IAEA-TECDOC-1320

Fuel behaviour under transient and LOCA conditions

Proceedings of a Technical Committee meeting held in Halden, Norway, 10–14 September 2001

INTERNATIONAL ATOMIC ENERGY AGENCY IAEA

November 2002

The originating Section of this publication in the IAEA was:

Nuclear Fuel Cycles and Materials Section
International Atomic Energy Agency
Wagramer Strasse 5
P.O. Box 100
A-1400 Vienna, Austria

FUEL BEHAVIOUR UNDER TRANSIENT AND LOCA CONDITIONS
IAEA, VIENNA, 2002
IAEA-TECDOC-1320
ISBN 92–0–114602–7
ISSN 1011–4289

Printed by the IAEA in Austria
November 2002

FOREWORD

At the invitation of the Government of Norway and in response to a proposal of the IAEA Technical Working Group on Water Reactor Fuel Performance and Technology (TWGFPT), the IAEA convened a Technical Committee Meeting on Fuel Behaviour under Transient and LOCA Conditions in Halden, Norway from 10 to 14 September 2001. The meeting was organized in co-ordination with OECD/NEA and was hosted by the Institutt for Energiteknikk — OECD Halden Reactor Project (HRP).

This meeting is the seventh in a series of IAEA meetings that were held in 1980 (jointly with OECD/NEA, Helsinki, Finland), 1983 (Risø, Denmark), 1986 (Vienna, Austria), 1988 (Preston, United Kingdom), 1992 (Pembroke, Ontario, Canada) and 1995 (Dimitrovgrad, Russian Federation). All of these activities have significantly contributed to the enhanced understanding of fuel behaviour at accident conditions.

In the six years since the last meeting took place, the demands on fuel duties have increased including higher burnup, longer fuel cycles and higher temperatures. To satisfy these demands, fuel vendors develop and introduce new cladding and fuel materials and designs to provide sufficient safety margins, especially under accident conditions. This has incurred a need for assessing the applicability of the database for clarification of safety criteria as well as models for accident evolution predictions. Thus, national and international experimental programmes have been launched, and models are being developed or adapted to consider the changed conditions, e.g. fission gas behaviour, relocation of cracked fuel, and physical property changes of the cladding.

Forty-three specialists in experiments and modelling of fuel performance at accident conditions from 15 countries and the OECD Nuclear Energy Agency and 10 observers (Norwegian and foreign representatives to the OECD HRP) took part in the meeting in order to gather and discuss existing knowledge on the subject and to identify the needs for further efforts. Twenty papers were presented at four sessions covering review of fuel research relevant to transient and accident conditions, transient analysis, cladding properties after high temperature oxidation and high burnup phenomena relevant to LOCA.

The IAEA wishes to thank all the participants for their contribution to the meeting and to this publication, especially J. Berger for assisting with administrative matters and M. McGrath of the Institutt for Energiteknikk - OECD HRP for summarizing the discussions during Panel Sessions. W. Wiesenack of the Institutt for Energiteknikk - OECD HRP chaired the meeting. P. Menut and V. Onoufriev of the Division of Nuclear Fuel Cycle and Waste Technology were the IAEA officers responsible for the organization of the meeting and the compilation of this publication.

EDITORIAL NOTE

This publication has been prepared from the original material as submitted by the authors. The views expressed do not necessarily reflect those of the IAEA, the governments of the nominating Member States or the nominating organizations.

The use of particular designations of countries or territories does not imply any judgement by the publisher, the IAEA, as to the legal status of such countries or territories, of their authorities and institutions or of the delimitation of their boundaries.

The mention of names of specific companies or products (whether or not indicated as registered) does not imply any intention to infringe proprietary rights, nor should it be construed as an endorsement or recommendation on the part of the IAEA.

The authors are responsible for having obtained the necessary permission for the IAEA to reproduce, translate or use material from sources already protected by copyrights.

CONTENTS

SUMMARY

SESSION 1. INTRODUCTION

The introductory session comprised two overview papers, one on the status of high burnup fuel safety research in the Republic of Korea and the other on OECD/NEA activities on fuel safety margins. Although covering different areas, it was apparent from both papers and the discussions that safety concerns are common and that international co-operation is required to address and resolve the issues with the necessary resources.

Safety research in the Republic of Korea is focused on providing the basis for licensing PWR fuel for burnup exceeding 60 MWd/kg U, the current licensing limit. To this end, a synergistic approach of fuel behaviour modelling and experimental activities is being pursued. The development of the fuel performance code INFRA takes account of important changes concurrent with increasing burnup, in particular rim microstructure formation, conductivity degradation, different modes of fuel swelling, cladding corrosion and ductility reduction, and creep-out behaviour due to fission gas release. Various hot cell tests and PIE will be conducted on irradiated pellet and cladding material, and some of the necessary facilities are being constructed. These will allow integral loss of coolant accident, (LOCA), simulations and investigations on fission product release properties of high burnup fuel.

The OECD/NEA activities on fuel safety margins are a part of the overall strategic plan of the Committee on the Safety of Nuclear Installations, CSNI. The Special Expert Group on Fuel Safety Margins, SEGFSM, conducted a topical meeting aimed at providing a forum for detailed discussions on the issues related to LOCA limits. These include:

- Effect of pre-transient oxidation
- Quenching & post quenching effects, changes in oxidation rate and embrittlement
- Ballooning and fuel relocation
- Beta-stabilising effects during ballooning & burst
- Sub-channel blockage
- Radiological consequences (extent of burst, release of fission products)
- Modelling adequacy & accuracy.

Considerable attention was given in the topical meeting to the origin of the Equivalent Cladding Reacted, ECR, and Peak Cladding Temperature, PCT, criteria. This was again the case in another session of the meeting reported here, underlining the importance of knowing the basis of the various criteria lest they be applied with the wrong premises. For example, the Baker-Just correlation must be used when estimating cladding oxidation for comparison with the 17% ECR criterion. Another important issue reported from the SEGFSM topical meeting was the limiting embrittlement of Russian Zr1Nb alloy (E110) already at 6% ECR in contrast to the performance of Zirlo and M5 alloys. A third focal point was axial fuel relocation into the ballooning area and its effect on heat-up, oxidation and quenching. Using code assessments, different conclusions were reached as to whether this effect requires special attention or whether it is already covered by conservative assumptions for more limiting effects.

Conclusions and recommendations for future work:

- Fuel behaviour modelling has to remain a continuous effort, relying on both empirical correlations and first principles. However, since different results can be obtained, e.g. on the consequences of fuel slumping, different groups (regulators, utilities) need to agree on the applicability and adequacy of models as well as underlying assumptions.

- There is still a need to provide an extended experimental basis in support of safety analyses for high burnup fuel. Among others, the effects of pre-existing oxidation, fuel relocation and the differences in behaviour of Nb-bearing Zr-alloys need to be resolved.

SESSION 2: NON-LOCA TRANSIENTS

This session dealt with the behaviour of nuclear fuel during transient (non-LOCA) conditions. The topics ranged from new simulation techniques, coupling of different codes, new results from experimental programs and new ways to perform them, as well as code development and new failure criteria.

The work on fuel performance evaluation under transients and accident conditions is being carried out in Alexandria University, Egypt. A Geno-fuzzy concept for nuclear reactors is used for this purpose. A new simulation technique, using this concept for the control of state variables, was demonstrated using a PWR Anticipated Transient Without Scram, ATWS, scenario.

The parallel coupling of codes enables step-by-step evaluation and the studying of the improvements and changes necessary in respective codes, and further features may be introduced easily. The work on coupling the USNRC fuel transient code FRAPTRAN and the VTT (Technical Research Center of Finland) thermal hydraulic subchannel model GENFLO was performed by VTT and STUK (Finnish Radiation and Safety Authority. The coupled code has been used for analyzing fuel behaviour during PWR and BWR transients and accidents. Some results of calculations for a large break LOCA, LBLOCA, in a WWER-440 and an instability accident in a BWR were shown.

The effect of cladding pre-oxidation on rod coolability during reactivity initiated accident, (RIA), has been investigated using the JAERI Nuclear Safety Research Reactor (NSRR). It has been shown that the presence of a minimum (several microns) oxide layer improves rod coolability during RIA conditions. The reason for this (better wettability) is probably the change in chemical potential instead of surface roughness.

Power ramp tests of high burnup BWR segment rods have been conducted in the Japanese Material Test Reactor, JMTR, after a basic 5 cycles irradiation in the Unit 2 of Fukushima Daini NPP. Satisfactory performance has been confirmed up to 60 GWd/t U, although some of the segments failed. Pinhole defect and axial cracks on high burnup BWR fuel cladding caused by the power ramp test, have been observed at 1 and 4 segments respectively.

The main features and status of qualification of the new 3.2 version of the SCANAIR code, developed by the Institut de Protection et de Sûreté Nucléaire, IPSN, in collaboration with Electricité de France, EDF, in the framework of the CABRI programme have been presented. The code's objective is to describe thermal mechanical behaviour of highly irradiated fuel (both UO_2 and MOX) PWR rods under RIA conditions. New features of SCANAIR include

improved mechanics, thermal hydraulics and fission gas release models. The interpretation of the experiments with the SCANAIR code has shown a satisfying status of qualification on the whole set of experimental results of the CABRI REP Na tests database. Planned evolution of the code is linked to the new CABRI international programme to be performed in the future Water Loop of the CABRI facility.

A new device to assess the mechanical behaviour of Zircaloy-4 during a RIA has been developed by CEA/Saclay in co-operation with IPSN and EDF in the framework PROMETRA programme to support CABRI tests. The device allows ring tests to be performed at high strain and heating rates. It is needed for better understanding of the behaviour of the cladding during RIA, including the correct failure mechanism.

A RIA failure criterion based on cladding strain has been proposed by C. Vitanza of the OECD/NEA. The criterion is based on CABRI data, but is also supported with NSRR experiments. This criterion predicts well the RIA data for high burnup UO_2 fuel. More tests are needed for MOX fuel to clarify any differences between UO_2 and MOX fuels. For what concerns mechanisms, fuel swelling is more important than FGR (fission gas release) for high burnup (~60 MWd/kg HM) fuel.

Conclusions and recommendations for future work:

- New simulations techniques are introduced in such classical fields as fuel behaviour modelling. In this case a paper presenting the use of genetic algorithms with fuzzy logic controlled variables was given. Another aspect that can be addressed is the generalization of the use of 3 dimensional, 3D, simulations.

- In the past, completely different codes were used for different disciplines. But in today's framework, the importance of considering the interactions among all the components in the system has been realized. Also the huge increment in computer capacity and speed has provided the possibility of performing the coupling between codes with different "physics". In the meeting a paper was presented coupling thermal hydraulics with thermal mechanics, but in the future there will also be coupling of the former with neutronics and systems codes.

- To feed the new codes, new knowledge of materials should be provided. To cope with this, new experimental programs are being carried out in different countries. These programs must deal with both microscopic and macroscopic properties of different fuel and cladding, as well as new operational circumstances such as higher burnup, longer cycles and higher operational temperatures.

- New results from different experimental programs were presented. Many of the programs are still running, and the results are therefore partial. Also, the conditions to perform the experiments must be thought about, in order to assure that the results are representative and valid for future operation or regulatory issues. Some of the experiments confirm previous research, whilst others show new results, such as new failure modes.

- There is evidence that some licensing criteria may not be valid any more. Enthalpy deposition for RIA must be rethought, both as the value of the limit and also as the correct failure mechanism. Thus, new criteria are needed. One criterion was presented based on cladding strain.

SESSION 3: CLADDING PROPERTIES AFTER HIGH TEMPERATURE OXIDATION

In this session, all papers but one were devoted to quench survival and post-quench ductility of several fuel cladding zirconium alloys during LOCA. During a typical LOCA transient, the fuel claddings are subjected to high temperature oxidation and finally quenched because of the reflooding of the core. The global oxygen and hydrogen contents and their distribution (due to irradiation or due to the transient) affect strongly the residual ductility of the cladding (zirconia layer thickness, oxygen-stabilized alpha phase thickness, oxygen and hydrogen content in the beta phase).

CEA presented ring-compression and other mechanical tests results performed on single-side steam oxidized low-tin Zircaloy-4 and M5 samples. KFKI presented hydrogen uptake measurements and ring-compression tests results performed on oxidized E110 and Zircaloy-4 (steam or separately argon-oxygen mixture followed by gaseous hydrogen). VNIINM presented quench tests results on steam oxidized simulators, deformed or not deformed, partially constrained or not, unirradiated and irradiated to 50GWd/t, cladded with E110 or E635 alloys, and ring-compression and other mechanical tests on steam oxidized E110. IPSN reviewed the rationale of current western criteria and transposed them to high-burnup Zircaloy-4, according to old JAERI results and recent KFKI results. OECD discussed these two kind of experimental results to derive LOCA safety limits.

All alloys survive nearly identically to unconstrained or partially constained thermal shock, i.e. with a large margin relative to the 17%-ECR limit below 1204°C; this is due to the fact that, for cooling rates typical of bottom flooding of core, most hydrogen atoms remain in solution in the beta phase at Leidenfrost temperature, and in such a state, hydrogen has little effect on the quench resistance of an oxidized zirconium alloy. The main problem is to have during the quench test, mechanical constraints representative of actual constraints occurring in large assemblies with grids and control rod guide tubes, as illustrated by a paper presented by JAERI in another session.

Survival to thermal shock is the main basis of the criteria used in Russia, whilst western countries' criteria (except Japanese ones), since the 1973 Emergency Core Cooling Systems (ECCS) rule-making hearing, are based on post-quench ductility. E110 alloy has relative total (elastic plus plastic) displacements up to the first main crack which are lower than for fresh Zircaloy or M5 during the ring-compression test, for comparable oxidation extent. This is due to higher hydrogen uptake during the steam oxidation transient, itself associated below ~1100°C with the oxide morphology (white, porous and layered oxide for E110 versus black, compact and adherent oxide for Zircaloy and M5. The reason for the difference between E110 and M5 alloys behavior, despite so similar compositions, remain unresolved.

Hydrided Zircaloy-4 (representing high-burnup Zircaloy-4) has also much lower displacements than fresh Zircaloy-4 during the ring-compression test, for comparable oxidation extent; high-burnup Zircaloy-4 suffers hydrogen uptake up to ~500wppm during irradiation.

A paper was devoted to the risk of blockage due to ballooning in WWER-1000 bundles. VNIINM presented coolability test results with 19 and 37 elements, cladded with E110 or E635. The conservative estimations of cross-section blockage do not exceed 70% for both E110 and E635 alloys.

Recommendations for future work:

- The effort of all counties developing and investigating ziconium alloys as fuel rod cladding materials has to be performed in such a way as to try to build a commonly recognized methodology for definition of LOCA limits and criteria.

- There is a need to compare mechanical test conditions of different zirconium-based alloys and to define common ones.

- There is a need for mechanical tests of high burnup irradiated Zircaloy-4.

SESSION 4: HIGH BURNUP PHENOMENA RELEVANT FOR LOCA

The influence of high burnup on fuel behaviour during a large break LOCA is an important issue, as very significant improvements of the fuel cycle economy can be achieved by increased burnup levels, and extensive analytical and experimental studies are going on in a number of countries.

The aspect discussed at this conference was the fuel damage limits (coolability criteria) at high burnup which for new advanced cladding alloys is normally expressed in terms of oxidation and temperature limits in combination with conservative correlations for metal/water reaction rates.

The main phenomena being investigated are:

- High temperature oxidation kinetics of high burnup cladding, including advanced alloys with improved performance during normal operation

- Resistance to thermal shock during quenching as a function of oxidation and of axial constraints

- Mechanical properties of cladding after a LOCA transient

- Fission gas release of high burnup fuel during a LOCA transient

- Ballooning and burst

- Fuel relocation.

Most of these phenomena were covered in Session 3. In Session 4, additional information was provided about the research program going on at JAERI in Japan. Extensive experiments have been performed on the influence of axial constraints during quenching, including the influence of pre-hydriding. The conservative 15% ECR limit used in Japan was based on the failure threshold determined in quenching tests with full axial restraint.

Fission gas release phenomena were addressed in a presentation of studies performed by CEA/Grenoble and CEA/Cadarache in France. Qualitative results of source term measurements were described and quantitative results will be published in the near future. Further developments of experimental facilities are going on in order to meet the requirements for special effects tests related to both RIA and LOCA transients.

Clad ballooning phenomena were discussed in a presentation of IPSN plans to perform new in-pile LOCA tests in France using bundles of high burnup fuel rods. The main concerns are possible fuel relocation into the ballooned area, effecting clad temperatures, and coolant flow blockage.

Conclusions and recommendations for future work:

- The fuel damage limits used in LOCA analyses should ensure that coolability is maintained. The basic requirement should be resistance to the thermal shock during quenching. The JAERI data show that larger axial constraints will lead to guillotine brakes of claddings at lower ECR values, which should be considered in the analysis of radiological consequences. However, such brakes should not significantly affect coolability. Other post-LOCA mechanical tests can provide additional insight into margins to other forces, for example during handling.

- The transient fission gas release during a LOCA event might contribute significantly not only to source term estimates but also to the ballooning and burst and thus to the oxidation. LOCA simulation experiments should if feasible be performed on high burnup rods with fuel pellets, for example in the tests planned within the Halden Programme, in order also to address this phenomenon. Tests with high burnup pellets will also provide better simulation of quenching behaviour.

- There is no full consensus about the importance of fuel relocation, but the tests planned within the Halden Programme will provide more information about this as well, if they can confirm when relocation occurs. The plans presented by IPSN include a very complete coverage of this aspect.

PANEL SESSION

During this session chairmen of the specific sessions raised issues of common interest revealed during the meeting, and Mr. C. Vitanza moderated a common round-table discussion and assisted in reaching a consensus for questionable issues.

1. Introductory session

Two points were put forward for discussion related to this session.

- Should modelling for RIA and LOCA be empirical or based on first principles and what level of detail is needed?

Enough should be learnt from testing to be sure that the simulations used in models are representative of what occurs in reality. Very detailed first principles knowledge is not needed in models – just in our understanding. The question is, what level of approximation should be used in models. Whilst models should be kept as simple as possible, the governing phenomena should be included. So far, RIA modelling was considered inline with these points, but it was felt that more fundamental issues could be included in LOCA modelling.

- Is there sufficient materials behaviour knowledge from RIA/LOCA studies to handle anticipated transient without scram (ATWS) modelling?

ATWS can be considered as a mild RIA with cladding temperatures similar to those during a LOCA being induced. Not much specific research has been done, but the important issue for fuel behaviour during an ATWS is considered to be whether fuel-clad contact exists or not. Before deciding if RIA/LOCA data from testing studies can help with ATWS investigation, all the physical processes occurring during an ATWS need to be identified and compared to those occurring during RIA/LOCA. Some are certainly not the same, indicating that specific material testing should probably be carried out.

From a utility point of view, whilst global reactor instability/oscillation is a real phenomenon, it always terminates with an automatic reactor scram. However, local instabilities could result in a seesawing effect that would not be detected by current monitoring. It was felt that adding extra core monitoring would prevent the Without Scram part of the phenomenon.

2. Transient analysis (non-LOCA)

This session covered new simulation techniques such as fuzzy logic and the coupling of codes from different disciplines. It was noted that there was a continued need for new knowledge due to the appearance of new or changing materials (higher burn-up / more aggressively operated). It was also felt that although new results were being made available, they were still insufficient for clear conclusions to be drawn. Licensing criteria validity was also discussed. Three issues were taken up in further discussion.

- Code coupling

It was mentioned that more complicated codes might be needed in the future, combining thermal-hydraulics with thermo-mechanics and perhaps neutronics and using 3D simulations. It was agreed that it was important to have thermal-hydraulics information at every time step to input to thermo-mechanical models and vice versa. Historically, codes have been developed separately in these two areas, but with increasing computer power, it should be possible to couple codes together with different “physics”. Although there was general support for this activity, it was pointed out that codes should be properly validated separately before they are coupled. Also, rather than making a permanently coupled, all encompassing code, it was felt a better approach would be to ensure all relevant codes had a “coupling protocol” which would allow them to be interfaced.

- MOX fuel during RIA

MOX fuel might have less margin for RIA than similar burn-up UO_2 fuel. It is important to extend materials testing for RIA studies to MOX fuel.

- New failure type: OD to ID cracking in power ramped, high burn-up fuel

Given that a new failure mechanism had been observed in high burn-up fuel exposed to high power ramping, it was questioned whether this was an important issue for RIA. High burn-up cladding is brittle due to the high hydrogen content which leads to hydride formation and thence hydride assisted crack propagation. The times associated with RIA may be insufficient for this mechanism to be relevant, given that hydride assisted crack propagation takes time to lead to clad failure. However, there are data from RIA studies - showing low enthalpy failures, with brittle cracks propagating from outside to inside, where the cladding had spalled oxide i.e. increased hydrogen pick-up. With no spalling, the failures were at higher enthalpy. It was pointed out that RIA studies should include current and advanced cladding materials,

and aim to encompass all realistic operating ranges expected in water reactors. Work is ongoing, particularly at CABRI, to address the issue for both current and future materials.

3. Cladding properties after high temperature oxidation

Most of the papers dealt with one of the two LOCA criteria: quench survival and post-quench ductility. Data from E110 and M5 cladding were compared to data from fresh Zry-4, which seemed to suggest a difference between the 1%Nb claddings, but a similarity between M5 and Zry-4. Whilst differing H-uptakes during the transient (due to differing oxide morphology) could account for this, differing testing conditions were felt to be a large issue. Also raised was the issue of testing hydrided Zry-4 as a substitute for high burn-up Zry-4. Three issues were discussed.

- Do we continue with the existing situation of two separate LOCA criteria, with the resulting two separate testing approaches for cladding?

Whilst survival to thermal shock is the basis of the Russian criteria, the Western criteria (except Japan) are based on post-oxidation ductility being above zero. This leads to two testing approaches, essentially one based on quench thermal shock, the other based on residual ductility, which makes a consistent comparison of test results from the different materials difficult. Extreme care must be taken not to draw any conclusions about Russian versus Western cladding based on different types of tests. A question for the future was thus if a common testing approach and safety criteria should be developed for all types of cladding. In designing such a test, simplicity and repeatability should be taken into account.

- Is the differing behaviour of E110 and M5 an issue?

The difference in behaviour was considered surprising because both alloys have a very similar composition. It was noted that the test loading conditions must be considered when results are being compared and that it would be ideal to use the same loading conditions, otherwise the test results of the two cladding types would always be different. It was mentioned that other advanced alloys with 1%Nb should be compared with E110 and M5, such as ZIRLO. There have been cases where M5 and E110 have been tested under the same conditions with differences in mechanical testing results still being observed. In this case the difference was accorded to differences in the oxide morphology. Although these are significant - M5 exhibits a black adherent oxide whilst that on E110 is white and layered - there was some debate as to whether this alone could explain the difference in the mechanical test results. A better understanding of the physical processes is needed to decide why similar clad types behave so differently. It was concluded that further experimentation was required and cladding users were encouraged to perform a Round Robin with common test conditions with M5, E110 and also to consider including ZIRLO and E635.

- Is hydriding an acceptable simulation of high burn-up material?

The most significant microstructural feature of high burn-up Zry-4 when considering cladding mechanical behaviour during a LOCA is its high levels of hydrogen uptake. Radiation damage effects anneal out very early in a LOCA, but because β-phase forms at the high cladding temperatures of a LOCA, it means that radial hydrides form during the subsequent quench. These have a deleterious effect on mechanical properties. High burn-up Zry-4 can thus be represented by pre-hydrided, unirradiated samples. However, in order to ensure that these samples are fully representative, “real” high burn-up samples should also be tested.

4. High burnup phenomena relevant for LOCA

The high fission gas inventory in fuel at high burn-up is an issue for LOCA as is the influence of the structure of high burn-up fuel on the relocation process during ballooning. Other high burn-up fuel assembly components could also be an issue for coolability after a LOCA, such as spacers and grids. Three points were raised for further comment.

- Will FGR from high burn-up fuel be a problem during transient heating?

This issue is being addressed experimentally, for instance at Halden, where both MOX and UO_2 commercial fuel are being extended to high burn-up for transient testing (power ramping) in a few years' time.

- Integral LOCA testing

LOCA type transient testing of single rods (i.e. not a bundle) will be carried out at Halden. The fuel has been identified, but some details are still to be resolved, such as pressurisation levels in the fuel.

- Coolability criterion

It was mentioned that fuel relocation during ballooning is a coolability issue whereas the previously discussed hydride induced cracking failure was not.

5. Final remarks

On the issue of criteria for RIA, it was noted that Switzerland, EPRI and OECD are making progress on provisional criteria and that SCANAIR will continue to develop.

On the issue of developing new criteria for LOCA, it would appear that the situation is less progressed than it is for RIA. As a first step, agreement is needed on a materials testing approach for continued studies, preferably consistent with the past as well as between different types of cladding.

INTRODUCTION

(Session 1)

Chairperson

W. WIESENACK
Norway

OECD/NEA ACTIVITIES ON FUEL SAFETY MARGINS

W. WIESENACK
OECD Halden Reactor Project, Institute for Energiteknikk, Halden, Norway

M. HREHOR
OECD/NEA, Paris, France

Abstract. In the paper a brief overview of the activities of the newly established CSNI Special Expert Group on Fuel Safety Margins (SEG FSM) is given. As specified in its mandate the objectives of the Group were to address cross-cutting issues related to fuel behaviour, including the work on relevant aspects of thermal-hydraulics, oxidation, chemistry, mechanical behaviour and reactor physics. Two Plenary meetings of the Group have been held so far: the kick-off meeting at the NEA Headquarters on 21-23 June 2000 and the second meeting organized in conjunction with a Topical Meeting on LOCA Fuel Safety Criteria in Aix-en-Provence, March 22-23, 2001. The first Topical Meeting on LOCA Fuel Safety Criteria belongs to the main events of the Group. The paper then focuses on some of the highlights of the Topical Meeting in the form of brief characteristics of presented papers. The SEG FSM will address issues raised during the meeting in its future activities.

1. INTRODUCTION

A new Strategic Plan of the OECD/NEA Committee on Safety of Nuclear Installations (CSNI) for the period 2000 - 2005 was approved in November 1999. The Plan included, among others:

- A review of the technical issues to be dealt with by the CSNI over the next few years
- The recommended structure of the CSNI and its working groups
- Recommendations on improved processes to ensure that the CSNI work is carried out efficiently.

It also recommended the creation of two Special Expert Groups for cross cutting issues, in particular:

- Special Expert Group on Fuel Safety Margins (SEG FSM)
- Special Expert Group on Human and Organizational Factors (SEG HOF)

The objectives of the Special Expert Group on Fuel Safety Margins (SEG FSM) were to address cross-cutting issues related to fuel behaviour, including the work on relevant aspects of thermal-hydraulics, oxidation, chemistry, mechanical behaviour and reactor physics. Its mandate included:

- Assessment the technical basis for current safety criteria and their applicability to high burn up, and to new fuel designs and materials.
- Identification of needs and priorities for future safety research programmes in the area of fuel safety behaviour
- Review from a safety point of view the methodologies used for reactor core assessments related to complex configurations, different fuel designs and types.
- Providing a forum to address emerging safety relevant fuel issues.

2. CURRENT ACTIVITIES OF THE SEG FSM

Two Plenary meetings of the Group have been held so far: the kick-off meeting at the NEA Headquarters on 21-23 June 2000 and the second meeting organized in conjunction with a Topical Meeting on LOCA Fuel Safety Criteria at Aix-en-Provence, March 22-23, 2001. During the second meeting the Group reviewed the status of ongoing activities, in particular

- Preparation of a CSNI report of fuel safety related R&D programmes in NEA Member States with the conclusion that some progress has been made in the compilation of ongoing and planned fuel safety research in NEA Member states.
- Preparation of a CSNI report on fuel safety criteria used in NEA Member States for which a revised questionnaire on high burnup fuel safety criteria has been issued and distributed to Member States
- Initiation of ISP based on a CABRI test was postponed due to controversial opinions regarding the value of such an exercise, taking into account the fact that number of codes able to simulate such test is very limited.

Based on the positive experience of the first Topical Meeting on LOCA Fuel Safety Criteria, the Group suggested to continue organizing a series of topical meetings devoted to high priority unresolved fuel safety issues. The second topical meeting (in March 2002) will focus on RIA related fuel safety criteria, especially with regard to high burnup. The Group also supported co-sponsoring the IAEA Technical Committee Meeting on Fuel Behaviour under Transient and LOCA Conditions planned for September 10 – 14, 2001 in Halden.

3. HIGHLIGHTS OF THE FIRST TOPICAL MEETING ON LOCA FUEL SAFETY CRITERIA

The first Topical Meeting on LOCA Fuel Safety Criteria belongs to the main events of the Group. The meeting was organised in co-operation with IPSN Cadarache and was chaired by Dr. Georges Hache from IPSN. In total 53 participants attended and 14 papers were presented in all by research and industry organisations from France, Hungary, Japan, the Russian Federation and the USA. The papers covered three main issues:

- Post-quench ductility
- The impact of axial constraint
- And fuel relocation.

The key paper on "***The Rationale of the LOCA 10CFR50.46b Criteria for Zircaloy and Comparison With E110 Alloy"*** was presented by Dr.G. Hache, IPSN, France. The paper highlighted the importance of post-LOCA ductility, a fact that had been largely forgotten during the last 25 years. The primary rationale of the 17% oxidation criterion was retention of cladding ductility at temperatures higher than 275°F (135°C), i.e., the saturation temperature during reflood. For oxidation temperatures 1204°C, the 17% oxidation limit (calculated with Baker-Just correlation) is adequate to ensure the survival of cladding under quenching thermal shock. However, the 17% ECR limit appears to be inadequate to ensure post-quench ductility at hydrogen concentrations >700wppm. The application of the 1973 ECCS Rule-making hearing methodology for VVER E 110 alloy (retention of cladding ductility) would lead to a 6% oxidation limit. This raised the question how is it with other Nb containg alloys, such as M5 and ZIRLO.

Dr. Ralph Meyer from US NRC briefly presented the ***"NRC Program for Addressing Effects of High Burnup and Cladding Alloy on LOCA Safety Assessment".*** He also informed on NRC meetings with Framatome and Westinghouse to discuss the concerns regarding the niobium alloys. Both Framatome and Westinghouse stated that their new alloys, in particular M5 and ZIRLO are in agreement with their earlier results on Zircaloy 4. The conflict with the Eastern European data remained unexplained. NRC proposed new co-operative work with Framatome and Westinghouse to address the high-burnup issues for the new claddings

Dr. Laszló Maróti, AEKI, Budapest, Hungary, gave an overview of the Hungarian "***Ring-Compression Test Results and Experiments Supporting LOCA PCT, Oxidation and Channel Blockage Criteria".*** Based on that he concluded that Zr1%Nb ring compression tests showed stronger embrittlement of this cladding after high temperature steam oxidation than Zry-4 which indicates that Zr1%Nb has most likely a higher H uptake predisposition during the oxidation than Zry-4. Nonetheless, their quench tests on 5 cm long fuel pieces confirmed the conservatism of the Russian 18% ECR criterion.

Mr. A. Le Bourhis, Framatome, France in his paper on ***"Justification of the M5^{TM} behavior in LOCA"*** stated that M5 alloy does exhibit embrittlement within the limits of the ECCS criteria, and that results on Zr1%Nb are not applicable to M5 claddings. Similarly Dr. W.J.Leech from Westinghouse, USA presented ***"Westinghouse Ductility Testing of Zircaloy-4 and ZIRLO^{TM} Cladding After High Temperature Oxidation in Steam"*** and concluded that there is strong similarity between ZIRLO and Zry-4 and that both alloys meet the 17% ECR criterion. He also opposed comparing ZIRLO with E110 alloy by saying that ZIRLO is behaving like Zry-4 and not like the E110 alloy.

Dr. Hee Chung, with his co-authors R.V. Strain, T. Bray, M.C. Billone from Argonne National Laboratory, USA described ***"Progress in ANL/USNRC/EPRI Program on LOCA".*** Their results show that

- Post-quench ductility is strongly influenced not only by oxidation but also by hydrogen concentration
- The threshold of hydrogen concentration for severe hydrogen-induced embrittlement in Zry-4 appears to be ‰600wppm.

According to published data, similar threshold hydrogen concentration for E110 appears to be lower.

Ms. L.N.Andreeva-Andrievskaya from VNIINM, Russian Federation presented with the co-authors Prof. Yu. K. Bibilashvili, Mr. N.B. Sokolov, , at al. a paper on ***"Thermomechanical Properties of Oxydized Zirconium Based Alloy Claddings in LOCA Conditions"***. Their thermal shock experiments confirmed the embrittlement criterion "1 200 °C PCT - 18% ECR" for the Zr1%Nb fuel rod claddings of VVER type. These experiments also showed that there is no difference in the residual ductility of the irradiated and unirradiated Zr1%Nb claddings.

Dr. Nicolas Waeckel and Patrickg Jacques, both from EDF, France, along with Dr. Rosa Yang and Mr. Robert Montgomery from EPRI, USA, tried to answer the following questions in the paper on ***"Analysis of Fuel Rod Axial Forces During LOCA Quench"***:

- Can the rods be locked-up at the grid locations during the LOCA?
- How strong might the axial forces be in case the rods are locked at the grid locations?

Their conservative analyses showed low values of axial forces if rod lock-up was assumed. The calculated maximum axial load was 5 times lower than the fully constrained load at failure upon quench experienced in JAERI LOCA tests. They also stated that the experimental data suggest that the rod-to-grid linkage is very unlikely and that fully constrained LOCA separate effect tests are atypical and overly conservative.

Dr. Hiroshi Uetsuka and F.Nagase, JAERI, Japan informed on ***"Progress in JAERI Program on High Burnup Fuel Behavior Under a LOCA Transient",*** in particular on the integral thermal shock test with pre-hydrided cladding tubes. They observed almost no influence of absorbed hydrogen on cladding failure by quenching under no restraint conditions. On the other hand the threshold ECR was obviously reduced by absorbed hydrogen for the restraint conditions.

Messrs. Michel Lambert, Yann Le Hénaff, both from EDF/SEPTEN, and Mr. Jean-Luc Gandrille from Framatome ANP, France presented a joint paper on ***"Synthesis of an EDF and FRAMATOME ANP Analysis on Fuel Relocation Impact in Large Break LOCA".*** Their analysis shows that the effect of fuel relocation on cladding temperature is very low and that the relocation phenomenon, if it exists, is limited to the burst area (a few centimetres), and to the hot rods only. They suggested that the relocation should not be taken into account in safety regulation.

Messrs. C. Grandjean, G. Hache, C. Rongier from IPSN, France focused on the same phenomenon but came to different conclusion in their paper ***"High Burnup UO2 Fuel LOCA Calculations to Evaluate the Possible Impact of Fuel Relocation After Burst"***:

- Fuel relocation in the ballooned region may increase significantly the peak clad temperature
- The maximum cladding oxidation rate exceeds the 17% acceptance limit when the initial (in service) oxidation rate is cumulated with the transient oxidation rate.

Mr. Hiroshi Hayashi from NUPEC, Japan summarized ***"High Burnup Phenomena Affecting the Failure Mode of Fuel Rods During LOCA",*** as observed in their experimental programme, in particular

- Cladding degradation due to hydrogen absorption and irradiation embrittlement
- Bonding layer between pellet and cladding
- RIM formation in the region of pellet peripheral
- Decreasing of thermal conductivity of pellets.

Mr. Smirnov V.P. at al. from RIAR, Russian Federation submitted a paper on ***"Results of the Experimental Research on High, Burnup VVER-type Fuel Behaviour in LOCA Conditions".*** Also these experiments confirmed that Zr1%Nb claddings do not fail during quenching and during subsequent transportation and manipulation. At typical LOCA temperatures (T>600ºC) the irradiated cladding mechanical properties don't differ from the properties of unirradiated claddings.

Dr. A. Mailliat from IPSN, France presented the paper on ***"IPSN Analysis of Experimental Needs Requested for Solving Pending LOCA Issues"*** in which he informed that IPSN is preparing the so called APRP-Irradié (High Burnup Fuel LOCA) programme consisting of in-pile experiments involving bundle geometries in the PHEBUS facility.

The LOCA Topical Meeting was closed by the discussion of Conclusions and Recommendations, which will become part of the meeting proceedings.

4. CONCLUSIONS

The first Topical Meeting on LOCA Fuel Safety Criteria was an important introduction of the SEG FSM into the subject. It pointed out that the origin US NRC 17% oxidation criterion, in particular its rationale "retention of post quench ductility", should be always kept in mind, otherwise the formal use of this criterion might be misleading. A number of experiments done so far show that the retention of post quench ductility is burnup dependent and that a hydrogen uptake, with its threshold concentration approx. 600 -700ppm, plays an important role in this respect. The meeting stressed, in addition, that for Nb containing alloys a combined effect of oxygen, hydrogen and niobium must be considered.

The meeting also showed that the "retention of post quench ductility" might be a rather conservative requirement as axial forces and overall loads during and after LOCA seem not to be as high as originally expected. Instead, a quench thermal shock survival might be a sufficient realistic requirement as shown in a number of other experiments.

SEG FSM will try to address the issues raised during the meeting in its future activities. One of them could be a definition of a representative test for further experimental studies of LOCA fuel safety criteria.

REFERENCES

[1] HACHE, G., IPSN, France, The Rationale of the LOCA 10CFR50.46b Criteria for Zircaloy and Comparison With E110 Alloy
Proceedings of the Topical Meeting on LOCA Fuel Safety Criteria Aix en Provence 22-23/03/2001, NEA/CSNI/R (2001)18

[2] MEYER, R., US NRC NRC Program for Addressing Effects of High Burnup and Cladding Alloy on LOCA Safety Assessment
Proceedings of the Topical Meeting on LOCA Fuel Safety Criteria Aix en Provence 22-23/03/2001, NEA/CSNI/R(2001)18

[3] MARÓTI, L., AEKI, Hungary, Ring-Compression Test Results and Experiments Supporting Budapest, LOCA PCT, Oxidation and Channel Blockage Criteria.
Proceedings of the Topical Meeting on LOCA Fuel Safety Criteria Aix en Provence 22-23/03/2001, NEA/CSNI/R(2001)18

[4] LE BOURHIS, Framatome, France, Justification of the M5TM behavior in LOCA ,
Proceedings of the Topical Meeting on LOCA Fuel Safety Criteria Aix en Provence 22-23/03/2001, NEA/CSNI/R(2001)18

[5] LEECH, W.J., Westinghouse, USA, Westinghouse Ductility Testing of Zircaloy-4 and ZIRLOTM Cladding After High Temperature Oxidation in Steam
Proceedings of the Topical Meeting on LOCA Fuel Safety Criteria Aix en Provence 22-23/03/2001, NEA/CSNI/R(2001)18

[6] CHUNG, H., STRAIN, R.V., BRAY, T., BILLONE, M.C., Argonne Nat. Lab., USA Progress in ANL/USNRC/EPRI Program on LOCA
Proceedings of the Topical Meeting on LOCA Fuel Safety Criteria Aix en Provence 22-23/03/2001,NEA/CSNI/R(2001)18

[7] BIBILASHVILI, Yu. K., SOKOLOV, N.B., ANDREEVA-ANDRIEVSKAYA, L.N., at al. VNIINM,Russian federation, Thermomechanical Properties of Oxydized Zirconium based Alloy Claddings in LOCA Conditions
Proceedings of the Topical Meeting on LOCA Fuel Safety Criteria Aix en Provence 22-23/03/2001, NEA/CSNI/R(2001)18

[8] WAECKEL, N., JACQUES, P., EDF, France, YANG, R., MONTGOMERY, R., EPRI, USA, Analysis of Fuel Rod Axial Forces During LOCA Quench
Proceedings of the Topical Meeting on LOCA Fuel Safety Criteria Aix en Provence 22-23/03/2001, NEA/CSNI/R(2001)18

[9] UETSUKA, H., NAGASE, F., JAERI, Japan, Progress in JAERI Program on High Burnup Fuel Behavior under a LOCA Transient
Proceedings of the Topical Meeting on LOCA Fuel Safety Criteria Aix en Provence 22-23/03/2001, NEA/CSNI/R(2001)18

[10] LAMBERT, M., HÉNAFF, EDF/SEPTEN, Y. L., GANDRILLE, J-L., Framatome ANP, France, Synthesis of an EDF and FRAMATOME ANP Analysis on Fuel Relocation Impact in Large Break LOCA
Proceedings of the Topical Meeting on LOCA Fuel Safety Criteria Aix en Provence 22-23/03/2001,NEA/CSNI/R(2001)18

[11] GRANDJEAN, C., HACHE, G., RONGIER, C., IPSN, France, High burnup UO2 Fuel LOCA Calculations to Evaluate the Possible Impact of Fuel Relocation After Burst
Proceedings of the Topical Meeting on LOCA Fuel Safety Criteria Aix en Provence 22-23/03/2001, NEA/CSNI/R(2001)18

[12] HAYASHI, H., NUPEC, Japan, High Burnup Phenomena Affecting the Failure Mode of Fuel Rods During LOCA.
Proceedings of the Topical Meeting on LOCA Fuel Safety Criteria Aix en Provence 22-23/03/2001,NEA/CSNI/R(2001)18

[13] SMIRNOV, V.P. at al., RIAR, Russian Federation, Results of the Experimental Research on High Burnup VVER-type Fuel Behaviour in LOCA Conditions
Proceedings of the Topical Meeting on LOCA Fuel Safety Criteria Aix en Provence 22-23/03/2001,NEA/CSNI/R(2001)18

[14] MAILLIAT, A., IPSN, France, IPSN Analysis Of Experimental Needs Requested for Solving Pending LOCA Issues
Proceedings of the Topical Meeting on LOCA Fuel Safety Criteria Aix en Provence 22-23/03/2001,NEA/CSNI/R(2001)18

STATUS OF HIGH BURNUP FUEL SAFETY RESEARCH IN THE REPUBLIC OF KOREA

J.G. BANG, C.B. LEE, D.H. KIM, Y.M. KIM, Y.S. YANG, Y.H. JUNG
Korea Atomic Energy Research Institute,
Yuseong, Daejeon, Republic of Korea

Abstract. UO_2 fuel for PWR in Korea is licensed up to the burnup of 60 MWD/kgU-rod avg. and further burnup extension is planned. In order to analyze the fuel rod behavior at high burnup under steady state and transient conditions, INFRA(INtegrated Fuel Rod Analysis), is being developed. Fuel performance models to analyze the pellet and cladding behavior at high burnup were newly developed, and the finite element analysis module was added for the mechanical analysis. To study the high burnup fuel behavior during the RIA and LOCA transient conditions, several hot cell tests are planned such as post-irradiation examination (PIE) for high burnup fuels, annealing test of high burnup pellet with rim region, and mechanical and high temperature oxidation tests of the irradiated cladding under LOCA condition by using high burnup fuel specimens.

1 INTRODUCTION

In order to increase the fuel cycle economy and reduce the quantity of spent fuels, fuel burnup has been increased continuously with improvement of corrosion resistant cladding. In the middle of 1990, UO_2 fuel reached up to 60 MWD/kgU-rod avg. In Korea, advanced fuel rod materials and components such as an advanced zirconium alloy, a new pellet, spacer grid, and top/bottom end piece, are being developed for the extension of fuel burnup. And also fuel performance analysis code, INFRA (INtegrated Fuel Rod Analysis, is being developed to analyze the high burnup fuel rod behavior under steady state and transient state up to the burnup higher than 70 MWD/kgU-rod-avg.[1]. For the prediction of pellet and cladding behavior at high burnup, several pellet and cladding models were newly developed.

Domestic fuels have been irradiated in PWR up to burnup higher than 55 MWD/kgU-rod avg., and further burnup extension is planned. Therefore, Korea is in the same situation as the other countries in high burnup fuel safety issues. Table 1 shows the status of fuel burnup being irradiated in PWR. Fuel safety tests in hot cell are planned by using high burnup fuel assembly irradiated in YGN-1 plant. Peak fuel rod burnup is about 55.4 MWD/kgU-rod avg.. Tests in hot cell such as post-irradiation examination (PIE) for high burnup fuels, annealing test of high burnup pellet with rim region, and mechanical and high temperature oxidation tests of the irradiated cladding under LOCA condition by using high burnup fuel specimens are planned.

TABLE 1. STATUS OF FUEL BURNUP IN KOREA

Reactor (Fuel Type)	Cycle Length (month)	Core Avg. Power (kW/ft)	Licensed FA Burnup (MWD/MTU)	Hot Channel Factor	Core Temperature	
					T_{in} (^oC)	T_{out} (^oC)
Kori-1 (OFA)	15	6.47	52 000	1.55	282.7	319.8
Kori-2 (STD)	15	5.37	43 000	1.55	287.7	326.1
Kori-3 (V5H)	18	5.44	53 000	1.65	291.7	328.2
YGN-1 (V5H)	18	5.44	53 000	1.65	291.7	328.2
UJN-1,2 (V5H)	18	5.44	53 000	1.65	286.2	324.9
YGN-3 (CE)	18	5.39	47 000	1.53	296.1	328.3

2 DEVELOPMENT OF FUEL ROD PERFORMANCE CODE, INFRA

As the fuel burnup increases beyond 60 MWD/kgU, the new issues for the fuel behavior have arisen. In order to predict the behavior of high burnup fuel, fuel rod performance code, INFRA is being developed [1]. Several models were newly developed to predict the high burnup fuel behavior. In particular, it is important to predict the behavior in pellet rim microstructure region at high burnup. Thermal conductivity in rim region, rim microstructure formation mechanism, and local radial burnup distribution are important parameters in predicting pellet behavior at high burnup. And creep-out behavior due to higher fission gas release, enhancement of corrosion rate and axial growth, and reduction of cladding ductility are among the important parameters in cladding behaviour at high burnup.

Neutron energy spectrum and magnitude are varying at radial position in UO_2 fuel pellet, then local fission density rates is changed. And it is necessary to predict those phenomena to analyze the high burnup fuel rim effects. Therefore, RAPID (RAdial Power and Burnup Prediction by following fissile Isotope Distribution in the Pellet) was developed to predict local power, burnup, and fissile isotope distribution as a function of radial position, pellet burnup and initial U-235 enrichment [2]. Figure 1 shows comparison of RAPID and Frapcon-3 predictions with the measured data. RAPID model predicts the measured data better.

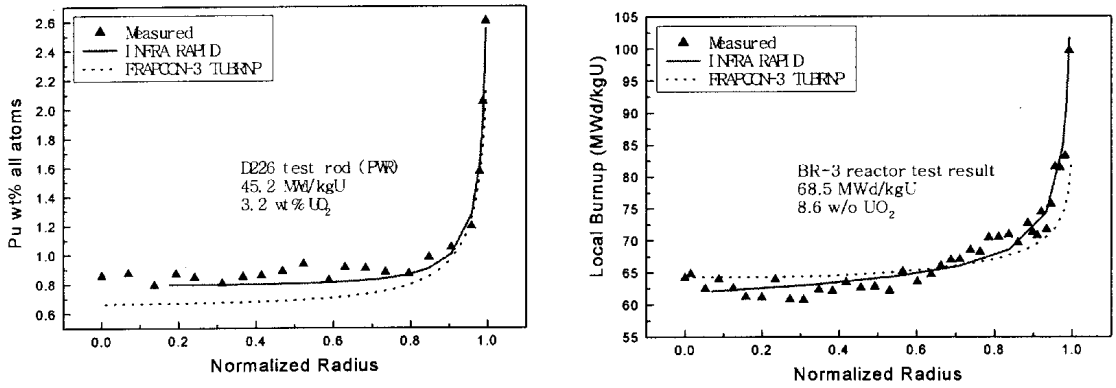

FIG. 1. Comparison of radial Pu nuclide and burnup distribution.

As UO_2 burnup increases, fission gas bubble generation increases gradually by the accumulated fission gases and therefore, swelling by fission gas bubble becomes non-negligible. In order to estimate the swelling caused by fission gas bubbles, gaseous swelling model was developed [3].

Thermal conductivity of irradiated UO_2 is an important parameter in fuel thermal behavior such as fuel temperature and fission release. In INFRA code, new thermal conductivity model was developed based upon the thermal diffusivity data of irradiated UO_2 fuel measured during annealing [4]. Since it considers the effects of solid fission product and gaseous fission product separately, it can be used to estimate the thermal conductivity of UO_2 rim microstructure region where most gaseous fission products are precipitated into fission gas bubbles.

Formation mechanism of rim microstructure was studied to show that the rim microstructure formation depends not simply local burnup but fission gas concentration in the UO_2 matrix [5]. At the critical fission gas concentration, fission gas bubbles are nucleated and stabilized,

followed by grain sub-division to form the rim microstructure. Therefore, it showed that as temperature increase, rim microstructure formation is delayed due to fission gas release and then at high temperature inner pellet region, rim microstructure would not be formed at all even at the higher burnup.

In order to predict the behavior of Zircaloy-4 cladding at high burnup, models of Zircaloy-4 cladding behavior at high burnup in the area such as creep-out and corrosion were developed. At high burnup, fuel rod internal pressure can exceed the external coolant pressure by fission gas release, which could result in the cladding lift-off. In order to analyze the phenomenon, it is necessary to estimate the cladding creep-out rate precisely. Comparison of the cladding creep-out prediction of the fuel performance analysis codes which were based upon the cladding creep-down test data with the Halden test data showed that the codes under-estimate the cladding creep-out rate. Therefore, based upon the existing creep model, new cladding creep-out model was derived by changing the dependence of the creep rate upon the fast neutron flux and stress [6]. Figure 2 shows the comparison calculation results by INFRA and Frapcon-3 prediction with measured data.

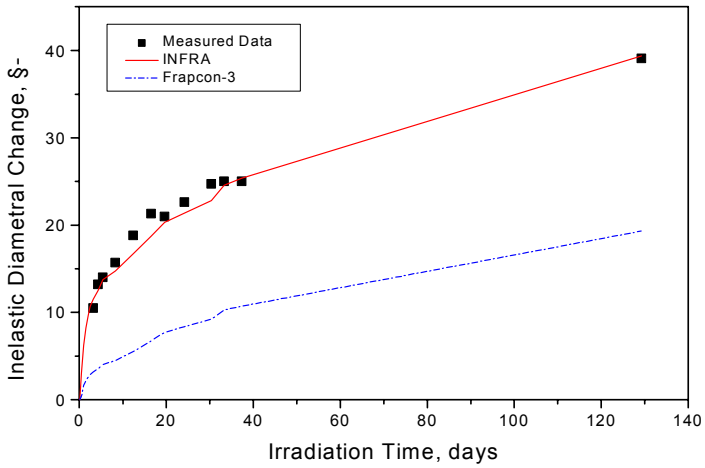

FIG. 2. Comparison of INFRA Prediction with Measured Data.

Corrosion model of Zircaloy-4 cladding was developed through the analysis of the corrosion mechanisms and other corrosion models. The parameters influencing the fuel cladding corrosion are the material and manufacturing characteristics of the cladding, coolant chemistry, hydride formation in the cladding and fast neutron flux. The model was derived taking into account the effect of each parameter on the Zircaloy corrosion. The derived model was evaluated by both the sensitivity analyses of the parameters and its predictability of such phenomena as the axial distribution of corrosion, the effect of water chemistry and acceleration of corrosion at high burnup [7].

For the accurate mechanical analysis of fuel pellet and cladding during steady state and transient, finite element analysis module was developed [8] and added to INFRA code. It receives the necessary data such as temperature and material properties from INFRA code and calculate local stress and strain of the fuel rod.

3. SAFETY RESEARCH OF HIGH BURNUP FUEL

Right after the result of RIA simulation tests in CABRI of France was presented in 1994, KAERI performed the analysis and the safety evaluation for domestic UO_2 fuel behavior [9], where 3-dimensional transient core analysis during RIA was first performed as a pioneering work and fuel failure criteria in terms of fuel enthalpy increase during RIA instead of total fuel enthalpy was first proposed, considering PCMI fuel failure mechanism. KAERI also performed the safety analysis for domestic nuclear power plant fuel in cooperation with other nuclear organizations such as KINS (Korea Institute of Nuclear Safety) and KEPCO [10].

KAERI has been developing advanced PWR fuel technology as a national nuclear project since 1997. In order to prepare for the development and the commercialization of high burnup fuel, high burnup fuel properties and related test data have been analyzed. Fuel behaviors under RIA and safety issues for high burnup fuel were analyzed. It was found that further tests would be necessary in such areas as fuel failure and dispersion under RIA, and high temperature cladding corrosion, and mechanical deformation under LOCA. Domestic fuel has been irradiated up to burnup higher than 55 MWD/kgU-rod average. The plan for safety research was established after the analysis of fuel safety issues and domestic fuel usage and development plan [11]. The objectives of fuel safety research were set as follows:

- Re-evaluation of Safety Criteria for PWR High Burnup Fuel
- Safety Tests, Verification and Buildup of Database for Domestic High Burnup Fuel
- Development of Safety Analysis Technology for High Burnup Fuel

2.1 Post irradiation test

Post irradiation examination for domestic high burnup fuel will be carried out in 2002. The optimum fuel for the examination will be selected through discussion with related institutes - KNFC, KEPCO and KINS - and transferred to hot cell in KAERI. PIE will be completed in 2002. And database for domestic high burnup fuel performance will be generated and be used for the verification of fuel performance and fuel performance analysis code.

3.2. Cladding tests

3.2.1. Design of Test Equipment and Establishment of Test Technology

For LOCA tests, integral LOCA simulator which can simulate the accident progress will be constructed by 2002. This equipment requires the high heating temperature of a maximum of 200 K/s, a high temperature oxidation test at a maximum of 1700 K and a quenching test by infusing water or steam. Figure 3 shows the schematic drawing of LOCA simulator. In order to simulate RIA, High Pressurization Equipment, which requires a strain rate of a maximum of 1.0/sec, will be constructed. This equipment will be installed by the end of 2002.

3.2.3 Out-of-pile Tests for Unirradiated Cladding

Using integral LOCA simulation equipment, baseline tests for criteria of ballooning, oxidation and failure on Zircaloy-4 and low tin Zircaloy-4 cladding will be carried out. And based on the above tests, a LOCA simulation test on new foreign cladding and domestic cladding will

be carried out, and analysis of the fracture mode will be performed through the destructive analysis.

Using high pressurization equipment, burst tests on foreign cladding and domestic cladding will be carried out, and the PCMI resistance will be evaluated.

3.2.3 In-pile Tests for Irradiated Cladding

After completion of transient tests on unirradiated cladding, test equipment will be transferred to hot cell. Zircaloy-4 cladding irradiated at domestic nuclear plant will be used. Integral LOCA simulation test, PCMI simulation test, and fracture toughness test will be carried out. After transient accident simulation test, post irradiation examination for irradiated specimen could be carried out in hot cell.

Analysis for behavior on high burnup cladding in RIA will be performed with data obtained from foreign countries and international cooperation. Finally integrating these test results, safety criteria for high burnup cladding and a new developed cladding will be confirmed and failure criteria will be re-established

3.3. Pellet tests

The problems of high burnup fuel in steady state are caused by the degradation of pellet material, therefore, in order to solve these problems it is necessary to improve and develop the UO_2 pellet material. The experimental data on low burnup fuel pellet behavior has been accumulated, but the experimental data on high burnup fuel pellet behavior are not sufficient.

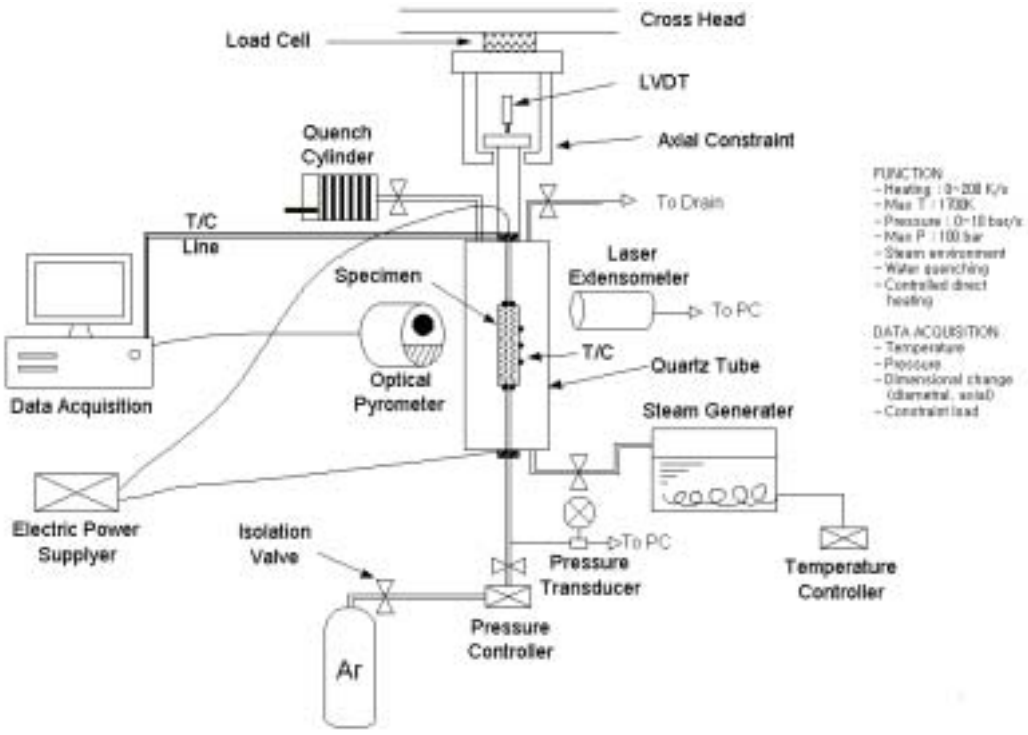

FIG. 3. Schematic Drawing of Integral LOCA Simulator.

Some of the experimental data on high burnup fuel shows that it is necessary to reevaluate the accident criteria established at low burnup.

Test of Microstructure of High Burnup Pellet

The state of pellet irradiated in steady state has an effect on fission gas release and fuel behavior under abnormal and transient conditions. Therefore, analysis of high burnup pellet microstructure is the starting point of pellet safety research. This analysis of domestic high burnup fuel will be carried out in hot cell in KAERI. Measurements of pellet density and dimension, etc., will be performed by the NDT method, and the measurements of microscopic distribution of pores and grains by optical microscope, microscopic distribution of fission product by EPMA, and chemical state of fission product by ICP will be carried out by the destructive test method.

In order to examine the rim formation mechanism, burnup distribution and fission gas release can be calculated and compared with measured data, and then model can be verified and established. And also FP bubble pressure, and bubble size, etc., can be calculated.

Fission Gas Release

Out of pile experiment will be performed in order to investigate fission product release. Figure 2 is the layout for post irradiation annealing experiment facility. This facility will be set in hot cell in KAERI by the end of 2002. Spent (irradiated) fuel fragments (total UO_2 : 30 - 500 mg) are heated in an induction furnace set in a hot cell. Carrier gas (mixture of He and H_2 gases) flows over the fuel fragments, and fission products which are released from the fuel fragments flow together with the carrier gas. Cs, I, and particles of the fission products are trapped in the hot cell, and thus the carrier gas containing only Xe and Kr flows into a glove box. In the glove box, we plan to measure the â-activity of Kr-85 continuously. Kr and Xe are then trapped in charcoal filter cooled by liquid nitrogen, and total accumulated Kr and Xe are measured by γ-activity. Carrier gas provided from a gas cylinder flows through furnace, FP-trap, β-counter, and charcoal filter, and finally returns to the hot cell.

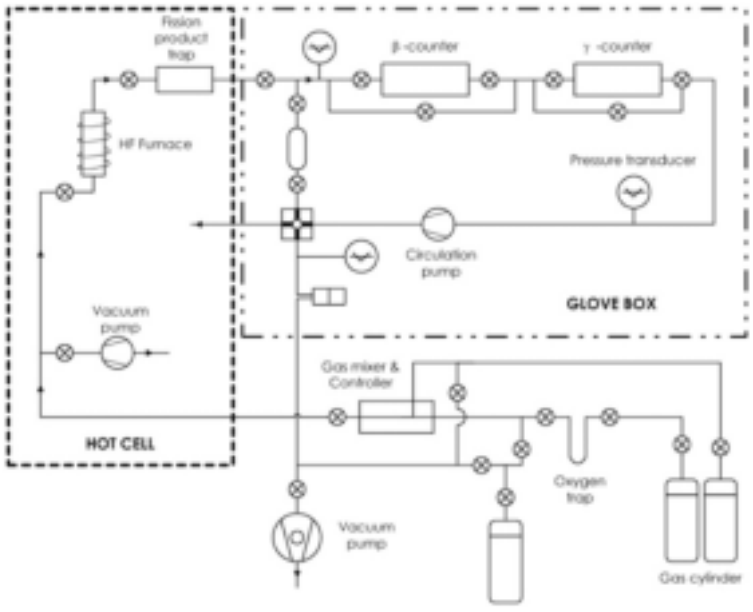

FIG. 4. Llayout for Post Irradiation Annealing Experiment.

3.4. Development of fuel safety analysis technology

Database obtained from PIE, RIA and LOCA test of cladding and pellet in the hot cell, and international joint program will be used for the reevaluation of safety criteria and the development of fuel performance analysis code in transient state. Fuel rod performance analysis code, INFRA has been developed to estimate the behavior of high burnup fuel at steady state, and this code would be finalized by 2002. Fuel rod performance analysis code under transient conditions will be followed. In transient state, fuel temperature and power are very high and the progressing time is very short, so that the performance models different from those in steady state would be developed. Therefore, by using the results of corrosion and mechanical strain tests for high burnup cladding, and gaseous swelling and fission gas release test for high burnup pellet, and international joint program fuel performance analysis code in transient state will be developed.

4. CONCLUSIONS

Fuel performance code is being developed in order to predict the high burnup fuel behavior under steady state and transient conditions. Fuel performance analysis models were newly developed to estimate the behavior of high burnup fuel: for the pellet, gaseous swelling model, thermal conductivity model, rim formation mechanism model, and RAPID program to predict local power and burnup, and for the cladding, creep-out model, mechanical property model, and corrosion model, and finite element analysis module for the mechanical analysis of fuel rod during the transient.

Domestic fuel has been irradiated in PWR up to a burnup of 55 MWD/kgU-rod avg. Therefore, Korea is in the same situation as the other countries in high burnup fuel safety issues. A safety research plan has been established. Simulation tests for RIA and LOCA will be performed by using high burnup fuel specimens and fuel safety criteria will be reevaluated and analysis tools for those transient will be developed.

REFERENCES

[1] LEE, C.B. et al., “Development of UO_2 Fuel Rod Performance Analysis Code, INFRA”, Proceedings of KNS 2001 Fall Meeting, 2001(to be published).

[2] LEE, C.B., , et al., "RAPID model to predict radial burnup distribution in LWR UO_2 fuel", J. of Nuclear Mater., vol.282, p.196, 2000.

[3] KIM, D.H. et al., “Fission Gas Swelling Model of high burnup Fuel”, Proceedings of KNS Fall Meeting, 1998.

[4] LEE, C.B. et al., "Development of Irradiated UO_2 Thermal Conductivity Model", IAEA Technical Committee Meeting on Nuclear Fuel Behavior Modelling at High Burnup and its Experimental Support, Windermere, UK, 2000.

[5] LEE, C.B., and Y.H. JUNG, "An Attempt to Explain High Burnup Structure Formation Mechanism in UO_2 Fuel", J. of Nuclear Mater., vol.279, p.207, 2000.

[6] BANG, J.G. et al., “Development of LWR Zircaloy-4 Cladding Creep-out Model”, Proceedings of KNS 1998 Fall Meeting, 1998.

[7] BANG, J.G. et al., “Development of LWR Fuel Zircaloy-4 Cladding Corrosion Model”, Proceedings of KNS 1999 Fall Meeting, 1999.

[8] KWON, Y.D. et al., “Development of Finite Element Module Technology”, KAERI/CM-399/99, KAERI, 1999.
[9] LEE, C.B. et al., “Analysis of the Fuel Rod Behavior Under the Rod Ejection Accident in the Pressurized Water Reactor”, OECD/NEA Specialists Meeting on Transient Behavior of High Burnup Fuel, Cadarache, France, 1995.
[10] LEE, C.B. et al., “Analysis of Fuel Behavior During Rod Ejection Accident in the Korea Standard PWR”, 1997 Int. Top. Mtg. on LWR Fuel Performance, Portland, 1997.
[11] LEE, C.Bet al., “Analysis of High Burnup Fuel Safety Issues”, KAERI/TR-1693/2000, KAERI, 2000.

NON-LOCA TRANSIENTS

(Session 2)

Chairperson

J.M. REY
Spain

FUEL PERFORMANCE UNDER TRANSIENTS, AND ACCIDENT MANAGEMENT USING GENO-FUZZY CONCEPT FOR NUCLEAR REACTORS

M.K. SHAAT, N.G. ABDEL-MOTTALEB, M. NAGUIB ALY, M.E. NAGY
Atomic Energy Authority, Cairo, Egypt
Faculty of Eng., Alexandria University, Alexandria, Egypt

Abstract. Simulation of Pressurized Water Reactor Power Plant (PWR) has been investigated by simulating all components installed in the power plant namely: the reactor core, steam generator, pressurizer, reactor coolant pumps, and turbine. All plant components have been introduced.

This simulator is useful for transient analysis studies, engineering designs, safety analysis, and accident management. Accidents in Pressurized Water Reactor Nuclear Power Plant (PWRNPP) may be occurred either due to component failures or human error during maintenance or operation. The main target of accident management is to mitigate accidents if it occurs.

The Geno-Fuzzy concept is the way to select some important plant state variables as a gene for the overall plant state chromosome. The selected genes are: reactor power, primary coolant pressure, steam generator water level, and onset boiling on clad surface which has direct impact on fuel behavior. Each of these genes has associated fuzzy level. The main objective of Geno-Fuzzy is turning the plant gene from abnormal states to the normal state by associated control variable using the inference wise fuzzy technique.

The Pressurized Water Reactor Nuclear Power Plant simulator has been tested for a typical PWR, for normal transients, Anticipated Transient Without Scram (ATWS), and using the proposed Geno-Fuzzy concept for accident management, which gives very good results in reactor accident mitigation. Some of these tested accidents are; reactor control rod ejection, change in turbine steam load, and loss of coolant flow, which have direct effects on fuel safety and performance. The parameters affecting the behavior of the reactor fuel integrity are analyzed to be considered in future reactor designs.

1. INTRODUCTION

Since Three Mile Island, many changes have increased safety in the nuclear industry. Reactor operators must be trained to handle emergencies, using computer simulator [1].

Licensed NPP operating personnel is responsible for nuclear power plant operation under normal, transient and accident conditions in accordance with instructions and regulations laid down in the operation manual.

The tasks of licensed nuclear power plant operating personnel require extensive skills and knowledge of plant design, operation and NPP accident behavior. To enhance training and qualification of NPP control room personnel different types of NPP simulators are used successfully during initial and retraining since many years [2-3].

The accurate diagnosis of accidents in a nuclear power plant has fundamental importance for decision making necessary to mitigate their consequences for the power plant as well as for the general public, on the basis of emergency planning [4].

Genetic Algorithms [5-7] (GAs) are stochastic optimization algorithms that also require only the value and not the derivative of the objective function to obtain an optimal solution. For this reason, GAs have been applied to nonlinear optimization problems in various fields including, in nuclear engineering, nuclear fuel management optimization [8-9]. The prediction of the severity of nuclear power plant transients [10], and the optimization of process variables of the core decontamination process using a weighted objective function [11].

Since 1965, when Zadeh first introduced the concept of fuzzy sets and linguistic variables, there has been a significant amount of work on theoretical and practical aspects of fuzzy control. Many researchers have exhaustively studied the theoretical issues involved in fuzzy control design such as fuzzification, defuzzification, and inference along with various operators that are used in fuzzy control [12-13].

PC simulators provide self-studies, support the instructors during lessons and can be modified easily if being developed by means of a standard programming language. Low costs and high flexibility in different training courses are main advantages of these systems.

2. MODEL DESCRIPTION

The PWR plant model comprises reactor core, primary coolant system, pressurizer; steam generator and steam dump system as well as important components of the safety and control system [14].

2.1. Core Kinetics Model

The thermal power by fission is calculated directly from the point-kinetics equations with six precursor concentration groups. Reactivity changes due to fuel and moderator temperatures, primary coolant system pressure, and control rod worth are taken into account. The linearized equations are:

$$\frac{d\delta P}{dt} = -\frac{\beta}{\Lambda}\delta P + \sum_i \lambda_i \delta C_i + \frac{\alpha_f P_o}{\Lambda} \sum_{\substack{fuel \\ nodes}} F_{fi}\delta T_{fi} + \frac{\alpha_p P_o}{\Lambda}\delta P_p + \frac{P_o}{\Lambda}\delta\rho_{rod} + \frac{\alpha_c P_o}{\Lambda} \sum_{\substack{coolant \\ nodes}} F_{ci}\delta T_{ci} \quad \text{------(1)}$$

$$\frac{d\delta C_i}{dt} = \frac{\beta_i}{\Lambda}\delta P - \lambda_i \delta C_i \quad \text{------(2)}$$

The fuel rod temperature is calculated to predict the reactivity feedback effect and the average heat flux from the cladding to the reactor coolant. In this model, a single, representative fuel rod is used, and only radial heat conduction is allowed.

The core heat transfer model used a nodal approximation for fuel and coolant temperatures. Each axial section included a fuel temperature node and two coolant temperature nodes. The equations are:

$$\frac{d\delta T_{fi}}{dt} = \frac{Q_{fi}}{(MC_p)_{fi}}\delta P - \left(\frac{UA_f}{MC_p}\right)_{fi}\left(\delta T_{fi} - \delta T_{cli}\right) \quad \text{------(3)}$$

$$\frac{d\delta T_{cli}}{dt} = \left(\frac{UA_f}{MC_p}\right)_{ci}\left(\delta T_{fi} - \delta T_{cli}\right) - \frac{2}{\tau}\left(\delta T_{cli} - \delta T_{cin}\right) \quad \text{------(4)}$$

2.2. Pressurizer Model

To simulate the dynamic behavior of a pressurizer, three kinds of pressurizer models are used.

$$\frac{d\delta T_{c2i}}{dt} = \left(\frac{UA_f}{MC_p}\right)_{ci} \left(\delta T_{fi} - \delta T_{c1i}\right) - \frac{2}{\tau}\left(\delta T_{c2i} - \delta T_{c1i}\right) \text{------(5)}$$

In the models, the control volume is not confined to the pressurizer, but extended to the entire RCS. Both the predicted pressurizer pressure and surge flow rate are adopted as boundary conditions for the RCS thermal-hydraulic model [15].

2.2.1. Normal Pressurizer model

When vapor and liquid phases exist simultaneously in the pressurizer, the conventional nonequilibrium two-region pressurizer model [16] is used.

The mass and energy conservation equations for the vapor region in the pressurizer are

$$\frac{d}{dt}(\rho V)_v = W_{fl} - W_{ro} - \beta W_{sp} - W_{rv} - W_{wc} - W_{cd} \text{-------(6)}$$

and

$$\frac{d}{dt}(\rho h V)_v = W_{fl}h_g - W_{ro}h_f - (\beta W_{sp} + W_{wc} + W_{cd})h_g - W_{rv}h_v + Q_i + V_v\frac{dP}{dt}, \text{------(7)}$$

Where

$$\beta = \frac{(h_f - h_{sp})}{h_{fg}}.$$

The mass and energy conservation equations for the liquid region in the pressurizer are

$$\frac{d}{dt}(\rho V)_l = W_{su} + W_{ro} - W_{fl} + (1+\beta)W_{sp} + W_{wc} + W_{cd} \text{------(8)}$$

and

$$\frac{d}{dt}(\rho h V)_l = W_{su}h_{su} + W_{ro}h_f - W_{fl}h_g + W_{cd}h_g + [(1+\beta)W_{sp} + W_{wc}]h_f - Q_i + Q_H + V_l\frac{dP}{dt}, \text{------(9)}$$

where

$$h_{su} = \begin{cases} h_l & \text{for } W_{su} < 0\ , \\ h_R & \text{for } W_{su} \geq 0\ . \end{cases}$$

The mass and energy conservation equations for the RCS region except for the pressurizer are

$$\frac{d}{dt}(\rho V)_R = -W_{su} - W_{sp} + W_{cont} - W_{break} \text{------(10)}$$

and

$$\frac{d}{dt}(\rho h V)_R = -W_{su}h_{su} - W_{sp}h_{sp} + W_{cont}h_{cont} - W_{break}h_{break} + Q_C - Q_{SG} + V_R\frac{dP}{dt} \text{------(11)}$$

where

$$V_v + V_l = V_{PR}$$

and

$$V_R = V_{RCS} - V_{PRZ}$$

2.2.2. Dry Pressurized Model

When the pressurizer empties, the volume of the RCS filled with steam and that of the pressurizer are considered as one node, and the remaining liquid volume in the RCS is considered as the other. The interface between the two regions is not fixed and is determined from the local properties calculated by the RCS thermal-hydraulic model at the old time step.

2.2.3. Solid Pressurizer Model

In the case of a solid pressurizer, the RCS is divided into two regions: the pressurizer and the RCS volume except the pressurizer.

2.3. RCS Thermal-Hydraulic Model

The RCS thermal-hydraulic model simulates the thermal-hydraulic behavior of the RCS excluding the pressurizer. The coolant loop is divided into four nodes: the hot leg, the primary side of the steam generator, the crossover leg between the steam generator outlet and the RCP, and the cold leg between the RCP and the reactor vessel. The reactor vessel is divided into three nodes: the downcomer and lower plenum, the core and upper plenum, and the upper head. Thus, the two-loop RCS excluding the pressurizer is modeled as 11 nodes. This nodalization is optimized to obtain a real-time simulation. The continuity equations are divided into a mixture continuity equation and a void propagation equation [17].

2.4. RCP Model

The RCS model describes the interaction of RCS fluid with a centrifugal pump. The flow across the pump is assumed to be homogeneous, and that the pump is merely a source of momentum with a zero volume. To obtain the relationship between the volumetric flow rate and the pump speed, the conservation equation of pump angular momentum is solved as follows:

$$I_o\frac{d\Omega}{dt} = T_m - T_h - T_f - T_w \text{------(12)}$$

The terms on the right side of Eq. (12) are motor, hydraulic, friction, and windage torques, respectively. In dimensionless form, the above equation is

$$I_o\Omega_o\frac{d\alpha}{dt} = -T_{ho}\tau(\alpha,\nu) - \sum C_i\alpha^i, \text{------(13)}$$

2.5. Steam Generator Model

The tube side of the U-tube steam generator is modeled with a single node. For simplicity, we assume that the heat transfer coefficient is constant along the tube and that the temperature of the shell side is constant.

The shell side and the pipe form the steam generator outlet to the main steam isolation valve (MSIV) are modeled with a single node. Thermal Equilibrium State is assumed in the node.

2.6. Steam Line Model

This model simulates the dynamics of a steam line. The control volume for this model is the main steam line volume from the MSIVs. The steam flow across the control volume includes two inlet flows from the MSIVs and five outlet flows to the turbine control valve, dump valve, moisture separator and reheater (MSR) valve, steam supply valve of the turbine-driven auxiliary feedwater (AFW) pump, and a normally closed pseudo valve to simulate steam line break accidents. As discussed previously, the conservation equations of mass and energy for the main steam line are solved simultaneously with those for the steam generators.

2.7. Control and Safety System Model

The control system can be represented as a combination of logic, on/off, lag, lead-lag, impulse, and proportional integral and differential units. The following control systems are modeled:

1) Turbine Flow-Control Valve Position Regulator
2) Dump-Flow Valve Actuator
3) Steam Drum Water-Level Regulator
4) Primary Flow/Pump Speed Regulator
5) Control Rod Position Regulator.

3. GENO-FUZZY CONCEPT

In reactor dynamic some variables (Genes) are selected in order to represent the plant state such variables are:

1. Reactor Power
2. Primary System Pressure
3. Existence of Boiling inside Reactor Core
4. Steam Generator Water Level.

The changes in these variables are divided into fuzzy levels, which may be one of the following:

NB: Negative Big
NM: Negative Medium
NS: Negative Small
ZO: Zero
PS: Positive Small
PM: Positive Medium
PB: Positive Big

This change in the variable is considered as the error, and the change in this error is also divided into fuzzy levels, which may be one of these symbols. Each of these variables is corrected using the associated inference rules in the accompanied control variables. Table (I) shows each gene, its fuzzy levels, and its control variable.

TABLE I. CONSIDERED GENES, ITS FUZZY LEVELS, AND ITS CONTROLLED VARIABLES

Gene	Fuzzy Level	Controller Variable
Reactor Power	NB, NS, ZO, PS, PB	Control Rod Reactivity
Primary Sys. Press.	NB, NS, ZO, PS, PB	Spray Flow Rate
Boiling Occurrence	Y, N	Primary Flow Rate
S.G. Water Level	NB, NS, ZO, PS, PB	Feed Water Flow Rate

1) In Case of Change of Gene, and Considering The Change of The Error in The Gene:

Due to the inherent characteristics of negative feed back of both fuel and coolant, and also get benefit from ATWS characteristics. The effort (the fuzzy level of the change in the controlled variable) is due to the error in gene, and also due to the change of the error in this gene. Table (II) shows the lookup table for the reactor power.

TABLE II. LOOKUP TABLE FOR THE REACTOR POWER

CE \ E	NB	NS	ZO	PS	PB
NB	ZO	ZO	ZO	ZO	NS
NS	PS	ZO	ZO	NS	NM
ZO	PB	PS	ZO	NS	NB
PS	PB	PS	ZO	NS	NB
PB	PB	PS	ZO	NS	NB

2) In Case of Change of Gene and Ignoring The Change of Error in The Gene:

In order to accelerate the corrective action in accident strategy, the effort had been decided based on the error only regardless the tendency of the system, which measured from the change of this error.

4. RESULTS AND ANALYSIS

Figure 1 shows the flowchart of the Geno-Fuzzy Controller program, and the results are shown in Figs 2-14 respectively for the first case “Geno-Fuzzy Controller with Change of Error”. While Figs 15-27 show the results for the second case “Geno-Fuzzy Controller without Change of Error”. The initiating event will be control rod withdrawal from normal critical condition to induce positive reactivity insertion by amount of half β (0.0032 $).

4.1. Geno-Fuzzy Controller With Change Of Error

Figure 2 represents the control rod maneuver to renormalized the main parameters of the reactor. The control rod will be inserted due to Geno-Fuzzy Controller signal that will beNegative Big.

Figure 3 shows the change of reactor power, which increased due the initiating event by increment considered Positive Big error. So the Geno-Fuzzy Controller will insert the control rod by Negative Big, then the power will decrease promptly and then smoothly due to negative feed backs of fuel and coolant temperatures.

As shown in Fig. 4 the reactor period decreases to become negative as a result of reactor shutdown. Fig. 5 represents the fuel temperature, which increases when power increases, and it decreases when power decreases. While the average coolant temperature almost constant in the first interval due to decrease in heat removal, then it will increase due to increase in fuel temperature as shown in Fig. 6.

The changes in surge flow rate in and out the reactor coolant Pressurizer according to increase and decrease of the primary coolant system temperatures are shown in Fig. 7. While the primary pressure increases and decreases according to changes in surge flow rate (in and out) as shown in Fig. 8.

Figures 9,10 show the changes in heater capacity and spray mass flow rate to renormalize the change in primary loop pressure. The Geno-Fuzzy Controller will actuate the spray system only because the primary loop pressure increases.

Figure 11 represents the total reactivity changes due to change in primary loop pressure, fuel temperature, reactor coolant temperature, and control rod movement, which will be the dominant parameter.

Figure 12 shows the secondary pressure changes to maintain the steam level constant. While Figure 13 represents the steam generator water level, which increased due to increase in secondary loop pressure.

4.2. Geno-Fuzzy Controller without Change of Error

Figure 14 represents the control rod maneuver to renormalize the main parameters of the reactor. The control rod will move due to Geno-Fuzzy Controller signal regarding to error only, and ignoring the change in error.

Figure 15 shows the change of reactor power, which increased due the initiating event by increment considered Positive Big error. So the Geno-Fuzzy Controller will insert the control rod by Negative Big, then the power will decrease promptly and then smoothly. Then the error will be considered Positive Medium, so the Geno-Fuzzy will insert the control rod by Negative Medium, and the power will decrease promptly and then will increase due to negative feed backs of fuel and coolant temperatures. This increment considered Positive Small error, and then the Geno-Fuzzy Controller will insert the control rod by Negative Small amount. So the power will decrease promptly and then will increase due to negative feed backs again. See Figs 14 and 15.

In Fig. 16 the reactor period increases to become positive or decreases to become negative as a result of reactor power changes. The fuel temperature, which increases when power increases, and it decreases when power decrease is represented in Fig. 17.

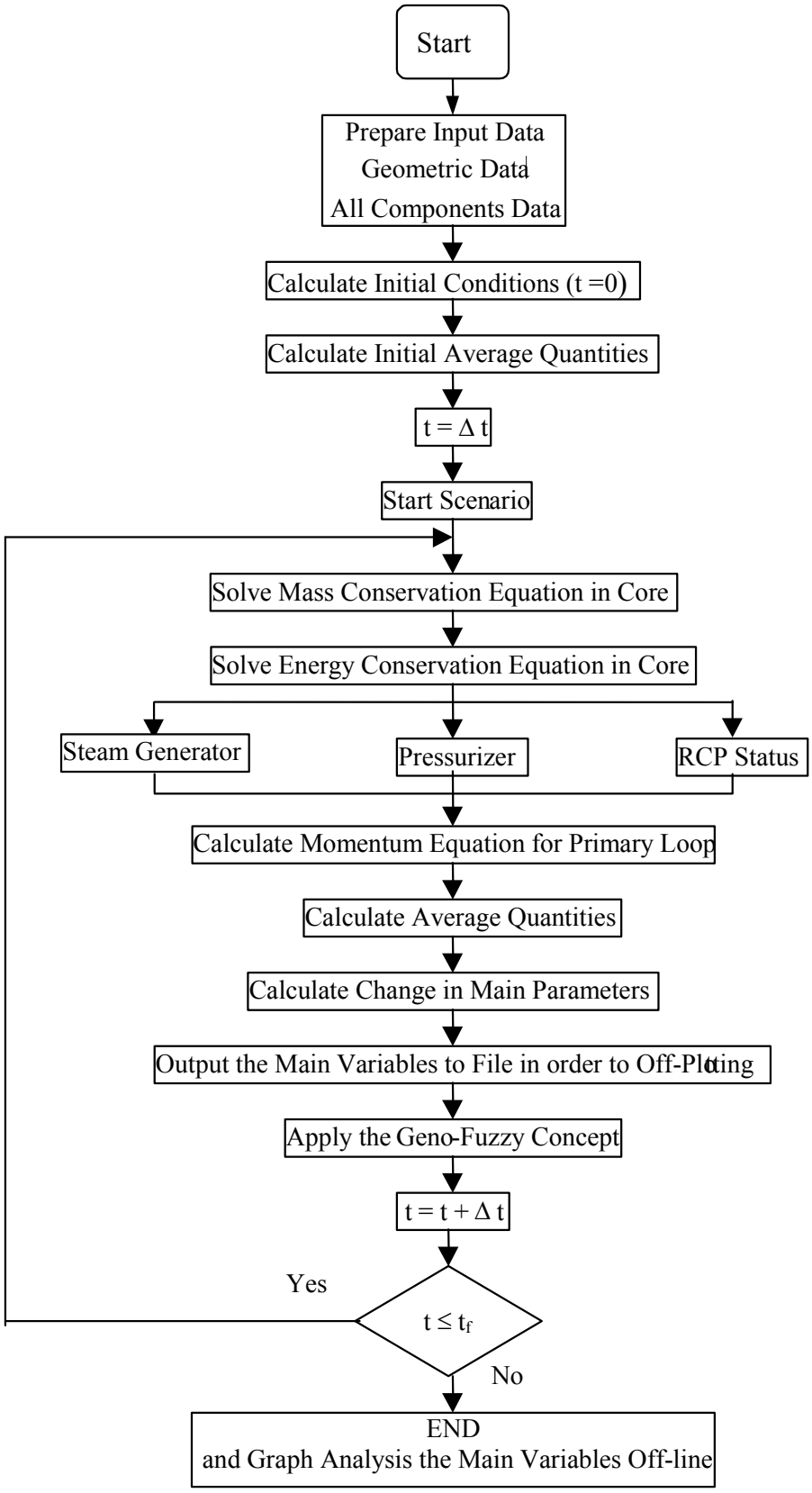

Fig. 1 Flowchart of the Geno-Fuzzy Controller Program

On Fig. 18 the average coolant temperature increased due to increase in fuel temperature, then decreased due to decrease in fuel temperature. There is interval in which the average coolant temperature increased due to decrease in heat removal, and then decreased due to decrease in fuel temperature.

The changes in surge flow rate in and out the reactor coolant pressurizer according to increase and decrease of the primary coolant system temperatures are shown in Fig 19. While the primary pressure increases and decreases according to changes in surge flow rate (in and out) as shown in Fig. 20.

Figs 21 and 22 show the changes in heater capacity and spray mass flow rate to renormalize the change in primary loop pressure. The Geno-Fuzzy Controller will actuate the spray system only because the primary loop pressure increases.

Figure 23 represents the total reactivity changes due to change in primary loop pressure, fuel temperature, reactor coolant temperature, and control rod movement, which will be the dominant parameter.

Figure 24 shows the secondary pressure changes to maintain the steam level constant. While Fig. 25 represents the steam generator water level, which increased due to increase in secondary loop pressure.

The following table contains the conversion of the British units, which used in this work to the SI units.

TABLE III. CONVERSION OF THE BRITISH UNITS TO SI UNITS

Parameter	British unit	SI unit
Heat Capacity	$9.478*10^{-4}$ Btu	1 Watt. sec
Length	3.281 ft	1 m
Mass	2.2046 lb_m	1 Kg
Pressure	14.22 lb_f/in^2	1 Kg/cm^2

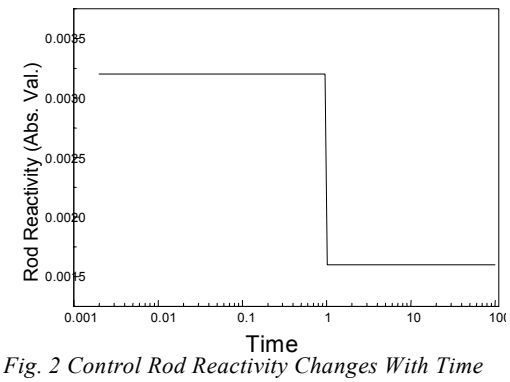

Fig. 2 Control Rod Reactivity Changes With Time With Change in Error

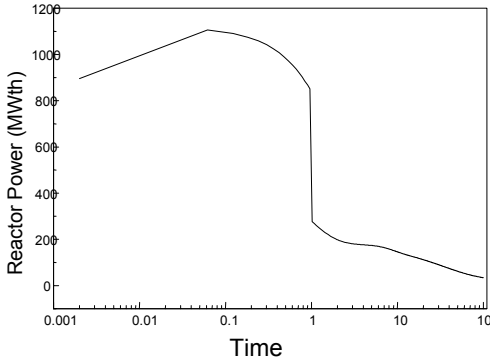

Fig. 3 Reactor Power Changes of Error.With Change With Time

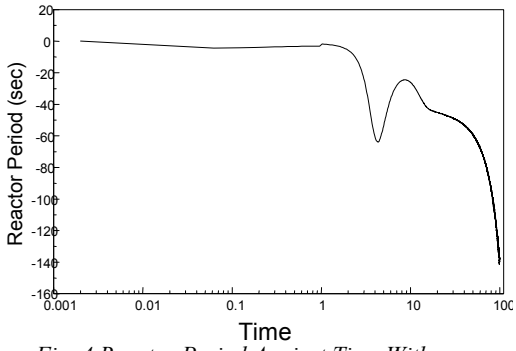

Fig. 4 Reactor Period Against Time With Change In

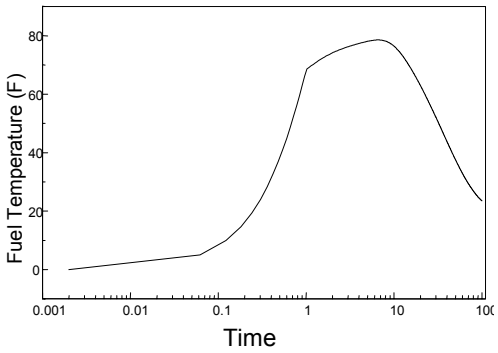

Fig. 5 Fuel Temperature Changes with Time with Change of

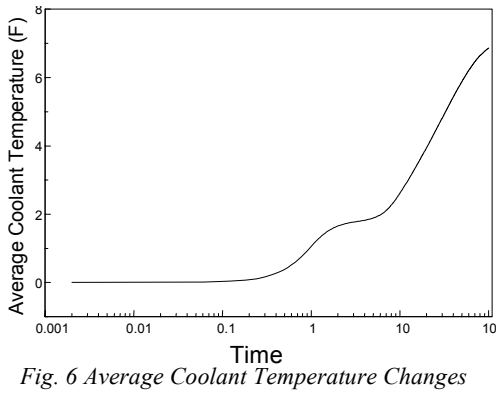

Fig. 6 Average Coolant Temperature Changes with Time with Change In Error.

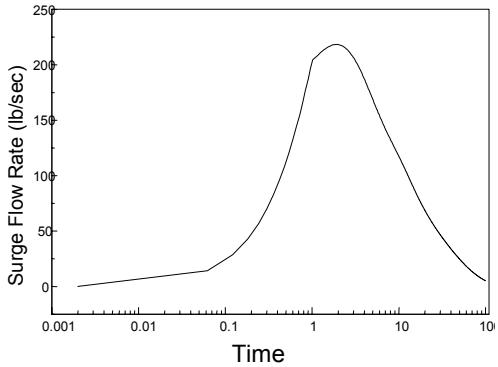

Fig. 7 Changes of Surge Flow Rate with Time with Change in Error

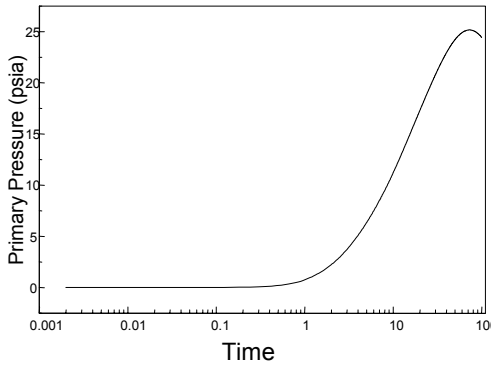

Fig. 8 Primary Pressure Changes with Change In Against Time

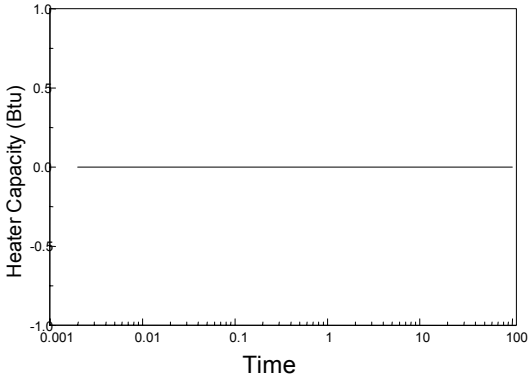

Fig. 9 Heater Capacity Against Time with Change In Error

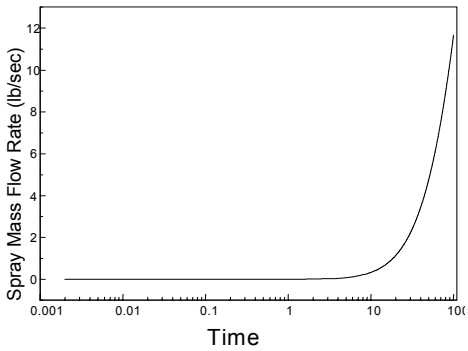

Fig. 10 Spray Mass Flow Rate Against Time With Change in

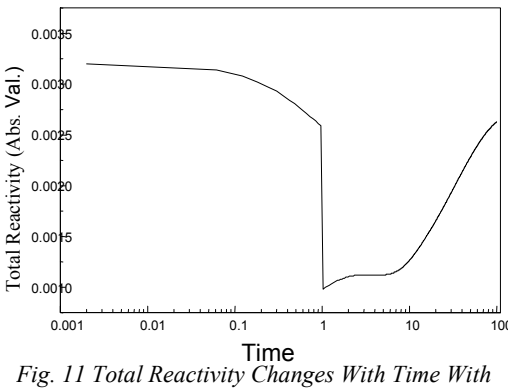

Fig. 11 Total Reactivity Changes With Time With Change In

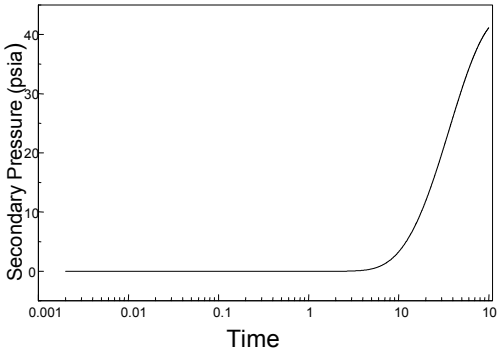

Fig. 12 Secondary Pressure Against Time With Change In Error.

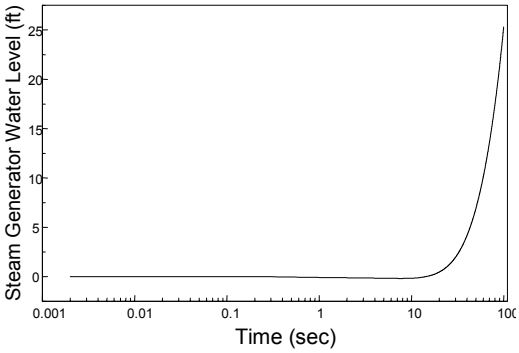

Fig. 13 Steam Generator Water Level Changes With Time with Change In Error.

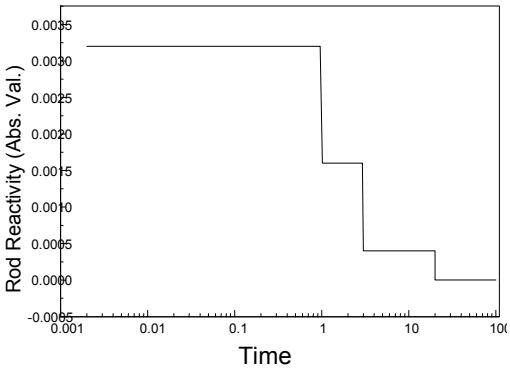

Fig. 14 Control Rod Reactivity Changes With Time Without Change In Error.

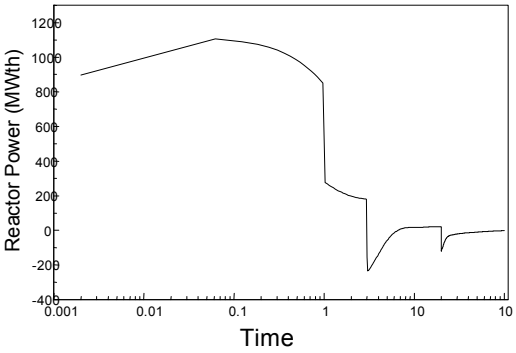

Fig. 15 Reactor Power Changes Against Time Without Change In Error.

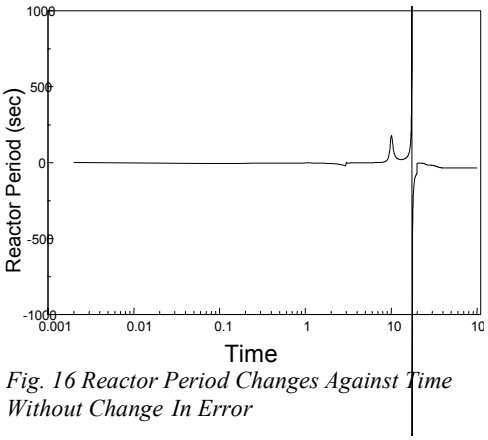

Fig. 16 Reactor Period Changes Against Time Without Change In Error

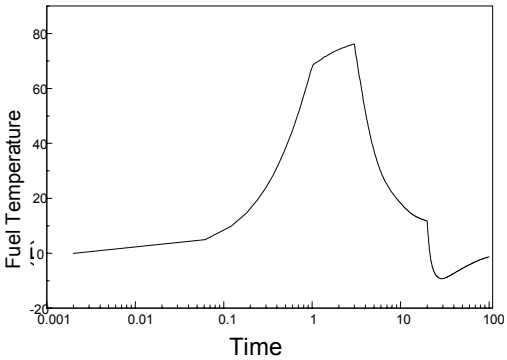

Fig. 17 Fuel Temperature Changes With Time Without Change In Error.

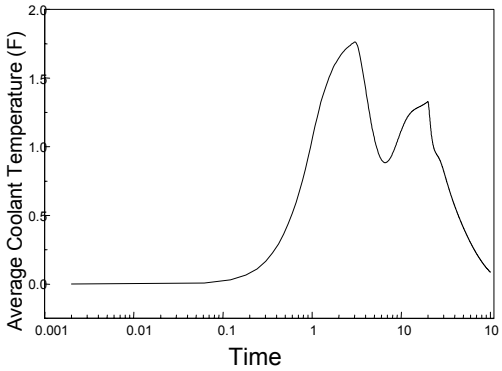

Fig. 18 Average Coolant Temperature Changes Against Time Without Change In Error.

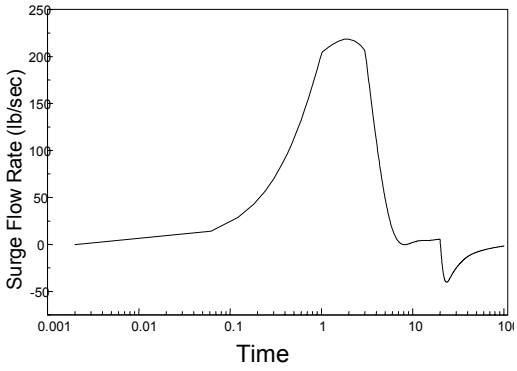

Fig. 19 Surge Flow Rate Changes With Time Without Change In Error.

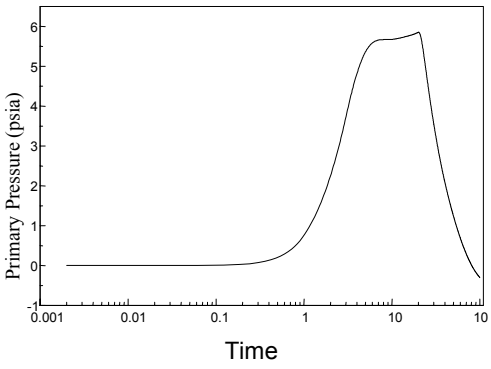

Fig. 20 Primary Pressure Changes With Time Without Change In Error.

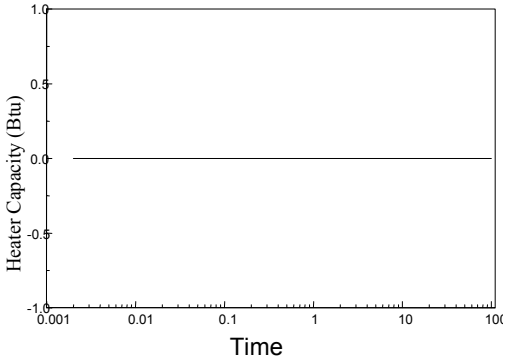

Fig. 21 Heater Capacity Against Time Without Change In Error.

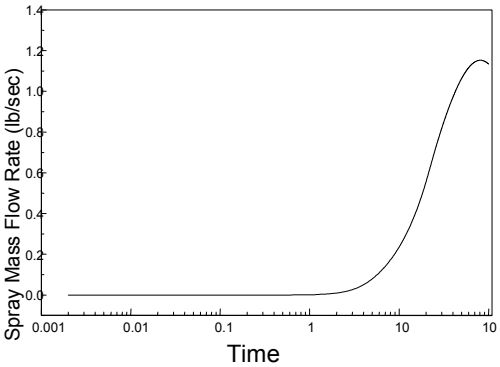

Fig. 22 Spray Mass Flow Rate Changes With Time Without Change

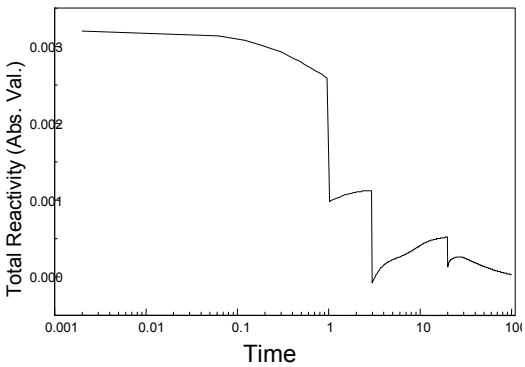

Fig. 23 Total Reactivity Against Time Without Change In Error.

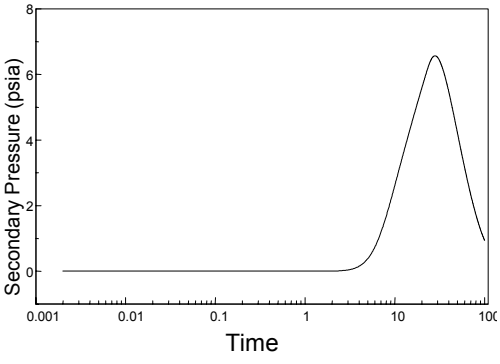

Fig. 24 Secondary Pressure Changes With Time Without Change In Error.

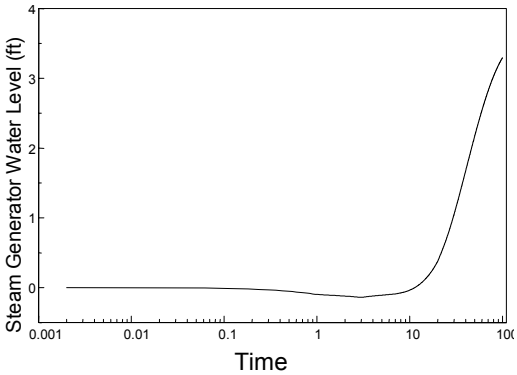

Fig. 25 Steam Generator Water Level Changes With Time Without Change In Error.

5. CONCLUSION

In this work, the nuclear power plant model has been used in order to simulate the normal accidents, which might be occurred due to reactivity transients. In geno-fuzzy model

which take care of reactor power, primary circuit pressure, boiling occurrence, and steam generator water level as a gene, and their fuzzy level as corrective parameters.

Two cases had been studied, the first geno-fuzzy without change of error ignoring the inherent characteristic of reactor elements. The second case with change of error in order to account to the negative feed back of both fuel and coolant, which enhance the safety characteristic of reactor control system.

6. NOMENCLATURE

$\mathbf{A_f}$: heat transfer area
$\mathbf{F_{ci}}$: reactivity importance for temperature changes in the i'th coolant node
$\mathbf{F_{fi}}$: reactivity importance for temperature changes in the i'th fuel node
h : enthalpy or dimensionless pump head
$\mathbf{h_{cont}}$: controlled enthalpy
$\mathbf{h_f}$: saturated liquid enthalpy
$\mathbf{h_g}$: saturated vapor enthalpy
$\mathbf{h_l}$: liquid phase enthalpy
$\mathbf{h_{sp}}$: spray enthalpy
$\mathbf{h_{su}}$: surge enthalpy
$\mathbf{h_v}$: vapor phase enthalpy
$\mathbf{(MC_p)}_{ci}$: total heat capacity of both coolant nodes associated with i'th fuel node
$\mathbf{(MC_p)_{fi}}$: total heat capacity for i'th fuel node
$\mathbf{P_o}$: initial steady-state power level

***Greek**:*
α_c : coolant temperature coefficient of reactivity
α_f : fuel temperature coefficient of reactivity
α_p : coolant pressure coefficient of reactivity
β : total delayed neutron fraction
β_i : delayed neutron fraction for the i'th delayed neutron group
δC_i : deviation of normalized precursor concentration from its steady-state value
δT_{ci} : deviation of coolant temperature in the i'th coolant node from its initial steady-state value

$\mathbf{Q_C}$: core volumetric flow rate
$\mathbf{Q_{fi}}$: fraction of total reactor power generated in fuel node i
$\mathbf{Q_H}$: electric heater heat source
$\mathbf{Q_{SG}}$: steam generator volumetric flow rate
$\mathbf{T_{c1i}}$: average coolant temperature in i'th fuel node
U : overall fuel-to-coolant heat transfer coefficient (includes resistance in fuel as well as film resistance)
V_v : vapor volume
$\mathbf{W_{cd}}$: condensation mass flow rate
$\mathbf{W_{cont}}$: controlled mass flow rate
$\mathbf{W_{fl}}$: flashing mass flow rate
$\mathbf{W_{ro}}$: rainout mass flow rate
$\mathbf{W_{rv}}$: relief valve mass flow rate
$\mathbf{W_{sp}}$: spray mass flow rate
$\mathbf{W_{wc}}$: wall condensation mass flow rate

$\mathbf{\delta T_{cin}}$: deviation in inlet temperature of the first coolant node from its initial steady-state value
$\mathbf{\delta T_{c2i}}$: outlet coolant temperature in i'th fuel node
$\mathbf{\delta T_{fi}}$: deviation of fuel temperature in the i'th fuel node from its initial steady-state value
Λ : neutron generation time
λ_i : delayed neutron decay constant for i'th delayed neutron group
$\rho \mathbf{r}_{rod}$: reactivity due to control rod movement
τ : dimensionless hydraulic torque
Ω : pump speed
Ω_O : rated pump speed

REFERENCES

[1] CUMMINGS, G. E. “Operator/Instrumentation Interactions During the Three Mile Incident”, IEEE Trans. Nuclear Science, NS-27,Vol. 1, (1980).

[2] HETRICK, D. L. "Power-Plant Simulation and Reactor Safety”, Nuclear Safety, Vol. 28, (1987).

[3] GONSALVES, J. B. and PROCTOR, J. E. “Nuclear Plant Simulators: The Past and Present”, Nuclear News, Vol. 30, (1987).

[4] ALVARENGA, M. A. B,. MARTINEZ, A. S. and SCHIRRU, R. “ Adaptive Vector Quantization Optimized By Genetic Algorithm For Real-Time Diagnosis Through Fuzzy Sets” Nuclear Technology, Vol. 120, Dec. (1997).

[5] HOLLAND, J. H. Adaptation in Natural and Artificial Systems, University of Michigan Press (1975).

[6] GOLDBERG,D.E. Genetic Algorithms in Search, Optimization and Machine Language, Addison-Wesley, Massachusetts (1989).

[7] DAVIS, L. ED., VAN NOSTRAND REINHOLD COMPANY, Handbook of Genetic Algorithms, New York (1991).

[8] POON, P. W., "Genetic Algorithms and Fuel Cycle Optimization", Nuclear Engineering, Vol. 31, (1990).

[9] DECHAINE, M. D. and M. A. FELTUS, "Nuclear Fuel Management Optimization Using Genetic Algorithms", Nuclear Technology, Vol. 111, (1995).

[10] LIN, J., BARTAL, Y. and UHRIG, R. E., "Predicting the Severity of Nuclear Power Plant Transients Using Nearest Neighbors Modeling Optimized by Genetic Algorithms on a Parallel Computer", Nuclear Technology, Vol. 111, (1995).

[11] OMORI, SAKAKIBARA, R. Y. and SUZUKI,A. "Optimization of Process Variables for Co-Decontamination Process Using Genetic Algorithms", J. Nucl. Sci. Tech., Vol. 32, (1995).

[12] SUGENO,M. "An Introductory Survey of Fuzzy Control", Information Sciences, Vol. 36, (1985).

[13] MIZUMOTO, M. "Fuzzy Controls Under Various Fuzzy Reasoning Methods", Information Sciences, Vol. 45, (1988).

[14] KERLIN,T. W., KATZ, E. M. and THAKKAR, J.G., and STRANGE, J.E., “Theoretical and Experimental Dynamic Analysis of the H. B. Robinson Nuclear Plant”, Nuclear technology, Vol. 30, Sep. (1976).

[15] JEONG, J. J., Y. OH, DEOG, NO, H.C., CHANG, S.H., CHO, S.J., JUN, H.Y., and LEE, Y.K., “FISA-2/WS, A Compact Real-Time Simulator for Two-Loop Pressurized Water Reactor Plants”, Nuclear Technology, Vol. 90, June (1990).

[16] MCFADDEN, J. F., et al., “RETRAN-02, A Program for Thermal-Hydraulic Analysis of Complex Fluid Flow Systems”, EPRI-NP-1850, CCM, Vol. 1, Electric Power Research Institute (1981).

[17] ZUBER N. and STAUB,. F.W., “The Propagation of the Wave form of the Vapor Volumetric Concentration in Boiling, Forced Convection System Under Oscillatory Conditions”, Int. J. Heat Mass Transfer, Vol. 9, (1966).

COUPLED CODE FRAPTRAN — GENFLO FOR ANALYSING FUEL BEHAVIOUR DURING PWR AND BWR TRANSIENTS AND ACCIDENTS

A. HÄMÄLÄINEN, J.O. STENGÅRD, J. MIETTINEN, R. KYRKI-RAJAMÄKI
VTT Energy, Finland

K. VALTONEN
Radiation and Nuclear Safety Authority, Helsinki, Finland

Abstract. Demands for reactor safety assessments and for the tools to make these are continuously growing. Apart from the general request for better accuracy and application of best-estimate type calculations, several concrete developments work to the same end. It may become necessary to consider new events, like Anticipated Transients Without a Scram (ATWS), in the basic licensing calculations. Also continuing is the quest for better fuel economy that is bringing around higher discharge burnups and increasingly complicated structural and neutronic solutions. Conventionally, the description of thermal hydraulics is kept simple in fuel transient behaviour codes. Attempts to combine proper models for the two have been made with varying success. Even in the best of the cases so far the result has been a gigantic assembly of codes the use of which has been limited by computing capacity at least until a few years ago. At VTT Energy in Finland, an effort was initiated to link a proven, fast running general thermal hydraulics module, developed in-house and known as GENFLO, with the U.S. Nuclear Regulatory Commission's (USNRC) renovated version of the FRAPTRAN fuel transient code. Preliminary results of the work are now available. In the paper, the codes and the main principles of the coupling are described. The first fuel rod calculation cases performed with the coupled code include a large break Loss-of-Coolant Accident (LBLOCA) in a VVER-440 power plant and an instability incident in a Boiling Water Reactor (BWR). Separately calculated system behaviour analyses were available for the two scenarios. Low and high burnup figures for the fuel were considered. Some results of these calculations are given to demonstrate the performance of the coupled code.

1. INTRODUCTION

Plans to include e.g. ATWS events into design basis accidents, demand of higher fuel discharge burnups as well as more and more complicated new fuel designs set new requirements for calculation models used in safety analyses. There have been attempts to meet these with approaches from two directions: by improving the fuel models of the reactor dynamics codes, and by introducing updated high-burnup models and more advanced thermal hydraulic models in fuel behaviour codes. To the latter belongs the effort to couple the general thermal hydraulic model GENFLO with the USNRC's FRAPTRAN code [1].

For fuel behaviour analyses, there are two assemblies of calculation tools available in Finland. One is based on the British ENIGMA steady state code and the transient code SCANAIR due to IPSN of France. The other combination relies on the USNRC fuel codes FRAPCON-3 and FRAPTRAN, for steady states and accidents, respectively. The steady state codes in the two can be used separately or to provide a burnup-dependent initial state for a transient analysis. The two calculation chains are intended to be in parallel use, the USNRC codes mainly for independent assessments serving the licensing office STUK. Common to all these codes is the simplicity of the thermal hydraulic description of the rod-to-coolant heat transfer. While not untypical, this restricts the spectrum of events that can be analysed. Customary way is to use passive links from so-called hot channel analyses with system codes. This, however, is too often seen to lead to numerical instabilities and physically unrealistic results in cases featuring

but the least complicated power-cooling conditions. The combination of the thermal hydraulic model GENFLO and FRAPTRAN is to offer an improvement to this unsatisfactory situation.

The GENFLO module, developed at VTT, is a fast-running five-equation model, in which models for the wetted wall heat transfer, dryout, post-dryout heat transfer and quenching are included. In the case of overheated core, also the cladding oxidation is modelled. At present the code has three totally different applications.

The system behaviour and boundary conditions needed for the fuel rod behaviour in FRAPTRAN-GENFLO analyses may be calculated with available system codes. In the coupled code, GENFLO calculates the thermal hydraulic parameters of which local fluid temperatures and heat transfer coefficients are provided for FRAPTRAN. FRAPTRAN routines are then used to yield the temperatures of the fuel rod, and the deformation of fuel pellets and cladding including potential ballooning. The parallel way the coupling has been made offers flexibility in changing the necessary data between the codes although the solution methods of the codes differ significantly.

The first power plant application of the coupled code was a case of a LBLOCA in the Loviisa VVER-440 plant. The system behaviour was calculated with the Finnish engineering simulator APROS. The second case studied an actual instability incident in a BWR reactor. There the system behaviour was calculated with the three-dimensional neutronics code TRAB-3D. The real event was extended by assuming a hypothetical failure of SCRAM leading to continued oscillations. The fuel rod in the latter was assumed to be one with a high burnup.

2. FRAPTRAN-GENFLO PAIR

The system behaviour and boundary conditions needed for detailed core simulation and studying the fuel rod behaviour with FRAPTRAN-GENFLO may be calculated with various system codes. At VTT this can be accomplished with RELAP5, the three-dimensional BWR or PWR reactor dynamics codes TRAB-3D or HEXTRAN, the fast-running small break LOCA and ATWS analysis model SMABRE, or the simulator APROS. The calculation system is introduced in Fig. 1. At present, the boundary conditions for the hydraulic model from the system code are the mass flow and enthalpy at the channel inlet, the pressure at the top of the channel, and the total power and power profile of the fuel rod.

The coolant mass, momentum and energy conservation equations are solved in GENFLO, including the calculation of the axial distributions of the fluid temperature and the void fraction. As a result, the fluid temperatures and heat transfer coefficients for each axial level at each time step are supplied for FRAPTRAN. The initial burnup, the temperatures in fuel rod, and the deformation of fuel pellets and cladding, including possible ballooning, are calculated in FRAPTRAN with burnup dependent models. Currently in GENFLO and FRAPTRAN, separate built-in models for the calculation of fuel and cladding temperatures, including cladding oxidation and hydrogen generation, are utilised. Nevertheless, FRAPTRAN supplies the local gas gap heat transfer coefficient for GENFLO. The axial power profile to FRAPTRAN and GENFLO comes from the system code. The axial mesh division of the fuel rods is the same in GENFLO and FRAPTRAN. In the future, models now performing in parallel will be unified so as to make tight code.

In the coupled code, FRAPTRAN is the master code calling GENFLO that will in turn provide the hydraulic conditions for the whole channel. This calculation is made only once for each time step, even if a number of iterations would be done in FRAPTRAN during the time step. In the beginning, there is a need from GENFLO for a steady state calculation before any coupled code calculation. In the coupled code calculation, the FRAPTRAN code dictates the length of the time step. A typical time step is short, 0.01 to 0.05 seconds. Even with such short steps, the actual FRAPTRAN-GENFLO calculation is not time-consuming thanks to the said non-iterative feature and effective numerical methods of the fast running hydraulics module.

The validation of the thermal hydraulic model GENFLO has been done elsewhere as a part of other codes. The verification and validation of the code pair FRAPTRAN-GENFLO is in progress.

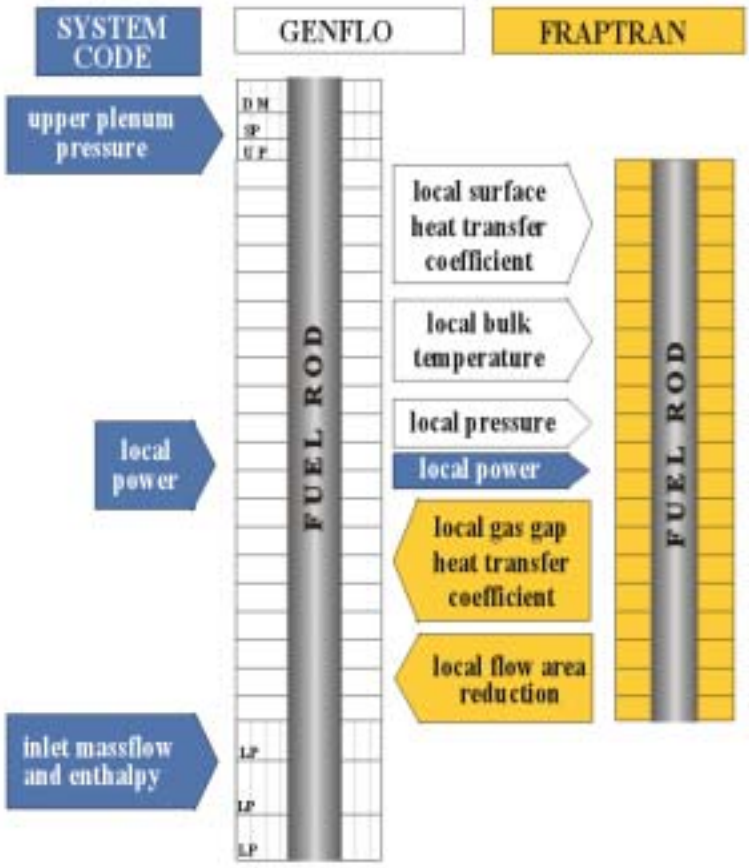

Fig. 1. Data change between system code, GENFLO and FRAPTRAN.

2.1. GENFLO code

At present, the GENFLO code is being used in three different applications. In a code called RECRIT, the model is coupled with the 2-D transient neutronics model TWODIN for calculating re-criticality accidents in a BWR plant. Then the whole BWR vessel is modelled for GENFLO. In APROS-SA application, the model is used to calculate the PWR pressure vessel thermal hydraulics during a severe accident until the core melting and relocation and pool generation at the bottom of the reactor vessel is simulated. And finally, in the current FRAPTRAN application the model is coupled with a transient fuel behaviour code to study complex fuel transients whereby special attention is given to realistic description of the thermal hydraulics in the sub-channel.

The thermal hydraulics solution principles of GENFLO are based on the models developed for the SMABRE [2] and RECRIT [3] codes. GENFLO is as a fast running, non-iterative, five-equation model, in which the wetted wall heat transfer, dryout, post-dryout heat transfer and quenching models are included. The main heat transfer and flow regimes of the code are depicted in Fig. 2.

The geometry described by GENFLO comprises one or several parallel fluid flow channels and optionally a related fuel structure. The lower and upper plena are always included but the core bypass and the downcomer may also be zeroed, as is done in the subchannel applications.

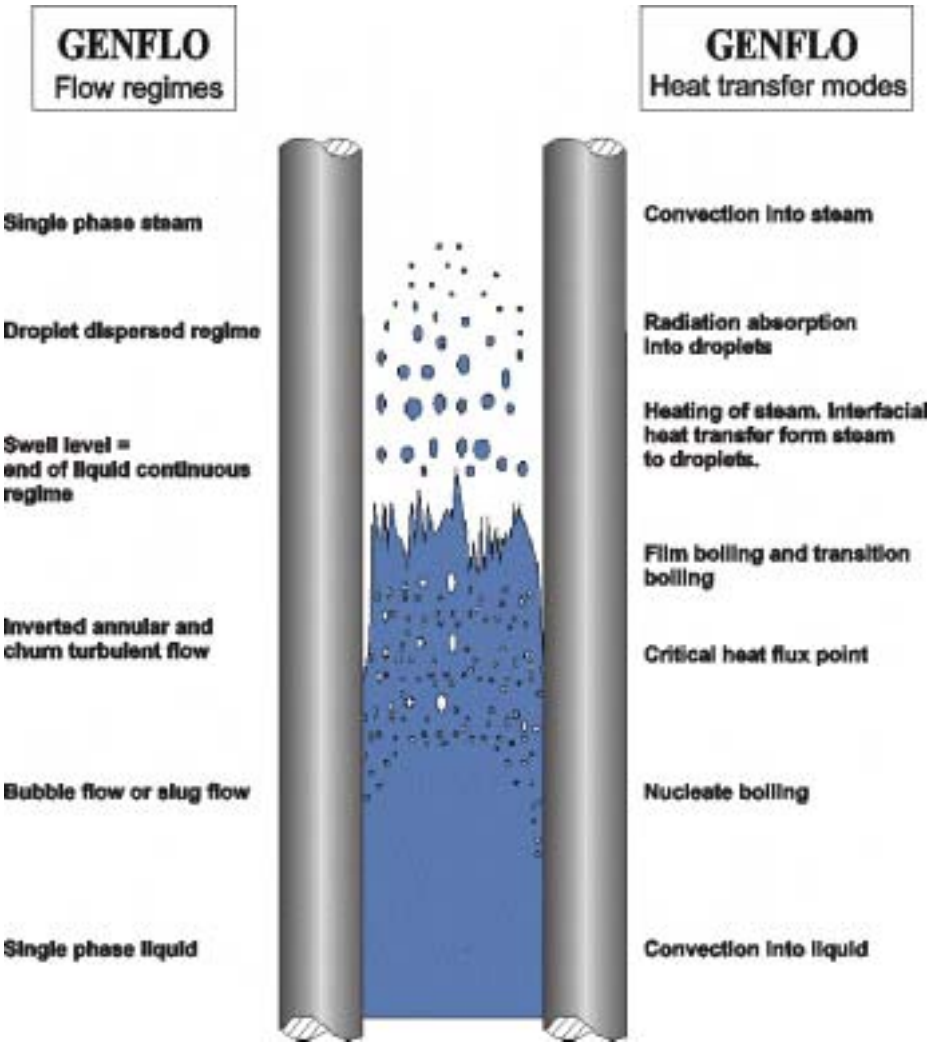

Fig. 2. Heat transfer and flow regimes in the GENFLO code.

At the top of a subchannel, the pressure is used as a boundary condition. The pressure is controlled by frictional leak from the top. The outside pressure of the leak follows the system pressure calculated by the system code. The pressure difference at the leak is 10 % of channel pressure.

The total mass flow and enthalpy are used for the boundary conditions at the channel inlet. The separate mass flows of vapour and water and the enthalpies are then calculated in GENFLO according to conservation of energy at the inlet. This calculation is needed when the enthalpy of the inlet flow exceeds the saturation enthalpy. Two assumptions are made for this

calculation. Firstly, the water inflow is either sub-cooled or saturated, and secondly, only outflow of water is allowed from the bottom.

Because the thermal hydraulic solution of GENFLO has been included in the RECRIT code, the validation of RECRIT also supports the GENFLO thermal hydraulics. RECRIT has been used for analysing recriticality incidents of BWRs in conditions, where the control rods have been melted at high temperatures, but after that the core cooling has been recovered. The validation cases for the RECRIT code includes ERSEC, ACHILLES, REWET-II, GÖTA, FLECHT and QUENCH experiments.

2.2. FRAPTRAN code

FRAPTRAN is an updated and improved version of the earlier FRAP-T family of codes, developed for prediction of LWR fuel rods performance during operational transients and hypothetical accidents. The phenomena modelled in FRAPTRAN include heat conduction within the fuel rod, heat transfer from cladding to coolant, elastic-plastic fuel and cladding deformation including cladding ballooning, cladding oxidation, fission gas release and fuel rod gas pressure. Burnup dependent parameters may be initialized with the FRAPCON-3 steady state code, which generates a link file for this purpose. In FRAPTRAN, MATPRO material properties package is used as is done with other NRC fuel codes. Some of the models have recently modified to reflect changes due to high burnup. The FRAPTRAN version used in the current work and calculations is Ver 1.4 (January 2000).

Dimensions of fuel rod components and coolant channel are needed as input, as well as information on rod materials and fabrication parameters, and a definition of the transient to be analysed. Essential data on the transient are 1) the average fuel rod power history, axial and radial power distributions in the rod and 2) the fuel rod boundary conditions including system pressure.

The thermal hydraulic boundary conditions can in simple cases be given in the normal input file, but more detailed conditions need an external file in a specified format. FRAPTRAN has no specific model for calculation of heat transfer from cladding to coolant during unstable or rapidly changing coolant flow conditions, which may occur during a LOCA transient. Depending on the type of the transient there is a possibility to employ thermal hydraulic functions of slowly changing non-reversal flow or to use pre-determined boundary conditions. The major disadvantage of using a pre-calculation with a thermal hydraulic code is the lack of feedback. Also differences in the fuel rod modelling between the thermal hydraulic code and FRAPTRAN may cause instabilities or physically non-realistic conditions.

The GENFLO model is thought to become to complement the selection of transient heat transfer models. Although the model has been tested in different surroundings, the coupled FRAPTRAN-GENFLO code will need some verification against the existing FRAPTRAN models. The first one mentioned above, the coolant enthalpy model, was considered able to give the best possibility for a comparison with results not strongly dependent on the properties of an external thermal hydraulic code. The raw transient data has to be slightly modified by filtering in order to avoid possible instantaneous coolant reverse flow, which could not be handled by the coolant enthalpy model. Hence, the comparison case is possibly not completely realistic in all details, but it is a test and an indication of the capabilities of the models and also serves as a tool for revealing deficiencies or necessary improvements in the models.

3. EXAMPLE 1: LOVIISA LBLOCA

There are results of LBLOCA analyses available for the Loviisa power plant that have been made by Fortum with the engineering simulator APROS. The thermal hydraulic boundary conditions, as well as geometry and safety factors used in hot channel analyses of LBLOCA that were applied in APROS calculations have been used for FRAPTRAN-GENFLO by averaging them for one subchannel. The safety factors of the hot rod account for the effects from linear power, enthalpy rise and position of hot rod inside the assembly. Initiating event in the transient is the double-ended break between the pressure vessel and the reactor coolant pump in one of the six cold legs. The LOCA transient is considered to occur when the fuel has no significant burnup.

In the transient the fuel rod temperatures increase in nearly dry core until injection from the emergency core cooling system quenches the core. Besides the high and low pressure safety injection, as simulated in the APROS calculation, two hydro accumulators start an injection to the downcomer. The other two accumulators, injecting to the upper plenum, are not operating in this transient.

3.1. Results of example 1

A reactor trip immediately follows the break. Due to the large break flow, pressure decreases quickly and the core is uncovered. In this situation, the small flow to the core is voided and is occasionally reversed. The real physical oscillation of inlet flow is difficult to separate from the numerical one seen in the APROS results. To eliminate the fastest numerical frequencies, the figures of core inlet mass flow and enthalpy have been filtered. The effects of filtering are seen in differences in the inlet liquid mass flow in Fig. 3 between the GENFLO and APROS curves. Another reason for using filtering was the decision to calculate the same transient also with the standard FRAPTRAN, which does not accept reversed flow.

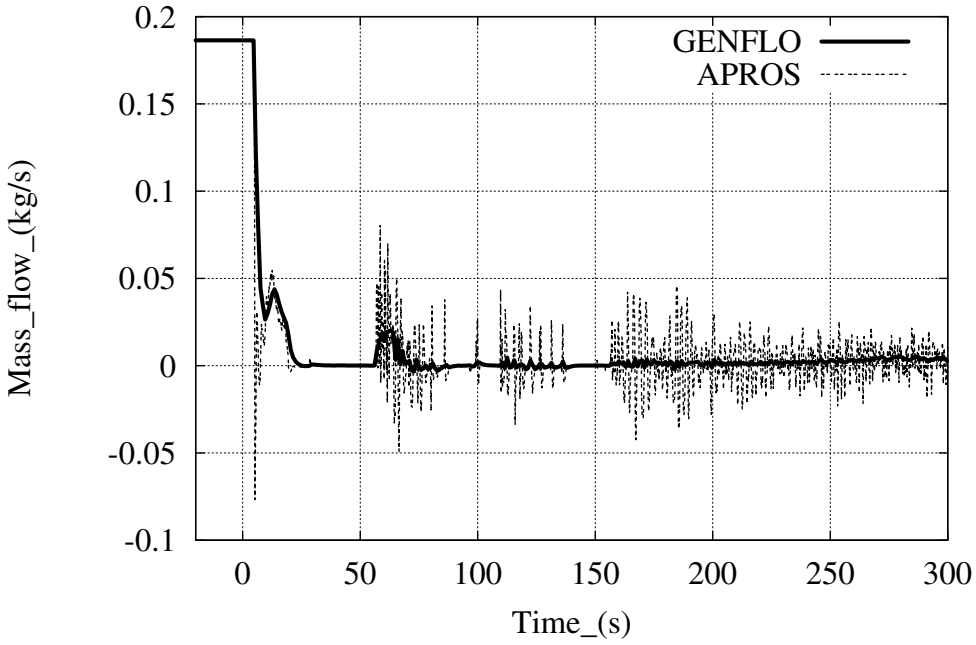

Fig. 3. Inlet liquid flow at bottom of channel

At the beginning of the transient, the fuel temperature drops according to the power decrease, shown in Fig. 4. Later, due to the loss of coolant inventory the fuel temperature starts increasing. The coupled code suggests that even a small amount of water in the channel inlet after 60 s is sufficient to stop the temperature increase, and then decrease the temperature temporarily.

Ninety seconds later the average void fraction is at its maximum with the water level at its minimum. The fuel temperatures increase, and the quenching front of the hydraulic channel drops until 200 sec after which the quenching front starts to rise again. At the time of maximum temperature, there is a quite sharp transition from one flow regime to another.

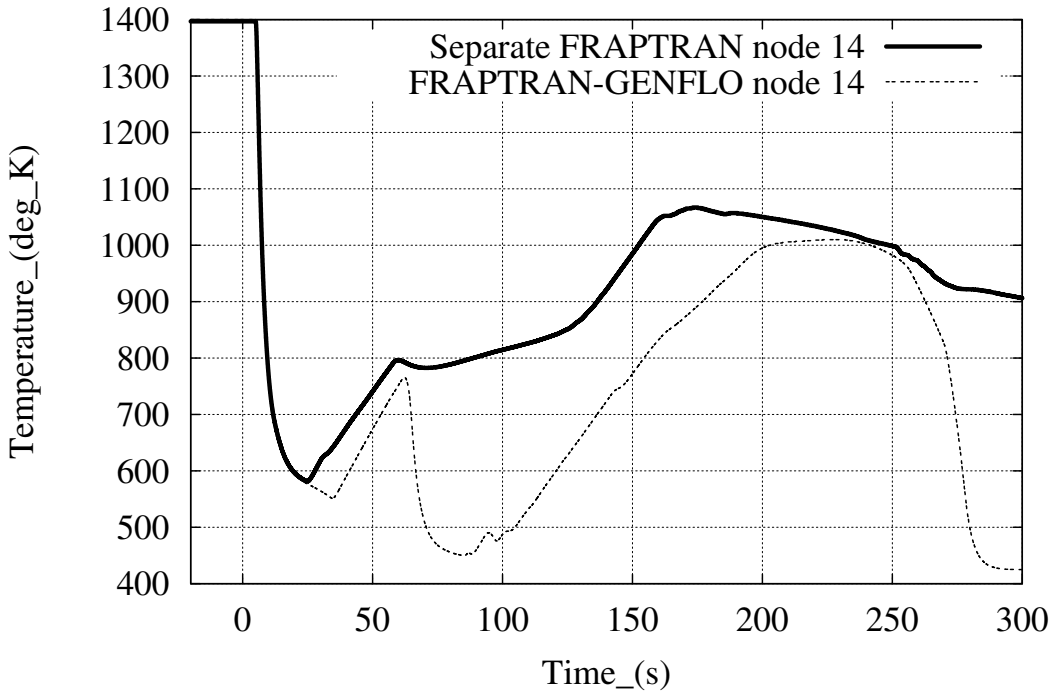

Fig. 4. Fuel centre temperature at level 14

In the separate FRAPTRAN calculation, enthalpy of the inlet flow may be unrealistic at the time of flow reversal, but basically the FRAPTRAN-GENFLO and FRAPTRAN cases described here, are the same.

The results with the separate FRAPTRAN and with FRAPTRAN-GENFLO are almost identical until the steam supply starts. The bulk temperature significantly increases due to high enthalpy values in the separate FRAPTRAN calculations. There are also corresponding differences in the heat transfer coefficients, rod temperatures and cladding deformation. Used separately, FRAPTRAN predicts that the clad starts ballooning at the time of the highest cladding temperatures. The internal pressure of the rod is seen to undergo rapid changes and then equals the channel pressure when the rod has failed (Fig. 5), whilst in the coupled code calculation rod failure does not occur.

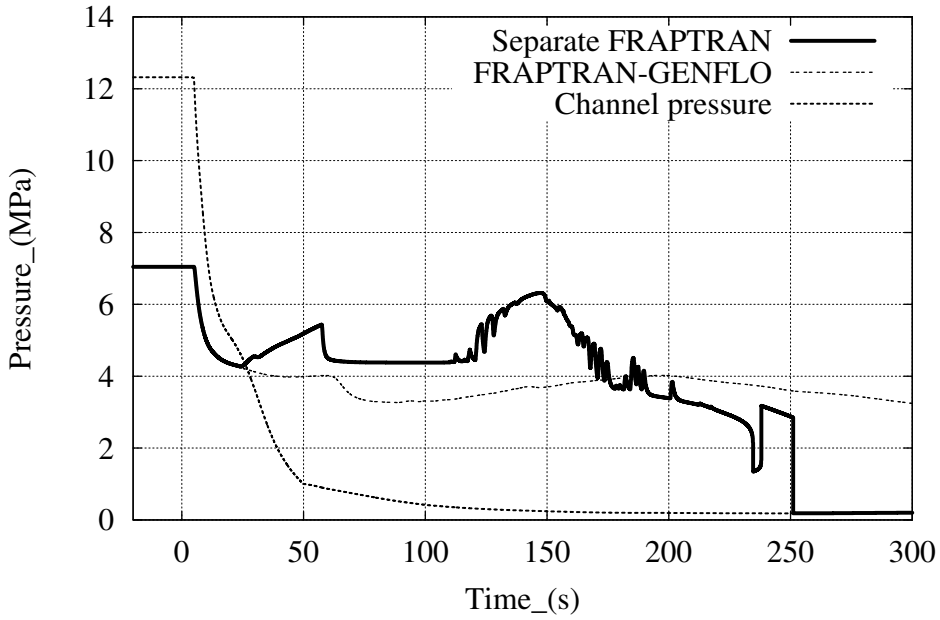

Fig. 5. Channel pressure and plenum gas pressure

4. EXAMPLE 2: BWR INSTABILITY

The second example is the instability transient during an ATWS in a BWR plant. The basis for the analysis was a real oscillation incident in a BWR reactor during the reactor startup procedure. The incident was safely terminated by normal operation of the reactor safety systems.

The incident was successfully simulated with the Finnish TRAB-3D showing good agreement with the real measurements [4]. TRAB-3D [5] is the latest member of the code system developed by VTT Energy for LWR reactor dynamics calculations. The code is used for three-dimensional calculations in rectangular geometry in the core. This instability transient has earlier been analyzed by STUK in Ref. [6]

The results of the TRAB-3D calculation agree with measurements (Fig. 6) and earlier analyses [6]. The oscillation frequency and the phase shift between the inlet and outlet flows in a channel of high relative power show good consistency. So do the out-of-phase oscillation of mass flows between high power channels and the core by-pass channel.

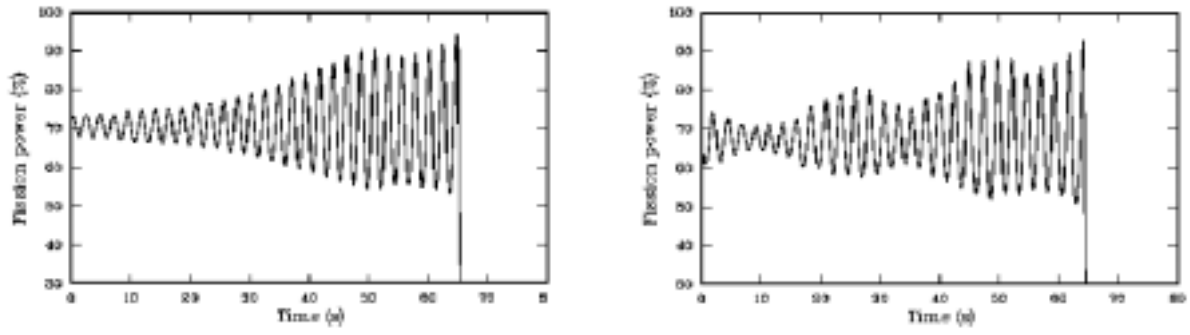

Fig. 6. TRAB-3D calculation and measurements in a BWR instability case.

To test the performance of the new model combination, the case was also hypothetically extended assuming no actions of safety system. The transient was recalculated with TRAB-3D as an ATWS case. The escalating oscillation phase of this calculation was chosen a subject of further studies in this FRAPTRAN-GENFLO analysis. The oscillations of boundary conditions were artificially continued in time and amplified. The total power in the hot assembly calculations with TRAB was multiplied by a factor of 1.3 for the hot rod analysis with FRAPTRAN-GENFLO. Also, the oscillating power was given a minimum value. Fig. 7 shows the boundary conditions of the average linear power and the core inlet mass flow. The flow rate oscillation finally leads to temporary flow reversals.

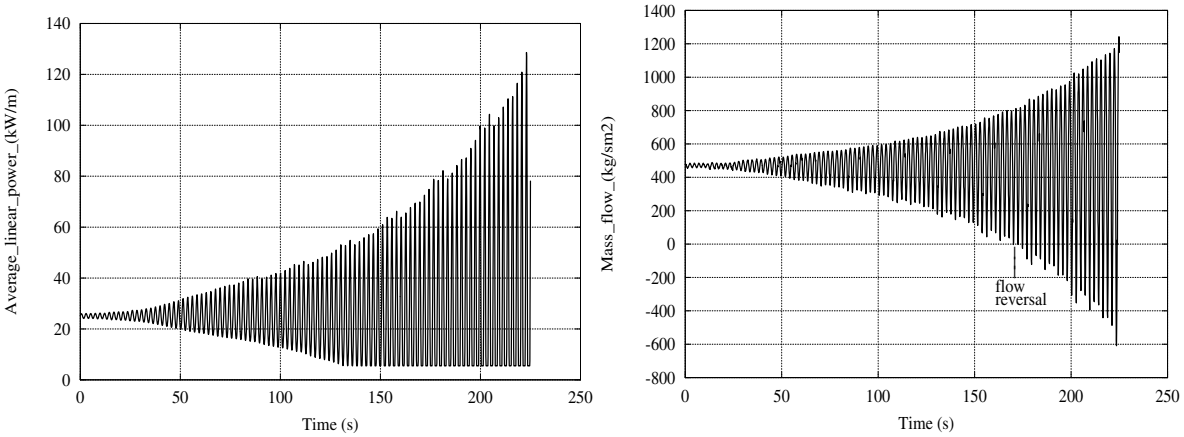

Fig. 7. Average linear power and mass flow rate boundary condition at core inlet in hypothetical BWR instability case

A continuously changing axial power profile was created to match the TRAB-3D calculations. The axial power profile was dynamically changed in GENFLO. For FRAPTRAN, an average profile was used. Contrary to the original TRAB-3D calculation, high burnup fuel was now assumed with a maximum set at 62.3 MWd/kgU. The frequencies of oscillations of boundary conditions were according to the TRAB-3D calculations.

4.1. Results of example 2

The results of the instability case of a BWR, show that the cycle length, about 2 seconds, is small enough to keep the fuel rod covered with water until the time of flow reversal. Then the quenching front starts dropping in the channel. Before the flow reversal, only local or temporary dryout or DNB conditions may be achieved. This will soon lead to high cladding temperatures at the upper part of the fuel rod (1 682 K). On the other hand, the highest fuel temperatures occur at the lower part of the rod (2 729 K), where the linear power is higher. The temperature profiles are shown in Figs 8 and 9. At the end of the calculation the cladding is quite soft and in contact with the fuel pellet (PCMI, pellet-to-cladding interaction). The plenum pressure remains below the fluid channel pressure during the whole transient, and no rod failure is predicted in spite of the fast deformation of the fuel rod (Fig. 10).

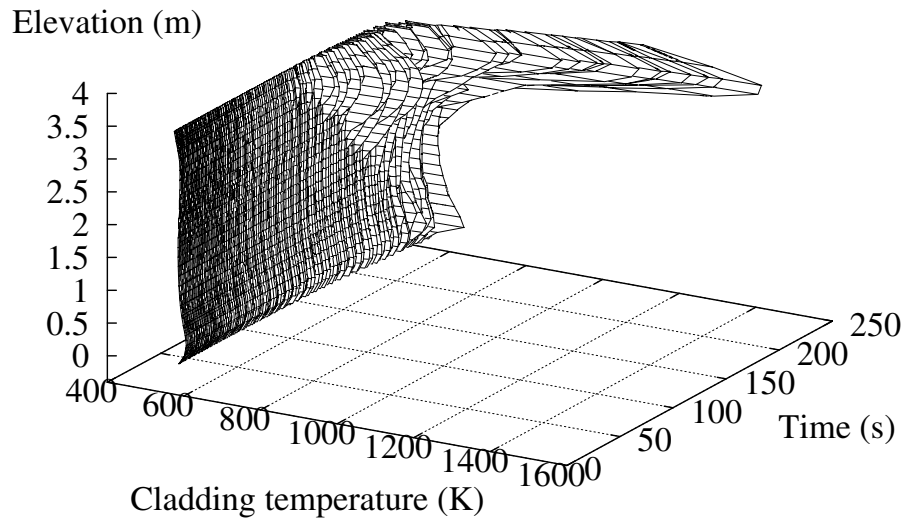

Fig. 8. Cladding surface temperature profile in hypothetical BWR instability case

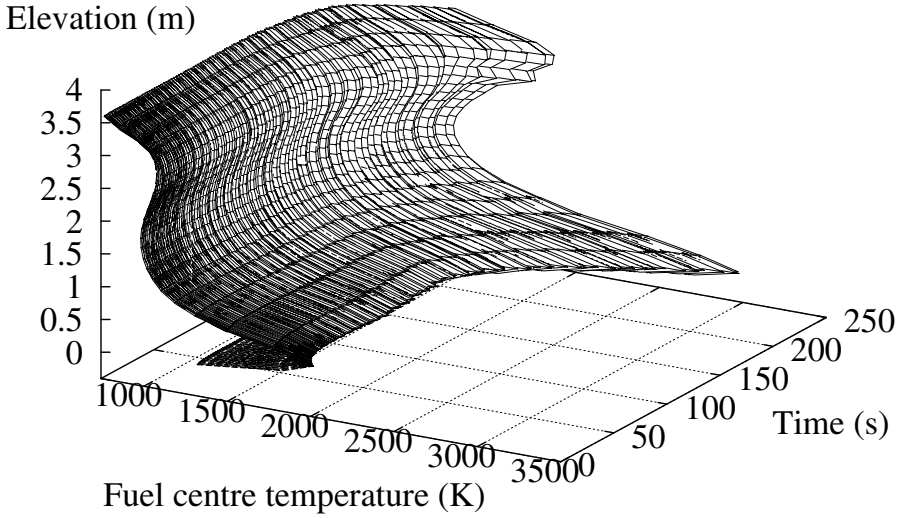

Fig. 9. Fuel centre temperature profile in hypothetical BWR instability case

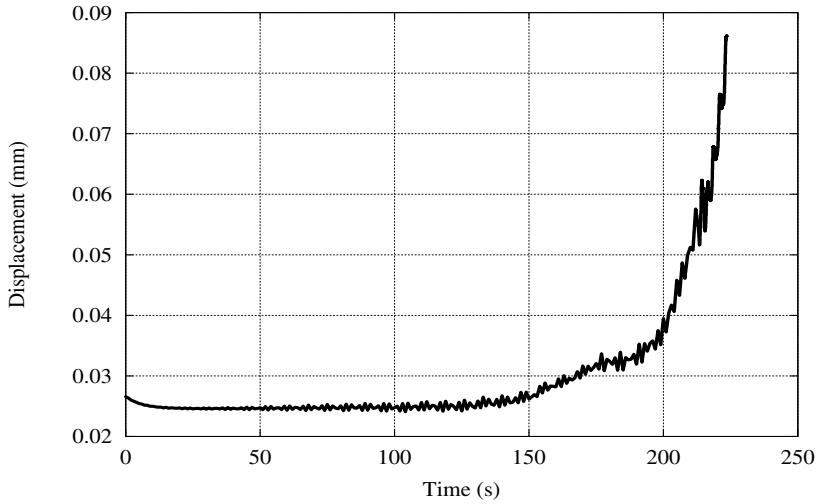

Fig. 10. Displacement of cladding outer surface in BWR instability case

FRAPTRAN-GENFLO has shown to be a proper tool for studying oscillation phenomena in a single subchannel, although continuation of the oscillation in real geometry may become totally different from the ones here that were artificially continued and amplified. Also the critical heat flux correlations of GENFLO need to be studied further.

5. DISCUSSION

The coupling of these two codes, FRAPTRAN and GENFLO, demonstrates a right direction to proceed with more detailed thermal hydraulic description in fuel transient analyses. However, improvements to both codes are being planned.

In order to benefit from more detailed thermal hydraulics, the FRAPTRAN code should take advantage of accepting dynamic axial power and pressure profiles. Also, an increasing number of the system code calculations are now providing dynamic power profiles from 1 and 3-dimensional neutronics calculations in the core.

Some features, already possible in GENFLO, are not enabled in the FRAPTRAN-GENFLO application. Such are the flexible hydraulic channel geometry in GENFLO due to ballooning and a possibility to use more than one subchannel in a single run. The several channels with different flow areas could describe the different positions of the rod in the assembly. Further, some GENFLO models, like DNB and CPR correlations suitable for a single hot rod, and especially suitable for BWR instability cases, need additional attention. At present in GENFLO, one has to rely on its material properties. For consistency, the same material properties, valid up to high burnups, should be used in the two codes.

Up to now the GENFLO still includes all the parts for the hydraulics in the pressure vessel, and the validation cases of RECRIT could also be calculated with GENFLO. The validation against QUENCH experiments is going on. Validation of the coupled code is needed against experimental high burnup fuel data.

6. CONCLUSIONS

A thermal hydraulic subchannel model GENFLO (=GENeral FLOw) has been developed at VTT and now coupled with the USNRC fuel transient code FRAPTRAN. The calculation of the example cases, Loviisa Large Break LOCA and a BWR instability case, with the coupled code has shown that GENFLO can be successfully used as a new hydraulic model of the FRAPTRAN code. Due to the non-iterative solution techniques and advanced numerical methods applied in GENFLO, the combined code preserves high performance with short running times.

The parallel coupling of the codes enables the evaluation and studying of the improvements and changes necessary in the FRAPTRAN and GENFLO codes step by step, and further features may be inserted easily. Several improvements for both codes have been introduced.

In the example case 1, no cladding ballooning was predicted with the coupled code. The separate FRAPTRAN calculation would suggest ballooning, cladding deformation and rod failure with these partly unrealistic boundary conditions. Calculation of the example case 2, the instability case of a BWR, shows that with small cycle time the channel is wetted and no sudden rod failures occur until flow reversal. Gas gap is expected to be closed at the end of

calculation. Definitive analyses would need more carefully studied input and boundary conditions for both cases.

The results of this first version of the coupled code are most encouraging and well warrant further development followed by careful validation against experimental data.

ACKNOWLEDGEMENT

This work has been done within the Finnish Research Programme on Nuclear Power Plant Safety (FINNUS, 1999-2002). The part of work described above, the coupling of the codes and the calculation of the example cases have been financed by the Radiation and Nuclear Safety Authority of Finland (STUK). The project would not have been possible without the USNRC providing the recent versions of the FRAPTRAN code. Our thanks go to the USNRC, and also to the Finnish utilities and colleagues who provided the system code calculations necessary for the boundary conditions.

REFERENCES

[1] CUNNINGHAM, M. E., FRAPTRAN: a Computer Code for the Transient Analysis of Oxide Fuel Rods, to be published as NUREG/CR report.

[2] MIETTINEN, J., HÄMÄLÄINEN, A., Development and Validation of the Fast Running Thermohydraulic Model SMABRE for Simulator Purposes, Proceedings of ICONE 8, 8th International Conference on Nuclear Engineering, April 2-6, 2000, Baltimore, MD USA.

[3] MIETTINEN, J., HOEJERUB, F., FRID, W., LINDHOLM, I., RECRIT Code for BWR Recriticality Analysis, Proceedings of ICONE 8, 8th International Conference on Nuclear Engineering, April 2-6, 2000, Baltimore, MD USA.

[4] DAAVITTILA, A, KALOINEN, E., KYRKI-RAJAMÄKI, R., RÄTY, H., Validation of TRAB-3D Against Real BWR Plant Transients, Proceedings of International Meeting on "Best-Estimate" Methods in Nuclear Installation Safety Analysis (BE-2000), November 2000, Washington, DC.

[5] KALOINEN, E., KYRKI-RAJAMÄKI, R., TRAB-3D a New Code for Three-dimensional Reactor Dynamics, CD-ROM Proceedings of ICONE-5, 5th International Conference on Nuclear Engineering, Nice, France, 1997, paper ICONE5-2197.

[6] VALTONEN, K., BWR stability analysis, Finnish Centre for Radiation and Nuclear Safety STUK-A-88, Helsinki, Finland, 1989.

POWER RAMP TESTS OF HIGH BURNUP BWR SEGMENT RODS

H. HAYASHI, Y. ETOH, Y. TSUKUDA
Nuclear Fuel Department, Nuclear Power Engineering Corporation, Tokyo, Japan

S. SHIMADA
Global Nuclear Fuel-Japan Co., Ltd, Ibaraki-ken, Japan

H. SAKURAI
Nippon Nuclear Fuel Development Co., Ltd, Ibaraki-ken, Japan

Abstract. Lead use assemblies (LUAs) of high burnup 8 × 8 fuel design for Japanese BWRs were irradiated up to 5 cycles in Fukushima Daini Nuclear Power Station No. 2 Unit. Segment rods were installed in LUAs and used for power ramp tests in Japanese Material Test Reactor (JMTR). Post irradiation examinations (PIEs) of segment rods were carried out at Nippon Nuclear Fuel Development Co., Ltd. before and after ramp tests. Maximum linear heat rates of LUAs were kept above 300 W/cm in the first cycle, above 250 W/cm in the second and third cycles and decreased to 200 W/cm in the fourth cycle and 80 W/cm in the fifth cycle. The integrity of high burnup 8 × 8 fuel was confirmed up to the bundle burnup of 48 GWd/t after 5 cycles of irradiation. Systematic and high quality data were collected through detailed PIEs. The main results are as follows.

- The oxide on the outer surface of cladding tubes was uniform and its thickness was less than 20 micro-meter after 5 cycles of irradiation and was almost independent of burnup.
- Hydrogen contents in cladding tubes were less than 150 ppm after 5 cycles of irradiation, although hydrogen contents increased during the fourth and fifth irradiation cycles.
- Mechanical properties of cladding tubes were on the extrapolated line of previous data up to 5 cycles of irradiation.
- Fission gas release rates were in the low level (mainly less than 6%) up to 5 cycles of irradiation due to the design to decrease pellet temperature.
- Pellet-cladding bonding layers were observed after the third cycle and almost full bonding was observed after the fifth cycle.
- Pellet volume increased with burnup in proportion to solid swelling rate up to the forth cycle. After the fifth cycle, slightly higher pellet swelling was confirmed.

Power ramp tests were carried out and satisfactory performance of Zr-lined cladding tube was confirmed up to 60 GWd/t (segment average burnup). One segment rod irradiated for 3 cycles failed by a single step ramp test at terminal ramp power of 614 W/cm with a pinhole due to PCI/SCC mechanism. One segment irradiated for 4 cycles failed by a single step ramp test at 551 W/cm with an outer side axial crack length of about 4 mm. Two segments irradiated for 5 cycles failed by a single step ramp test between 420 to 430 W/cm with outer side axial crack lengths of about 10 and 6 mm, respectively. Detailed discussions on these failures are in another paper of this meeting.

1. INTRODUCTION

Under the sponsorship of the Ministry of Economy, Trade and Industry (METI), Nuclear Power Engineering Corporation (NUPEC) is carrying out irradiation test program “The Verification Test on BWR High Burnup Fuel" to verify fuel integrity and to study fuel behaviors of the lead use assemblies (LUAs) of high burnup 8 × 8 fuel (BWR Step II Fuel) at high burnup [1], [2].

The time schedule of the program, which includes the power ramp test on irradiated rods and post irradiation examinations (PIEs), is shown in Figure 1.

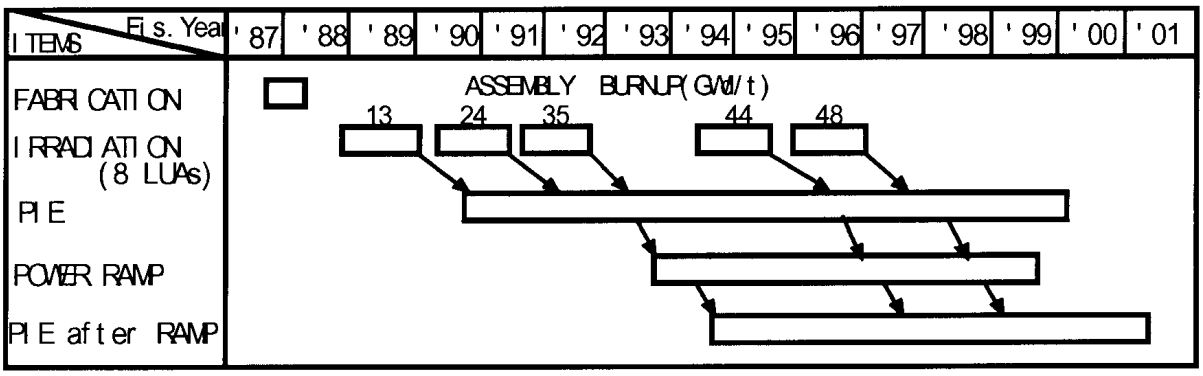

Fig. 1. Test schedule of BWR high burnup fuel.

The LUAs of high burnup 8 × 8 fuel were irradiated up to 5 cycles in Fukushima Daini Nuclear Power Station No. 2 Unit. Segment rods were installed in LUAs and used for power ramp tests in Japanese Material Test Reactor (JMTR). PIEs of segment rods were carried out at Nippon Nuclear Fuel Development Co., Ltd. (NFD) before and after ramp tests.

In this paper, fuel behaviors at high burnup during both base irradiation in the commercial BWR and ramp tests are presented.

2. OUTLINE OF VERIFICATION TEST

2.2. Test Fuel Assemblies

Step II fuel has an 8×8 lattice configuration of 60 fuel rods in which Zr-liner and high corrosion resistant cladding tubes are used. Its design maximum bundle burnup is 50GWd/t. The bundle design has a central large diameter water rod to soften the neutron spectrum. It uses ferrule-type spacers in place of the earlier grid-type ones to improve thermal hydraulic performance. Furthermore, some design improvements to reduce fission gas release, such as an increased initial He pressure, increased pellet density and decreased gap width between pellet and cladding, are incorporated. The design parameters and fuel rod arrangement in the fuel assembly are shown in Figure 2 [1].

Eight test assemblies, some of which were equipped with segment rods for power ramp tests, were fabricated by Japan Nuclear Fuel Co., Ltd.

2.3. Irradiation

Eight test assemblies were loaded in a relatively high power position in the core of Fukushima Daini Nuclear Power Station No. 2 Unit, operated by Tokyo Electric Power Co., in 1989. They were irradiated up to 5 irradiation cycles under normal BWR conditions and one assembly was discharged after each cycle for detailed PIEs. The reactor was operated at almost full power through the five cycles.

Irradiation history of 5-cycle irradiated fuel assembly is shown in Figure 3. Maximum linear heat rates of LUAs were kept above 300 W/cm in the first cycle, above 250 W/cm in the second and third cycles and decreased to 200 W/cm in the fourth cycle and 80 W/cm in the fifth cycle. The integrity of high burnup 8 × 8 fuel was confirmed up to the bundle burnup of 48 GWd/t after 5 cycles of irradiation.

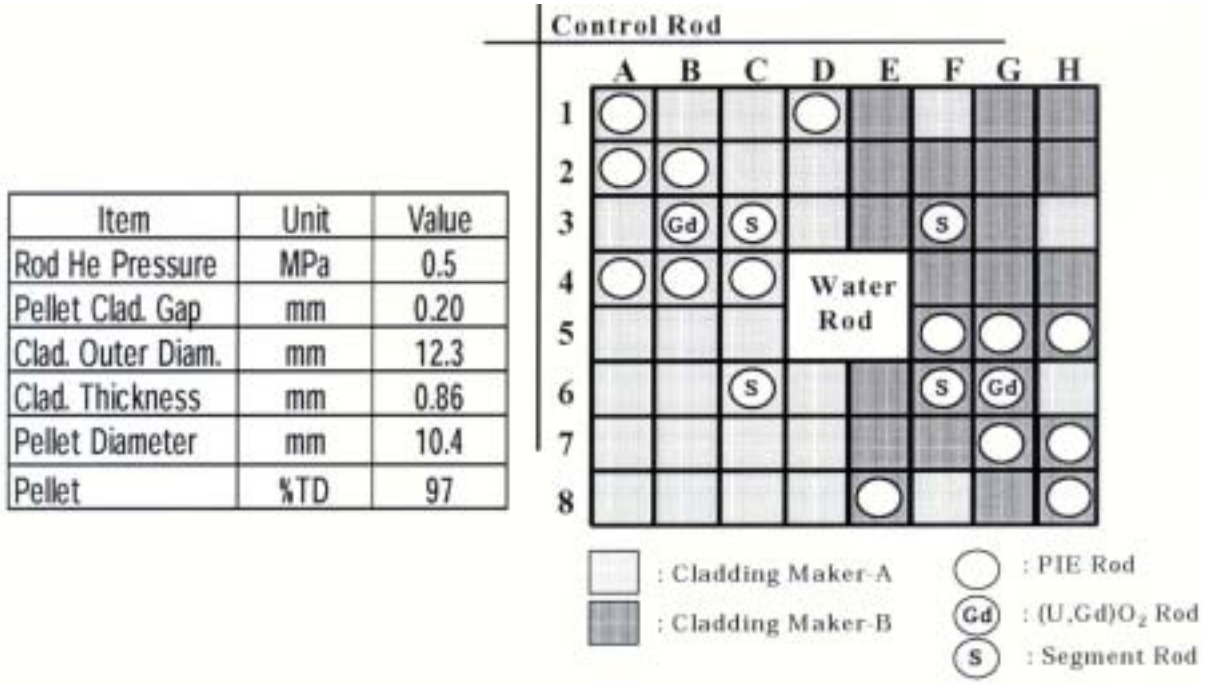

Item	Unit	Value
Rod He Pressure	MPa	0.5
Pellet Clad. Gap	mm	0.20
Clad. Outer Diam.	mm	12.3
Clad. Thickness	mm	0.86
Pellet Diameter	mm	10.4
Pellet	%TD	97

Fig. 2. Design parameters and rods arrangement of STEP II LUA.

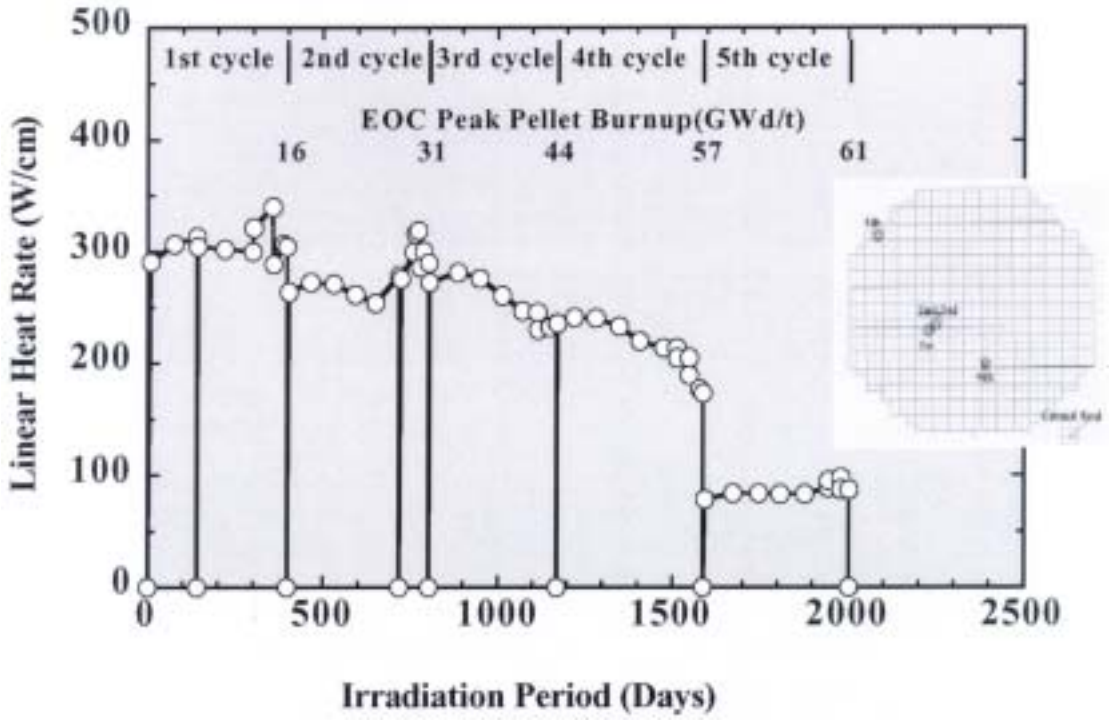

Fig. 3. Irradiation history of step II LUAs.

2.4. Power Ramp Tests

In order to confirm both the integrity of fuel rods during normal/off-normal operational transients and the margin of ramp performance, a power ramp test series were executed using 25 segment rods irradiated for three to five cycles (burnup range: from 43 to 61GWd/t).

The ramp sequences are a stair case power ramp (Ramp sequence A), a single step power ramp (Ramp sequence B), and a power cycling test (Ramp sequence C). Ramp sequence A is used to calibrate heat generation by He-3 gas pressure and to determine power to failure. There are three types of ramp sequence B, that is, Bs, Bt and Br. Ramp sequence Bs is employed to confirm the integrity of fuel during normal operational transients as is ramp sequence C also. In this case, ramp terminal power (RTP) corresponds to the designed maximum power level. Ramp sequence Bs is also employed to investigate the margin of ramp performance by increasing RTP up to about 150% of the designed maximum power level. The integrity of fuel rods under abnormal operational transients, such as control rod withdrawal, is studied by ramp sequence Bt in which RTP and the holding time are selected as about 125% of the designed maximum power level and 10 minutes, respectively [2]. RTP and the cumulative holding time of ramp sequence Br are the same as those of ramp sequence C, so it is possible to obtain the characteristics of fuel behavior during cyclic operation by comparing with ramp sequence Br. Four typical power ramp sequences (two Bs, Bt and C) are shown in Figure. 4.

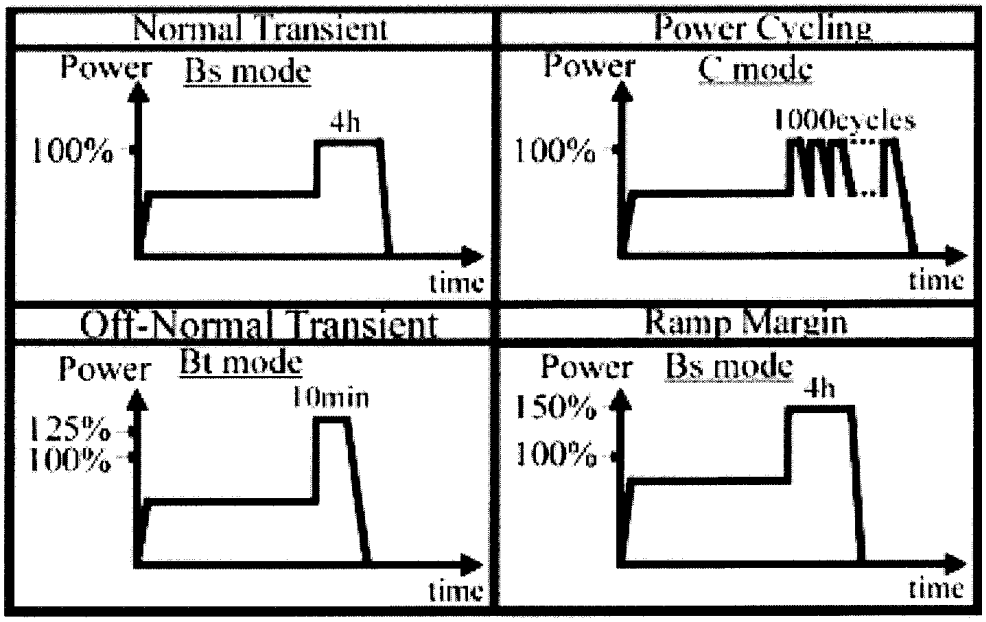

Fig. 4. Power ramp sequence.

2.5. Post-Irradiation Examination

After each of the reactor cycles, test assemblies were subjected to basic non-destructive examinations in the spent fuel pool, including visual examination with an underwater TV camera. Five assemblies have been examined in the hot laboratory of Nippon Nuclear Fuel Development Co., Ltd. (NFD) and detailed PIE data were systematically obtained. The burnups of these five assemblies were about 13, 24, 35, 44 and 48GWd/t, respectively. At each burnup stage, non-destructive tests (NDT) were executed on 16 rods and destructive tests (DT) were performed on 2 or 3 rods, including a $(U,Gd)O_2$ rod.

Segment rods were dismantled from the assemblies and examined non-destructively at NFD before the power ramp test. After the power ramp test, both non-destructive and destructive PIEs were carried out.

3. STEADY STATE BEHAVIOR

3.2. Water-side corrosion of cladding tube

Cladding water-side corrosion and resulting hydrogen uptake are considered to potentially limit fuel burnup extension. High corrosion resistant cladding tubes have been used for Step II fuel.

Visual appearances and cross-sectional micrographs of the cladding are shown in Photo 1. Two types of corrosion were observed. Nodular corrosion was clearly observed at the gas plenum region, although the oxide layer of fuel stack region was uniform and the thickness was 10 - 20 micro-meter in the transverse sections of each fuel rod, as shown in Photo 1.

Burnup dependence of maximum oxide thickness in fuel stack regions of Step II LUAs is shown in Figure 5, which also includes those of 8 × 8 fuels and Step I LUAs [3], [4]. In this figure, oxide thickness obtained by metallography is plotted as a function of specimen burnup. Maximum oxide thickness of Step II LUAs was less than one half of 8 × 8 fuels throughout their irradiation cycles.

The improvement in the corrosion resistance was attributed to the controlled chemistry within Zircaloy-2 specifications and the application of appropriate heat treatments. Microstructural observations of the cladding showed that radiation-induced dissolution of intermetallic precipitates seemed to be faster than that in the conventional cladding, because of a smaller precipitate size as a result of the heat treatments, which would improve the corrosion resistance.

3.3. Hydrogen pickup of fuel rods

The content of hydrogen in cladding was measured by an inert gas fusion method. Hydrogen content of BWR fuel cladding is shown in Figure 6, as a function of irradiation period. Maximum hydrogen content of Step II LUA cladding was less than that of 8×8 fuels up to three irradiation cycles, but it tended to increase with an increase in irradiation period thereafter, and after five irradiation cycles, the content was almost the same as those of the reported.

Hydride morphologies in the cross-sectional metallography of the cladding are shown in Photo 2. Hydrides in the cladding irradiated for 3 cycles are small and distribute uniformly. Hydrides increase with burnup after 4 cycles of irradiation and hydride densities in outer peripheral and Zr-liner are high.

3.4. Mechanical properties of fuel cladding

Tensile, burst and micro hardness tests were carried out to characterize the mechanical properties of the irradiated cladding tubes. Figure 7 shows the dependency on fast neutron fluence of 0.2% offset yield strength.

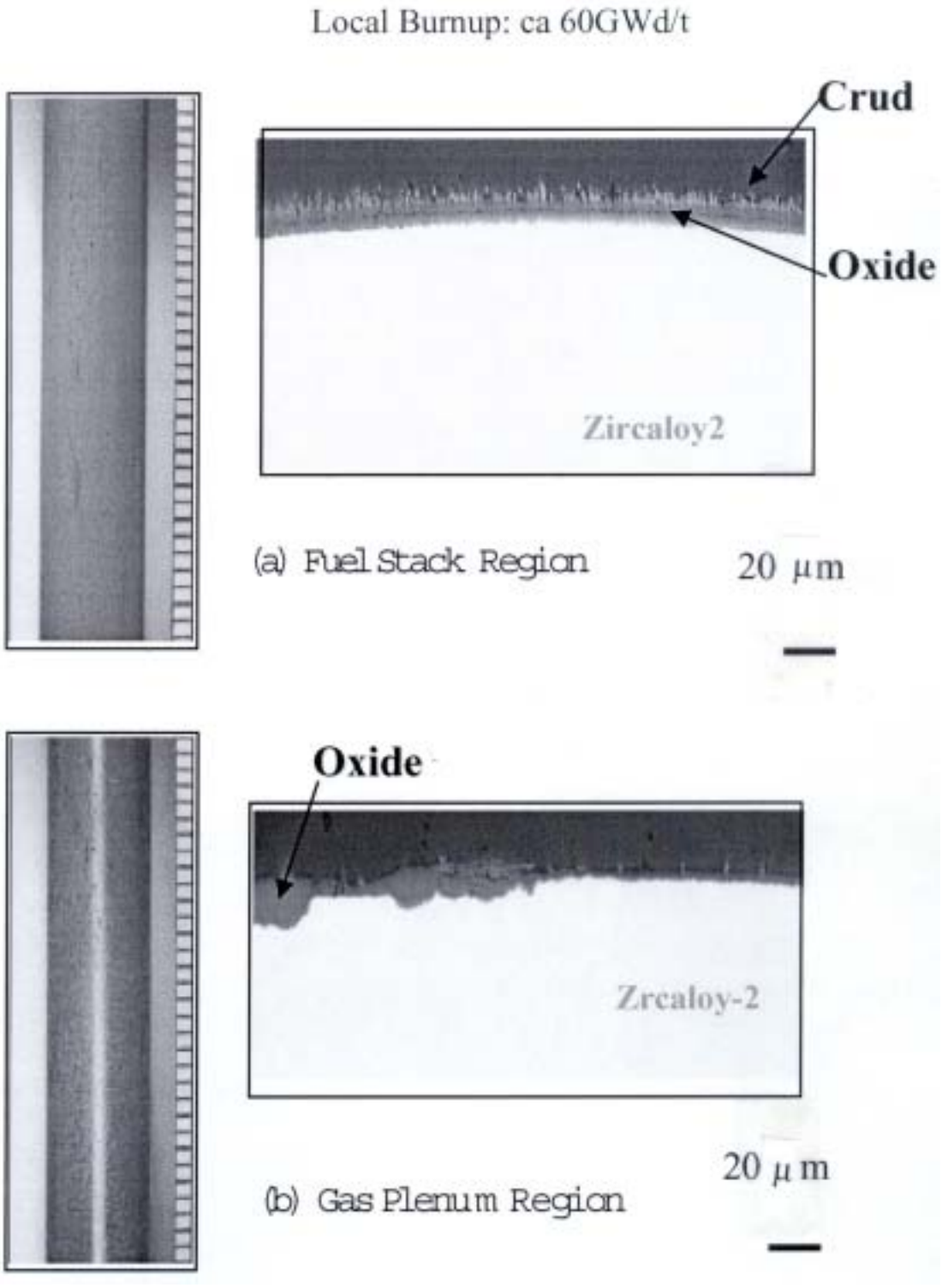

Photo 1. Visual appearance and cross sections of oxides on fuel rods.

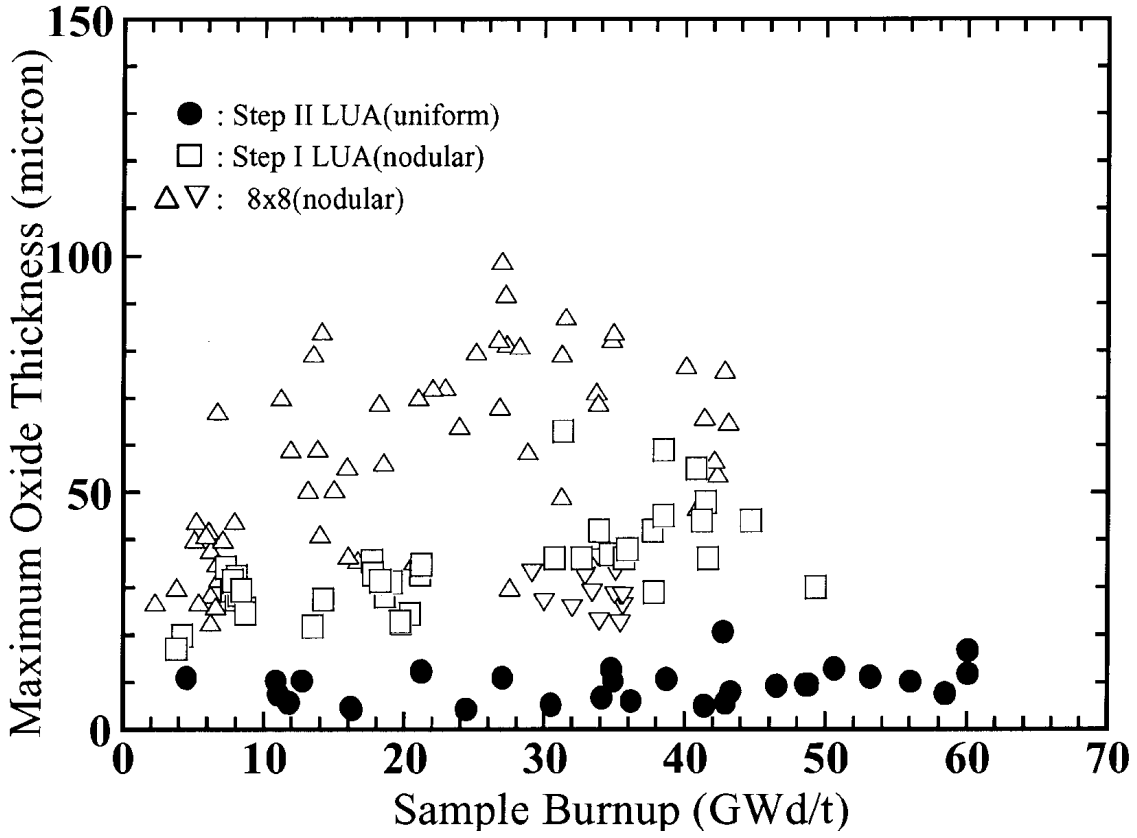

Fig. 5. Burnup dependence of maximum oxide thickness.

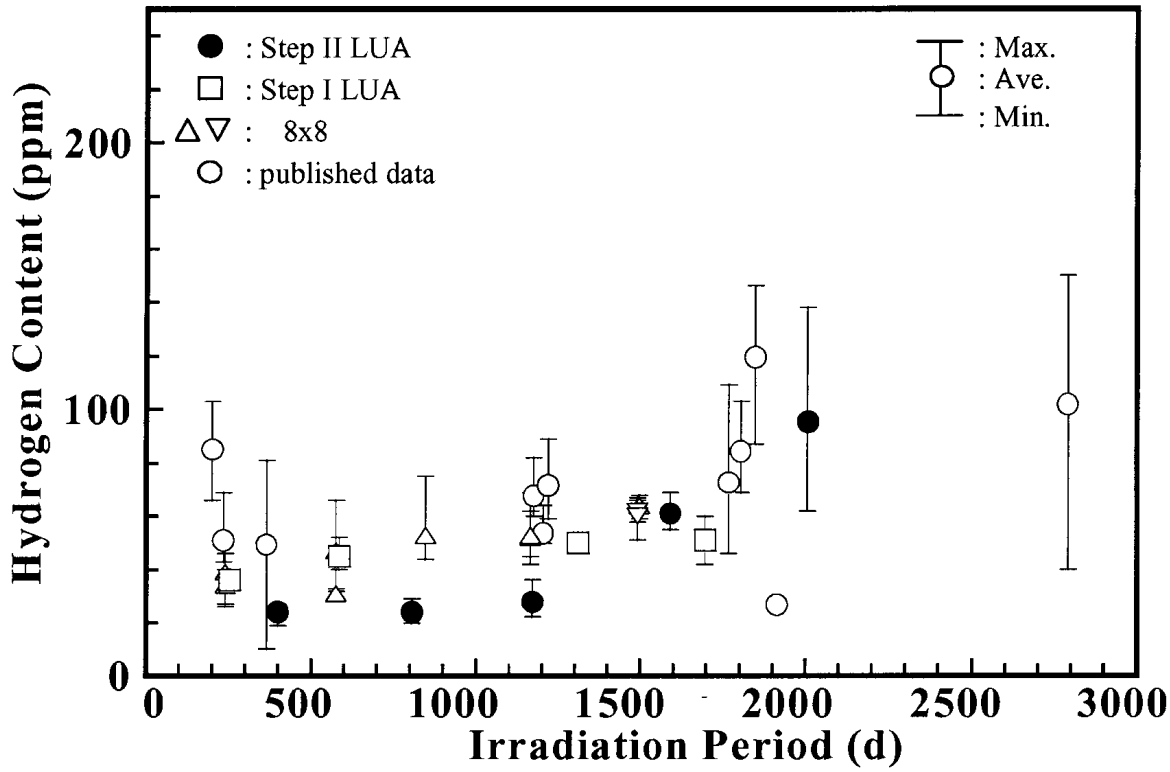

Fig. 6. Hydrogen content in cladding v.s. irradiation period.

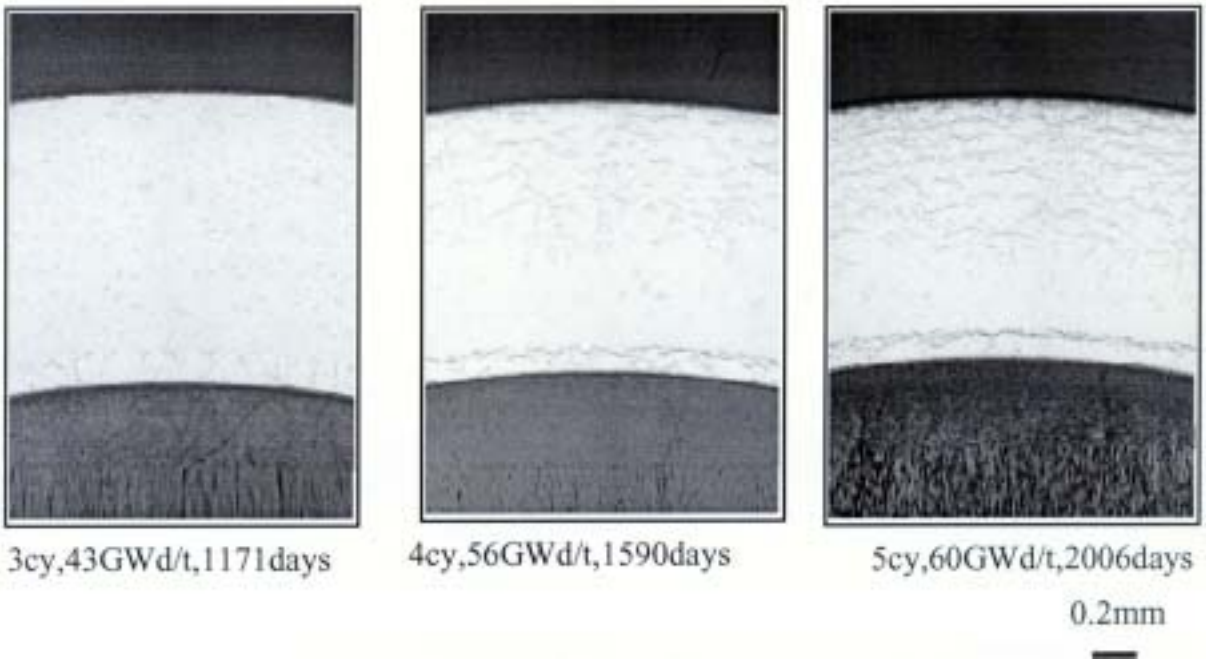

Photo 2. Hydryde morphology of step II fuel cladding.

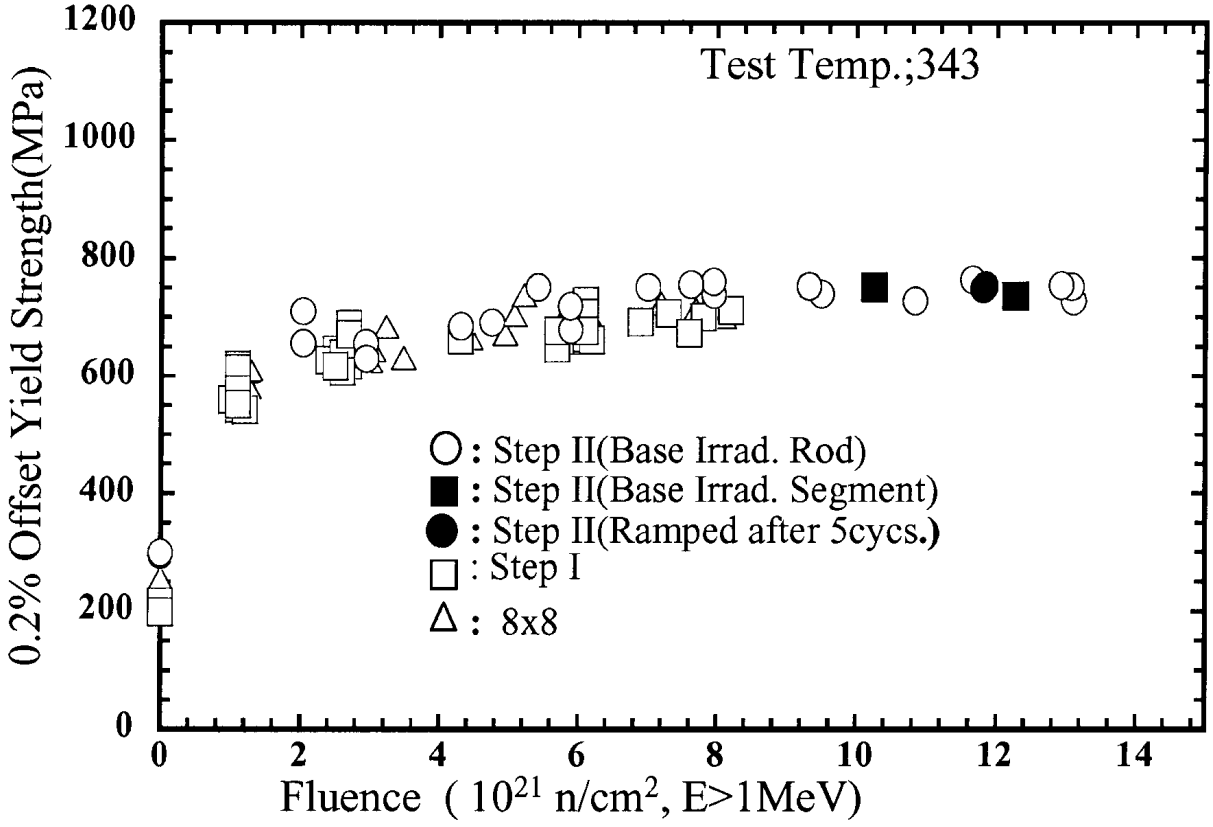

Fig. 7. Mechanical properties of cladding (yield strength).

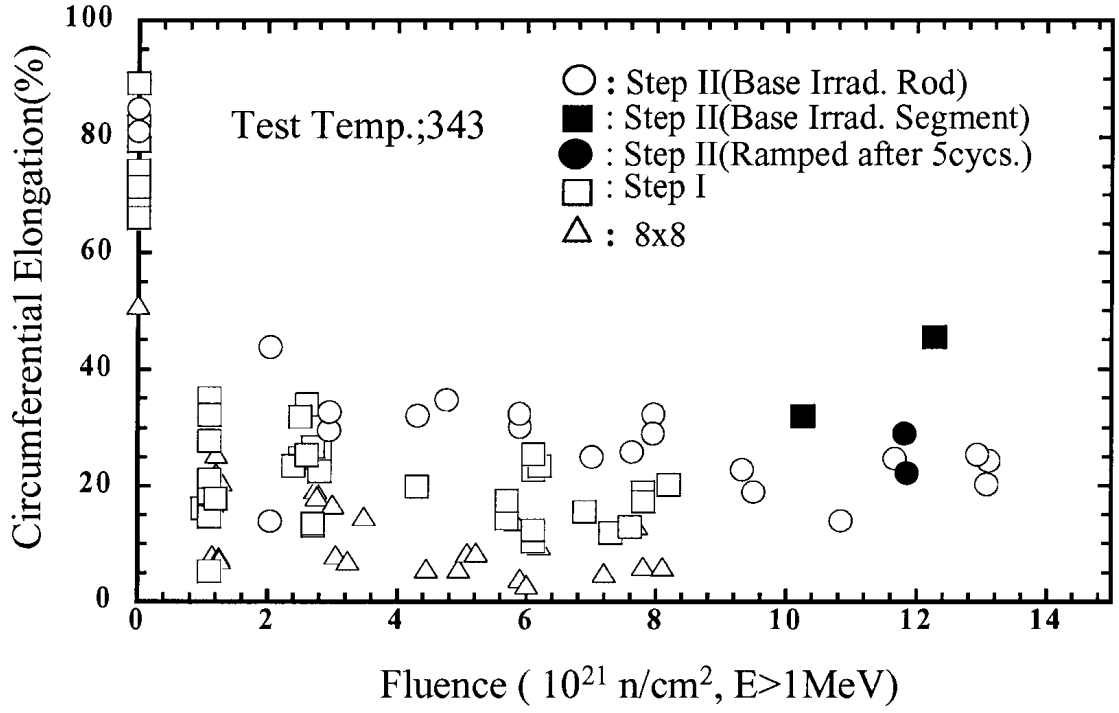

Fig. 8. Mechanical properties of cladding (elongation).

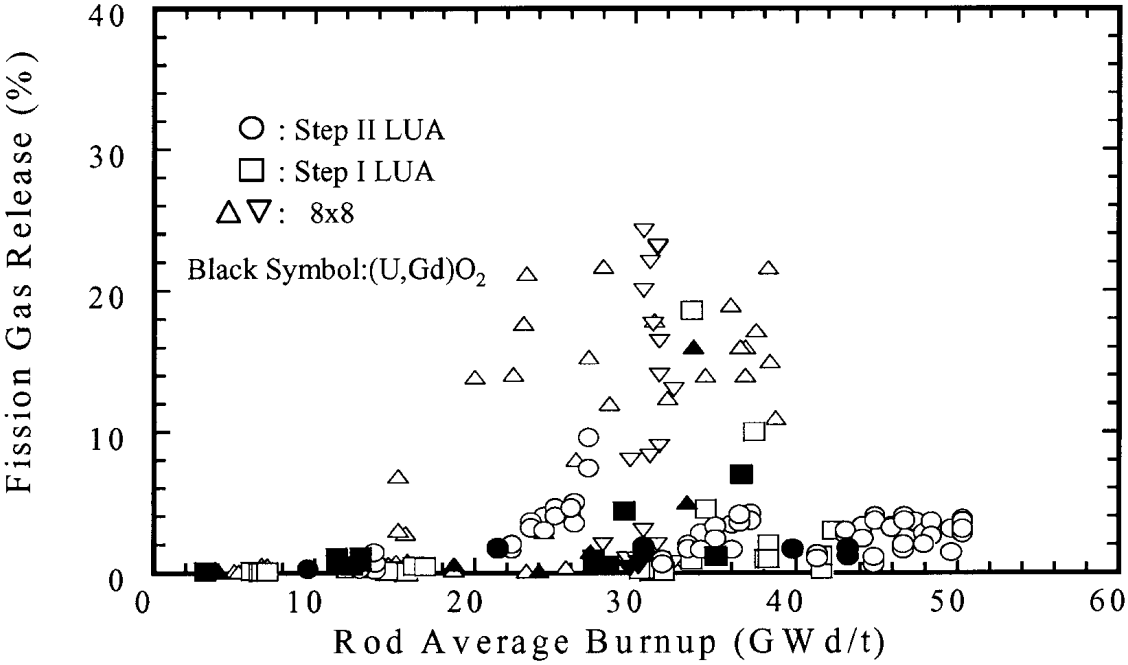

Fig. 9. Burnup dependence of fission gas release.

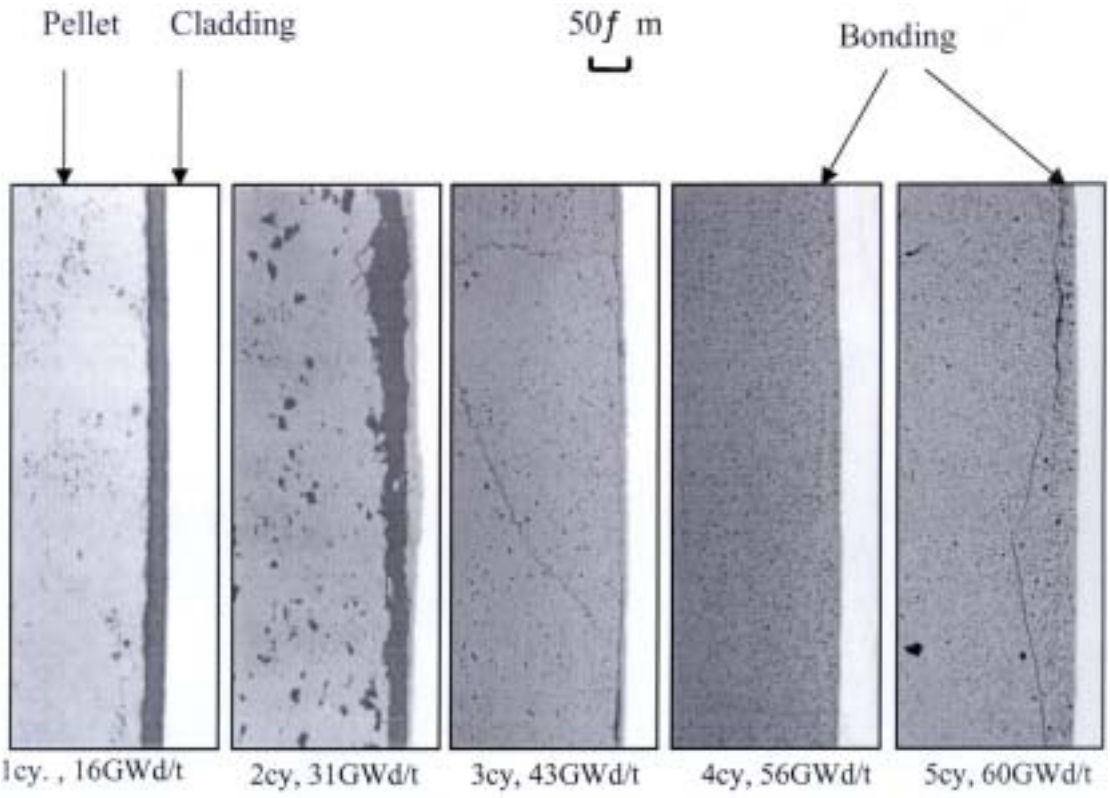

Photo 3. Cross-sectional metallography at pellet-cladding interface.

Uniaxial tensile properties of the irradiated cladding were measured at room temperature and 343 degree centigrade. Burst test was carried out at 343 degree centigrade. Circumferential yield strength of the heat-treated cladding tubes adopted in the Step II LUA were almost the same as those of the 8 × 8 fuel claddings [3] as shown in Figure 7. Circumferential failure strain of the Step II LUA's cladding was slightly higher than those of the 8 × 8 fuel claddings and the failure strains were greater than 10% up to 1.3×10^{22} cm^{-2} as shown in Figure 8.

The tensile properties and micro hardness saturated with the exposure after the first cycle, which is the same tendency as that of the burst properties.

From these results, it was concluded that the mechanical properties of the heat-treated cladding tubes did not essentially differ from those of the 8×8 fuel cladding irradiated in commercial BWR reactors.

3.5. Fission gas release

As fission gas release (FGR) is considered to potentially limit fuel burnup extension, fuel design improvements to reduce FGR have been adopted in Step II fuel.

FGR was measured by Krypton-85 gamma intensity measurements at the plenum position of the rod (for all NDT rods) and by puncturing tests (for DT rods). FGR of Step II LUAs is compared with published BWR data [3], [4] in Figure 9. Except for two fuel rods, in which highly enriched UO_2 was loaded and which showed about 10% FGR at 27GWd/t rod average burnup after two irradiation cycles, FGR of Step II LUAs was up to about 5% throughout the irradiation cycles. When compared at the same power experienced during irradiation, FGR of Step II LUAs was less than that of the previous types of fuel rods, indicating the effect of the design improvements to reduce FGR.

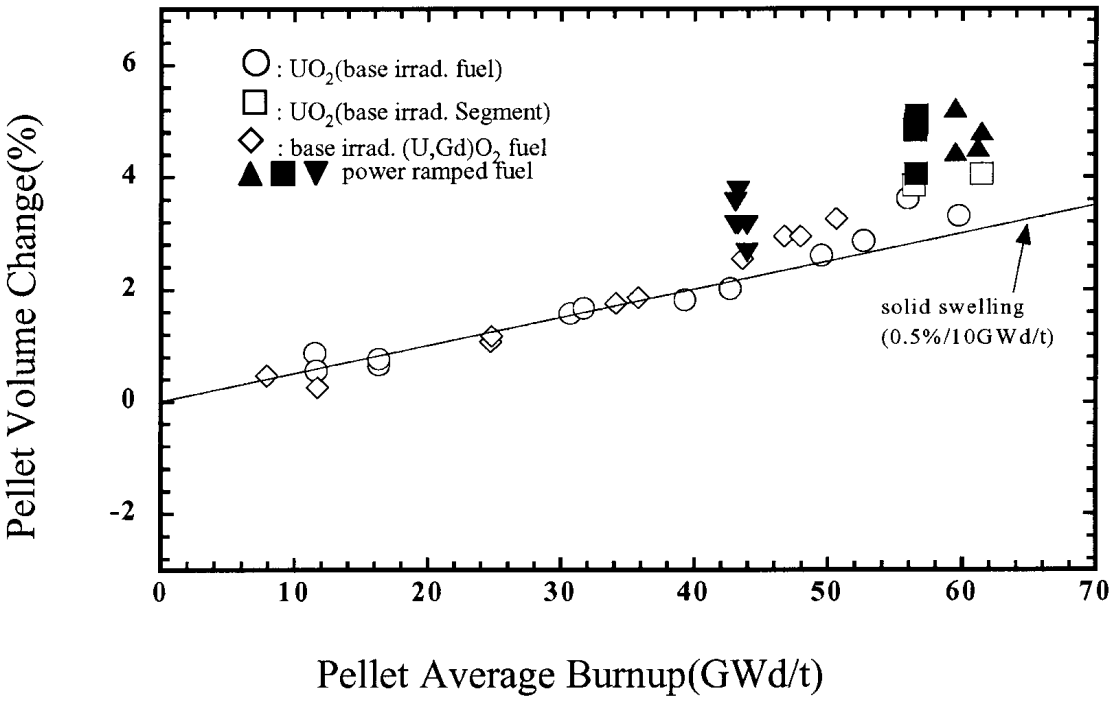

Fig. 10. Pellet volume change depending on burnup.

3.6. Pellet-cladding bonding layer

With increasing burnup, pellet-cladding gap in fuel rods tends to close due to pellet swelling and cladding creep-down, and eventually a bonding layer is formed between the pellet and cladding under hard contact conditions at high burnups. The bonding layer was observed for Step II LUAs after three cycles of irradiation (Photo 3). The thickness of the layer is about 10–20 μm and remained almost constant in spite of the increase in burnup. Considering EPMA measurement results at the pellet-cladding interface and published information [5], this layer may be produced by subsequent mutual diffusion of UO_2 and ZrO_2.

3.7. Pellet volume

Pellet densities of irradiated for one to five cycles were measured by immersion method. As shown in Figure 10, pellet volume increased with burnup in proportion to solid swelling rate up to the forth cycle. After the fifth cycle, slightly higher pellet swelling was confirmed.

4. TRANSIENT BEHAVIOR

A ramp test series for 25 segment rods with burnup range from 43 to 61GWd/t were executed in JMTR using the Boiling Water Capsule under simulated BWR temperature and pressure conditions. RTP ranged from 330 to 620W/cm based on the designed maximum power level. The cumulative holding times were 10 minutes (Bt), 4 hours (A, Bs) and 321 hours (Br, corresponding to 1 000 cycles power cycling test). Test segments were preconditioned for more than 6 hours prior to power ramp. The ramp rate was 250 W/cm/min.

Table I. Power ramp results of STEP II LUAs segment rods

Test No.	Bundle No.	Burnup (GWd/t)	Ramp Mode	Pre-Conditioning Power (W/cm)	Ramp Terminal Power (W/cm)	Results	Hold Time
1		43.4	A	310	616	Sound	4 hours
2		43.4	Bs	282	412	Sound	4 hours
3		42.7	Bt	279	505	Sound	10 minutes
4	2F2D3	42.7	Bs	279	517	Sound	4 hours
5		42.7	Bt	280	511	Sound	10 minutes
6		43.4	Bs	279	623	Sound	4 hours
7		43.4	Bs	279	614	Failed	9 minutes*
8		42.7	Bs	277	517	Sound	4 hours
9		43.7	Br	208	414	Sound	321 hours
10		43.7	C	207	412	Sound	100 cycles
11		56.3	A	250	592	Sound	4 hours
12		56.3	Bs	220	350	Sound	4 hours
13	2F2D4	56.3	Bt	220	432	Sound	10 minutes
14		56.2	Bs	220	433	Sound	4 hours
15		56.3	Bs	283	551	Failed	149 minues*
16		56.2	Bs	261	501	Sound	4 hours
17		60.8	A	252	446	Failed	22 minutes*
18		60.8	Bs	201	333	Sound	4 hours
19		60.8	Bs	214	399	Sound	4 hours
20	2F2D8	59.5	Bt	204	399	Sound	10 minutes
21		59.5	Br	166	336	Sound	321 hours
22		61.1	Bs	203	421	Failed	100 minutes*
23		61.1	Bs	202	402	Sound	4 hours
24		61.1	Bs	202	428	Failed	68 minutes*
25		59.5	C	168	326	Sound	1000 cycles

* : The hold time when the failure was detected.

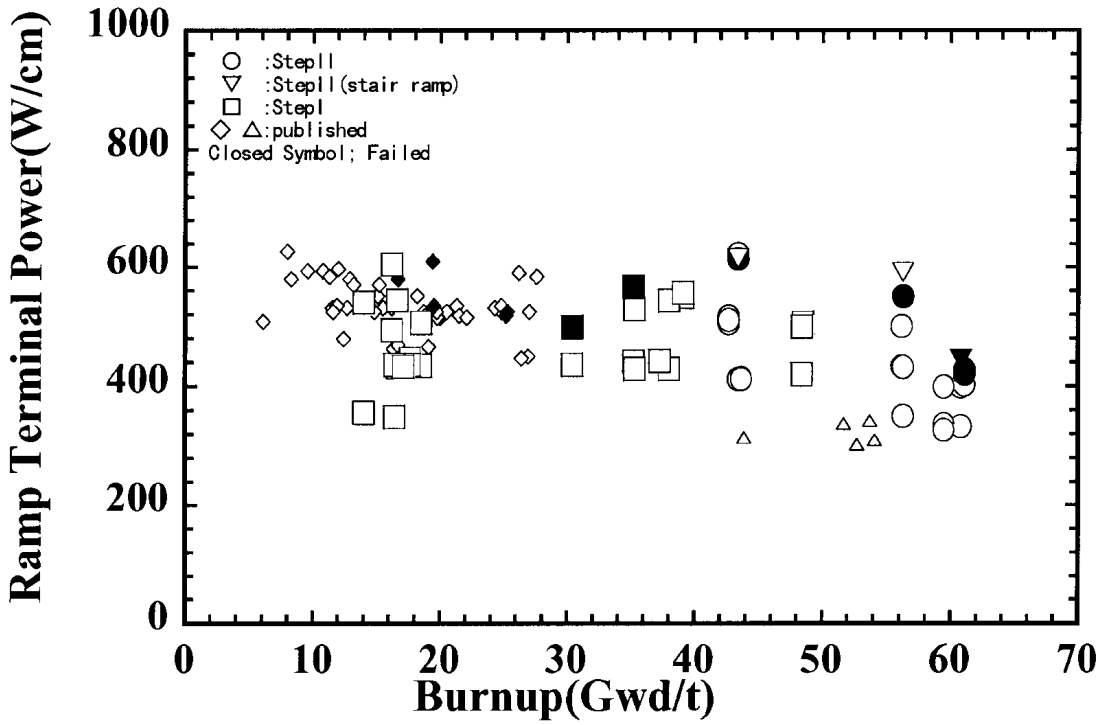

Fig. 11.Power ramp test results for Zr-lined fuel rod.

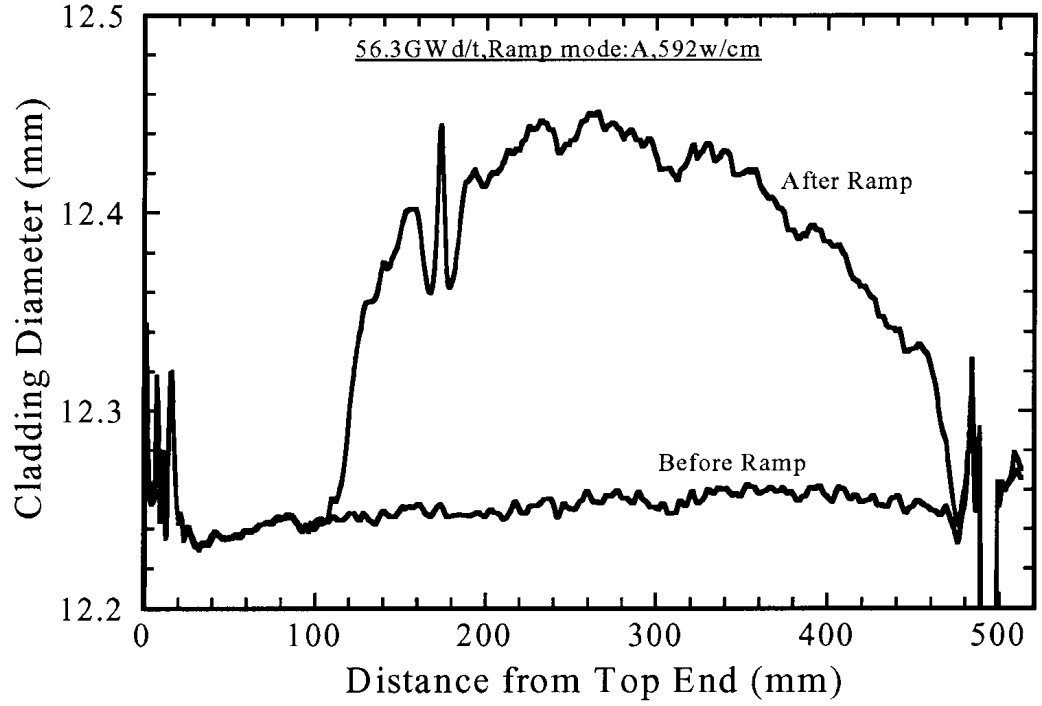

Fig. 12. Cladding deformation due to power ramp.

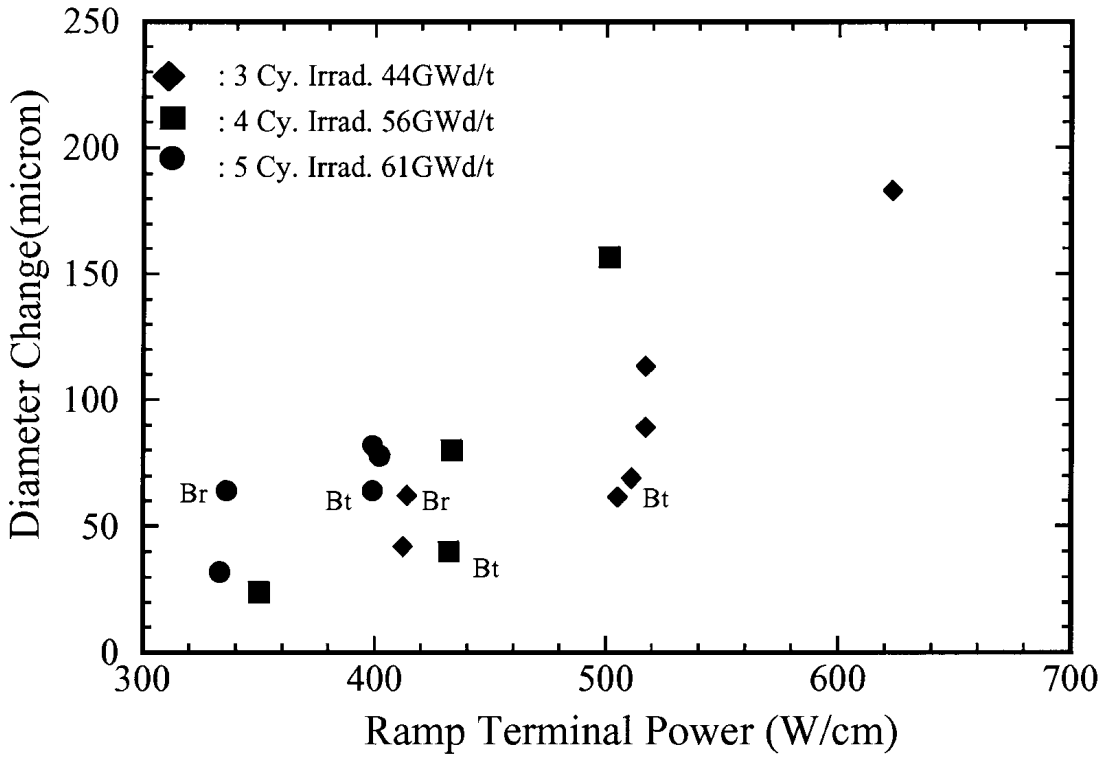

Fig. 13. RTP dependence of cladding diameter increase.

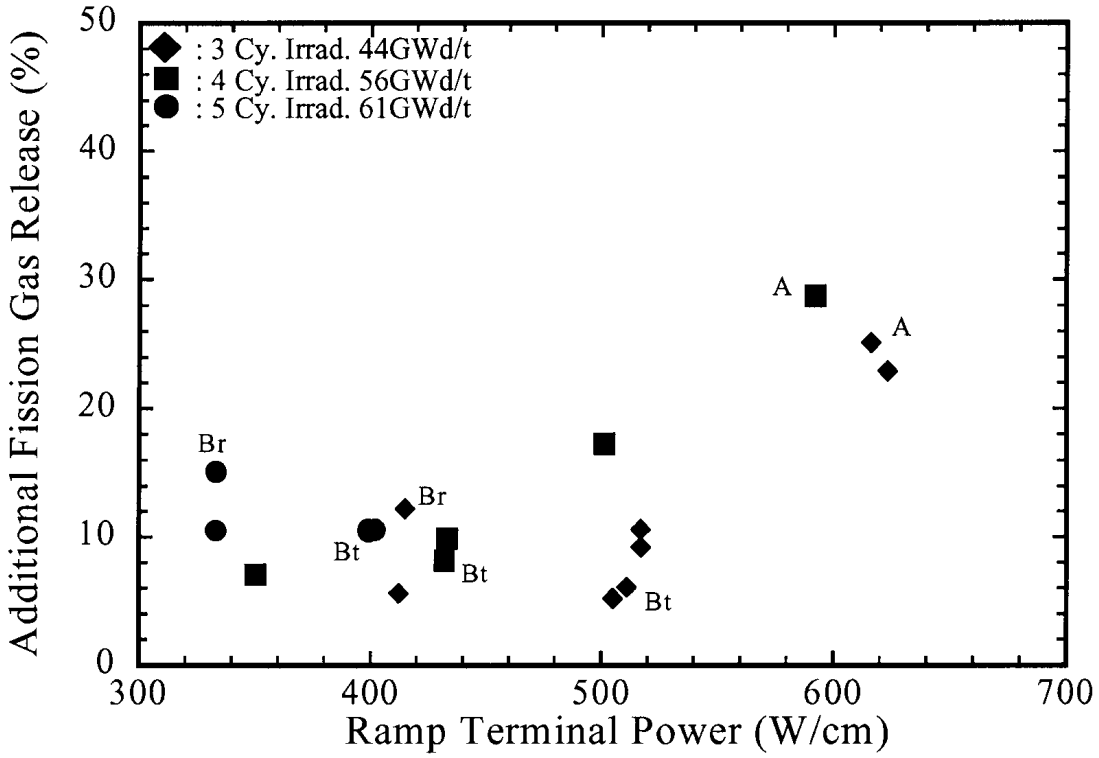

Fig. 14. RTP dependence of fission gas release.

4.2. Power ramp performance

Power ramp test results are shown in Table 1 and Figure 11 with published data [2], [6]. In the case of single step power ramp, RTP of the failed segment rod irradiated for 3 cycles (43 GWd/t) is higher than those of Step I fuels and published data whose burnup are less than 35 GWd/t. The RTP of the failed segment rod irradiated for 4 cycles (56 GWd/t) is 551 W/cm and those for 5 cycle irradiated (61 GWd/t) are 421 and 428 W/cm, respectively. The decreasing tendency of failure threshold for higher burnup segment rods is clear and the failure mode of higher burnup segment rods is different from that of low burnup (less than 43 GWd/t) segment rods.

Although the failure threshold power had a tendency to decrease at the high burnup region as shown in Figure 11, these failure levels corresponded to about 140% of the designed maximum power, and it was considered that, in spite of decreasing the gap width between pellet and cladding, Step II fuel had sufficient integrity for normal/off-normal operational transients and a good margin for ramp performance.

4.3. Fuel rod deformation

Figure 12 shows an example of diametral profiles of a segment rod before and after the power ramp test. Each segment showed permanent diametrical deformation, which increased with RTP at the fuel stack. The average diameter increase during power ramp tests (Ramp sequence B) is shown in Figure 13 as a function of RTP [7]. From this figure, it could be seen that diameter increase depended on RTP, burnup and the cumulative holding time.

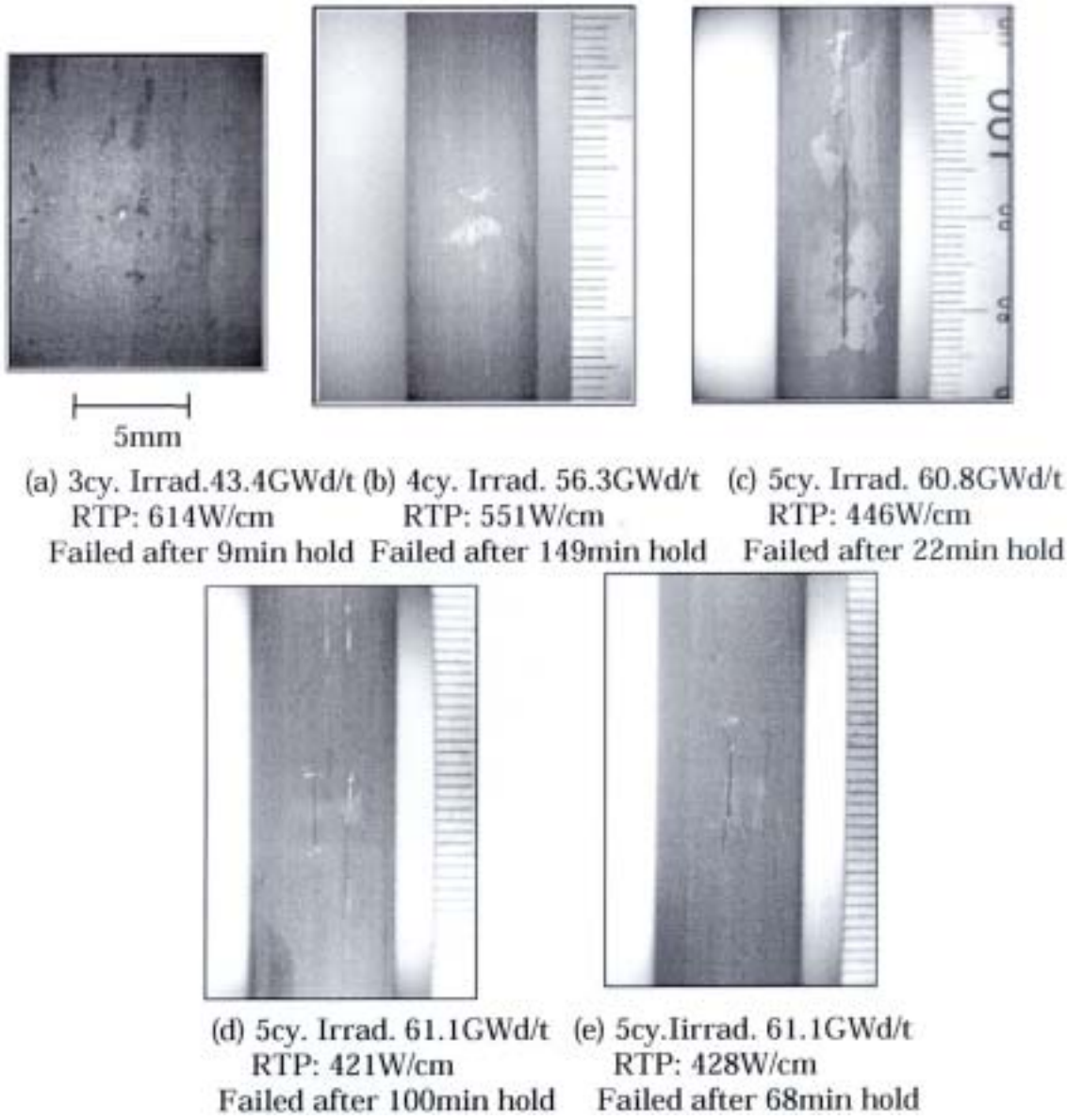

Photo 4. Visual appearances of failed segment rods.

4.4. Fission Gas Release

Krypton-85 gamma intensities at the plenum position of the segment rods were measured before and after the power ramp test and puncturing tests were performed after the power ramp test. FGR of the segment rods before the power ramp test ranged from 7 to 12% and was higher than those of full-length rods. This may be caused by the difference in the experienced power during base irradiation between full-length and segment rods.

FGR during the power ramp test is shown in Figure 14 as a function of RTP. FGR depended strongly on RTP and burnup, and dependency on the cumulative holding time was also observed. As FGR is closely related to pellet temperature, pellet grain growth, local fission gas release determined by EPMA (Electron Probe Micro Analysis) and Cs redistribution obtained by micro gamma scanning also showed dependency both on the RTP and on the cumulative holding time.

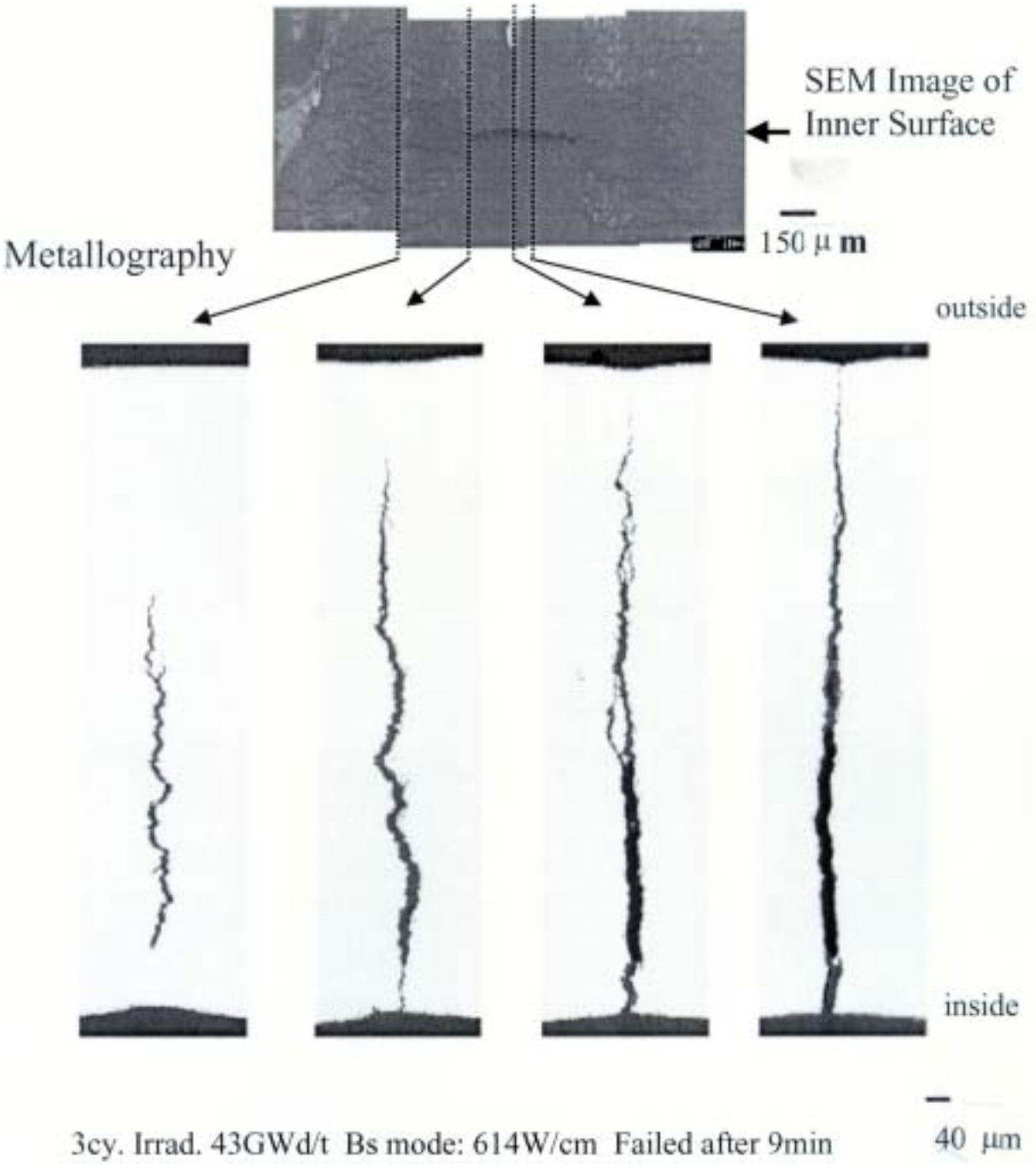

Photo 5. SEM image and cross-sectional metallography of failed segment (3cy. Irradiated).

4.5. Failed segment rods

The visual appearances of five segment rods failed during power ramp are shown in Photo 4.

Among the five failed segment rods, the one irradiated up to about 43 GWd/t failed after 9 minutes at 614 W/cm. A small pinhole is observed on the outer surface in Photo 4 (a). By the detailed PIE, the failure mechanism was confirmed to be stress corrosion cracking (SCC) and the penetrated crack was initiated at the pellet/pellet interface [2] as shown in Photo 5. The other four, higher burnup segment rods have different appearance from SCC as shown in Photo 4 (b) to Photo 4(e).

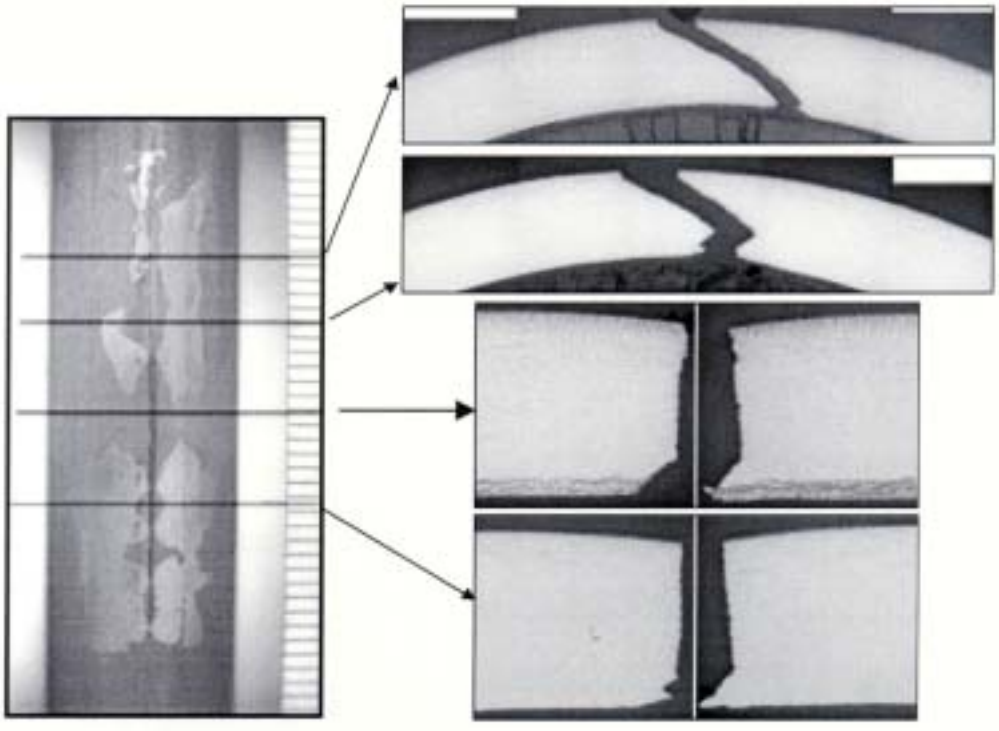

Photo 6. Visual appearance and cross sectional metallography of failed segment rod. (5cy. Irrad., RTP: 446W/cm, failed after 22min hold).

Photo 4 (b) shows the appearance of a failed segment rod of 56 GWd/t burnup, which was subjected to a single step power ramp with RTP of about 551 W/cm and failed after a holding time of 149 minutes. An axial crack with a length of about 4 mm was clearly seen on the outer surface.

Two segment rods irradiated for 5 cycles failed by a single step ramp test at 421 and 428 W/cm also caused outer side axial cracks with lengths of 10 and 6 mm as shown in Photos 4 (d) and 4 (e), respectively. Similar appearance was also observed on the segment rod with burnup of 61 GWd/t, which was subjected to a stair case power ramp and failed after about 22 minutes at power level of 446 W/cm as shown in Photo 4(c). Four cross-sections of the segment rod at the crack portion are shown in Photo 6. Crack started from the outer surface of the cladding tube and propagated to radial and axial directions and finally failed by ductile fracture.

Taking into account the proposed mechanisms of crack propagation [4], [8], detailed PIEs (such as scanning electron microscopy, hydrogen content measurement and so on) are being conducted on the rods with outer side axial splits with an emphasis on understanding the mechanism of cracking initiation and propagation observed in this test.

Detailed discussions on these failures are in another paper of this meeting.

5. SUMMARY

In this verification test program, well-characterized LUAs of high burnup 8 × 8 fuel were irradiated in a typical commercial BWR in Japan, Fukushima Daini Nuclear Power Station

No. 2 Unit, under normal operational conditions. After each irradiation cycle, detailed PIEs at a hot laboratory were carried out on five assemblies. Power ramp test also carried out on segment rods, which were installed in LUAs. As the results of these examinations, irradiation performances of Step II LUAs irradiated up to about 48 GWd/t assembly burnup can be summarized as follows.

(1) The oxide on the outer surface of cladding tubes was uniform and its thickness was less than 20 micro-meter after 5 cycles of irradiation and was almost independent of burnup.

(2) Hydrogen contents in cladding tubes were less than 150 ppm after 5 cycles of irradiation, although hydrogen contents increased during the fourth and fifth irradiation cycles.

(3) Mechanical properties of cladding tubes were on the extrapolated line of previous data up to 5 cycles of irradiation.

(4) Fission gas release rates were in the low level (mainly less than 6%) up to 5 cycles of irradiation due to the design to decrease pellet temperature.

(5) Pellet-cladding bonding layers were observed after the third cycle and almost full bonding was observed after the fifth cycle.

(6) Pellet volume increased with burnup in proportion to solid swelling rate up to the forth cycle. After the fifth cycle, slightly higher pellet swelling was confirmed.

(7) Although high burnup BWR fuel showed sufficient integrity for normal/off-normal operational transients and a good margin of ramp performance, it is important to understand the failure mechanism in the high burnup region.

ACKNOWLEDGEMENTS

This study was carried out mainly under the direction of committees of NUPEC. The authors wish to express their gratitude to the members of the “Committee of Verification Tests on High Burnup Fuel", especially Dr. T. Okubo and Dr. M. Yamawaki for their discussions and evaluations with respect to this program. The authors also gratefully acknowledge METI for the sponsorship on this project.

REFERENCES

[1] KUROSU, T., et al., “Verification Test Program of High Burnup Fuel", Japan-Russia Experts Meeting on Power Reactor Fuels, held in Tokyo, Japan, 19-21 September (1994).
[2] HAYASHI, H., et al., “Irradiation Characteristics of BWR Step II Lead Use Assemblies", Proc. 1997 ANS Int. Mtg. on LWR Fuel Performance, Portland, Oregon, (1997), 296.
[3] SAKURAI, H., et al., “Irradiation Characteristics of High Burnup BWR Fuels”, Proc. 2000 ANS Int. Mtg. on LWR Fuel Performance, Park City, Utah, (2001), 151.
[4] MISHIMA, Y., et al.,“Proving Test on Reliability for BWR Fuel Assemblies", J. At. Energy Soc. Japan, 29, (1987), 90.

[5] OISHI, M., et al.,“High Burnup Fuel Behavior Studies in NUPEC", IAEA Mtg. on Fuel Performance at High Burnup for Water Reactors, held in Studsvik, Sweden, 5-8 June (1990).
[6] KOIZUMI, S., et al.,“Study on Fission Gas Release from High Burnup Fuel", IAEA Mtg. on Fuel Performance at High Burnup for Water Reactors, held in Studsvik, Sweden, 5-8 June (1990).
[7] NOGITA K., and UNE, K., “Formation of Pellet-Cladding Bonding Layer in High Burnup BWR Fuels”, J. Nucl. Sci. and Tech., 34 (1997) 679.
[8] OHARA, H., et al.,“Fuel Behavior During Power Ramp Tests", Proc. 1994 Int. Topical Mtg. on LWR Fuel Performance, West Palm Beach, Fl, (1994).
[9] SCHRIRE, D., et al., “Testing Cladding Integrity at High Burnup”, IAEA Tec. Committee Mtg., Nyköping, Sweden, (1998).

AXIAL CRACK ON HIGH BURNUP BWR FUEL CLADDING CAUSED BY POWER RAMP TEST

H. HAYASHI, Y. ETOH, Y. TSUKUDA
Nuclear Fuel Department, Nuclear Power Engineering Corporation, Tokyo, Japan

S. SHIMADA
Global Nuclear Fuel-Japan Co., Ltd, Ibaraki-ken, Japan

H. SAKURAI
Nippon Nuclear Fuel Development Co., Ltd, Ibaraki-ken, Japan

Abstract. Lead use assemblies (LUAs) of high burnup 8 × 8 fuel design for Japanese BWRs were irradiated up to 5 cycles in Fukushima Daini Nuclear Power Station No. 2 Unit. Segment rods were installed in LUAs and used for power ramp tests in Japanese Material Test Reactor. Post irradiation examinations (PIEs) of segment rods were carried out at Nippon Nuclear Fuel Development Co., Ltd. before and after ramp tests. One segment rod irradiated for 3 cycles failed at the ramp terminal power of 610 W/cm by PCI/SCC mechanism, while some segment rods irradiated for 4 and 5 cycles failed at about 550 and 420 W/cm, respectively, and showed axial cracks starting in the outer surface of cladding tubes.Following characteristics on failure segment rods were observed through detailed PIEs before and after ramp tests.

- Radial hydrides were observed at the outer rim of the cladding tubes irradiated for 4 and 5 cycles and ramp-tested rods, while no radial hydrides were observed before ramp tests.
- The fractography showed that the fracture surface is composed of three regions. The region near outer surface is strongly brittle, but that of the near inner surface is ductile while the middle region is macroscopically brittle but microscopically the mixture of brittle and ductile features. The width of strongly brittle region is about 50 to 80 micro-meter and that of macroscopically brittle crack is about 700 micro-meter from outer surface.
- Many hydrides perpendicular to the crack were found on both sides of the crack.
- Small hydrides along crack propagation direction were observed at the crack tip.
  Estimated failure mechanism by axial crack is as follows.
- Hydrogen contents in the cladding tubes increased with burnup and exceeded solubility limits during base irradiation of segment rods.
- During power ramp tests, some hydrogen diffused from inner to outer region in the cladding tube due to temperature gradient. Diffused hydrogen precipitated radially at the outer region due to coupled effects of high hydrogen content and high tensile stress by PCMI.
- Radial hydride was cracked by high stress and/or strain.
- New, small hydride precipitated at the crack tip due to stress concentration and cracked repeatedly.
- When stress exceeded the yield strength of residual cladding thickness, it failed ductilely.

1. INTRODUCTION

Under the sponsorship of the Ministry of Economy, Trade and Industry (METI) , Nuclear Power Engineering Corporation (NUPEC) is carrying out irradiation test program“The Verification Test on BWR High Burnup Fuel" to verify fuel integrity and to study fuel behaviors of the lead use assemblies (LUAs) of high burnup 8 × 8 fuel (BWR Step II Fuel) at high burnup [1], [2].

The time schedule of the program, which includes the power ramp test on irradiated rods and post irradiation examinations (PIEs), is shown in detail in previous paper of the same meeting [3] (Figure 1).

The LUAs of high burnup 8 × 8 fuel were irradiated up to 5 cycles in Fukushima Daini Nuclear Power Station No. 2 Unit. Segment rods were installed in LUAs and used for power ramp tests in Japanese Material Test Reactor (JMTR). PIEs of segment rods were carried out at Nippon Nuclear Fuel Development Co., Ltd. (NFD) before and after ramp tests.

In this paper, characteristics observed through PIEs on failed segment rods during power ramp tests and estimated failure mechanism are presented.

2. OUTLINE OF VERIFICATION TEST

2.1. Test Fuel Assemblies

Detailed description of test fuel assemblies is given in paper [3], including design parameters and fuel rod arrangements (see Fig. 2, [3]). Eight test assemblies, some of which were equipped with segment rods for power ramp tests, were fabricated by Japan Nuclear Fuel Co., Ltd.

2.2. Irradiation

Irradiation history is given in detail in previous paper, see paragraph 2.2 and Fig. 3 in [3].

2.3. Power Ramp Tests

Power ramp tests are described in detail in previous paper including four typical power ramp sequences, see Fig. 4 in [3].

2.4. Post-Irradiation Examination

PIE methodology was described in detail in previous paper [3]. Five assemblies have been examined in the hot laboratory of Nippon Nuclear Fuel Development Co., Ltd. (NFD) and detailed PIE data were systematically obtained. Segment rods were dismantled from the assemblies and examined non-destructively at NFD before the power ramp test. After the power ramp test, both non-destructive and destructive PIEs were carried out.

3. POWER RAMP TEST RESULTS

3.1. Power Ramp Performance

A series of ramp tests for 25 segment rods of burnup ranging from 43 to 61 GWd/t was carried out in JMTR using the Boiling Water Capsule under simulated BWR temperature and pressure conditions. The ramp test results are shown in Figure 11 of previous paper [3] with published data [2, 4, 5]. Five segment rods failed during the power ramp tests. The appearances of failed segment rods are shown in Photo 1. One segment rod irradiated for 3 cycles failed at RTP of 610 W/cm by PCI/SCC mechanism, while four segment rods irradiated for 4 and 5 cycles failed at about 550 and 420 W/cm respectively and had axial cracks starting from the outer surface of cladding tubes.

3.2. Results of Post Irradiation Examination

Following characteristics on failed segment rods were observed through detailed PIEs before and after ramp tests.

The cross-sectional micrographs at four elevations of the through wall crack of the segment rod irradiated for 5 cycles are shown in Photo 2. The shape of cross section near the center of the axial crack is perpendicular to the outer surface of the cladding tube and the failure mode is strongly brittle. At the upper part of the crack, there is a small brittle portion in the outer rim of the cladding tube and a large ductile area in the middle part.

Radial hydrides are observed at the outer rim of the cladding tubes in Photo 3 of which was taken from the failed segment rod during power ramp test after 5 cycles irradiation. The length of radial hydrides is about 70 micro-meter. These radial-oriented hydrides were observed on all rods failed by ramp-tests after 4 and 5 cycle irradiations, and the length of the hydrides depended on RTP. No radial-oriented hydrides were found on rods before ramp tests.

Photo 4 shows the fractography of the crack taken by SEM. The fracture surface is composed of three regions. The region near outer surface is strongly brittle, but that of the near inner surface is ductile while the middle region is macroscopically brittle but microscopically the mixture of brittle and ductile features. The width of strongly brittle region is about 50 to 80 micro-meter and that of macroscopically brittle crack is about 700 micro-meter from outer surface. The width of strongly brittle region is close to the length of radial hydrides at the outer rim of the cladding tubes. In Photo 5 two pairs of the two opposing fracture surface are shown. It is evident that there is a good fit between the two sides of the crack, i.e., a “hill” on one fracture surface corresponds to a “valley” on the matching fracture surface [8].

The cross-sectional micrographs of another crack sample from the segment rod irradiated 5 cycles are shown in Photo 6. There are many hydrides perpendicular to fracture surface. These hydrides are also seen in Photo 3.

In order to get the root cause of the crack from the outer surface of the cladding tube, many metallurgical observations were done, from three different directions, i.e. axial, radial and circumferential directions. Photo 7 shows the view from axial direction at non-penetrated cracks. There are many hydrides perpendicular to the crack on both sides and some hydrides are gathering at the crack tips. There is a small hydride just at the crack tip as shown in Photo 8. View from radial direction close to the cladding outer surface at the axial ends of crack indicates a nest of hydrides at the small crack tip as shown in Photo 9. These photos tell us the crack propagation is strongly connected with hydrides gathering at the crack tip.

4. FAILURE MECHANISM [6-8]

Estimated failure mechanism by axial crack is as follows.

1) Hydrogen contents in the cladding tubes increased with burnup as shown in Figure 6 of previous paper [3] and exceeded solubility limits of cladding material after 4 and 5 cycle of base irradiations. Photo 10 shows the distribution of hydride in the cladding tubes irradiated 4 and 5 cycles. In the outer region of the cladding tube there are many circumferentially oriented hydrides. Inner portion of the cladding tube, Zr liner has more hydrides due to lower solubility than Zircaloy-2. Estimated relative hydrogen content

distributions are shown in Figure 1. These hydrogen contents were evaluated using the densities of hydrides in the micro photos.

2) During power ramp tests, some hydrogen diffused from inner to outer region in the cladding tube due to temperature gradient. The distribution of hydrogen solubility limit in the cladding tube is so steep as shown in Figure 2 under power ramp conditions. Diffused hydrogen precipitated radially at the outer region due to the combined effects of relatively lower solubility and high tensile stress in the cladding caused by PCMI.

3) Radial hydride was cracked by high stress or strain by PCMI at first stage of the power ramp.

   This is the initiation of the failure due to crack and the schematic diagram is shown in Figure 3 (1).

4) When initial crack formed in the power ramp test, hydrogen came to the area of stress concentration at the crack tip and small hydride was formed as shown in Photo 7 and Photo 9. These small hydrides at the crack tip cracked and formed "hill" and corresponding "valley" on matching fracture surface as shown in Photo 5 by the stress due to PCMI. Then fresh crack tip is formed as shown in Photo 8.

5) These stress concentration, hydrogen diffusion, hydrogen precipitation and the cracking of hydride repeated and the crack propagated. This is the propagation mechanism of the crack and the schematic diagram is shown in Figure 3 (2).

6) When stress exceeded the yield strength of residual cladding thickness, ductile failure appeared.

5. SUMMARY

In this verification test program, well-characterized LUAs of high burnup 8 × 8 fuel were irradiated in a typical commercial BWR in Japan, Fukushima Daini Nuclear Power Station No. 2 Unit, under normal operational conditions. After each irradiation cycle, detailed PIEs at a hot laboratory and power ramp tests on segment rods, which were installed in LUAs, were carried out.

As the results of these examinations, some segment rods irradiated for 4 and 5 cycles failed at about 550 and 420 W/cm, respectively, during power ramp tests and showed axial cracks initiated at outer surface of cladding tubes.

Estimated failure mechanism by axial crack can be summarized as follows.

- Hydrogen contents in the cladding tubes increased with burnup and exceeded solubility limits during base irradiation of segment rods.

- During power ramp tests, some hydrogen diffused from inner to outer region in the cladding tube due to temperature gradient. Diffused hydrogen precipitated radially at the outer region due to coupled effects of high hydrogen content and high tensile stress by PCMI.

- Radial hydride cracked by high stress and/or strain.

- New, small hydride precipitated at the crack tip due to stress concentration and cracked repeatedly.
- When stress exceeded the yield strength of residual cladding thickness, it failed ductilely.

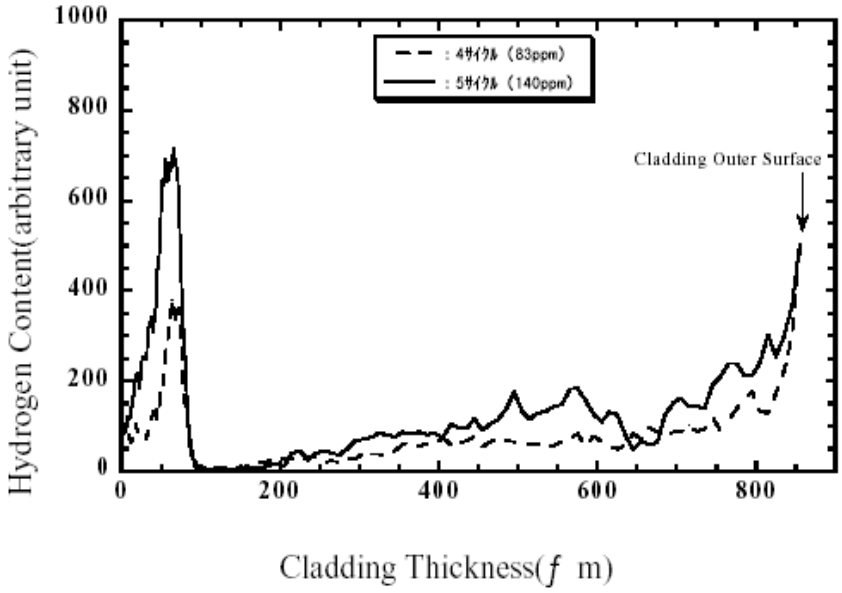

Fig. 1. Hydride Distribution in Cladding after Base Irradiation.

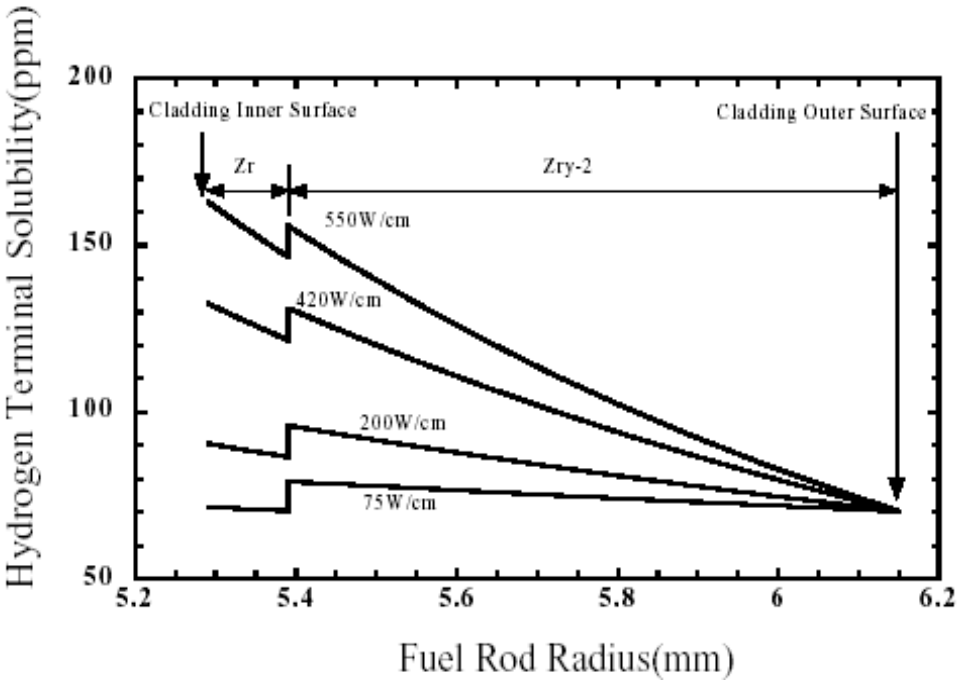

Fig. 2. Hydrogen Solubility Limits in Cladding.

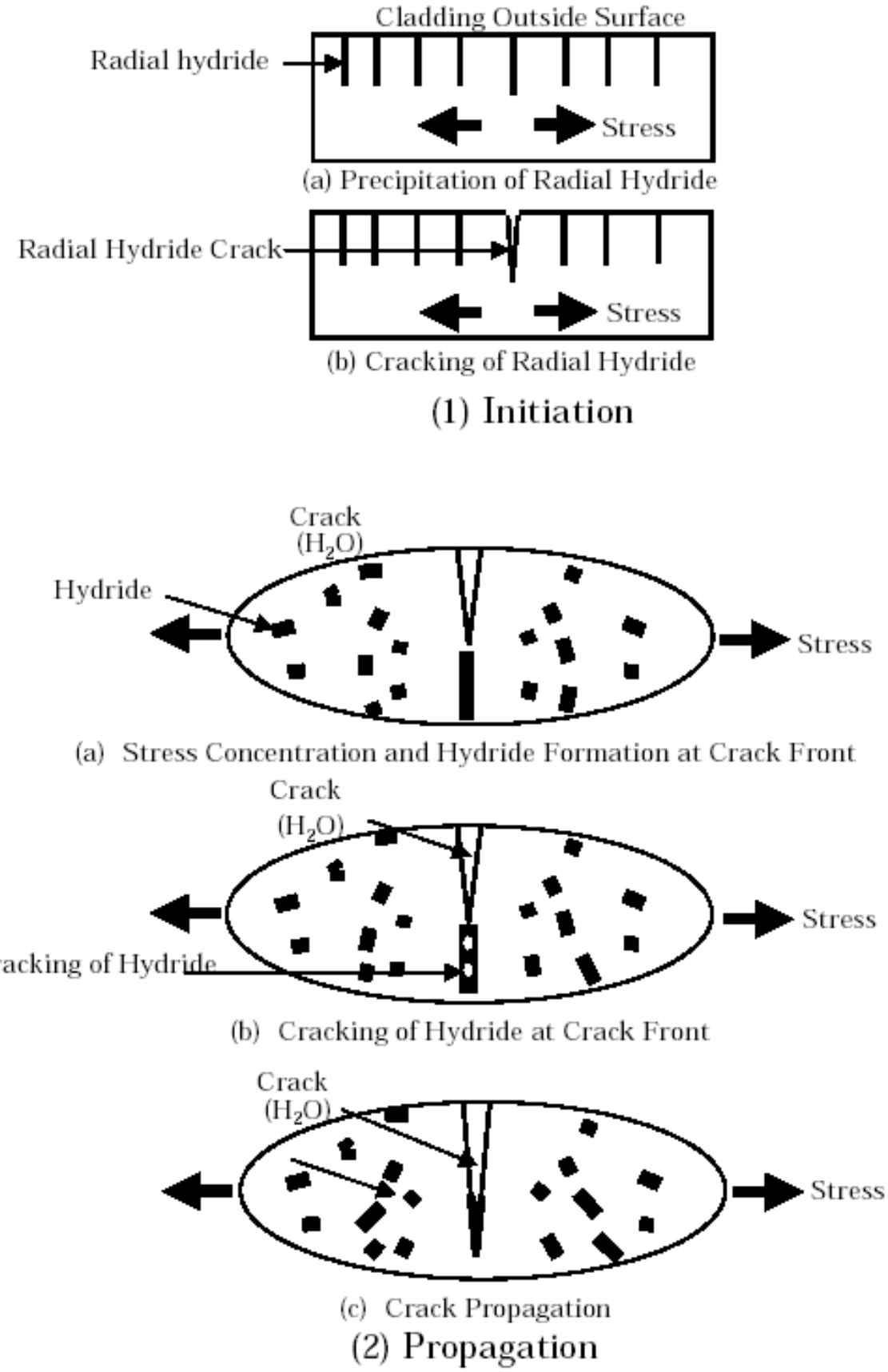

Fig. 3. Schematic Diagram of Crack Initiation and Propagation.

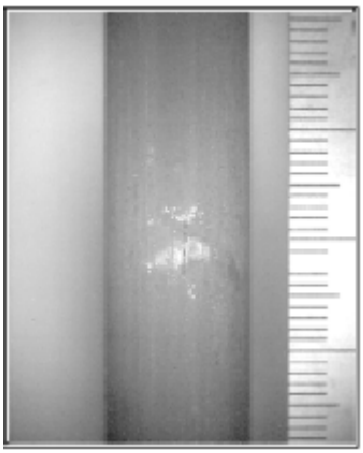

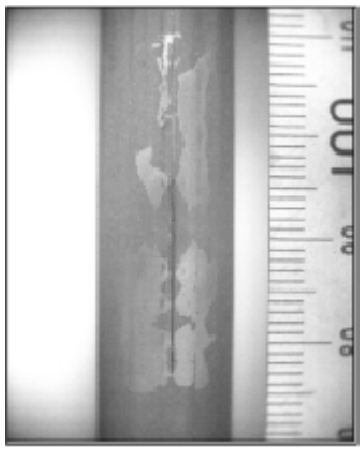

(a) 3 Cycles Irrad.43.4GWd/t
RTP: 614W/cm
Failed after 9min hold

(b) 4 Cycles. Irrad. 56.3GWd/t
RTP: 551W/cm
Failed after 149min hold

(c) 5 Cycles Irrad. 60.8GWd/t
RTP: 446W/cm
Failed after 22min hold

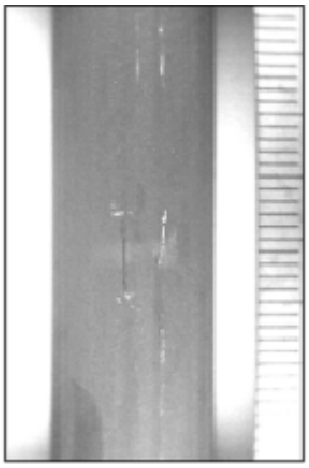

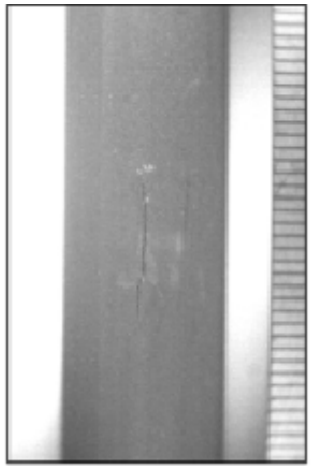

(d) 5Cycles Irrad. 61.1 GWd/t
RTP: 421W/cm
Failed after 100min hold

(e) 5 Cycles Irrad. 61.1GWd.t
RTP: 428W/cm
Failed after 68min hold

Photo 1. Visual Appearances of Failed Segment Rods.

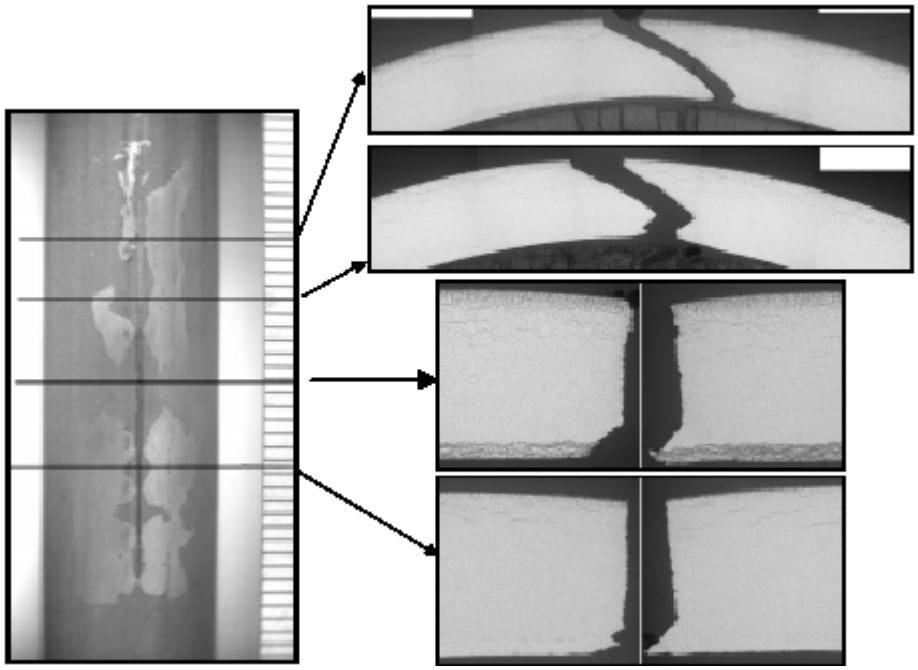

Photo.2. Visual Appearance and Cross Sectional Metallography of Failed Segment Rod (5 Cycles Irrad., RTP: 446W/cm, Failed after 22min hold).

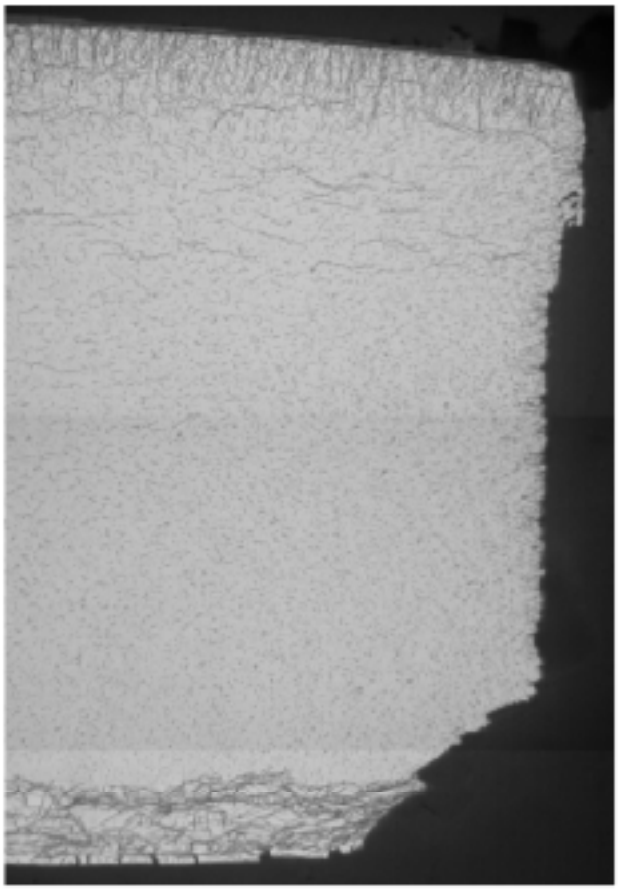

Photo 3. Hydride Distribution in Cladding of Failed Segment Rod (5 Cycles Irrad., RTP: 446W/cm, Failed after 22min hold).

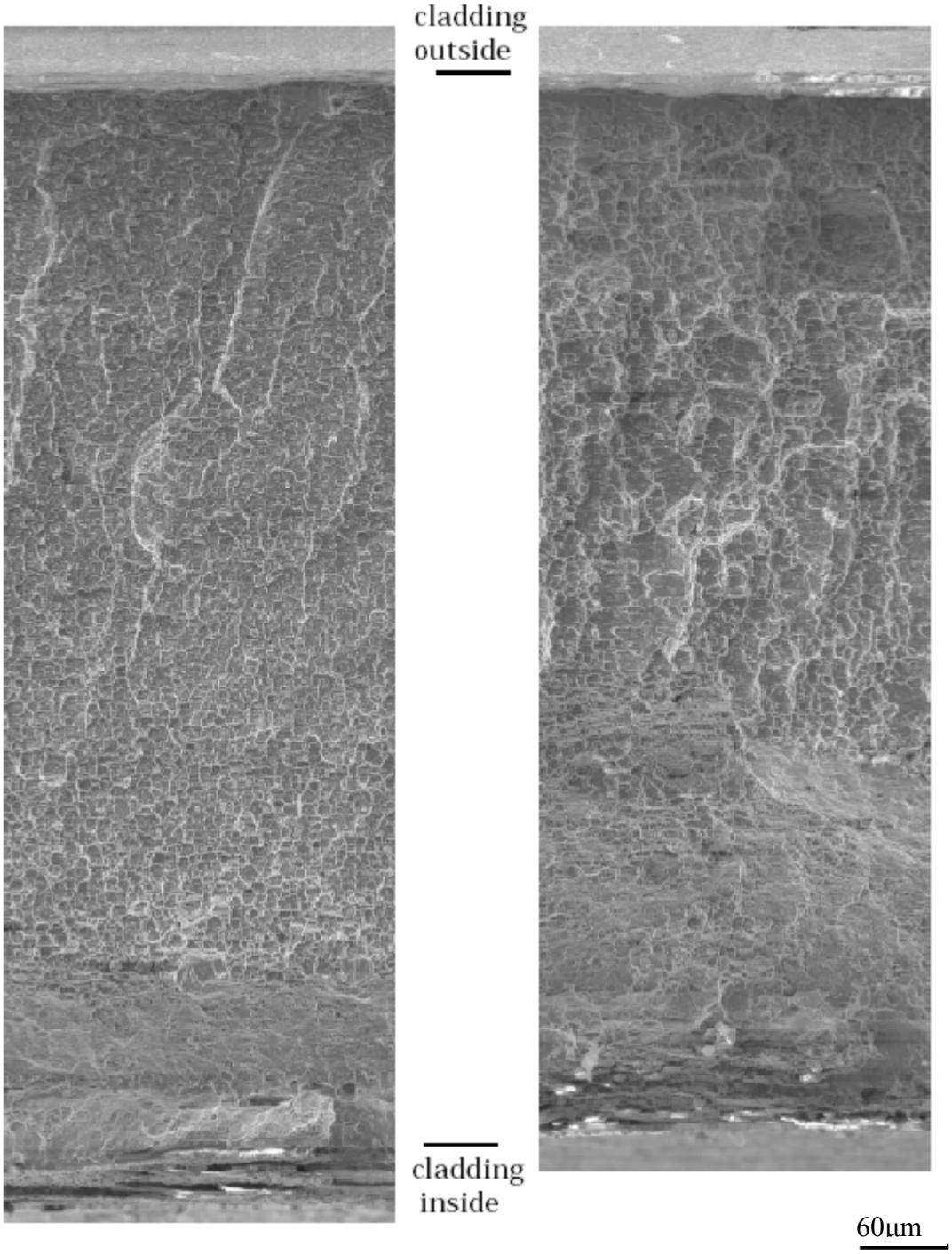

Photo 4. SEM Images of Fracture Surfaces (5 Cycles Irrad., RTP: 446W/cm, Failed after 22min hold).

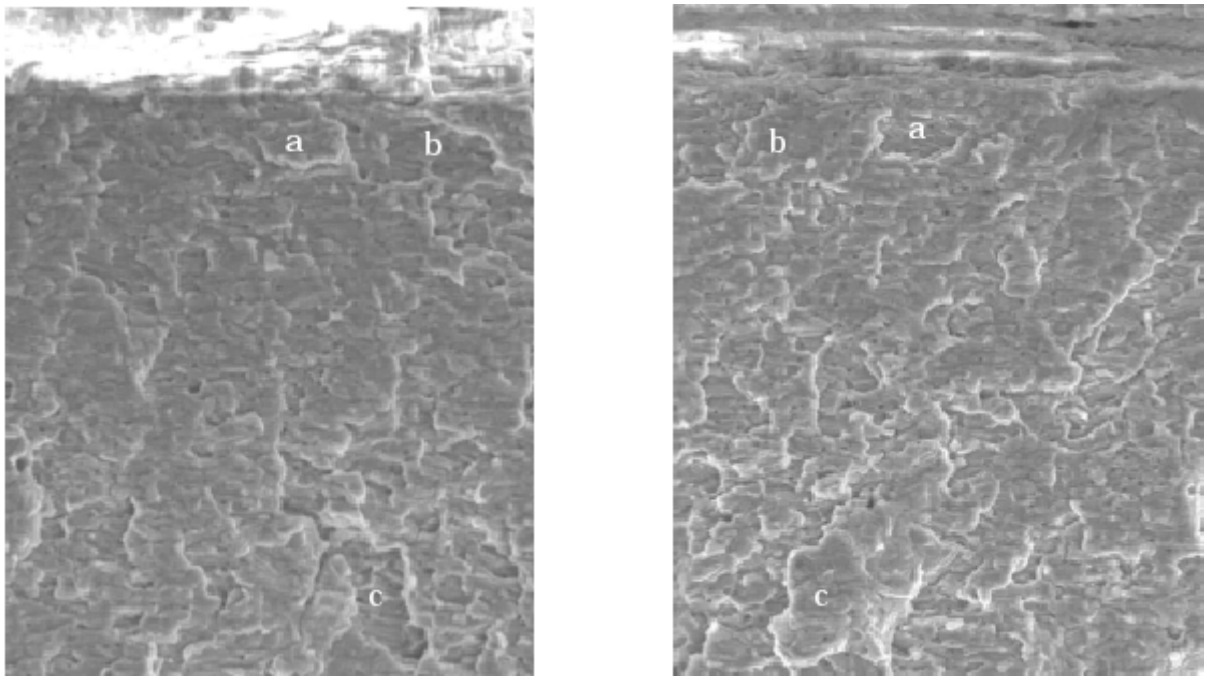

(a) close to the cladding outer surface

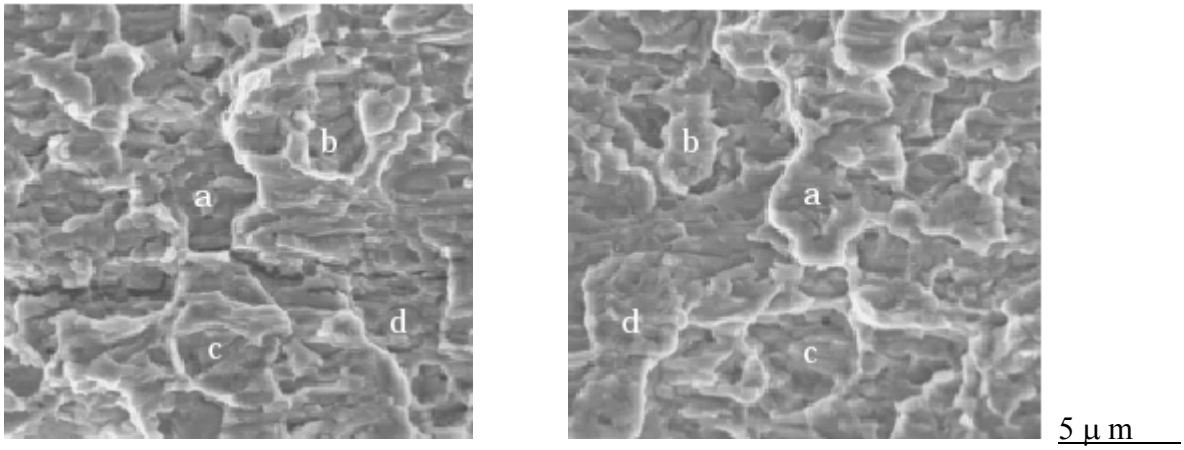

(b) about 120 μ m inside from the cladding outer surface

Photo 5. SEM Images of two Matching Fracture Surfaces. (5 Cycles Irrad., RTP: 421W/cm, Failed after 100min hold)

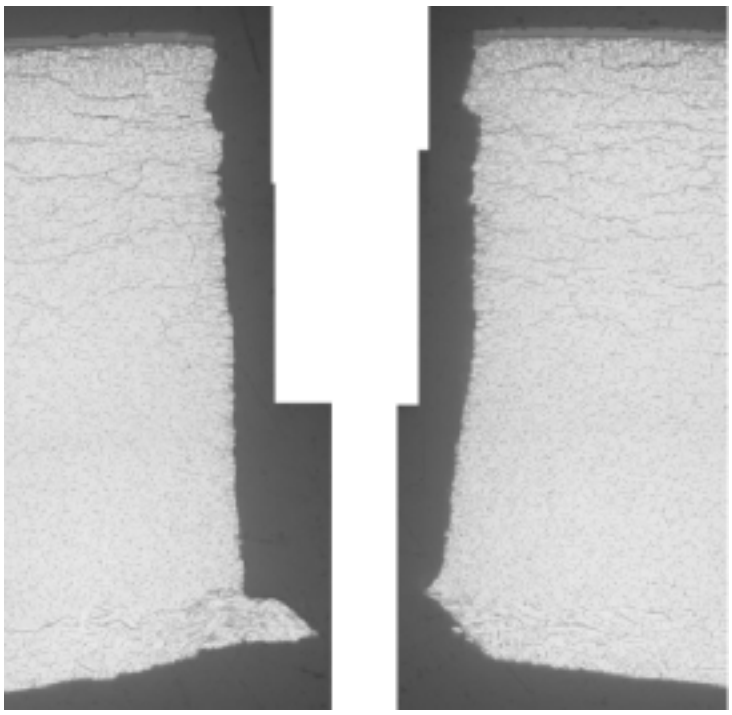

Photo 6. Hydride Metallography at the Crack.

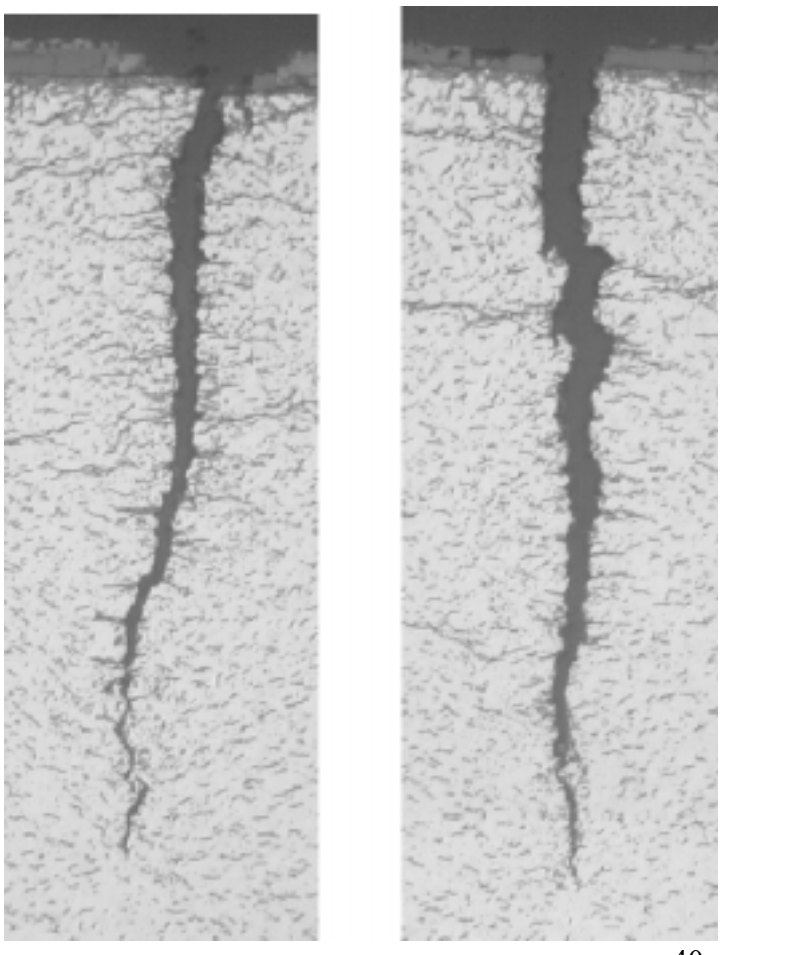

Photo 7. Hydride Distribution at Non Penetrated Cracks.

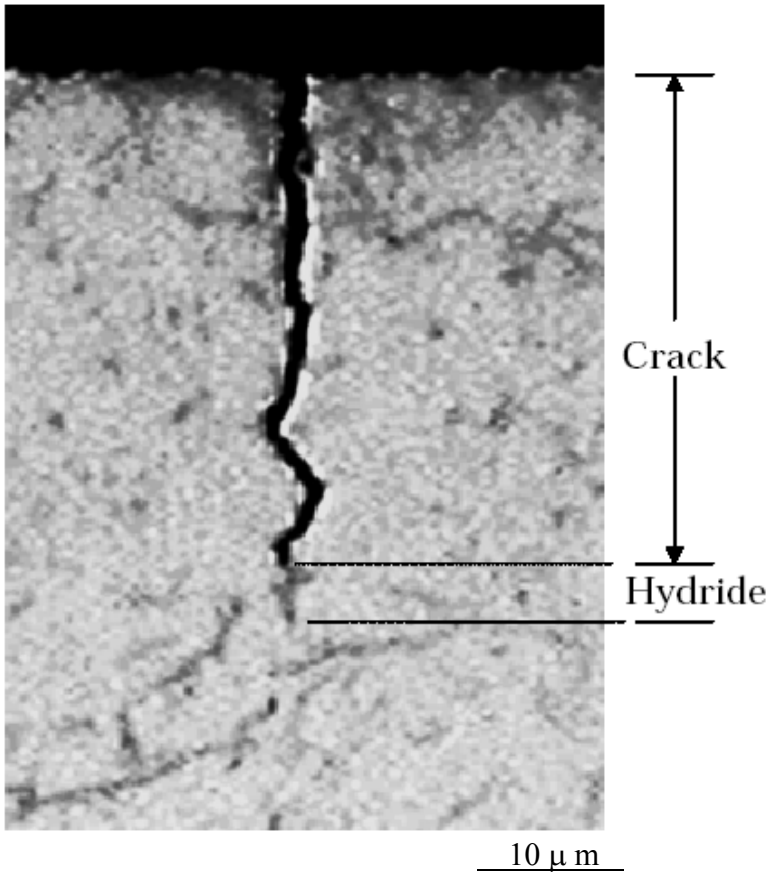

Photo 8. Hydride Observed at Crack Tip (Radial Cross Section).

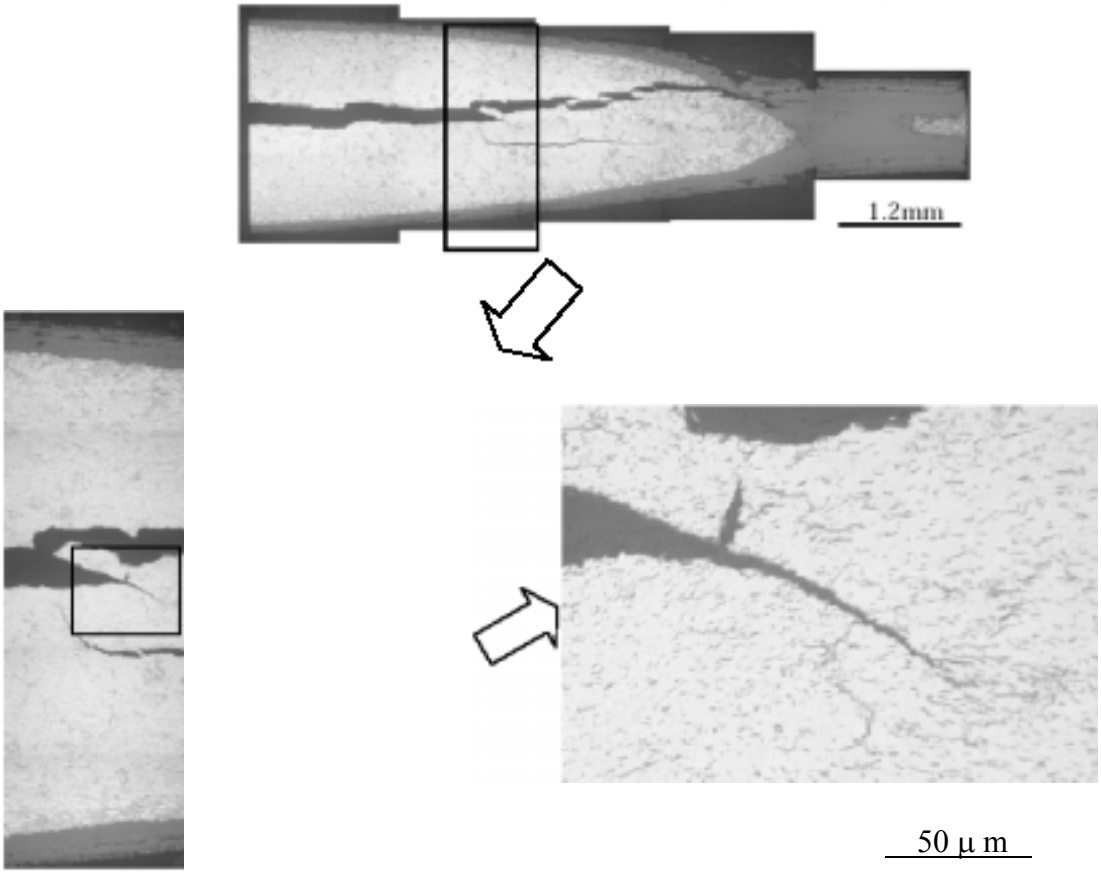

Photo 9. Hydride Observed at Crack Tip (Tangential Cross Section).

Base Irradiated Fuel Rod

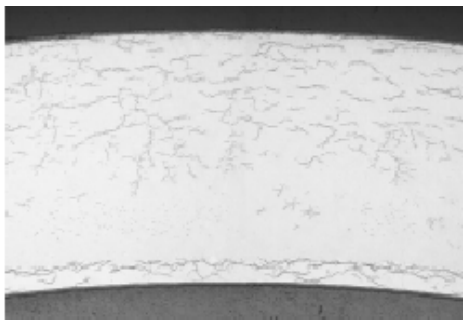

(4 Cycles Irrad.; 56.0GWd/t 67ppm H_2)

Base Irradiated Segment Rod

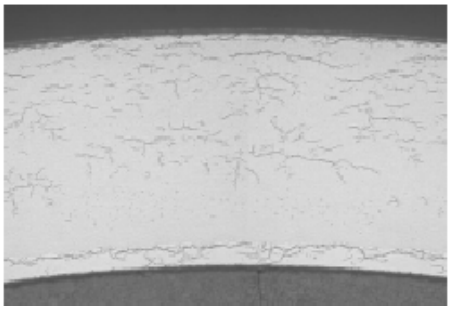

(4 Cycles Irrad.; 56.5GWd/t 82ppm H_2)

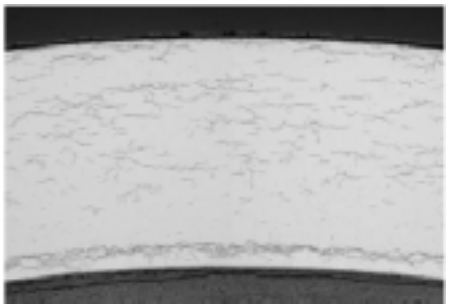

(5 Cycles Irrad.; 59.9GWd/t 76ppm H_2)

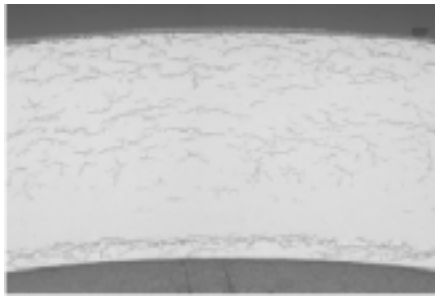

(5 Cycles Irrad.; 56GWd/t 122ppm H_2)

Photo 10. Hydride Distribution in Cladding of Base Irradiated Fuel Rod and Segment Rod.

ACKNOWLEDGEMENTS

This study was carried out mainly under the direction of committees of NUPEC. The authors wish to express their gratitude to the members of the “Committee of Verification Tests on High Burnup Fuel", especially Dr. T. Okubo and Dr. M. Yamawaki for their discussions and evaluations with respect to this program. The authors also gratefully acknowledge METI for the sponsorship on this project.

REFERENCES

[1] KUROSU, T., et al., “Verification Test Program of High Burnup Fuel", Japan-Russia Experts Meeting on Power Reactor Fuels, held in Tokyo, Japan, 19-21 September (1994).
[2] HAYASHI, H., et al., “Irradiation Characteristics of BWR Step II Lead Use Assemblies", Proc. 1997 ANS Int. Mtg. on LWR Fuel Performance, Portland, Oregon, (1997), 296.
[3] HAYASHI, H., ETOH, Y., TSUKUDA, Y., SHOMADA, S., SAKURAI, H., “Power ramp Tests of High Burnup BWR Segment Rods”, in Proc. of the same meeting.
[4] SAKURAI, H., et al., “Irradiation Characteristics of High Burnup BWR Fuels”, Proc. 2000 ANS Int. Mtg. on LWR Fuel Performance, Park City, Utah, (2001), 151.
[5] OHARA,H., et al.,“Fuel Behavior During Power Ramp Tests", Proc. 1994 Int. Topical Mtg. on LWR Fuel Performance, West Palm Beach, Fl, (1994).

[6] SCHRIRE, D., et al., “Secondary Defect Behavior in ABB BWR Fuel”, Proc. 1994 Int. Topical Mtg. on LWR Fuel Performance, West Palm Beach, Fl, (1994) 338.
[7] SCHRIRE, D., et al., “Testing Cladding Integrity at High Burnup”, IAEA Tec. Committee Mtg., Nyköping, Sweden, (1998).
[8] LYSELL, G., et.al., “Axial Splits in Failed BWR Fuel Rods”, Proc. 2000 ANS Int. Mtg. on LWR Fuel Performance, Park City, Utah, (2001), 216.

THE SCANAIR CODE VERSION 3.2: MAIN FEATURES AND STATUS OF QUALIFICATION

E. FEDERICI*, F. LAMARE, V. BESSIRON, J. PAPIN
Institut de Protection et de Sûreté Nucléaire (IPSN),
CE-Cadarache,
DRS/SEMAR,
Saint Paul lez Durance, France

Abstract

The SCANAIR code is developed in order to describe the thermo-mechanical behavior of highly irradiated PWR fuel rods under Reactivity-Initiated Accident (RIA). The main features of the newly delivered version of the code (version 3.2) are presented. Zircaloy-4 cladding mechanical properties have been updated with the results of tests performed in the frame of the PROMETRA program. Fuel-cladding gap thermal conductance modeling, and its behavior at high temperature and large contact pressure, is presented. Current features of the fission gas behavior modeling are described. Then, the status of the physical qualification of the code is given, and focuses on the cladding-related mechanical behavior (cladding hoop strain and transient elongation), and on the fission gas release. Finally, the planned evolution of the code is outlined.

1. INTRODUCTION

The SCANAIR code is developed by the French "Institut de Protection et de Sûreté Nucléaire" (IPSN), in collaboration with "Electricité de France" (EDF) in the frame of the CABRI PWR program. Its objective is the description of the thermo-mechanical behavior of highly irradiated PWR rods (including UO_2 and MOX fuels) under Reactivity Initiated Accident (RIA) (Ref. 1, Ref. 2, Ref. 3).

The code is able to take into account the following physical phenomena and their strong coupling occurring during rapid transients: thermal dynamics including clad-to-coolant heat transfer modeling in sodium or water conditions, structural mechanics for the rod constitutive elements, and fission gas (FG) transient behavior.

In this paper, the main new improvements of the latest version of the code (version 3.2) will be reviewed. Then, the status of qualification, performed thanks to experimental results obtained in the French reactor CABRI, will be given. Finally, the planned evolution of the code will be presented.

* *Corresponding author:* eric.federici@ipsn.fr

2. MAIN FEATURES

2.1. Structural mechanics: update of cladding mechanical properties

In this part, we are interested in obtaining the mechanical properties of "sound" irradiated Zircaloy-4 (i.e. corroded, but with no significant hydrided layer): ultimate tensile strength (UTS) and total elongation (TE).

A selection has been made among the IPSN data base related to the compilation of available mechanical tests performed in the frame of the PROMETRA program (Ref. 4), in order to remove tests performed on non-irradiated cladding, and to keep only tests performed on standard and low tin Zircaloy-4.

The UTS results show little anisotropy from the values obtained in hoop or axial tensile tests (i.e. the differences lie in the point scatter); so both types of data have been used to fit a UTS law, taking into account temperature and strain rate dependencies.

The analytical adjustment (see Fig. 1) shows a slight "strain rate" hardening: UTS values are higher for higher strain rates. However, the difference resulting from the use of both strain rates (10^{-2} s^{-1} and 5 s^{-1}) in the analytical law, although qualitatively correct, is not statistically significant (less than 2σ). Thus, only a temperature dependency can be taken into account for use in computer codes.

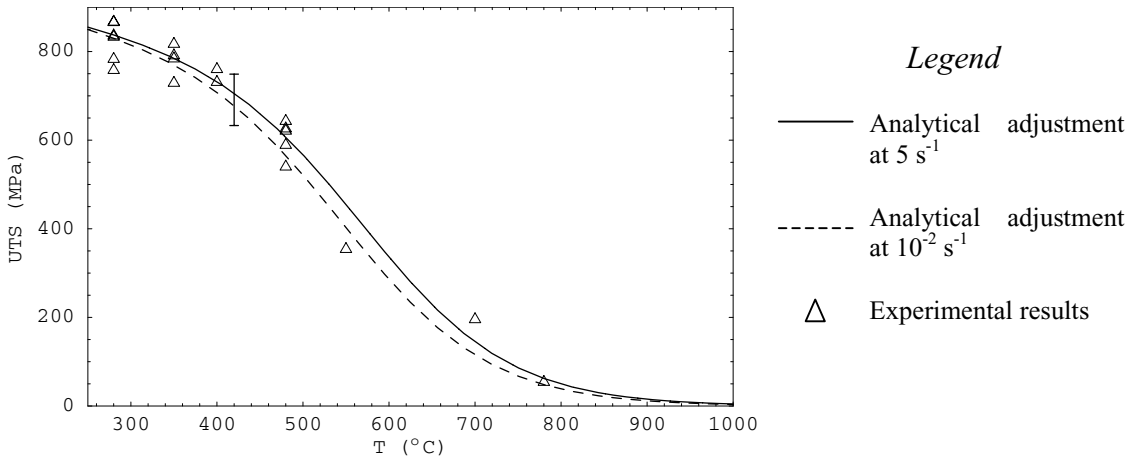

Fig. 1. Irradiated Zircaloy-4 UTS law versus temperature.

The PROMETRA hoop tensile tests have been carried out up to the failure of the samples. However, the obtained failure modes are not representative of the ones observed in RIA conditions such as observed in the CABRI REP Na tests for instance. In effect, hoop tests between 150 and 400 °C usually show a typical failure mode in a plane at 45 ° from the axial direction (above 600 °C, a necking appears) while in RIA conditions, failures along the axial direction have been observed, e.g. in the CABRI REP Na-8 test (Ref. 5).

New studies are currently under way worldwide to elaborate new designed specimens in order to better simulate the actual mechanical loading of the cladding during the transient. A new type of specimen has been proposed by the Penn State University (Ref. 6). It leads to a state of plane deformation in approximately a 2 mm range across

the gauge width. However, up to now, only tests on non-irradiated specimens have been conducted. Thus, as a first guess for the TE values (to be used for failure criteria calculations), the results from the PROMETRA program on standard geometry ring specimens have been used to derive a first law depending on temperature and strain rate. This law will be corrected gradually when the results obtained on Penn State geometry specimens are available (Ref. 7).

From the Fig. 2 showing TE values at 10^{-2} s^{-1} and 5 s^{-1} obtained from tests performed on PROMETRA ring specimens, it is clear that the strain rate plays an important role. At high strain rate, TE values are relatively low (~17%) and seem independent of the temperature. At low strain rate, TE values are higher (about 2.5 times higher at 480 °C), and seem to vary quadratically with temperature.

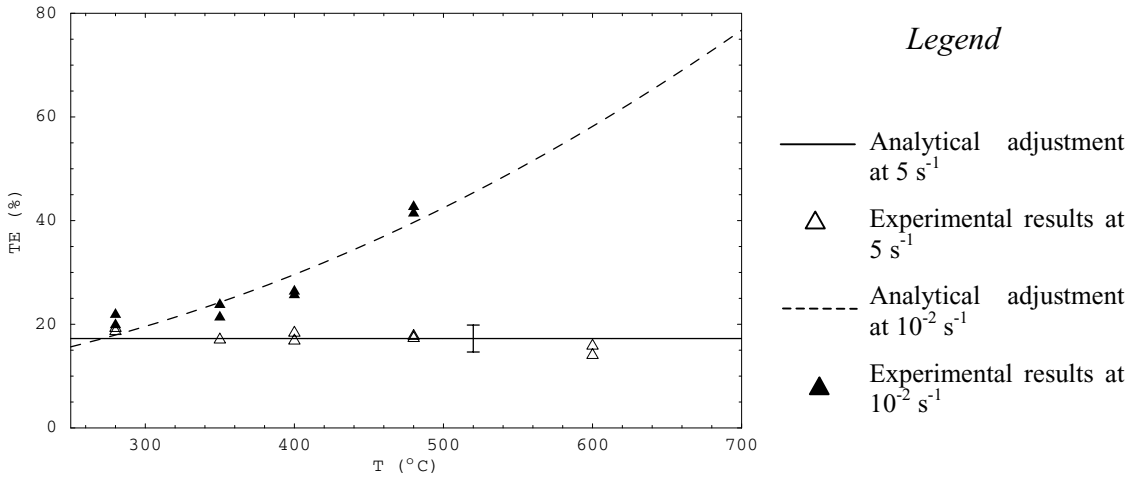

Fig. 2. Zircaloy-4 TE values from the PROMETRA tests on ring specimens.

However, in the frame of the proposed approach, two remarks have to be taken into account:

- the tests performed on Penn State geometry specimens will validate or invalidate the strain-rate effect on TE values deduced from the tests performed on PROMETRA standard ring specimens,
- if the strain-rate influence is confirmed, the prediction of the failure of the cladding in RIA transients will require measurements at another strain rate; a strain rate lower than 5 s^{-1} but still close to the one reached during a RIA would be suitable, typically 0.5 or 1 s^{-1}.

2.2. Thermal dynamics: calculation of the fuel-cladding gap thermal conductance

A solid-solid conductance term (Ref. 8) has been added into the fuel-clad heat exchange coefficient, which was previously composed of a gaseous thermal conduction term and a radiation term. The use of such a contribution is necessary in order to get a better estimation of heat exchanges between fuel and cladding at high temperatures, when materials become softer and tend to crush the residual gaseous volumes linked to

the surface roughness of the materials, and also at high contact pressures that could be reached during highly energetic power pulses.

The key parameter of this modeling that controls the magnitude of the solid-solid contact contribution is the ratio of the contact pressure over the hardness of the softest material. Presently the experimental Meyer hardness values are available for non-irradiated cladding (Ref. 9), but irradiation tends to harden the material and thus to increase its hardness. An estimation of the hardness of irradiated Zircaloy-4 can be deduced from the relationship between the hardness (H) and the yield strength (YS), valid for materials that do not strain-harden: $H = 3 \times YS$ (Ref. 10).

Fig. 3 shows the comparison between the hardness of the irradiated Zircaloy-4 cladding, as deduced from the use of the previous theoretical relationship, and experimental values obtained on non-irradiated material (Ref. 9).

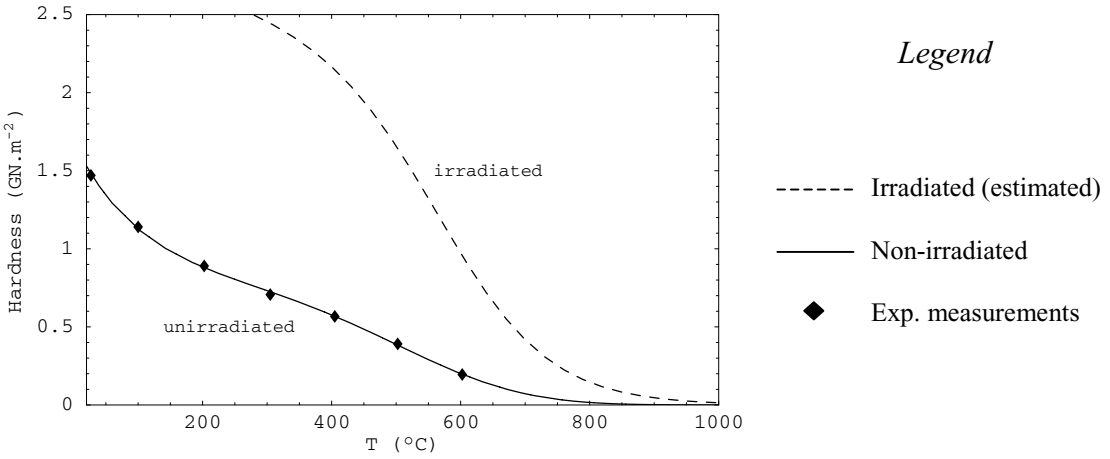

Fig. 3. Zircaloy-4 hardness.

At high temperatures, the cladding hardness tends towards zero. UO_2 hardness has a similar behavior: it starts from a relatively large value at room temperature (about 8 $GN.m^{-2}$, Ref. 11), and decreases rapidly with temperature (about 1 $GN.m^{-2}$ at 650 °C, Ref. 11). Thus, as the temperature increases, the contact between the two materials improves, and the difference between the two surface temperatures decreases.

In the CABRI REP Na tests, due to the high thermal conductivity of the sodium that insures a good coolability of the cladding, the maximum inner temperature of the cladding is of the order of 600–850 °C, depending on the test case. However, in the future Water Loop tests (Ref. 12), after the occurrence of the DNB, higher clad temperatures are expected, and due to a lack of available experimental data of hardness values in this range of temperature, it could be necessary to assume a perfect thermal contact between fuel and cladding (i.e. an infinite thermal conductance) in order to better evaluate the temperatures in this case.

Fig. 4 shows the result of the calculation of the heat flux between fuel and cladding at peak power node (PPN) versus time, for the CABRI REP Na-5 test (see Ref. 13 and Table I). This test uses a short power pulse (pulse width: 9 ms), and has a relatively high linear power (about 220 $kW.cm^{-1}$ at maximum, also shown in Fig. 4). In this case,

the solid-solid contact contribution to the total heat flux amounts to about 15% as a maximum value. One can also see clearly the beginning of fission gas (FG) release to the free volumes (at ~0.075 s), and the subsequent sharp decrease in the heat flux, due to the drop of the average gaseous thermal conductivity in the gap.

In the case of REP Na-5, the effect of the use of the solid-solid contact contribution in the heat exchange calculation between fuel and cladding leads to an increase of 20 °C in the maximum clad temperature, 5 °C in the maximum sodium temperature, and a decrease of 18 °C in the maximum fuel temperature.

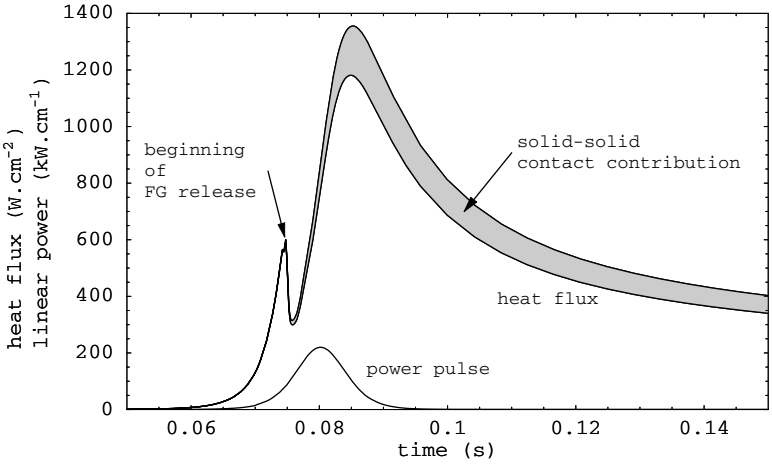

Fig. 4. Fuel-cladding heat flux at PPN in the CABRI REP Na-5 test.

2.3. Fission gas behavior: status of the current modeling

Based on the interpretation of experiments performed in CABRI and NSRR reactors on UO_2 and MOX fuels under RIA transients (Ref. 13 and Ref. 14), it has been suggested that the grain boundary (GB) gases play an important role, both in the fission gas release and on the cladding mechanical loading during the transient.

The grain boundary gases are composed of gases in the fuel porosities (coming from the fabrication of the fuel or developed during irradiation, such as the rim porosity) and gases in intergranular bubbles, coming from the diffusion of intragranular gases towards the grain edge.

The assumed mechanism is as follows. Due to the rapid energy deposit and to the burnup radial profile inside the fuel, a peaked temperature profile towards the edge of the pellet arises, and tends to over-pressurize the gas bubbles. At the grain scale, the most significant effect is that a tensile stress is being developed on the grain boundary surface (between the intergranular bubbles) that can lead to the grain boundary opening if the grain boundary rupture stress is reached (see Fig. 5).

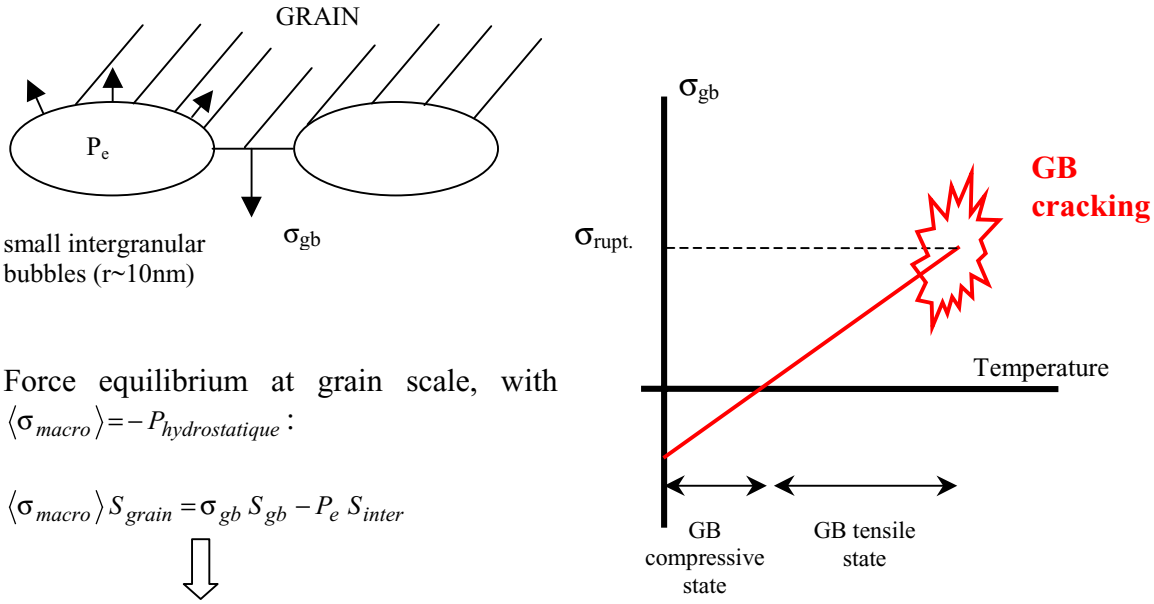

Force equilibrium at grain scale, with $\langle \sigma_{macro} \rangle = -P_{hydrostatique}$:

$$\langle \sigma_{macro} \rangle S_{grain} = \sigma_{gb} S_{gb} - P_e S_{inter}$$

$$\Downarrow$$

$$\sigma_{gb} = \frac{S_{inter}}{S_{gb}} P_e + \frac{S_{grain}}{S_{gb}} \langle \sigma_{macro} \rangle$$

>0 **<0**

Fig. 5. Grain boundary opening mechanism.

The opening of the grain boundaries leads to the linkage of the gases in intergranular bubbles and in the porosities. A large fuel expansion can occur if pressure equilibrium is assumed between these gases and the fuel hydrostatic pressure (justified by the grain boundary cracking), and can result in an increase of the cladding mechanical loading, if the resulting pressure is sufficient. This effect is enhanced in high burn-up UO_2 fuels by the presence of a large amount of gas in the rim porosity, and also in highly irradiated MOX fuels with important fission gas retention and porosity in the $UPuO_2$ agglomerates.

After the grain boundary opening, a flow of gases towards the free volume is possible, and is presently modeled in SCANAIR by a Darcy law (the gas velocity is proportional to the pressure gradient) with a constant permeability. Fig. 6 illustrates some results of this modeling on the CABRI REP Na-5 test at PPN, at the end of the test. Here is shown the radial distribution of the grain boundary gases between released gas (from open porosities towards the free volume) and retained gas (in open or closed porosities). The proportion of released gases increases with the pellet radius, but outside the rim zone, most of the GB gases are still retained inside the fuel (maximum fraction of GB released gas on the order of 30%). In the rim zone, the proportion of released gases increases sharply, and the maximum value of GB released gases reaches about 85% at the edge of the pellet. This modeling is currently being qualified through experiments to be performed in the ADAGIO facility (Ref. 15).

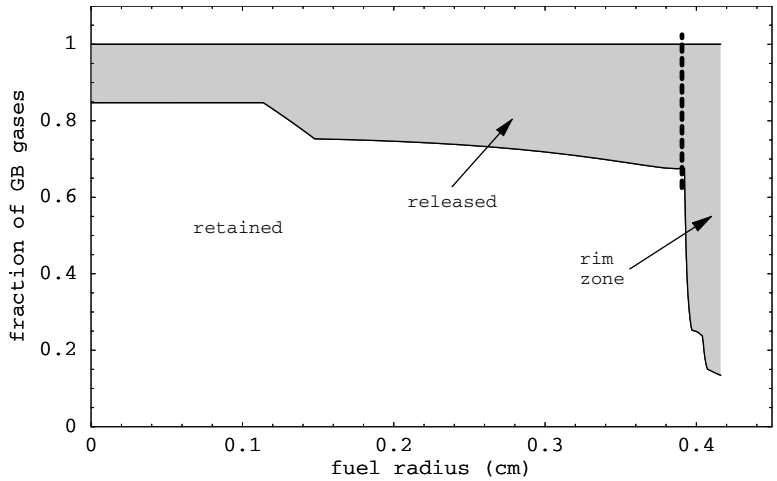

Fig. 6. Distribution of GB gases between retained part and released part in the CABRI REP Na-5 test.

3. STATUS OF QUALIFICATION

3.1. Introduction

The physical qualification of the SCANAIR code is performed, thanks to the available experimental results of the tests performed in CABRI and NSRR reactors. In this part, we will show results obtained on the following tests performed on irradiated fuels with non-spalled Zircaloy-4 cladding: UO_2 tests CABRI REP Na-3, 4 and 5, and MOX tests CABRI REP Na-9, 6 and 7.

The main characteristics of these tests are summarized in Table I and Table II (Ref. 13). We will focus on the comparison between calculated results and experimental measurements on the cladding deformation (maximum plastic hoop strain and transient elongation) and on total fission gas release.

Concerning the MOX test CABRI REP Na-7 which led to rod failure, an estimation of the axially averaged total hoop strain, including thermal strain of the cladding, is available from a preliminary study of the sodium flow-meter measurements, just before failure (approach based on the integration of displaced sodium volume and taking into account the sodium thermal dilatation). The corresponding calculated value given by SCANAIR (i.e. axially averaged total hoop strain at time of failure) is used in the comparison to this result.

Test Characteristics		REP Na-3	REP Na-4	REP Na-5
Max. burnup	$GWd.tM^{-1}$	52.8	62.3	64.3
Corrosion thickness(1)	μm	40	80	20
Energy deposit(2)	$J.g^{-1}$ ($cal.g^{-1}$)	502 (120)	404 (96)	439 (105)
Pulse width	ms	9.5	64	9
Calculated peak fuel enthalpy(3)	$J.g^{-1}$ ($cal.g^{-1}$)	523 (125)	414 (99)	481 (115)
Clad max. plastic hoop strain	%	2.1	0.37	1.11
Fission gas release	%	13.7	8.3	15.1

(1): maximum value, (2): for fast ramps at 0.4 s, for slow ramps at 1.2 s, (3): radially averaged.

Table I. CABRI UO_2 tests REP Na-3, 4 and 5 characteristics.

Test Characteristics		REP Na-9	REP Na-6	REP Na-7
Max. burnup	$GWd.tM^{-1}$	28	47	55
Corrosion thickness(1)	μm	20	35	40
Energy deposit	$J.g^{-1}$ ($cal.g^{-1}$)	1007 (241)	691 (165)	720 (172)
Pulse width	ms	34	35	40
Calculated peak fuel enthalpy(4)	$J.g^{-1}$ ($cal.g^{-1}$)	879 (210)	620 (148)	490(2) (117(2))
Clad max. plastic hoop strain	%	7.4	2.5	1.6(2), (3)
Fission gas release	%	33.3	21.6	**-failure** **-fuel dispersal** **-pressure peaks**

(1): maximum value, (2): at time of failure, (3): axially averaged total hoop strain, (4): radially averaged.

Table II. CABRI MOX tests REP Na-9, 6 and 7 characteristics.

3.2. Cladding hoop strain

Fig. 7 shows a very good agreement between the measured and calculated values of the cladding plastic hoop strains at PPN, both on UO_2 and MOX fuels. One can particularly note that the large value of the cladding deformation reached in the MOX test REP Na-9 and the cladding deformation just before failure in REP Na-7 are well reproduced.

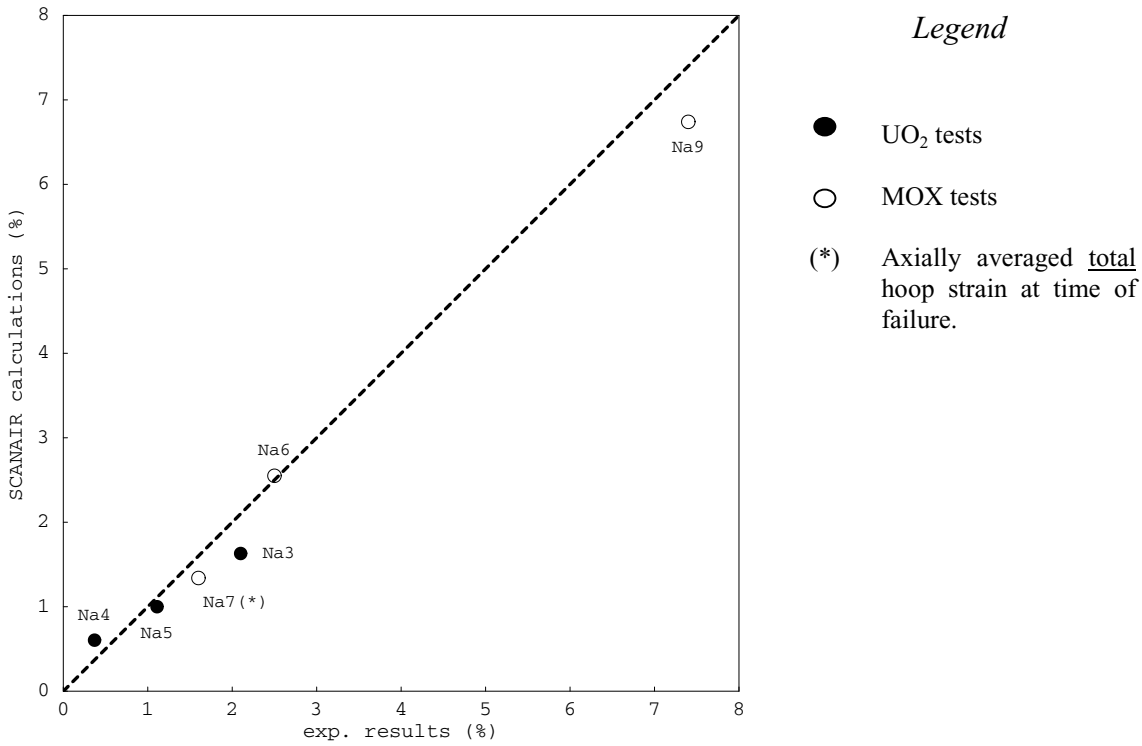

Fig. 7. Comparison between calculated and measured maximum cladding plastic hoop strain in some UO_2 and MOX CABRI tests.

Other experimental data are used to assess the qualification of the modeling, and particularly the cladding-related mechanical results. Among them, the on-line measurements of the cladding elongation in CABRI are useful.

In Fig. 8, one can see the comparison between the calculated cladding elongation during the transient and the experimental on-line measurement. The range of experimental results shown on the figure (shaded area) is obtained by taking or not into account a deconvolution process from the rough signal. The comparison with the SCANAIR results gives some interesting conclusion. The beginning of the increase of the cladding elongation starts at the same time than the measurement and with the same magnitude, thus confirming the modeling assumption that as soon as the fuel-cladding gap closes, there is a non-slipping contact between the fuel and the cladding (standard option of SCANAIR). This assumption seems to be valid all along the duration of the pulse (apart from the region close to 0.1 s, where the overshoot in the deconvoluated signal is not to be taken into account), and the longer term calculated value of the cladding elongation (close to 6 mm at ~0.3 s) is in good agreement with the measurement.

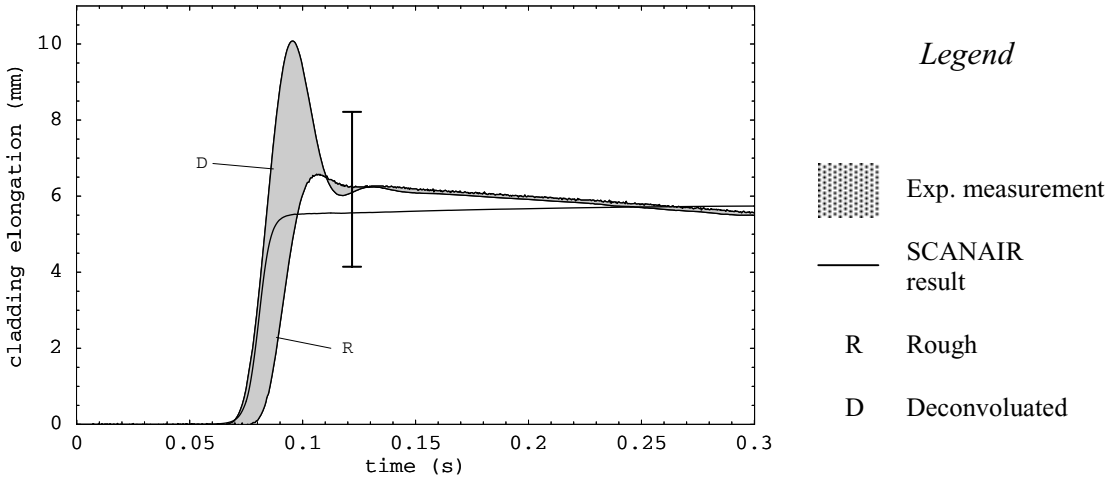

Fig. 8. CABRI REP Na-5 cladding elongation. Comparison between experimental measurements and calculation.

3.3. Fission gas release

Fig. 9 shows the result of the comparison between the calculated and measured fission gas release in some UO_2 and MOX CABRI tests. It is to be recalled that the calculated results depend on some input parameters and modeling hypotheses whose qualification is in progress.

First of all, the initial state of the gases before the transient (resulting from the base irradiation), and particularly the distribution between intragranular gas, intergranular gas and gas in the porosities are given by an irradiation code. Then, the release during the transient depends on the modeling of the opening of the grain boundaries (see §2.3) and also on the way the FG migrate from the open porosities towards the free volume (mechanism presently controlled by the fuel permeability).

The Fig. 9 shows best-estimate results of the final FG release. However, it is also important to estimate correctly the fission gas release kinetics, used in the calculation of the heat transfer between fuel and cladding and of the cladding mechanical loading by gas pressure. The physical qualification of this part of the modeling will use results from tests planned in the French SILENE reactor (see §4).

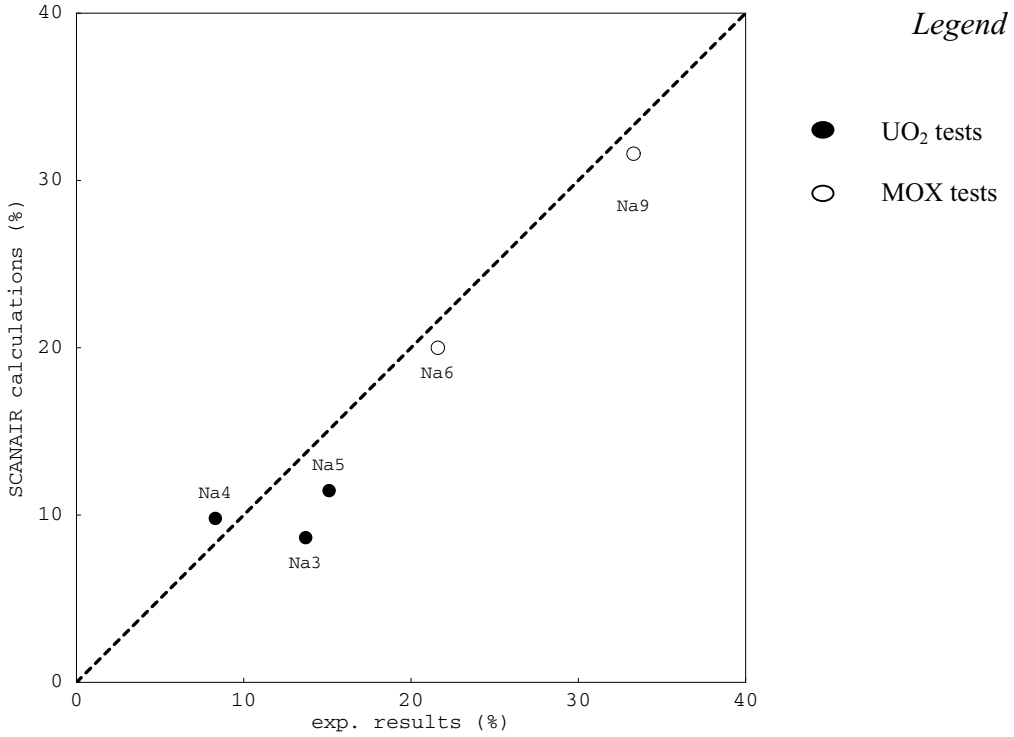

Fig. 9. Comparison between calculated and measured fission gas release in some UO_2 and MOX CABRI tests.

4. PLANNED EVOLUTION OF THE SCANAIR CODE

The mid-term planned evolution of the SCANAIR code is now oriented consistently with the new CABRI Water Loop Program (Ref. 12) devoted to the study of the behavior of high burn-up advanced fuels submitted to RIA, under representative reactor conditions.

Cladding mechanics. Cladding mechanical properties will be updated gradually, when the results of the on-going or planned PROMETRA mechanical tests are available, and particularly on the advanced cladding materials (M5 and Zirlo cladding, …). In parallel, a failure criterion approach is currently under progress. Its objective is to get a prediction of the potential risk of failure of the cladding under different types of loadings: either induced by Pellet-Cladding Mechanical Interaction (PCMI), either induced by a gas pressure loading. This latter type of loading is more likely to occur with the use of highly irradiated UO_2 and MOX fuels, with a high gas content. Extension of the modeling is planned on the rod-failure-related phenomena: cladding failure prediction (possibly by clad ballooning), subsequent gas ejection into the coolant with possible Fuel-Coolant Interaction (FCI).

Thermal-hydraulics. An update of the heat-exchange coefficient correlations between the cladding and the water is in progress. These correlations are deduced from the PATRICIA experimental program in which the cladding is submitted to a rapid transient, representative of a RIA transient, under PWR conditions (water pressure: 155 bar, water inlet temperature: 280 °C) and NSRR conditions (stagnant water at atmospheric pressure and room temperature). Correlations concern the forced

or natural convection regime, the Departure from Nucleate Boiling (DNB) phase, with adapted critical heat flux correlations, and the post-DNB phase.

Fission gas behavior. Progress in the fission gas behavior modeling, related to the role of the grain boundary gases, are expected from the availability of separate effect tests planned in the French SILENE reactor on highly irradiated UO_2 and MOX fuel samples, devoted to the study of kinetics of fission gas release, pressure gas loading and impact of initial internal pressure. In parallel, results of grain boundary inventory measurements are expected from the analyses of ADAGIO tests performed on irradiated fuel samples, before and after transient (Ref. 15).

Physical qualification process. Physical qualification of the code will continue to be improved by a thorough comparison of the code results to the available experimental measurements obtained in the CABRI and NSRR reactors. In addition, the physical qualification of the code on CABRI and NSRR tests will be extended to highly irradiated UO_2 and MOX fuels.

5. CONCLUSION

The SCANAIR code is presently able to take into account the following physical phenomena and their strong coupling occurring during rapid power transients representative of RIA conditions, such as a control rod ejection: thermal dynamics including clad-to-coolant heat transfer modeling in sodium or water conditions, structural mechanics for the rod constitutive elements, and fission gas (FG) transient behavior.

The interpretation of the experiments with the SCANAIR code has shown a satisfying status of qualification on the whole set of available experimental results of the CABRI REP Na tests data base.

The planned evolution of the code is linked to the new CABRI international program to be performed in the future Water Loop of the CABRI facility. It mainly concerns the implementation of a rod failure criterion together with the adaptation of the mechanical properties of the advanced cladding materials (M5 and Zirlo cladding, …), the update of clad-fluid heat-transfer modeling under rapid transient, the improvement of the fission gas transient behavior modeling based on on-going separate effect experimental programs and the post-failure phenomena modeling. In addition, the physical qualification of the code on CABRI and NSRR tests will be extended on highly irradiated UO_2 and MOX fuels.

REFERENCES

Ref. 1. Latché J.-C., Lamare F., Cranga M., *"Computing Reactivity Initiated Accidents in PWRs"*, SMIRT-13 Meeting, Porto Alegre, Brazil, August 13-18, 1995

Ref. 2. Papin J., Rigat H., Lamare F., Cazalis B., *"The SCANAIR code for the description of PWR fuel rod behavior under RIA: validation on experiments and extrapolation to reactor conditions"*, International Topical Meeting on Light Water Reactor Fuel Performance, Portland, Oregon, March 2-6, 1997

Ref. 3. Fédérici E., Lamare F., Bessiron V., Papin J., *"Status of development of the SCANAIR code for the description of fuel behavior under Reactivity Initiated Accident"*, International Topical Meeting on Light Water Reactor Fuel Performance, Park City, Utah, April, 10-13, 2000

Ref. 4. Balourdet M., Bernaudat C., Basini V., Hourdequin N., *"The PROMETRA programme: assessment of mechanical properties of Zircaloy-4 cladding during an RIA"*, SMIRT-15 Meeting, Seoul, Korea, August 1999

Ref. 5. Schmitz F., Papin J., *"REP Na-10, another RIA test with a spalled high burnup rod and with a pulse width of 30ms"*, WRSM 26th, Washington, October 1998

Ref. 6. Bates D. W., *"Influence of stress state and hydrogen on deformation and failure of Zircaloy-4"*, Master of Science, Pennsylvania State University, December 1998

Ref. 7. Yvon P., Sainte-Catherine C., Duguay C., Carassou S., Hourdequin N., Cazalis B., Bernaudat C., *"Development of new techniques to assess the mechanical behavior of Zircaloy-4 during an RIA"*, IAEA Technical Committee Meeting on fuel behavior under transient and LOCA conditions, Halden, Norway, September, 10-14, 2001

Ref. 8. Todreas N., Jacobs G., *"Thermal contact conductance of reactor fuel elements"*, Nucl. Sci. Eng., 50 (1973) 283

Ref. 9. Peggs I. D., Godin D. P., *"The yield-strength-hot hardness relationship of Zircaloy-4"*, Journal of Nuclear Materials, 57 (1975) 246

Ref. 10. Courtney T. H., *"Mechanical Behavior of Materials"*, McGraw-Hill series in materials science and engineering, Second Edition, 2000

Ref. 11. Wolfe R. A., Kaufman S. F., WAPD-TM-587 (1967)

Ref. 12. Papin J., Mélis J.-C., Lecomte C., *"Definition and status of the CABRI international program with a sodium and a water loop"*, WRSM 28th, Bethesda, USA, October 2000

Ref. 13. Lemoine F., *"The role of fission gases on the high burnup fuel behavior in reactivity initiated accident conditions"*, 10th international Symposium on Thermodynamics of Nuclear Materials (STNM-10), Halifax (Canada), 6-11 Aug. 2000

Ref. 14. Fuketa T., Sasajima H., Sugiyama T., *"Behavior of high-burnup PWR fuels with low-tin Zircaloy-4 cladding under Reactivity-Initiated-Accident conditions"*, Nuclear Technology 133 (2001) 50

Ref. 15. Ravel S., Muller E., Eminet G., Caillot L., *"Partition of grain boundary and matrix gas inventories: results obtained using the ADAGIO facility"*, Seminar on Fission Gas Behavior in Water Reactor Fuels, Cadarache, France, September, 26-29, 2000

EFFECT OF CLADDING PRE-OXIDATION ON ROD COOLABILITY DURING REACTIVITY ACCIDENT CONDITIONS

T. SUGIYAMA, T. FUKETA
Department of Reactor Safety Research,
Japan Atomic Energy Research Institute,
Tokai-mura, Ibaraki-ken, Japan

Abstract. Effect of cladding pre-oxidation on rod coolability during reactivity initiated accident was investigated using the Nuclear Safety Research Reactor. Pulse irradiation experiments were carried out on fresh fuel rods with three cladding surface conditions: without oxide layer, with 1μm-thick and 10μm-thick oxide layer. Temperature measurements showed that a threshold of departure from nucleate boiling increases at the pre-oxidized cladding in terms of surface temperature and peak fuel enthalpy. Quenching temperature also increases at the pre-oxidized cladding, and duration of film boiling reduces. Both the critical heat flux point and the minimum heat flux point accordingly move in the direction of higher heat flux and higher temperature due to the cladding surface pre-oxidation. Some previous studies showed such tendency in boiling curve as a function of surface wettability controlled by surface roughness. In the present case, the wettability change is possibly dominated by chemical potential change at the cladding surface due to oxidation rather than by surface roughness change, because the present results indicate the effects depending on the presence of the oxide layer, not on the oxide layer thickness.

1. INTRODUCTION

In order to clarify fuel behaviour under reactivity initiated accident (RIA) conditions, pulse irradiation experiments have been carried out in the Nuclear Safety Research Reactor (NSRR) at Japan Atomic Energy Research Institute (JAERI). One of the most important variables measured in a reactivity transient is cladding temperature, because it provides information about rod coolability and mechanical properties of cladding materials. Accumulated data from a large number of fresh fuel experiments have been utilized to establish safety guidelines and to verify computer codes predicting transient fuel behaviour. However, irradiated fuel experiments, which were started in 1989, show different tendency of cladding temperature histories. Generally, cladding temperature of irradiated fuel rods is lower than those of fresh fuel rods with a same condition of the peak fuel enthalpy.

FIG. 1 shows cladding surface temperature histories for two test fuel rods. Both the rods have identical specifications, but one fuel rod had been irradiated in the Japan Materials Testing Reactor (JMTR) up to the burnup of 21.2 MWd/kgU. For the peak fuel enthalpy of 670 J/g, the fresh fuel rod shows a quick temperature increase at the departure from nucleate boiling (DNB), a high temperature state from 900 K to 1500 K during a stable film boiling and a sudden temperature drop at quenching. On the other hand, the irradiated rod shows lower peak temperature and shorter duration of film boiling even for the higher peak fuel enthalpy of 740 J/g [1]. FIG. 2 shows another case from an iterative irradiation experiment. A fresh test fuel rod was pulse-irradiated three times with a same peak fuel enthalpy condition. Temperature history at the first irradiation shows typical behaviour of a fresh fuel rod, but histories after the second irradiation show lower peak temperature and shorter duration of film boiling [1].

The following factors can reduce cladding surface temperature: (a) reduction of pellet thermal conductivity due to cracking, relocation, or increased porosity with burnup increase, (b) reduction of heat transfer at the pellet/cladding gap due to a change of contact state by pellet cracking or cladding creep down, or due to a change of gas composition by FP release, and

(c) enhancement of heat transfer at the cladding surface due to some reasons such as oxidation. The factors related with burnup increase can be neglected, because the cladding temperature reduction was observed in the iterative irradiation experiment using a fresh fuel rod. Thus, remaining factors are pellet cracking and relocation, and enhanced heat transfer at the cladding surface. In association with the surface effect, some studies show possible effect of cladding surface oxidation on the cladding coolability. Moreaux [2] and Kikuchi [3] reported enhanced heat transfer at the surface coated with low thermal-conductive materials like metal oxide. On the other hand, Chowdhury [4] suggested surface roughness could change the boiling curve through a change of surface wettability. In order to confirm the effect of cladding oxidation on the rod coolability, fresh fuel rods with pre-oxidized cladding were pulse-irradiated in the NSRR. The factor of pellet cracking and relocation was removed by using a new fuel rod for each experiment. Furthermore, pellets with a large diameter were used to reduce the initial pellet/cladding gap and to uniform the heat transfer condition at the gap.

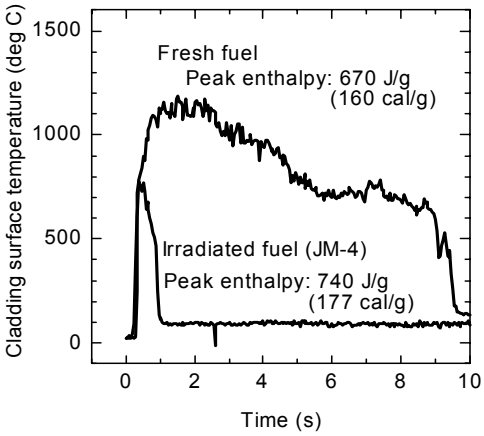

FIG. 1. Comparison of cladding surface temperature between fresh and irradiated fuel experiments

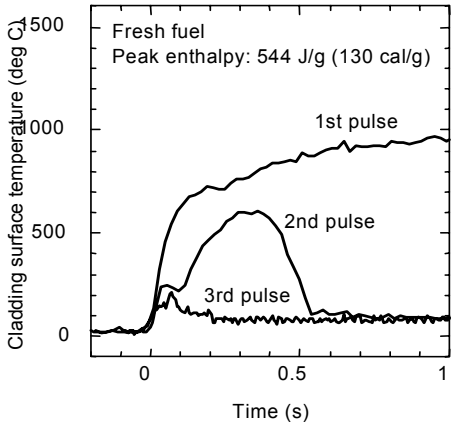

FIG. 2. Comparison of cladding surface temperature in an iterative pulse irradiation experiment

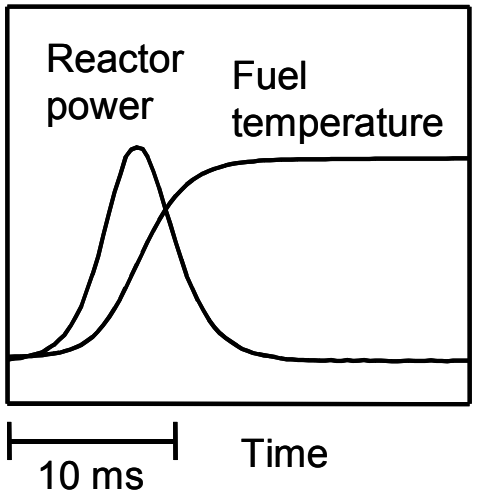

Fig. 3. Typical histories of NSRR power and test fuel temperature

2. NSRR FACILITY

The NSRR is a modified TRIGA type reactor with a capability to produce large pulsing power. A test fuel rod contained in a test capsule with coolant water is set at the centre of the experimental cavity in the reactor core and is subjected to pulse irradiation. FIG. 3 shows typical histories of reactor power and test fuel temperature. Behaviour of the test fuel rod is measured with instrumented thermocouples, pressure sensors, elongation sensors and other sensors. Signals from these sensors are transmitted to the high-speed recorder. Further information on the NSRR facility is provided in the reference [5].

3. TEST CONDITIONS

3.1 Test Fuel Rod

Test fuel rods are short-sized 17×17 PWR type and consist of a Zircaloy-4 cladding and 12 UO_2 pellets of 4.1%-enrichment. In order to examine the effect of surface oxide layer on rod coolability, three surface conditions were prepared: without oxide layer (normal surface), with 1μm-thick and 10μ-thick oxide layer. FIG. 4 shows a cross section of the 10μm-oxidized fuel rod. The pre-oxidation was carried out in an autoclave with conditions listed in Table I. Hydrogen absorption level in the 1μm-oxidized fuel rod is low, so influence of hydride on rod coolability is neglected. The UO_2 pellets have larger diameter than the standard design and the pellet/cladding radial gap size is 20μm. Hence, the gap is immediately closed during pulse irradiation and similar gap condition in terms of heat transfer can be expected for all tests. The upper 4 pellets have centre hole of 1.9 mm in diameter for fuel centreline temperature measurement. The filling gas of the rod is helium.

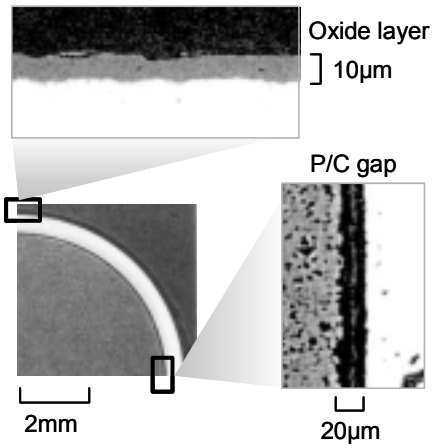

TABLE I. CLADDING PRE-OXIDATION CONDITIONS

Oxide layer thickness (μm)	1	10
Atmosphere	Steam	Air
Temperature (deg C)	400	430
Pressure (MPa)	1	0.1
Holding time (hour)	2	1739.5
Hydrogen concentration (wt ppm)	38	-

FIG.4. Cross section of test fuel rod

3.2 Test Capsule and Coolant Water

The test fuel rod is set at the centre of a stainless steel capsule with an inner diameter of 120 mm. The fuel rod is cooled by stagnant water of atmospheric pressure. The initial temperature of the coolant water is 20±4 degrees C.

3.3 Instrumentation

FIG. 5 shows thermocouple installation on the fuel rod. Cladding surface temperatures are measured at 6 elevations (Tc #1 - #6) with directly welded thermocouples. Fuel centreline temperature is measured at the elevation of the Tc #5. The fuel centreline temperature should be corrected with the following equation, because response of the thermocouple at the fuel centre is not quick due to its large heat capacity. The time constant is 0.31 second according to a preliminary test.

$$T_f(t) = T_m(t) + \tau \frac{dT_m(t)}{dt},$$

where t is time, T_f is corrected fuel centreline temperature, T_m is measured temperature and τ is the time constant. Other sensors are also instrumented to measure coolant water temperature, capsule internal pressure and elongations of the cladding and the pellet stack.

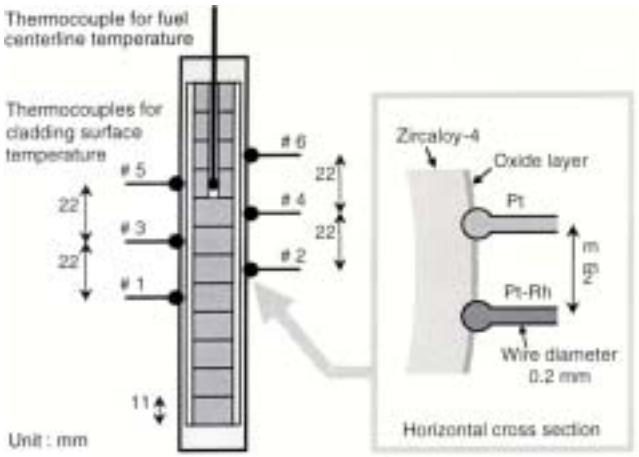

TABLE II TEST MATRIX AND TEST ID

Peak fuel enthalpy J/g (cal/g)	Oxide layer thickness (μm) None	1	10
335 (80)	NL	1L	10L
460 (110)	NM	1M	10M
565 (135)	NH	1H	10H

FIG. 5. Thermocouple installation

3.4 Pulse Irradiation

For each cladding surface condition, 3 fuel rods were pulse-irradiated with different conditions of peak fuel enthalpy: 335, 460 and 565 J/g (80, 110 and 135 cal/g, respectively). Hence, total 9 experiments were performed. Table II shows the test matrix and test ID for each condition.

4. TEST RESULTS AND DISCUSSION

4.1 Results of temperature measurements

Transient records of cladding surface temperature are shown in FIG. 6. It should be noted that nuclear heating by pulse irradiation is almost finished in 30 ms and there is no heat source after the time. For the low peak fuel enthalpy condition (335 J/g), a clear difference is observed between normal and oxidized rods. DNB occurred at all elevations on the non-oxidized rod (NL), but it occurred at only two elevations on the 1μm-oxidized rod (1L) and no DNB occurred on the 10μm-oxidized rod (10L). For the middle and high peak fuel enthalpy

conditions (460 and 565 J/g), almost all temperature histories indicate the occurrence of DNB. However, duration of film boiling is longer on the normal rods than on the oxidized rods. Consequently, it is suggested that pre-oxidized cladding prevents DNB and reduces duration of film boiling. FIG. 7 shows relation between the cladding surface temperature and the fuel centreline temperature at a same elevation of a rod. For a same level of the peak fuel enthalpy, cladding temperature histories without DNB or with an early quenching always correspond to quick degradation of fuel centreline temperature. In other words, preventing DNB or reducing the duration of film boiling enhanced the rod coolability. The test results suggest these effects were caused by pre-oxidized cladding. The mechanism of the effects will be discussed in the following sections.

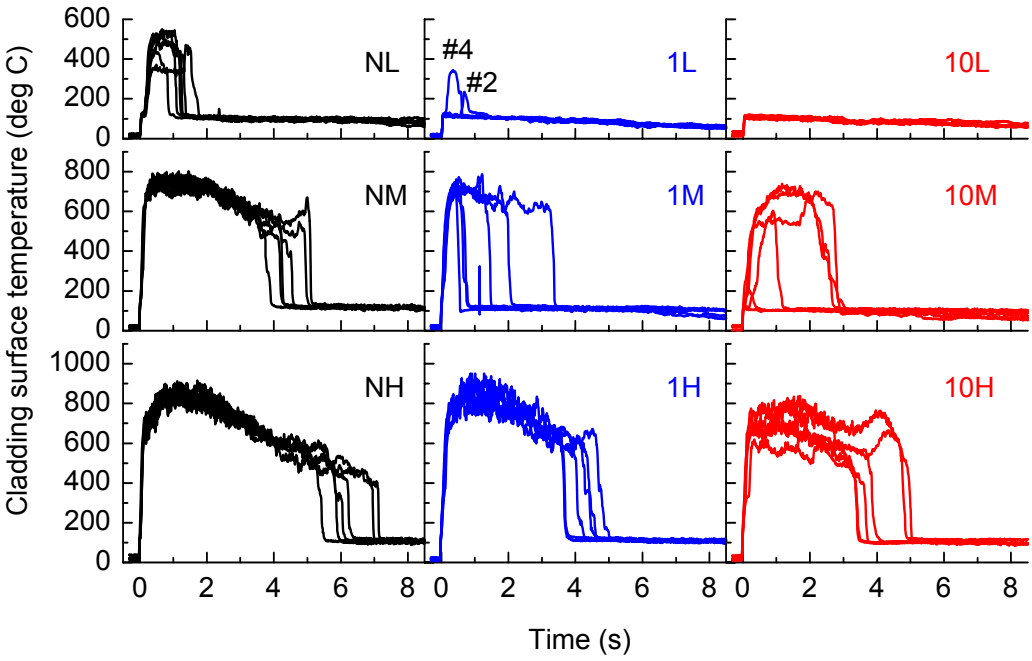

FIG 6. Transient records of cladding surface temperature

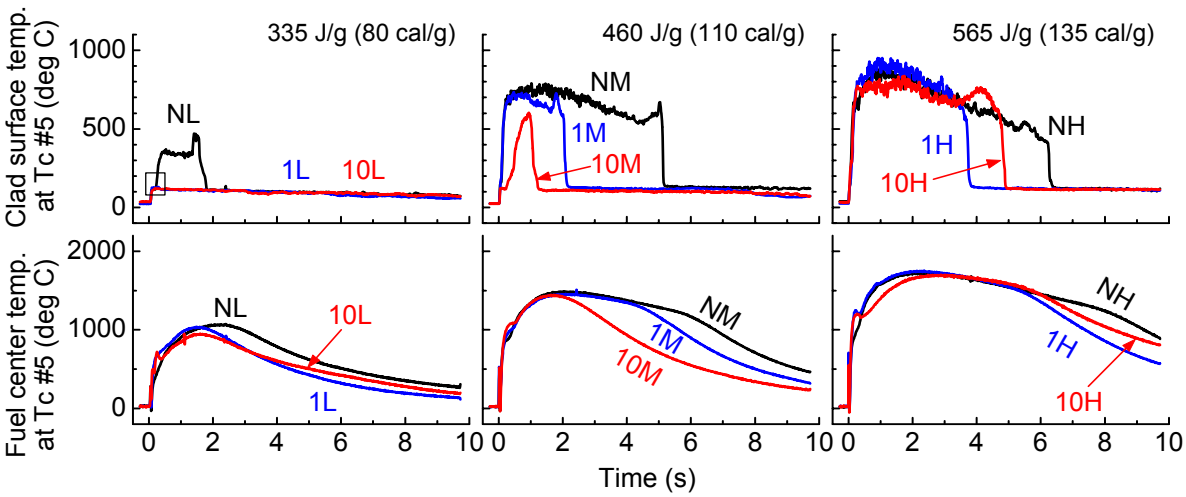

FIG. 7. Transient records of cladding surface temperature at Tc #5 and fuel centreline temperature

4.2 DNB threshold

FIG. 8 shows a magnified view of cladding surface temperature histories for the low peak fuel enthalpy condition (NL, 1L and 10L). The range is indicated by a rectangle in FIG. 7. Since the coolant pressure is atmospheric, saturation temperature is 100 deg C. DNB did not occur in the tests 1L and 10L, even though their cladding surface temperatures reached the level, at which DNB occurred in the test NL. This suggests that temperature threshold of DNB was raised by the cladding pre-oxidation. Chowdhury and Winterton showed possible movement of the critical heat flux (CHF) point [4]. They controlled surface wettability, or contact angle of water with a surface, by changing a surface roughness and showed that boiling curve could be modified as shown in FIG.9. Their results indicated that the CHF point and the minimum heat flux (MHF) point move in the direction of higher heat flux and higher temperature when the surface wettability is higher. In FIG. 8, all the cladding temperature histories are similar before the DNB time in the test NL. Hence, the oxidized surface and the normal surface possibly have a common boiling curve up to the CHF temperature of the normal surface. This suggests that the CHF points for the tests 1L and 10L moved also in the higher heat flux direction as shown in FIG. 9.

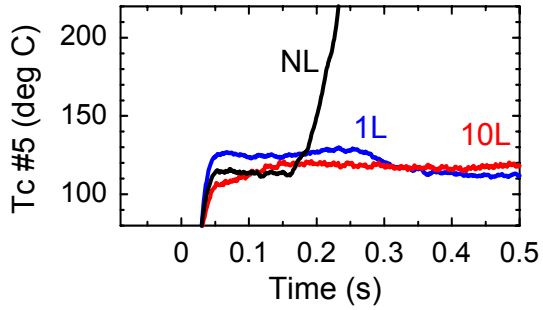

FIG. 8. Magnified view of cladding surface temperature at Tc #5 for 335 J/g

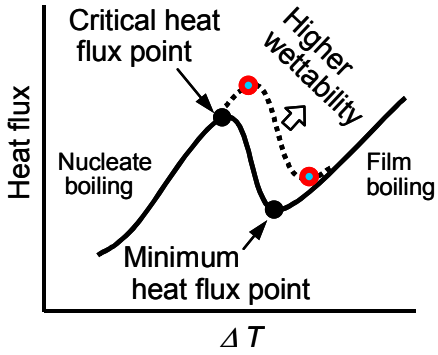

FIG. 9. Anticipated change of boiling curve

The wettability effect on the CHF point is easily understandable. As shown in FIG. 10, the contact area of water with the cladding surface should be larger on the more wettable surface than on the less wettable one. High wettability causes easy separation of vapor bubbles from the cladding surface during a nucleate boiling and possibly prevents the vapor layer from covering the surface. Thus, the temperature threshold of DNB is raised. The wettability depends on surface energy, or surface tension, at each phase-interface as illustrated in FIG. 10. According to the current test results, it is anticipated that cladding surface wettability was increased due to pre-oxidation. Two possible factors affecting wettability exist. One is a development of surface roughness during the pre-oxidation. The order of roughness magnitude was 1μm in the experiments by Chowdhury and Winterton. However, developed roughness larger than 1μm cannot be expected on the 1μm-oxidized cladding. Hence, the clear differences in temperature history between the 1μm-oxidized and the normal rods cannot be explained only by surface roughness. Another possible factor is a change of chemical potential level at the cladding surface due to oxidation. In case that the surface energy at water/cladding interface is decreased, the wettability at the cladding surface will be increased and subsequently the rod coolability can be enhanced. Comparison of contact angles between Zr/water and ZrO_2/water can prove the above speculation. However, available measured data could not be found at the present.

4.3 Duration of film boiling

The speculation of wettability increase can also explain the reduced duration of film boiling on the oxidized rods. According to the Chowdhury's results, the minimum heat flux (MHF) point moves in the higher heat flux and higher temperature direction as well as the CHF point. Thus, quenching can occur at higher surface temperature and the duration of film boiling will be consequently reduced. The cladding surface histories for 565 J/g shown in FIG. 7 clearly indicate that quenching occurred at higher temperature on oxidized rods than on the normal rod. Similar behaviour was observed in reflooding experiments performed in Halden reactor [6]. Quenching occurred earlier on the oxidized rods than on the unoxidized rods.

FIG. 11 shows averaged duration of film boiling for each test. Here, each duration is an average for 6 elevations of a rod. According to linear extrapolations, DNB thresholds in terms of the peak fuel enthalpy are evaluated as 280 and 400 J/g for the normal and the two oxidized rods, respectively. Thus, the DNB threshold level was raised 120 J/g by the cladding pre-oxidation. The test result suggests that there is no difference between 1μm and 10μm-oxidized rods. This supports the speculation of the chemical potential change as the dominant factor, because the chemical potential at the cladding surface should depend on the presence of the oxide layer, not on the oxide layer thickness. If the surface roughness, which was developed in the pre-oxidation, is the dominant parameter in the present experiments, the 10μm-oxidized rod should have larger surface roughness and indicate more significant effect than the 1μm-oxidized rod.

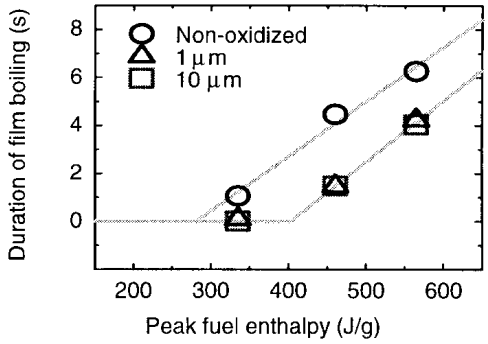

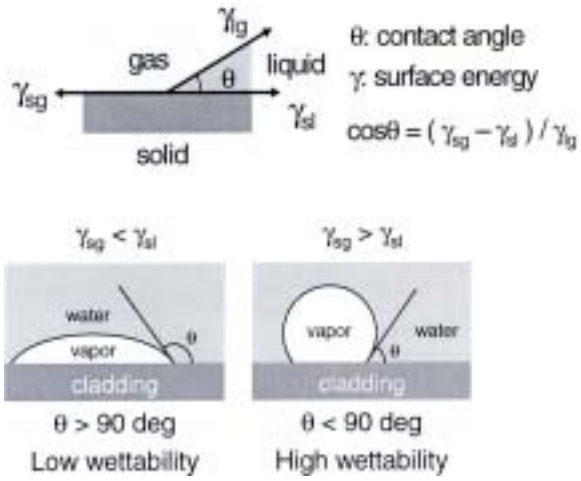

FIG.10. Relation between wettablility and surface energies

FIG.11. Averaged duration of film boiling

Effect of the pre-oxidation on quenching is not easy to understand intuitively, when it is expected that the cladding surface should be covered with vapor and perfectly separated from water during a film boiling. However, there could be water/cladding direct contacts even at a stable film boiling. FIG. 12 shows a schematic of film boiling at the surface of a vertical fuel rod. Since the rod length is finite, there should be a boundary between nucleate boiling and film boiling. Typically, the boundary on the bottom side is a quench front where quenching starts at. The thickness of vapor layer is non-uniform due to hydrodynamic unstabilities and the vapor/water interface flutters. Hence, there can be direct contacts of water with the cladding. In case of a non-wettable surface, the vaporization rate exceeds the spreading rate of the contact area and consequently the direct contact disappears in a short time. On the other hand, the contact area can spread at a highly wettable surface. In such case, the contact point

can be a new quench front and the quenching occurs at higher temperature than on the non-wettable surface. This speculation is supported by test results. FIG. 13 shows quenching time at each elevation of fuel rod in the tests NH, 1H and 10H (565 J/g). One rod has 6 thermocouples (#1 – #6), but markers for odd and even numbers are separately jointed in order to indicate they are on opposite sides of a rod as shown in FIG. 5. Results for non-oxidized rod suggest that quenching started on the bottom side and that quench front came up gradually. On the other hand, results for oxidized rods show earlier quenching at an upper position than at a lower poison. The strange order of quenching positions is explainable with the speculation of the water/cladding direct contacts resulting in quenching at high temperature.

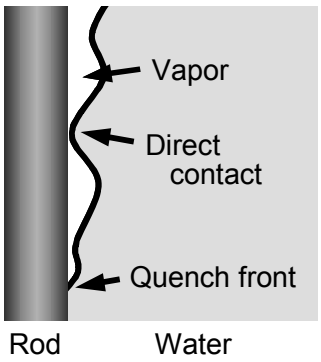

FIG.12. Water/cladding direct contact during film boiling

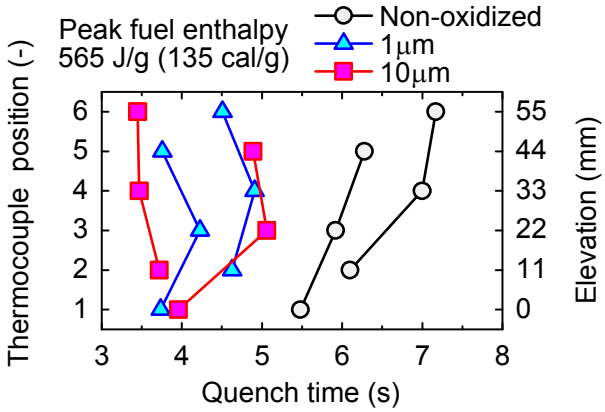

FIG.13. Quenching time at each elevation

4.4 Pre-oxidation effect under power reactor conditions

The NSRR experiments were performed with different coolant conditions from power reactors, such as high subcooling temperature (80 deg C), low coolant pressure (0.1 MPa) and natural convection. The effects by cladding pre-oxidation under power reactor conditions should be confirmed in order to discuss coolability of real fuel rods.

High subcooling temperature in the NSRR experiments causes thin vapor layer around a fuel rod during a film boiling. In the thinner vapor layer, the water/cladding direct contact is expected more frequently and the wettability effect becomes more remarkable. On the other hand, high coolant pressure and forced convection in power reactors also make the vapor layer thin. Hence, the pre-oxidation effect is possible also under the power reactor conditions, if the direction of wettability change due to oxidation is same as that under the NSRR conditions. Quantitative discussion is quite difficult at the present, because wettability data are not enough especially for high temperature and high pressure states.

5. SUMMARY

RIA-simulating experiments were performed on fresh fuel rods with three cladding surface conditions: without oxide layer (normal surface), with 1μm-thck and 10μm-thick oxide layer. For each surface condition, three fuel rods were tested with different levels of the peak fuel enthalpy, 335, 460 and 565 J/g. Thus, total 9 tests were carried out.

Temperature histories measured at the cladding surface and at the fuel centre showed that the pre-oxidized rods have higher coolability than the normal rod. The coolability depends on whether DNB occurs or not, and how long film boiling continues. Test results for the peak fuel enthalpy of 335 J/g suggest that the CHF point of the oxidized rods moved in the direction of higher heat flux and higher temperature. On the other hand, results for the peak fuel enthalpy of 460 and 565 J/g indicate the MHF point also moved in the same direction as the CHF point. The movement of the CHF and MHF points can be explained by a wettability change at the surface as shown by Choudhury and Winterton. In the present study, the wettability can be dominated by a chemical potential change or a roughness change at the cladding surface due to pre-oxidization. Test results indicate the coolability enhancement depends on the presence of the oxide layer, not on the oxide layer thickness, because the averaged durations of film boiling show no difference between the 1μm and 10μm-oxidized rods. Accordingly, the wettability is possibly dominated by a chemical potential change rather than by a surface roughness change.

The coolability enhancement due to the cladding pre-oxidation is anticipated also in power reactors. However, wettability data for water/Zr and water/ZrO_2 at high temperature and high pressure states are necessary to discuss the effect quantitatively.

ACKNOWLEDGEMENT

The authors are most grateful to JAERI colleagues in NSRR Operation Division for assembling and disassembling of test capsules and performing pulse irradiations.

REFERENCES

[1] FUKETA, T. et al., “Behavior of Pre-irradiated Fuel under a Simulated RIA Condition (Results of NSRR Test JM-4)”, JAERI-Research 95-013, March 1995
[2] MOREAUX, F., CHEVRIER, “Destabilization of Film Boiling by Means of a Thermal Resistance”, J. C. and Beck, C., Int. J. Multiphase Flow, Vol. 2, pp.183-190, 1975
[3] KIKUCHI, Y., HORI, T. and MICHIYOSHI, I., “Minimum Film Boiling Temperature for Cooldown of Insulated Metals in Saturated Liquid”, Int. J. Heat Mass Transfer, Vol. 28, No. 6, pp.1105-1114, 1985
[4] CHOWDHURY, S. K. R. and WINTERTON, R. H. S., “Surface Effects in Pool Boiling”, Int. J. Heat Mass Transfer, Vol. 28, No. 10, pp.1881-1889, 1985
[5] ISHIKAWA, M. and SHIOZAWA, S., J. Nucl. Mater., Vol. 95, pp.1, 1980
[6] SVANHOLM, K. et al., “Halden Reactors IFA-511.2 and IFA-54X: Experimental Series under Adverse Core Cooling Conditions”, Experimental Thermal and Fluid Science, Vol. 11, No. 1, pp.77-100, 1995.

DEVELOPMENT OF NEW TECHNIQUES TO ASSESS THE MECHANICAL BEHAVIOUR OF ZIRCALOY-4 DURING AN RIA

P. YVON, C.S. CATHERINE, C. DUGUAY, N. HOURDEQUIN
DMN/SEMI, France

S. CARASSOU
DMN/SRMA, CEA/Saclay, Gif-sur-Yvette, France

B. CAZALIS
IPSN/SEMAR, CEA/Cadarache, Saint Paul lez Durance, France

C. BERNAUDAT
EDF/SEPTEN, Villeurbanne, France

Abstract. Hoop and axial tensile tests have been carried out by the CEA to assess the behaviour of irradiated Zircaloy-4 cladding during Reactivity Initiated Accidents (RIA) : this series of tests, termed PROMETRA, is intended as a support to the CABRI program related to the studies of the behaviour of high burnup UO_2 and MOX fuel in RIA situation, undertaken by IPSN in collaboration with EDF. Ring and longitudinal samples, machined by spark erosion from defueled cladding have been performed up to high temperatures (1 100°C) and high strain rates (up to 5 s^{-1}). The axial tensile tests were carried out using the Joule effect, and heating rates up to about 500°C.s^{-1} were obtained, which enabled us to perform the axial tests in a satisfactory manner. However, the tensile ring tests were first done in a vertical furnace with a heating rate about 0.5°C/s. For temperatures above 480°C, the mechanical characteristics showed a sharp drop which could be attributed to irradiation defect annealing. Therefore, we have recently developed an induction heating system to reach heating rates high enough (200°C.s^{-1}) to prevent any significant annealing before performing the ring tensile tests. The raw data have been corrected via a finite element analysis which provided us with reliable constitutive laws for Zircaloy-4 under transient conditions, but the failure mode of the rings could not lead to a failure criterion. Therefore we are implementing the approach developed by PSU, using wider notched rings. This particular geometry is designed in order to get axial plane strain ($\varepsilon_{zz}=0$) state in its central ligament part. Thus, the failure mode obtained is comparable to the one observed for the first stage of RIA (PCMI stage) and notably different from the one obtained on ring tensile tests. Furthermore, finite element analysis of these tests is carried out in order to get a good understanding of the mechanical stress and strain state obtained with this specimen geometry.

1. INTRODUCTION

Economic considerations have promoted the use of high burnup fuel in nuclear power plants. However, the behaviour of the high burnup UO_2 and MOX must be assessed: one of the requirements is that high burnup fuel does not lead to core degradation during a design basis reactivity initiated accident (RIA), i.e. in a pressurized water reactor (PWR) a rod control cluster accident leading to fast power increase (in a few ms). In this framework, the RIA CABRI REP-Na programme [i] has been run jointly by IPSN and EDF in order to analyse the high burnup fuel behaviour under RIA transients and to check the validity or adapt the current safety criterion. In the frame of this programme and to support these studies, the CEA runs the PROMETRA (which stands for "Transient Mechanical Properties") programme [i] which is devoted to the assessment of the mechanical properties of Zircaloy-4 cladding under thermomechanical conditions representative of the first phase of an RIA. Behaviour laws of irradiated Zircaloy-4 cladding, taking into account irradiation hardening, hydriding, waterside

oxidation and spalling, are derived and implemented in the SCANAIR code developed by IPSN [ii] in order to simulate more accurately fuel behaviour during accidents.

In an RIA, a control rod ejection or drop causes a sudden increase in reactor power, which deposits a large amount of energy into the fuel. The resulting thermal expansion of the fuel pellets, possibly reinforced by fission gas swelling first loads rapidly the cladding into the plastic regime. In a second phase, plenum pressure driven clad ballooning may occur, depending on conditions in the coolant channel. But, in this paper, we will focus on the first stage of the accident which is dominated by the Pellet Clad Mechanical Interaction (PCMI). This phase is characterised by high heating rates (~10^3 °C.s^{-1}). and high strain rates (~1 s^{-1}). The typical temperatures reached are between 280 and 600°C. The cladding is submitted to hoop and axial stresses, with a σ_z/σ_θ ratio ranging between 0.5 (pure gas pressure) and 1 (PCMI). The samples tested originated from cold work stress relieved Zircaloy-4 claddings, irradiated up to five annual cycles in a PWR and taken from different grid spans, in order to observe the influence of corrosion (oxide, hydride and possibly spalling). First, uniaxial tensile tests have been performed and the results have been published elsewhere [iii]. Then, ring tests on machined tubing have been realized [iv] in order to measure the relevant mechanical properties (such as yield strength, ultimate tensile strength, uniform elongation, stress-strain curve,..). These tests were complemented by an iterative finite element analysis (FEA) to estimate constitutive laws in spite of the heterogeneous stress and strain fields encountered during these hoop tests. However, there was concern about the significance of values obtained at temperatures higher than 480°C, due to the potential annealing of irradiation defects : the samples were heated with a conventional furnace with slow heating rates (~0.2 °C.s^{-1}) and consequently, annealing, redistribution of hydrides and even recrystallization for the higher temperatures could be expected. Therefore, we have decided to develop a fast heating technique (200 °C.s^{-1}) to minimise the impact of annealing. Another concern was the difficulty to establish a reliable failure criterion given the geometry and the failure mode of the rings used, and we are now adapting in our institute the plane strain specimen developed by Penn State University (PSU) [v-vii].

2. RAPID HEATING TESTS

2.1. Experimental techniques

The materials stem from grid spans 2 to 6 of irradiated Zircaloy-4 cladding with tin contents of 1.5% (former standard) and 1.3% (present standard). The oxide thickness of these claddings has been determined using Eddy current measurements. The samples are machined with a ram spark erosion machine which requires the prior mechanical removal of the oxide layer. For these tests, the samples were rings machined from tubes with an external diameter of about 9.5 mm and a thickness of about 0.6 mm. The rings have a 5 mm current width with two gauge lengths of 3 mm length and 2 mm width (gauge length to width ratio equal to 1.5). The rings are placed around two half cylinder (double-D) inserts which are attached to the cross heads and pulled apart inside the rings as shown in Figure 1. The fixtures are placed on a servo hydraulic tensile testing machine equipped with load and displacement sensors. In opposition to the tests performed earlier [iv], the samples are heated up rapidly with an induction coil as shown in Figure 2. The heating rate obtained is 200 °C.s^{-1} (to be compared to 0.2 °C.s^{-1} obtained with a conventional furnace) and temperature up to 900°C can be reached. The inductor coil is located around the mandrel. In order to protect this coil during the test, the range of displacement of the jack is limited to 5 mm. The temperature is regulated using a K-type thermocouple spot welded in the middle of one of the gauge lengths. Prior to the introduction in hot cell, the temperature measured by the thermocouple has been validated by

measurements with a monochromatic pyrometer from 375 to 900°C. A typical temperature ramp, illustrated in Figure 3, shows the good agreement with both types of measurements. The tests were performed satisfactorily with a strain rate of 5 s^{-1} and with a heating rate of 200 °C.s^{-1} followed by a short stabilisation time: typically about 7 s elapsed between the start of the heating ramp and the completion of the test. The test matrix is given in Table 1.

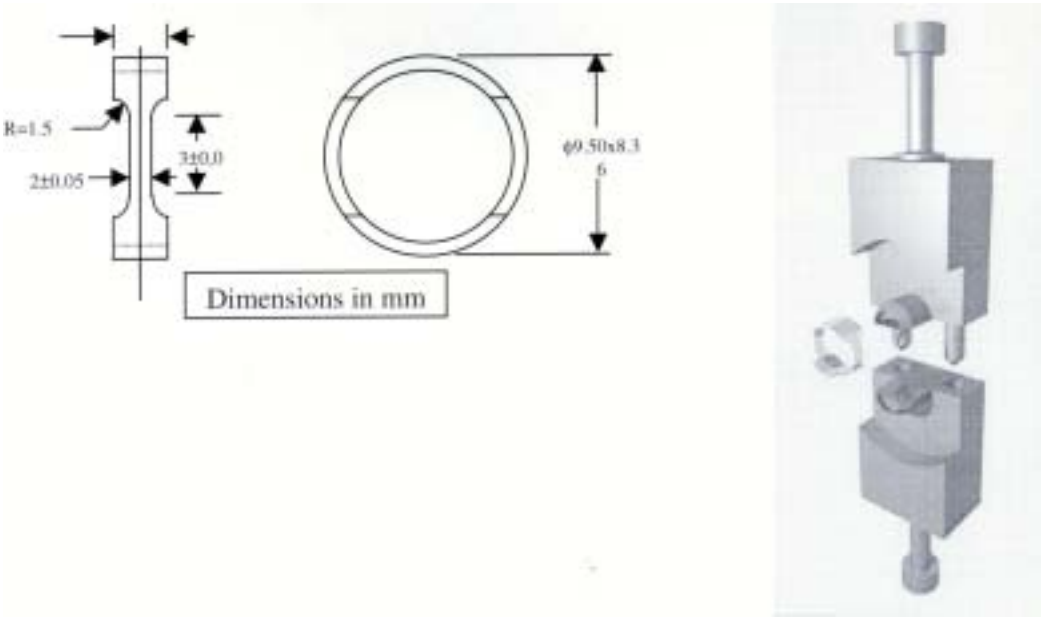

FIG. 1. Ring specimen geometry and 3D view of the mandrel and ring test sample.

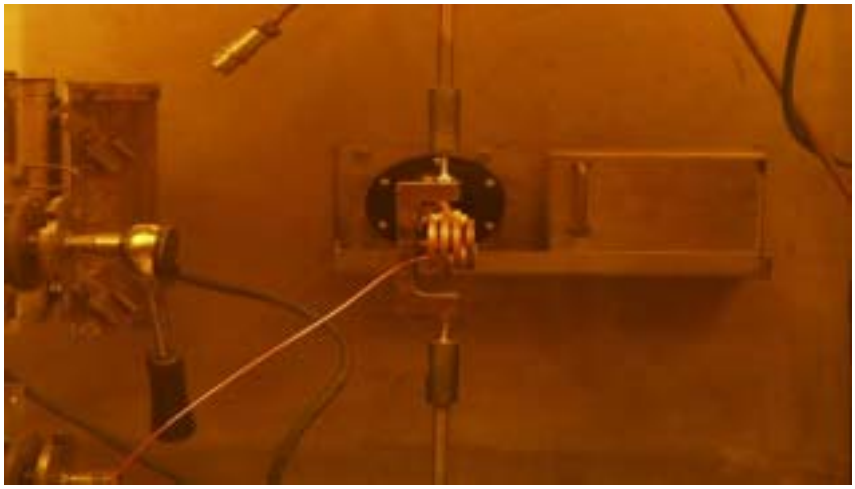

FIG. 2. Rapid heating device.

TABLE I. TEST MATRIX GIVING TEMPERATURE RANGES (IN °C) COVERED FOR SLOW HEATING RATES [iv] AND FAST HEATING RATES.

Heating rate	Oxidation of the cladding (ZrO_2 thickness)				
°C.s^{-1}	Unirradiated	<30µm	30 to 60	60 to 100	>100µm
0.2	20-600	280-600	280-600	280-600	280-480
200		480-600	480-600		

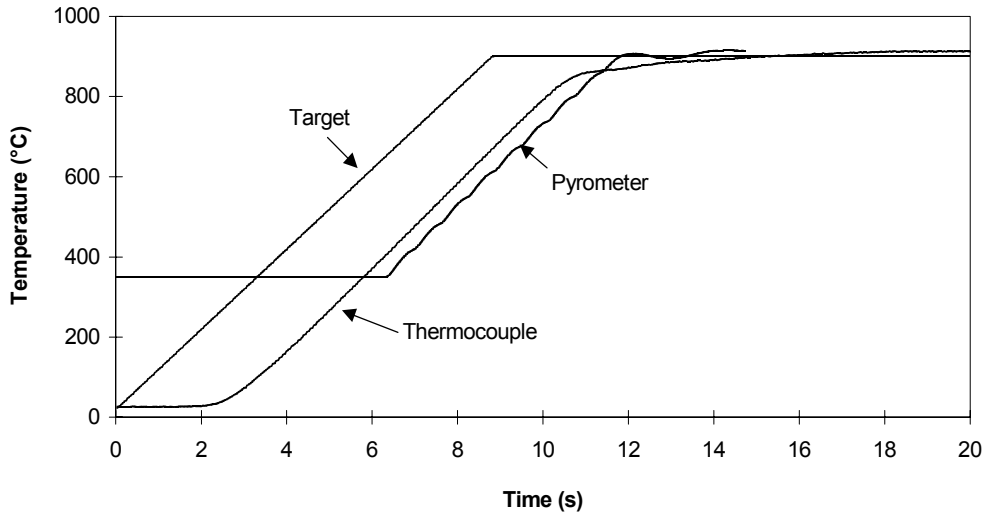

FIG 3. Typical temperature ramp achieved on ring specimen with induction heating.

2.2. Results

Figures 4 and 5 show the hoop ultimate tensile strength and the uniform elongation plotted versus the temperature for the tests carried out with a slow heating rate [iv] and the results obtained with the rapid heating technique. These figures show that for the tests at 480°C, there are no differences between the results obtained with the two heating techniques. This suggests that no significant annealing takes place during the heating ramp to 480°C and that the results obtained with a conventional furnace are valid up to this temperature. For the tests at 600°C, important differences between the mechanical properties obtained with conventional heating and induction heating are observed. As expected, the ultimate tensile strength increases and the uniform elongation decreases, which shows the necessity of using induction techniques for temperatures higher than 480°C. This is due to the fact that the time allowed to reach the target temperature and proceed to the test (<10 s) is insufficient to allow significant microstructural changes to occur.

2.3. Inverse method used to derive stress-strain curve from ring specimens

For the ring tensile tests, a procedure that combines both 3D FEA analysis and testing results is used to determine the true stress-strain curve. The machine compliance and offset displacement are determined by standard means and confirmed by FEA. Conventional engineering stress strain curves are determined from the load-displacement curves using the following formulae:

$\sigma_c = \frac{Load_{exp}}{S_u}$ and $\varepsilon_c^t = \frac{u_{mes}}{L_u}$ with S_u the initial calibrated section, u_{mes} the measured displacement and L_u the length of the calibrated section (3 mm)

True stress-strain curves are then derived from engineering stress-strain curves, using the following approximated formulation up to the offset:

$$\begin{cases} \varepsilon_r^p = ln\left(1+\varepsilon_c^p\right) \\ \sigma_r = \sigma_c\left(1+\varepsilon_c^p\right) exp\left(\frac{2\nu}{E}\sigma_r\right) \end{cases}$$

Then, the true stress-strain curve up to the plastic strain at rupture is extrapolated using the following Hollomon relation:

$$\sigma_r = a \cdot \left(\varepsilon_r^p\right)^n$$

where a and n are identified from $n = \dfrac{\varepsilon_{r\,m}^p}{1 - \dfrac{2\nu}{E}\sigma_{rm}}$ *and* $a = \dfrac{\sigma_{rm}}{\left(\varepsilon_{r\,m}^p\right)^n}$.

Finally, the elastic strain from the material Young's modulus is added to obtain the true stress-total strain relationship to be used as an input in the FEA.

FEA and a detailed 3D model (see Figure 6 below) of the specimen are used to calculate the mechanical response of the specimen. The calculated load vs. plastic displacement is calculated and compared to the experimental data shown in Figure 7, assuming a constant elastic stiffness during the tensile test.

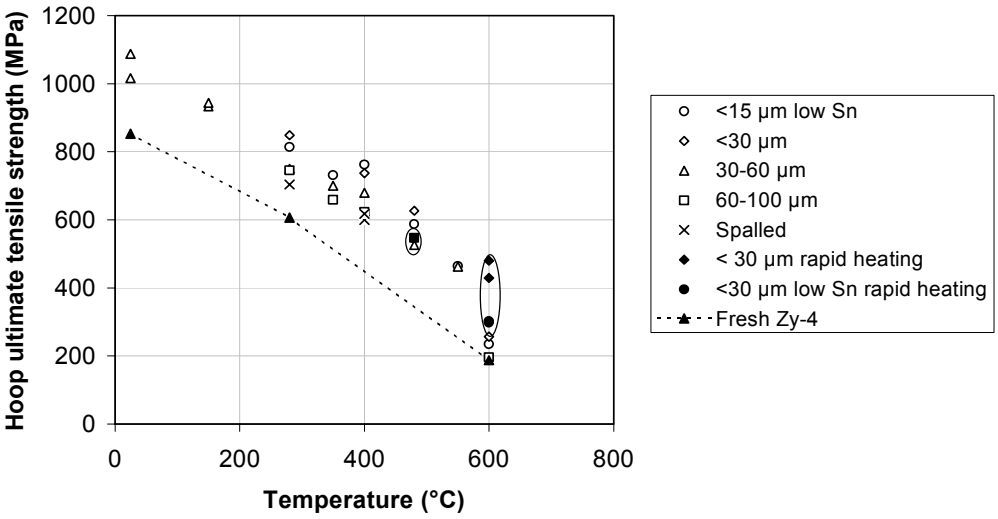

FIG 4. Hoop Ultimate tensile strength versus temperature

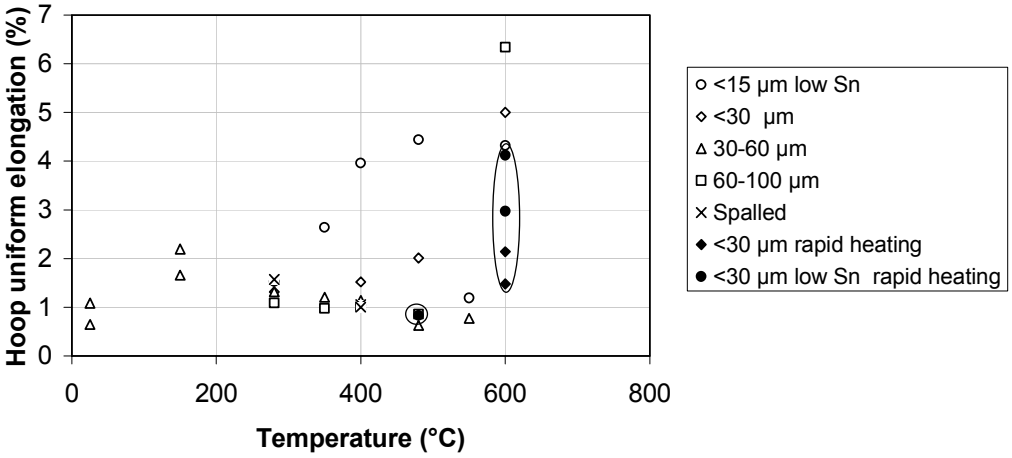

FIG 5. Uniform elongation versus temperature

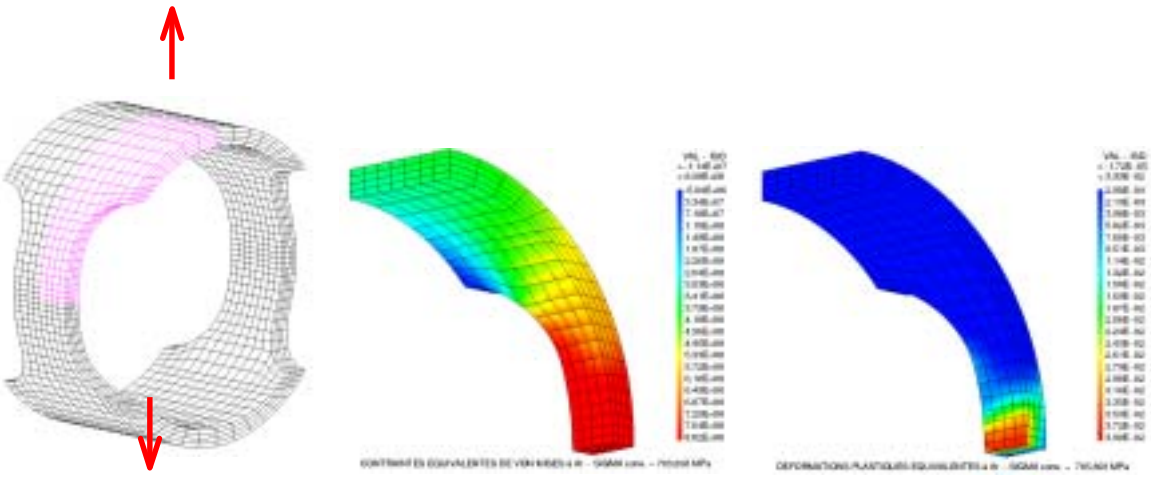

3D FEA model of the ring | Equivalent Von Mises stress at maximum load | Equivalent plastic strain at maximum load

FIG 6. FEA calculations of the ring test

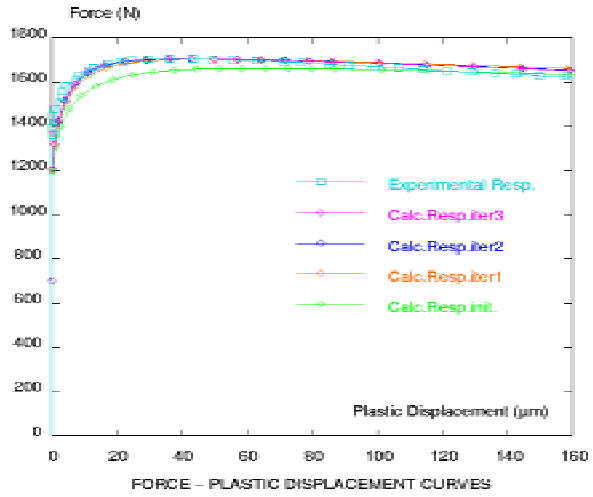

FIG 7 Calculated versus measured load –displacement curve

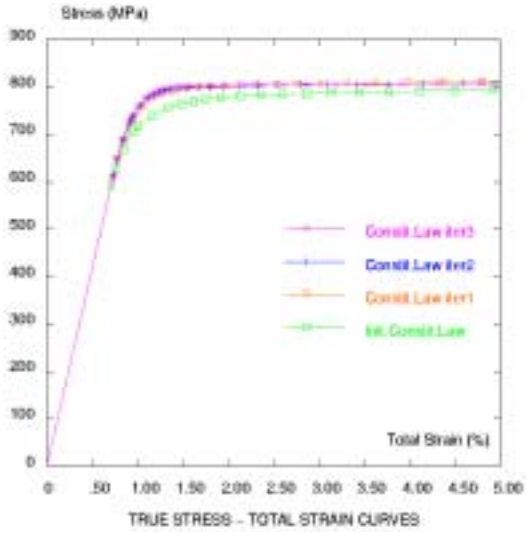

FIG 8. True representation of iterated constitutive equations

The true stress-strain curve is corrected with a factor issued from a comparison of the experimental and calculated loads and this iterative process is carried out until a good correlation between the experimental and calculated load vs. plastic displacement is reached. The true stress-strain curves resulting from this iterative process are shown in Figure 8. Using the FEA procedure leads to a corrected uniform elongation divided by a factor 2 to 3 as compared to the raw experimental values.

3. DEVELOPMENT OF PLANE STRAIN SAMPLES

As mentioned in the introduction, another concern is to determine an appropriate failure criterion. The fracture mode obtained on standard tensile ring specimens is not representative of those obtained on tubes during bust tests or RIA experiment. So, a notched wide ring geometry was developed by PSU [4] for this particular purpose and will be hereby referred as PSU geometry. At CEA Saclay, we tested this PSU geometry and we checked experimentally and by FEA that, as outlined by PSU, it gives rise to axial plane strain deformation on more than 1/3 of the ligament. Furthermore, the indentation technique gives access to local strain measurements and after this validation step it will be used for the measurement of critical hoop strain.

3.1. Experimental techniques

On standard ring specimens used for the determination of the true stress-strain relation, the gauge section is not wide enough in order to avoid shearing in the axial direction. So, slip bands are activated and are giving rise to the X rupture type as shown in Figure 9. This is of course not representative of the rupture mode obtained on tubes.

The PSU ring specimen (Figure 10) was developed at PSU [4]. There are four notches on this specimen and they are oriented towards the pulling direction and not on the middle plane as for ring specimen. This configuration was selected in order to avoid bending problem in the ligaments between two notches. On these rings, we realized two types of indentation lines (as shown in figure 10) to measure local strains. The indents are located 0.2 mm apart and were made with a Vickers indenter applying a load of less than a kg. The depth of these indents is estimated to be less than 30 μm and therefore they are not expected to have any influence on the deformation and rupture of the sample. The first indentation line is located along the ligament between the two notches and is dedicated to the validation of this technique and to check that the axial strain is close to zero in the central part of the gauge length. This line will not be present in the next experiments. Two other pairs of indentation lines are located along the circumference of each gauge length. The measurements on one of the gauge lengths will give access to the plastic instability, where the measurements on the other one will give the strain at rupture. The samples are tested up to rupture with or without intermediate unloadings. After each phase of loading, the distance between indents is measured using an optical microscope.

The failure modes obtained with these notched specimens are completely different from those obtained on standard ring specimens. Figure 11 shows that the fracture line is quite straight except near the two notch roots. It can be observed that the location of the rupture is uncorrelated to the indentation lines which confirms that these indents do not affect the rupture of the sample. Furthermore, SEM observation (Figure 12) of the fracture area clearly show that ductile cavities are oriented in hoop direction in the central part of the ligament. Near the notch tips, the ductile cavities are oriented in the axial direction as observed on the standard ring specimen. Finally, the measurements of hoop deformation are shown in Figure 13.

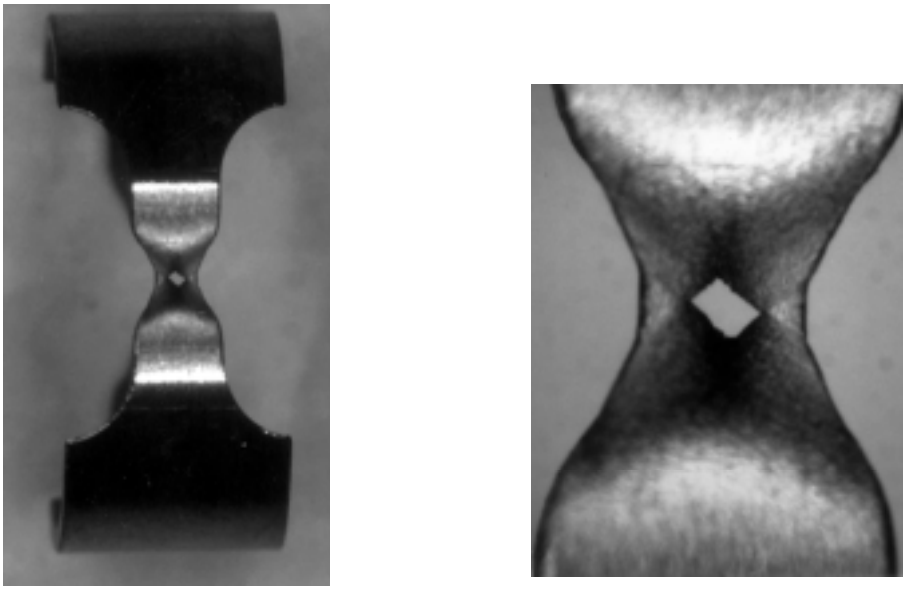

FIG 9. Typical failure of standard ring specimen

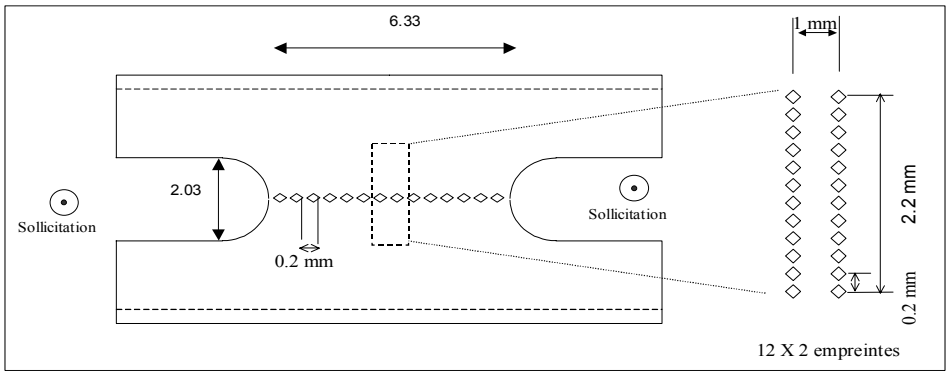

FIG 10. Geometry of PSU notched rings

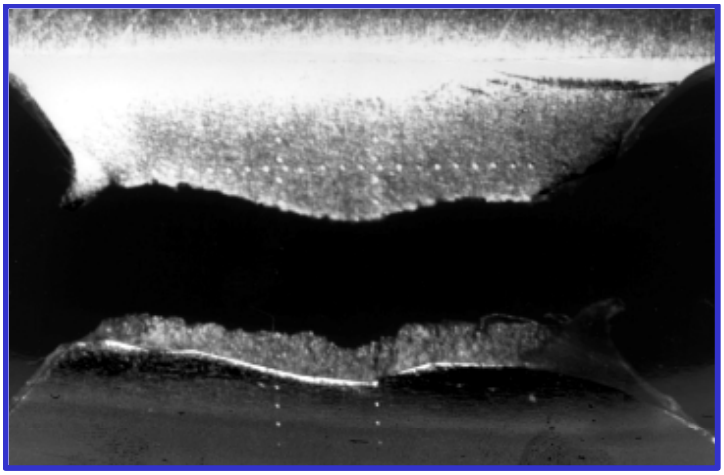

FIG 11. Typical failure of PSU notched rings

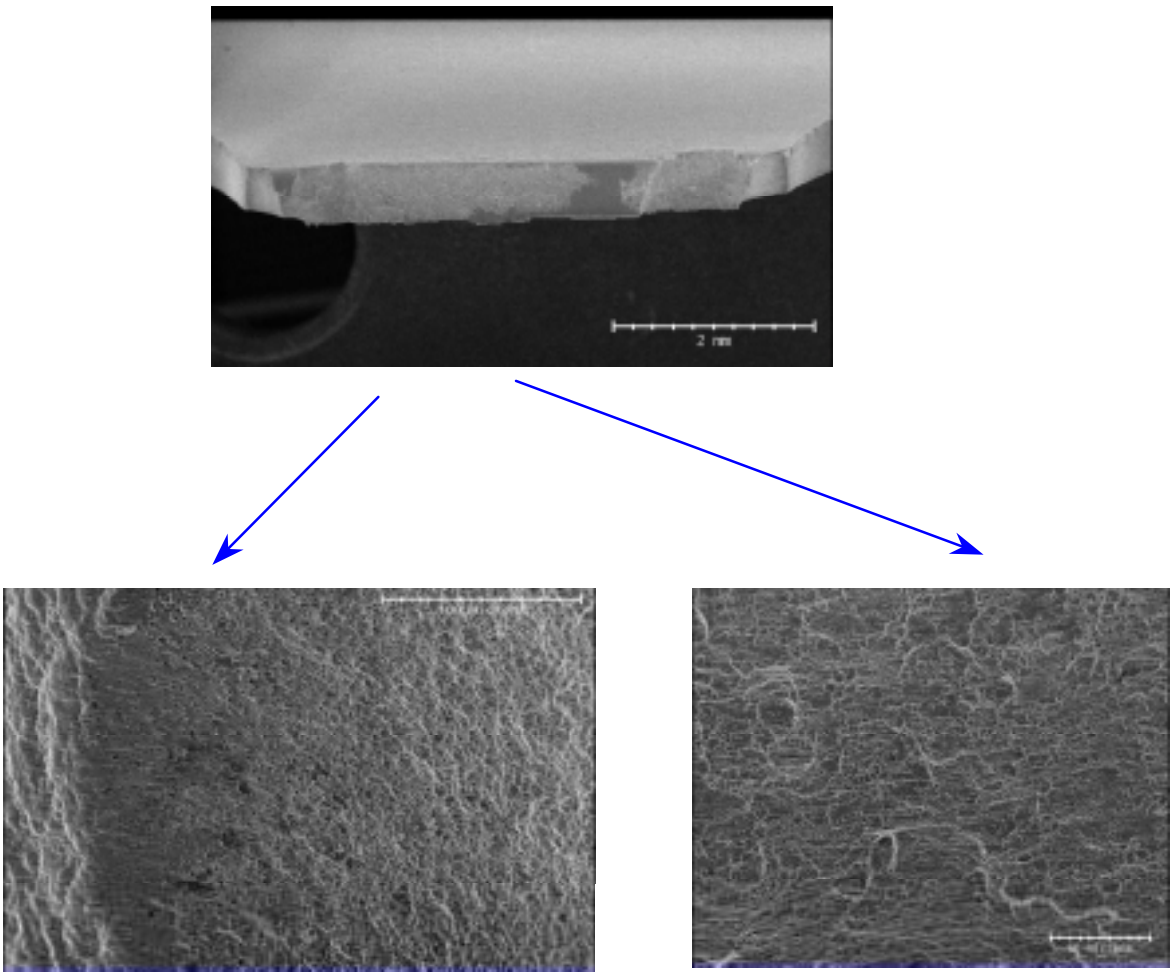

FIG 12. MEB photograph of failure mode observed on PSU notched ring

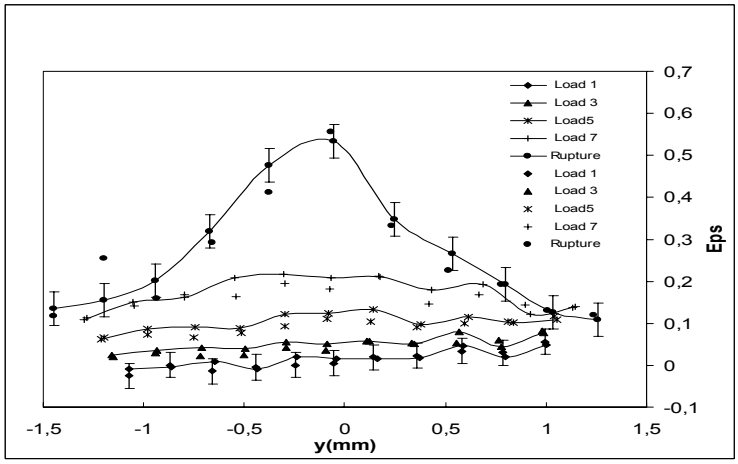

FIG 13. Measurement of the hoop deformation

3.2. Finite element modelling

FEA analysis of PSU notched ring specimen was achieved with two objectives. The first one is, as in the experimental phase, to check that the axial strain is zero between the notches where the rupture process will take place. The second objective is to be able to compute a failure criterion and determine its critical value when the fracture is experimentally observed.

Due to specimen symmetry and loading mode, only 1/8 of the PSU specimen is modelled in 3D (Figure 14). The mesh used is composed with full integration cube elements (CUB20) with 20 nodes and 27 Gauss points. As for the standard ring specimen, the double-D insert boundary and loading conditions were simulated with special imposed geometric relations for the mesh nodes located on the inner surface and on the ligament. This type of boundary conditions of course does not represent any friction coefficient between the specimen and the double-D insert. By doing so, the load level is not well represented for these specimen because the friction is more important than for the conventional ring specimen. This is due to the fact that the notched section which is the part under deformation is located on the double-D while for the standard ring specimens, it is located between the double-D insert. Nevertheless, it is not very important for this particular geometry because the objective is not to use the global load-displacement curve, but rather to obtain local strain values.

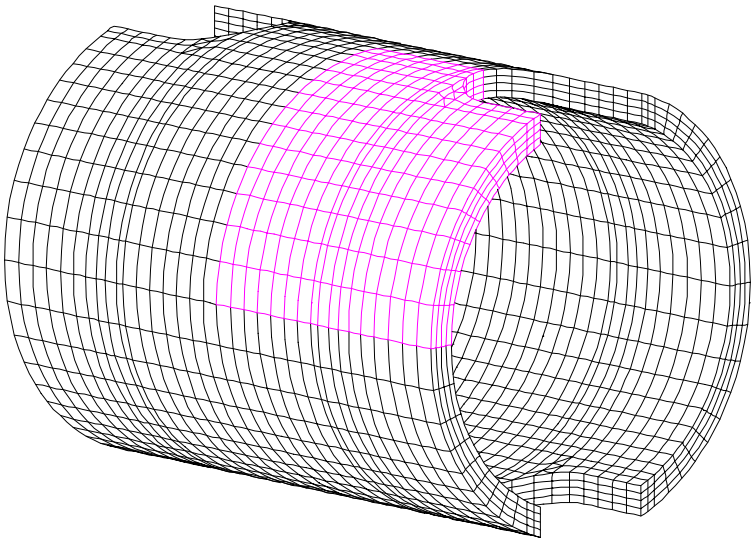

FIG 14. Mesh of PSU notched ring specimen

3.3. Results

For these FEA calculus, a true stress-strain curve was derived from a tensile test on a Zircaloy-4 standard ring in the hoop direction at room temperature with the inverse method presented in § 2.3. The simulation was conducted up to a displacement corresponding to the experimental failure point. Two characteristic points are considered during this analysis. The first one is corresponding to maximum load and the second one to the failure point. They can be used as different failure criteria : plastic instability and failure.

Figure 15 shows the distribution of axial plastic strain for an imposed displacement which corresponds to the failure point. The red colour is corresponding to values very close to zero and so the non-zero axial strain is located around the notch tip. Figure 16 is giving a profile of this result along the ligament and shows that the axial strain is nearly zero on 1/3 of its width. The comparison with experimental results, derived from micro-indentation measurements, is very favourable. The width of axial plane strain conditions seems to be a little more reduced in the experimental results than in numerical one but it remains more than half of the ligament width. Furthermore, interrupted tests have also been performed in order to check that this type of results is valid during the whole loading. Very similar results were obtained by PSU [v].

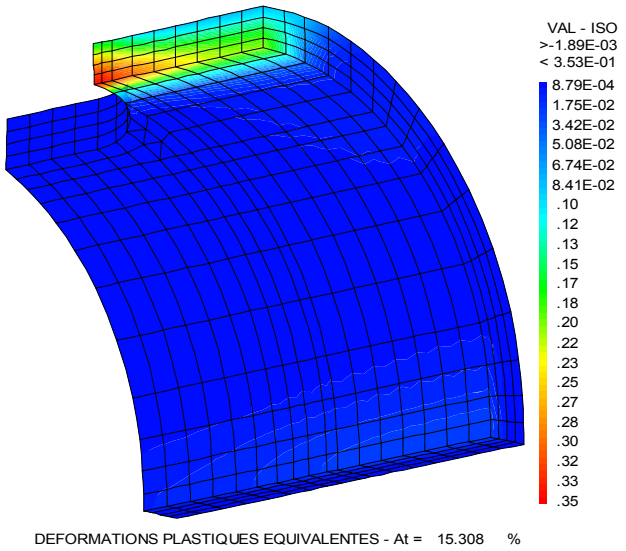

FIG 15. Inelastic axial strain distribution for an imposed displacement of 0.4 mm

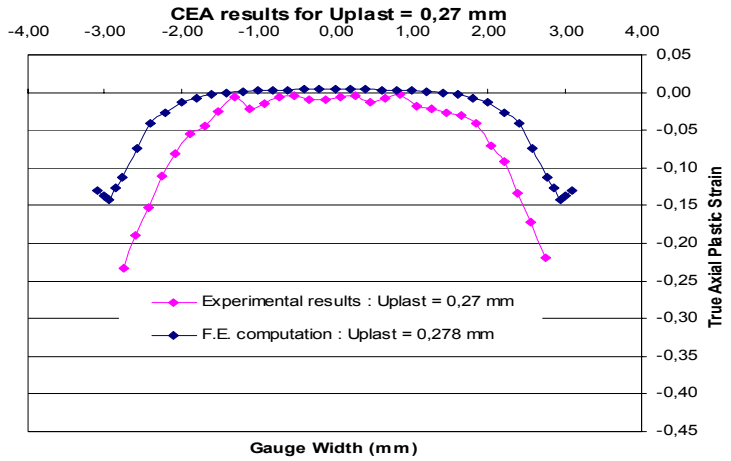

Fig 16. Ccomparison modelling-experiment for the axial strain

On going work is now concerning hoop strain experimental and numerical determination. Future computations will also include local strain energy density, which can then be used as a failure criterion in SCANAIR code [1]. Other stress, strain components are examined in order to get a good knowledge of the mechanical stress state achieved in the PSU notched specimen and to compare it with the one obtained in RIA experiments.

4. CONCLUSIONS

Mechanical tests up to high strain rates (~5 s^{-1}) are needed in support of the RIA studies led by EDF and IPSN. Up to now, the PROMETRA program has yielded important data on transient mechanical properties of irradiated Zircaloy-4 cladding, and the influence of waterside corrosion up to 480°C. In this work, we have developed and implemented in hot cell a rapid heating device which enables us to perform tests up to 900°C with a heating rate of 200 °C.s^{-1}.

Also, even if the constitutive laws obtained with the ring tests performed are valid and useful to computer codes, the failure mode of these rings was uncharacteristic of tube failures, hence the need of specific samples to determine a failure criterion. In this work, we adapted the ring geometry developed by PSU, and showed that on these rings, there is a large part of the gauge length where we observe no axial strain. The next step is to implement these tests (along with the indentation technique and the rapid heating) in hot cell.

REFERENCES

[1] PAPIN, J., BALOURDET, M., LEMOINE , F., FRIZONNET, J.M., SCHMITZ, F.,"French Studies on High-Burnup Fuel Transient Behavior Under RIA Conditions", Nuclear Safety **37(4)** (1996) pp. 289-327.

[2] FEDERICI, E., LAMARE, F., BESSIRON, V., PAPIN, J. , "The SCANAIR code version 3.2 : mean features and status of qualification", AIEA Technical Committee Meeting on " Fuel Behaviour under transient and LOCA conditions " Halden, Norway, September 10-14, 2001

[3] BALOURDET, M., and BERNAUDAT, C., "Tensile Properties of Irradiated Zircaloy 4 Cladding Submitted to fast transient loading", Proceedings of the CSNI Specialist Meeting on Transient Behavior of High Burnup Fuel, Cadarache, France, September 12-14 1995, pp. 417-431

[4] BALOURDET, M., BERNAUDAT, M., BASINI, V., and HOURDEQUIN, N., "The PROMETRA Programme: Assessment of Mechanical Properties of Zirclay 4 Fuel Properties During an RIA", Transactions of the 15th International Conference on Structural Mechanics in Reactor Technology (SMiRT-15) Seoul, Korea, August 15-20, 1999, pp. II-485-492.

[5] LINK,T.M., KOSS, D. A., and MOTTA A.T., "Failure of Zircaloy Cladding under Transverse Plane Strain Déformation", Nuclear Engineering and Design **186** (1998) pp. 379-394.

[6] BATES, D.W., KOSS, D.A., MOTTA, A.T., and MAJUMDAR, S. "Influence of Specimen Design on the Deformation and Failure of Zircaloy Cladding", Proceedings of the ANS Light Water Reactor Fuel Performance, Park City, USA, April 10-13, 2000, pp. 296-305.

[7] DAUM, R.S., MAJUMDAR, S., TSAI, H.C., BILLONE, M.C., KOSS, D.A. and MOTTA, A.T., "Embrittlement of Hydrided and Irradiated Zircaloy-4 Under RIA-Type Conditions", Proceedings of the 13th Symposium on Zirconium in the Nuclear Industry, Annecy, France, June 11-14, 2001 (to be published).

A RIA FAILURE CRITERION BASED ON CLADDING STRAIN

C. VITANZA

OECD Halden Reactor Project, OECD/NEA, Paris, France

Abstract. This note intends to contribute to the interpretation of the RIA tests that have been performed during the last decade on high burn-up PWR and BWR rods and that have been reported in the open literature. A failure threshold based on cladding deformation is proposed. This criterion predicts well all CABRI data with the exception of one. NSRR fuel failures are also reasonably well predicted by the proposed criterion. Further MOX tests are needed in order to clarify differences between MOX and UO_2. For what concerns mechanisms, fuel swelling is important and FGR less important for the failure mechanism at high burnup (~60 MWd/kg).

1. INTRODUCTION AND SUMMARY

The RIA test data available in the literature, and in particular the CABRI REP Na test data (Table 1), provide a very consistent basis for the assessment of fuel behaviour mechanisms relevant for RIA transients. For the CABRI REP Na rods that did not fail, valuable information on fission gas release and especially on cladding deformation have been generated in the test programme. REP Na cladding strain data have been used as a start point for deriving an admittedly simple RIA failure criterion. This is based on a maximum strain which can be tolerated by the cladding, i.e. failure can occur only when this strain level is exceeded.

- For cladding that still retains ductility, failure at high burn-up (50-60 MWd/kg) is predicted beyond a 1% (permanent) diameter strain.
- For cladding that has been embrittled due to e.g. large corrosion, spalling and hydriding, a zero ductility is assumed, i.e. the failure threshold is at onset (0%) of permanent strain.

The conditions under which the ductility decreases from 1% to zero are provisionally set in the paper, taking into account the evidence from the CABRI tests and from ANL laboratory tests. Based on the above, one derives that the lowest failure limit at 60 MWd/kg is ~65-70 cal/g, which applies to heavily corroded/hydrided fuel, i.e. for oxide thickness of ~80 μm and in presence of oxide spalling. For corrosion resistant fuel, i.e. for oxide thickness well below 80 μm and in absence of spalling, the failure threshold at the same burnup is ~100 cal/g.

This failure criterion predicts well three of the four failed REP Na tests, but not the REP Na-1 test. For this, the predicted failure threshold is 63 cal/g, whereas the reported experimental value is 30 cal/g. For CABRI unfailed rods, the predicted failure limit is very close to the enthalpy achieved during the test. When used at its higher degree of conservatism (i.e. ductility = 0), the proposed failure threshold predicts reasonably well also the failed NSRR PWR and BWR rods. In general, more data at prototypical conditions are needed in order to arrive to comprehensive, best-estimate failure predictions.

The PIE data of unfailed REP Na rods show a remarkable similarity between the trend exhibited by the cladding strain and by the fission gas release. This is briefly discussed in this paper with regard to a possible FGR mechanism (i.e. it is implied that the gas may mostly be released upon cooling, when cladding constraints are reduced). In any case, it appears that FGR as such has little to do with the mechanism of failure when this occurs at low enthalpy.

TABLE I. THE CABRI REP NA TESTS

Test	Rod	Pulse (ms)	Energy end of peak (cal/g)	Corrosion (μ)	RIM (μ)	Results and observations
Na-1 (11/93)	GRA 5 4.5% U 64 GWd/t	9.5	110 (at 0.4 s)	80 initial spalling	200	- Failure, brittle type for HF = 30 cal/g. - Hydride accumulation - Fuel dispersion 6 g., including fuel fragments outside RIM (>40 μ) - Pressure peaks in Na of 9-10 bars
Na-2 (6/94)	BR3 6.85% U 33 GWd/t	9.1	211 (at 0.4 s)	4		No failure H_{MAX} = 210 cal/g Max. strain: 3,5% average, 3.1% mid-pellet, FGR: 5.5%
Na-3 (10/94)	GRA 5 4.5% 53 GWd/t	9.5	120 (at 0.4 s)	40	100	No failure H_{MAX} = 125 cal/g Max. strain: 2% FGR: 13.7%
Na-4 (7/95)	GRA 5 4.5% U 62 GWd/t	# 75	95 (at 1.2 s)	80 no initial spalling	200	No failure H_{MAX} = 99 cal/g Cladding spalling under transient Max. strain: 0.4% FGR: 8.3%
Na-5 (5/95)	GRA 5 4.5% U 64 GWd/t	9.5	105 (at 0.4 s)	20	200	No failure H_{MAX} = 115 cal/g Max. strain: 1% FGR: 15.1%
Na-8 (07/97)	GRA 5 4.5% 60 GWd/t	75	106 (at 0.4 s)	130 lim. initial spalling	200	Failure $H_F \leq$ 82 cal/g, H_{MAX} = 110 cal/g no fuel dispersion
Na-10 (07/98)	GRA 5 4.5% 62 GWd/t	31	107 (st 1.2 s)	80 important initial spalling	200	Failure at H_F = 79 cal/g, H_{MAX} = 110 cal/g no fuel dispersal Examinations to be performed
Na-9 (04/97)	MOX 2 cycles 28 GWd/t	34	197 at 0.5 s 241 at 1.2 s	< 20		No failure H_{MAX} = 210 cal/g Max. strain: 7.4% average FGR: ~34%
Na 6 (03/96)	MOX 3 cycles 47 GWd/t	35	125 at 0.66s 165 at 1.2 s	35		No failure H_{MAX} = 148 cal/g Max. strain: 3.2% (2.5% average) FGR: 21.6%
Na 7 (1/97)	MOX 4 cycles 55 GWd/t	40	125 at 0.48s 175 at 1.20s	50		Failure H_F= 120 cal/g (t=0.452 s) Strong flow ejection, pressure peaks of 200-110b, fuel motion in the lower half zone

A comparison MOX versus UO_2 fuel based on the REP Na tests is also attempted. The data do indicate possible differences between the two fuels at low burnup (~30 MWd/kg). However, at higher burnup the difference between MOX and UO_2 fuel is not so clear (possibly except for fuel ejection), at least on the basis of the limited MOX data available so far.

In conclusion, the REP Na test series have proven to constitute a very valuable and consistent data set. The information on cladding strain fits very well together and has enabled to derive a failure criterion, which predicts reasonably well three out of four REP Na failures and the NSRR failures. However, the reported failure level of the REP Na-1 test cannot be explained based on the present analysis, a point which is discussed in the paper.

2. CLADDING STRAIN, CABRI REP NA TESTS WITH UO_2 FUEL

Unfailed UO_2 fuel rods tested in the REP Na series have been examined in hot cells after the tests in the CABRI reactor. Through the post-test diameter profilometry one can determine how the diameter permanent strain at a given axial position depends on the fuel enthalpy deposited at that position during the transient. This has been done for the UO_2 fuel rods and the outcome is shown in Fig. 1.

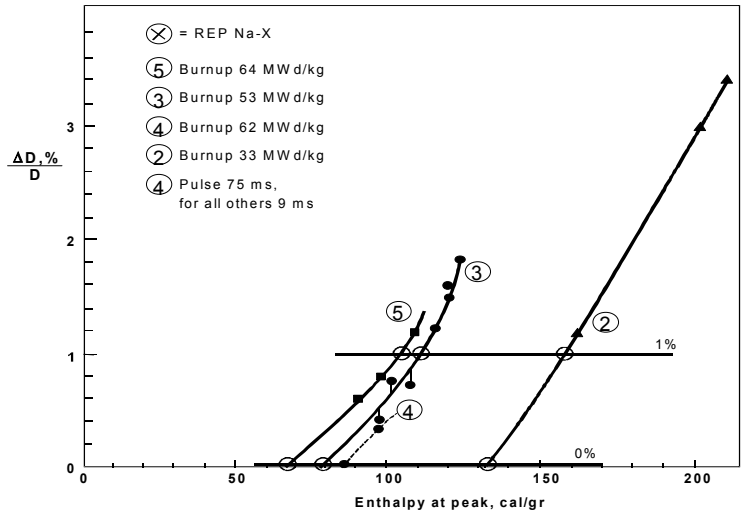

FIG. 1. Permanent diameter strain versus enthalpy as derived from the post-test rod profilometry of the four REP Na UO_2 fuels that did not fail. One can see that the curves tend to shift towards left at increasing burn-up. The pulse width also has an effect as shown by the comparison of curve 4 and 5.

The burnup effect on cladding strain can be seen in Fig. 1 by comparing curve 2, which refers to a fuel rod of 33 MWd/kg, with curves 3 and 5, which are for 53 and 64 MWd/kg respectively. One can also discern a slight difference between 3 and 5, which is attributed to the burnup difference between these two fuel rods.

The cladding strain as derived in Fig. 1 is substantially greater than what it would be expected from fuel thermal expansion only, typically 2 to 4 times greater. In fact, fuel swelling is believed to be the most important contributor to cladding strain.

The plots in Fig. 1 show that for the high burnup fuel the slope of the strain vs. energy curve tends to increase gradually, indicating that the fuel swelling might become progressively more pronounced (see curve 3 and 5). The difference between curve 4 and 5 is ascribed to the difference of pulse width, which was larger in test 4 (75 ms versus 9.5 ms).

3. CLADDING STRAIN AS BASIS OF A FAILURE CRITERION

Regardless of the details on the mechanisms involved, the ability of the fuel to withstand a RIA transient depends on its capability to accommodate cladding strain. The criterion suggested here reflects this, as it is based on a maximum tolerable cladding strain, i.e. failure can occur for cladding strain exceeding a given limit.

- For cladding that has not been embrittled by hydrogen, the (permanent) strain limit at 50-60 MWd/kg is set at 1%. This is certainly a conservative value, since REP Na tests show that fuel rods with burnup from 53 to 64 MWd/kg could tolerate cladding strains in the range 1 to 2% without failing (See REP Na-3 and -5, Fig. 1).
- The REP Na tests provide evidence that large cladding oxidation and presence of oxide spalling may reduce the cladding ductility due to hydrogen embrittlement, making the cladding more prone to failure. In this case the threshold of cladding failure is set at onset of permanent strain (i.e. permanent strain = 0).

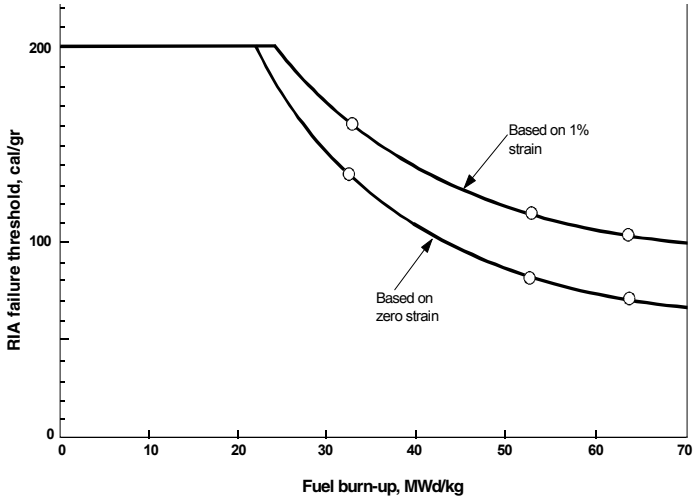

FIG. 2. Failure threshold derived from the experimental cladding strainplots (in Fig.1). The upper curve is the failure limit for cladding that still retains ductility (1% ΔD/D permanent). The lower curve is forembrittled cladding (0% ΔD/D). For fuel at burnup of 60 MWd/kg, the lowest failure threshold is approximately 65-70 cal/g.

The enthalpy failure limits corresponding to the 1% and 0% ductility threshold are derived from Fig. 1 in a straightforward manner. The resulting enthalpy failure limit when the above strain limit is set over the entire burn-up range, is shown in Fig. 2. It can be seen that the enthalpy limit decreases with burnup. At 60 MWd/kg the threshold is as low as ~70 cal/g for embrittled cladding and ~110 cal/g for cladding which has no hydrogen embrittlement. As Fig. 2 shows, an upper limit of 200 cal/g is set on the curves in the low burnup range, since failure mechanisms other than PCMI prevail for high energy depositions.

4. INFERENCE OF A RIA FAILURE THRESHOLD

4.1. Correlation for the RIA failure threshold

A correlation for the fuel failure limit has been derived based on the consideration made in the previous sections and on a closer analysis of the data, taking into account that larger strains can be accommodated at lower burn-up. The correlation is as follows

$$H_F = \left[200 \cdot \frac{25 + 10\,D}{Bu} + 0.3\,\Delta\tau \right] \left(1 - \frac{0.85\,OX}{W} \right)^2 \qquad /1/$$

where H_F is the fuel enthalpy failure limit, cal/g
If H_F from (1) is > 200,. set H_F = 200
Bu is burnup in MWd/kg
D is the (ductility or) hoop strain limit at high burn-up (1% for cladding with residual ductility and 0% for embrittled cladding), in percent
$\Delta\tau$ is the pulse width in ms (≤ 75 ms, use 75 ms beyond that)
OX is the oxide thickness in μm
W is the as-fabricated wall thickness as-fabricated in μm (576 μm for the REP Na rods)

The parameter D varies from 1 for ductile cladding to 0 for embrittled cladding. Embrittlement occurs for large oxide and in presence of spalling. The REP Na tests indicate that for cladding having an oxide thickness of 80 μm, embrittlement (D=0) occurs for spalled cladding oxide, whereas ductility is maintained (D=1) for un-spalled cladding. Recently published ANL data indicate that cladding ductility can gradually decrease to zero also for uniform oxides [1]. These data show that ductility decreases with increasing thickness of the peripheral hydride layer, approaching zero when this thickness goes beyond ~100 μm. For the purpose of this analysis, these findings have been provisionally converted in decreasing ductility vs. oxide thickness. The resulting picture is given in Fig.3, which shows how ductility drops to zero for spalled oxide (inferred from the failed REP Na rods) and for un-spalled oxide (inferred from [1]). One should notice that in most practical cases one does not know a-priori if the cladding is spalled or not, except that spalling may occur for thick oxide. For such cases, the use of the left curve of Fig. 3 is conservatively recommended.

The oxide thickness in equation /1/ is important not only because it affects the ductility term D. Oxidation causes also a reduction of cladding metal wall thickness and an increases of hydride formation at the cladding periphery, which both lower the constraint posed by the cladding on the swelling fuel. This is accounted for by the last term of equation /1/. In practice, the above means that low or moderately oxidised fuel will fail at appreciably higher enthalpy than heavily oxidised fuel.

In addition to oxide thickness, burnup is very important. Swelling both during normal operation and during a RIA transient become more pronounced with burnup, causing larger cladding strains. This is acknowledged in equation /1/ by the inverse relation between failure enthalpy and burnup.

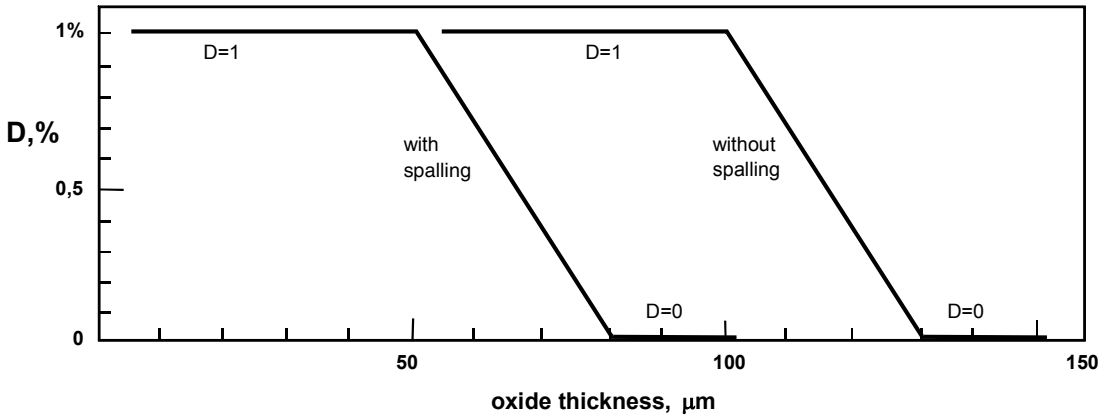

FIG. 3. Suggested dependency of the term D on cladding oxide

Since the oxide thickness is also a function of burnup, at the end of the day the failure threshold can be expressed only in terms of burnup, once the relation between oxide thickness and burnup can be anticipated. Two practical examples are shown in Fig. 4, which gives the failure limits for two types of fuel cladding, one having significant corrosion and spalling, the other one having moderate corrosion. The predictions give a threshold that is ~40 cal/g lower for the more oxidised/spalled cladding. (The cases of Fig. 4 are only meant as examples, as oxide dependency on burnup may be different for different reactors/materials). For cladding having oxide thickness larger than 130 μm, the predicted failure threshold at 60 MWd/kg is lower than ~55 cal/g.

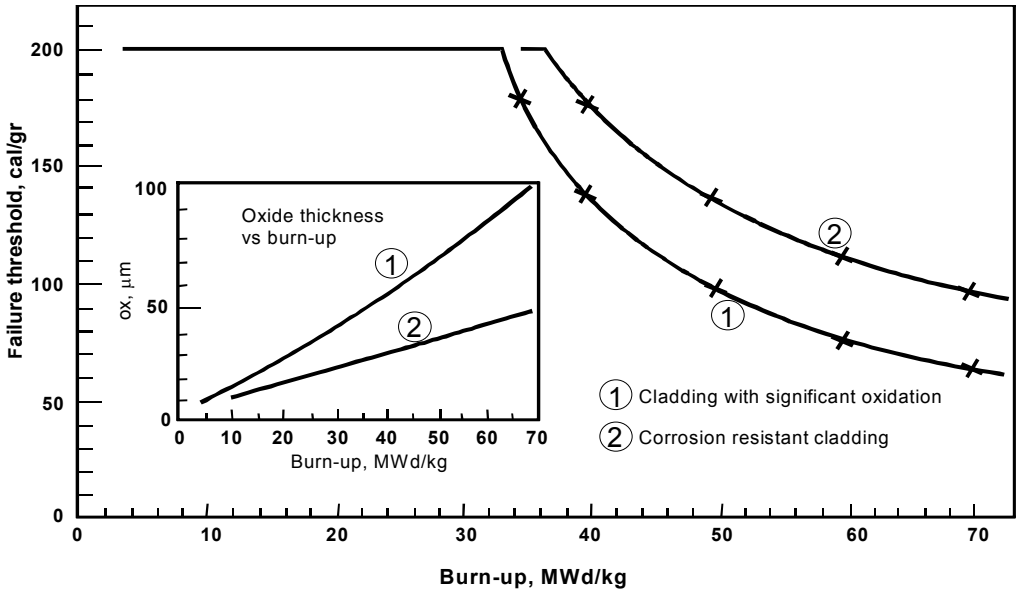

FIG. 4. RIA failure threshold as predicted by Eq./l/in the case of a cladding exhibiting significant oxidation and spalling (curve 1) and in case of a corrosion resistant cladding (curve 2). At 60 MWd/kg, the predicted enthalpy-to-failure threshold is~40cal/gr higher for the corrosion resistant cladding (70 vs. 110 cal/gr).

In this evaluation, burnup and oxide thickness are kept as independent, separate variables that affect failure levels in the way expressed by Eq. /1/. They are considered as separate variables because the corrosion-burnup relation may vary substantially from case to case, depending on cladding alloy, water chemistry and fuel duty during service in a commercial reactor. It is possible that some sort of duty index can be used as better parameter to predict fuel failure enthalpy, but such refinements are beyond the purpose of this note. Burnup and oxide thickness are used here simply because they are parameters of common use which have a direct physical meaning– in other words, everyone knows what these parameters represent.

Equation /1/ acknowledges only a moderate effect of pulse width ($\Delta\tau$). In fact, the predicted failure threshold increases by only ~5 cal/g when the pulse width increases from 9 to 30 ms. Since in the REP Na series the $\Delta\tau$ ranged between 9 and 75 ms, a maximum value $\Delta\tau$ = 75 ms should be used when the pulse width exceeds 75 ms.

4.2. Predictability of the REP Na tests

The calculated enthalpy to failure based on equation /1/ for the various REP Na tests is given in Table 2.

For the rods that had failed, the comparison between predicted and actual failure enthalpy is shown in Fig. 5. Three tests are well predicted by Eq. /1/, but REP Na-1 is not. In this case the failure is predicted at 63 cal/g, whereas the quoted enthalpy to failure is a factor of 2 lower.

TABLE II. FAILURE PREDICTIONS OF REP NA TESTS BASED ON EQ. /1/

Test	$\Delta\tau$	Bu	OX	D	Experiment fuel enthalpy	H_F (Eq. 1)	
REP Na – 1	**9.5**	**64**	**80 (**spalled)	**0**	***H_{Fail} = 30**	**63**	
REP Na-2	9.1	33	4	1	H_{MAX} = 210	200	
REP Na-3	9.5	53	40	1	H_{MAX} = 125	119	
REP Na-4	75	62	80	1	H_{MAX} = 99	105	
REP Na-5	9.5	64	20	1	H_{MAX} = 115	107	
REP Na-6	35	47	35	1	H_{MAX} = 148	142	MOX
REP Na-7	**40**	**55**	**50**	**1**	***H_{Fail} = 120**	**120**	**MOX**
REP Na-8	**75**	**60**	**130** (spalled)	**0**	***$H_{Fail} \leq$ 82**	**70**	
REP Na-9	34	28	20	1	H_{MAX} = 210	200	MOX
REP Na-10	**31**	**62**	**80** (spalled)	**0**	***H_{Fail} = 79**	**71**	

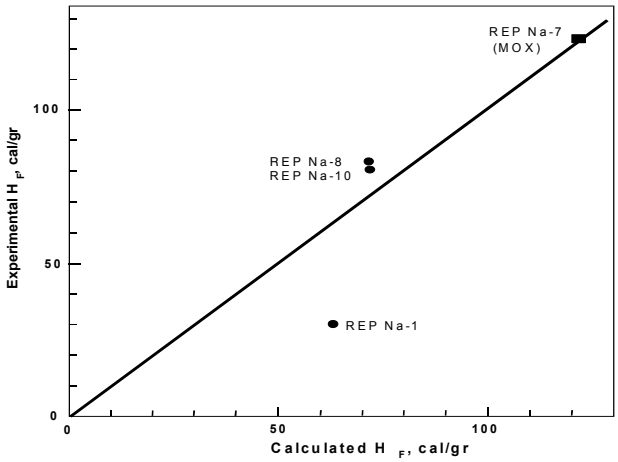

FIG. 5. Comparison of calculated vs experimental enthalpy to failure for the four REP Na tests that failed. Three tests, including a MOX test, are well predicted. The REP Na-1 test cannot be predicted by the proposed correlation (Eq./1/).

A prediction of the failure limit has been done also for the REP Na tests that did not fail. The results are shown in the diagram of Fig. 6. One can observe that all data points lay rather close to the 1:1 diagonal, typically ~5-10 cal/g above it. This confirms that, with reference to the REP Na-1 database, the proposed correlation is conservative by ~5-10 cal/g, i.e. it is not an "unreasonably" conservative one. One should observe that all the three failed UO_2 fuel rods had spalled oxide, where none of the rods with un-spalled oxide failed. This implies that for the latter category of rods, i.e. those with un-spalled oxide, the failure threshold given by Eq. /1/ contains an inherent conservatism in that the database has only unfailed rods. As shown in Fig. 6, the failure predictions are only 5-10 cal/g away from the actually achieved enthalpy, but we do not know how far this is from the actual failure level - simply because none of such rods failed. In other words, one knows that (for rods with un-spalled oxide) Eq. /1/ provides failure limits which are conservative by at least 5-10 cal/g, but the actual conservatism (or margin to failure) can be greater than that.

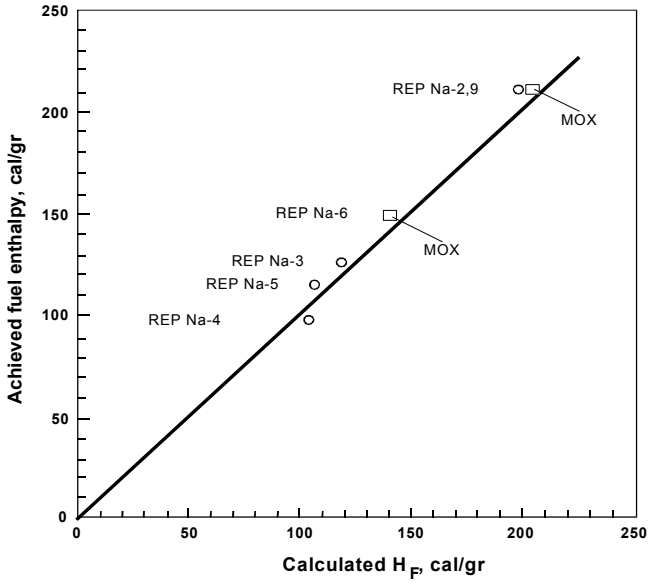

FIG. 6. Comparison between the calculated enthalpy to failure and the actually achieved fuel enthalpy for the REP Na tests that did not result in fuel failure.

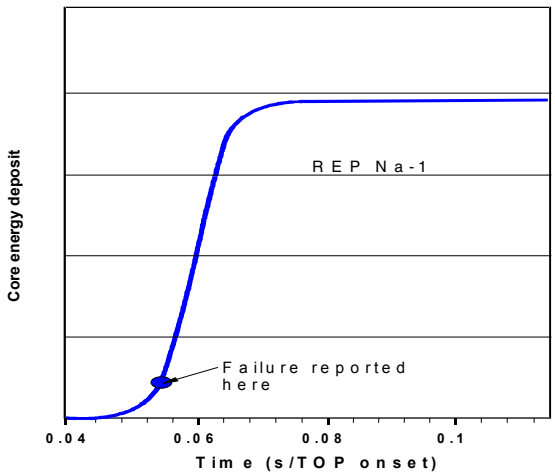

FIG. 7 Core energy deposit versus but time for REP Na-1 test.

Returning to the discrepancy of the REP Na-1 test (calculated failure at 63 cal/g versus a reported experimental value of 30 cal/g), one should notice that the transient started at a steady temperature of 280°C, corresponding to ~20 cal/g (Fig 7). The tests, which was to achieve 110 cal/g, resulted in a fuel failure that reportedly occurred when the transient had just started (see figure on the right side). At that point-in-time, only 8.9 cal/g had been injected onto the fuel, bringing the total enthalpy to (~20 + 8.9) = ~30 cal/g. Fuel failure at such conditions is difficult to explain and to reconcile with the experimental evidence from other tests, in CABRI and elsewhere.

A ΔH = 8.9 cal/g means an average fuel temperature of ~400°C. Fuels are not expected to fail at such conditions, also considering that in this case the fuel was likely exposed to more challenging conditions for a long time during service in the power reactor. The fact that the temperature was higher than 400°C in the pellet rim does not change the substance of this observation. The REP Na-1 test will remain unexplained unless an effort is made to re-examine the details of the test or fuel specimens condition that might have led to such a low failure enthalpy.

4.3. Generic failure threshold, application to the NSRR tests

While Eq. /1/ already contains a reasonable degree of conservatism, the correct setting of the parameter D must be considered further for cases different than the REP Na tests. As said earlier, in REP Na tests it is apparent that an inverse relation does exist between oxide thickness/spalling and cladding ductility. However, other factors than oxide morphology may also contribute to ductility degradation for fuel and conditions different than the ones of the REP Na tests. Changes of cladding type may result in different residual ductility at high burnup, as affected by irradiation as well as by hydrogen content and distribution in the cladding. The coolant temperature during irradiation at normal conditions as well as during the transient may also affect the residual ductility in that it affects the balance between irradiation induced embrittlement and temperature induced annealing.

If well-characterised cladding ductility data are available, the value of the parameter D can be set on the basis of such data. In lack of this information, the most conservative setting, i.e. D=0, should be used for failure prediction based on Eq. /1/.

For applications to other cases than the REP Na tests, another point to consider is the temperature or enthalpy at the start of the test. In Eq. /1/, H_F is the total enthalpy to failure, with a start enthalpy level of [Cp · 280°C] = 20 cal/g [1]. For generic applications to a lower (or different) initial temperature, such as in the NSRR tests, the failure threshold should be expressed in terms of enthalpy increase above the initial value. Thus for those generic applications to cases other than the REP Na ones, the failure threshold should be expressed by

$$\Delta H_F = \left[200 \cdot \frac{25}{Bu} + 0.3\Delta\tau\right]\left(1 - \frac{0.85\,OX}{W}\right)^2 - Cp \cdot (280 - T_i) \qquad /2/$$

which is equivalent to Eq. /1/ except that D is set D=0 and the enthalpy increase ΔH_F above the initial instead of total enthalpy. The terms T_i is the test initial temperature (which was 280°C in the REP Na tests).

The performance of Eq. /2/ is predicting the NSRR PWR and BWR tests where failure occurred is shown in Table 3.

TABLE III. COMPARISON OF THE NSRR PWR/BWR EXPERIMENTAL ENTHALPY AT FAILURE WITH THE VALUES PREDICTED BY EQ. /2/

4.3.1. Test	*Δτ*	*Bu*	*OX*	*Exp. ΔH at failure*	*ΔH_F (Eq. 2)*	*Fuel type*
NSRR						
HBO-1	5	50	48	60	67	PWR
HBO-5	5	44	60(1)	77	75	PWR
TK-2	5	48	35	60	73	PWR
TK-7	5	50	30	86	73	PWR
NSRR/BWR						
FK-6	5	61	~20	70	59	BWR
FK-7	5	61	~20	62	59	BWR
FK-9	5	61	~20	86	59	BWR

(1) Maximum value

5. FISSION GAS RELEASE, TESTS WITH UO_2 FUEL

An evaluation has been made in order to derive the dependency of FGR on enthalpy, on the reasonable assumption that the release depends mainly on fuel enthalpy and burnup. The resulting FGR versus enthalpy curves for REP Na rods having different burnup are shown in Fig. 8. Not surprisingly, one can observe that the release increases with fuel burnup and enthalpy. By comparing this figure with Fig. 1, one can also note that the onset of FGR is very close to the onset of permanent deformations.

As an additional exercise, the enthalpy at 5% FGR has been derived for the four curves given in Fig. 8, and then plotted as function of the corresponding fuel burnup, as shown in Fig. 9. In the same figure, the onset of cladding permanent strain curve has also been plotted. One can again note that the 5% FGR curve is remarkably close to the onset of cladding strain curve, which was derived in Fig. 2.

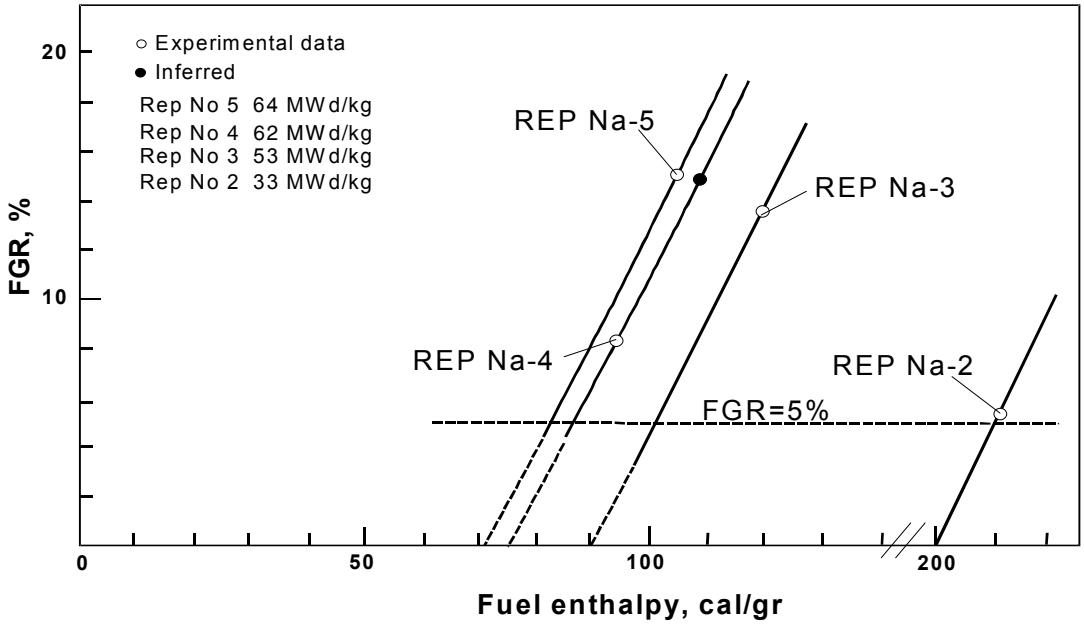

FIG. 8. Fission gas release (FGR) data, plotted as function of the fuel enthalpy, for the UO_2REP Na tests.

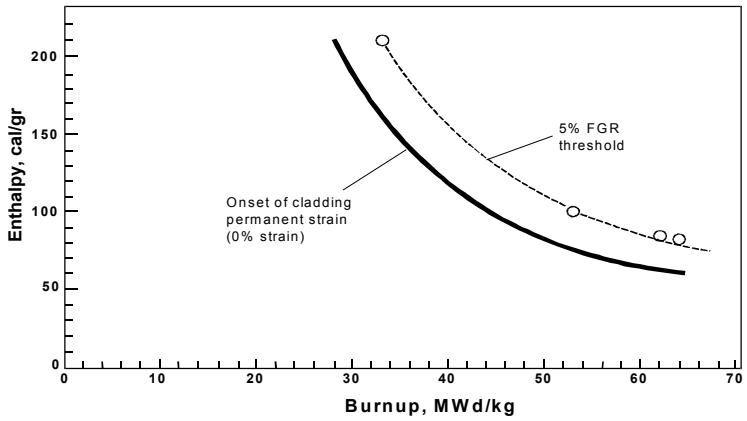

FIG. 9. Plot of the 5%FGR threshold derived from the previous figure (FIG.8). together with it, the curve for onset of cladding plastic deformation is also plotted. The latter is identical to (the lower curve of) FIG.2 and is derived from the cladding strain data shown in FIG. 1. The trend of the two curves is remarkably similar.

Fig. 9 basically says that appreciable fission gas release is observed beyond the onset of permanent cladding strain. Since the latter is also the failure threshold for brittle cladding, it

(1) $Cp = 0.30\ J/g^oC$ or $Cp = 0.072\ cal/g^oC$

follows that FGR "occurs" beyond the low-enthalpy failures (i.e. those related to brittle cladding). Said in other terms, while fission gas induced fuel swelling is important, FGR has little to do with the failure mechanism for these low enthalpy failures. Fission gas release - more than the cause of clad diameter deformation - seems to be the consequence of it. This can be rationalised, for instance, if the gas release takes place mainly in the cooling phase, i.e. after the cladding has been deformed and, upon cooling, does not provide any more constraint to the fuel.

6. MOX FUEL

The diameter strain for the two unfailed MOX tests are compared with the diameter stain of the unfailed UO_2 tests in the diagram of Fig. 10. Although this is only an indicative comparison, one can observe that the diameter strain observed in REP Na-6 are comparable with the ones observed for UO_2 fuel at high burnup. Instead, REP Na-9 gave larger deformations than the UO_2 test at corresponding burnup (REP Na-2). It should be noted, however, that the REP Na-2 fuel was of quite different source than the rest of the REP Na series. Fig. 11, where the FGR of MOX and UO_2 fuel are compared, gives approximately the same picture, i.e. the MOX REP Na-6 FGR is compatible with UO_2 fuel, whereas the REP Na-9 gives higher release than REP Na-2.

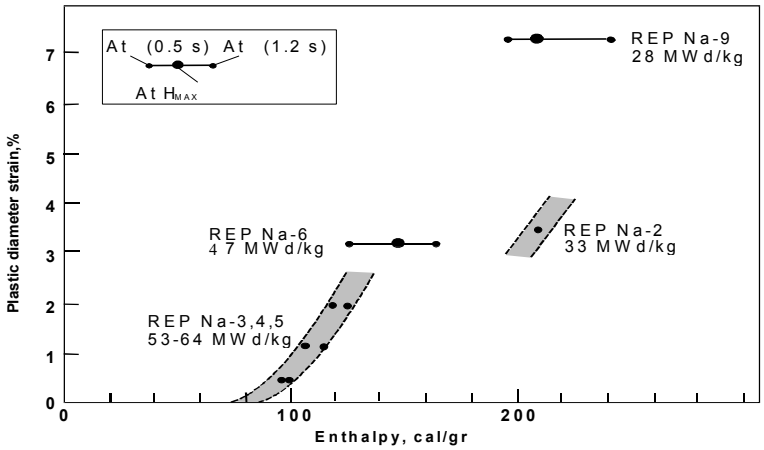

FIG. 10. Comparison of the percent diameter strain in UO_2 and MOX fuel. The REP Na-6 test gave strains comparable with the UO_2 tests at high burnup. The RER Na-9 MOX test strains appreciably greater than the REP Na-2 UO_2 (test at comparable burnup). Note however that the REP Na-2 was

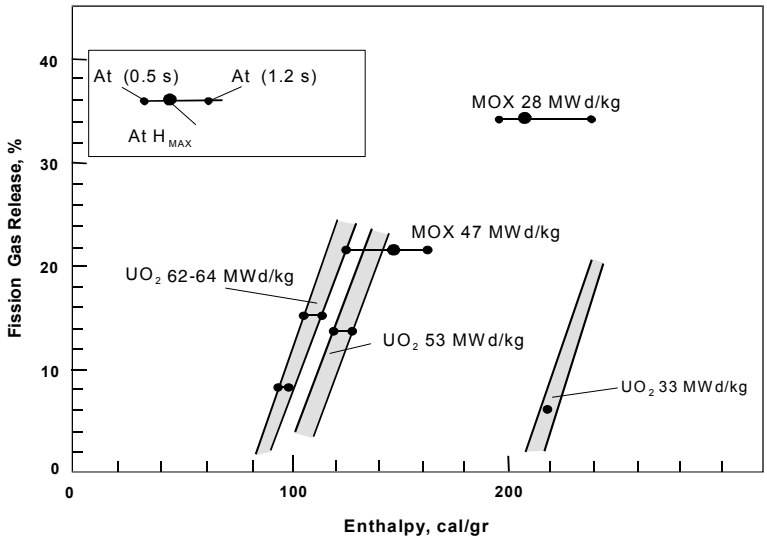

FIG. 11. Comparison of the fission gas release UO_2 and MOX fuel. The REP Na-6 MOX test (47 MWd/kg) gave FGR compatible with the REP Na-3 UO_2 test (53 MWd/kg). The REP Na-9 MOX test (28 MWd/kg) gave much higher gas release than the REP Na-2 UO_2 test (33 MWd/kg)-Note however that the latter has a "special" type of fuel.

In conclusion, the high burnup MOX data (REP Na-6) on cladding strain and FGR are comparable with UO_2 high burnup data. Whether the differences observed at lower burnup between REP Na-9 and 2 are due to the MOX vs. UO_2 fuel differences or to other factors (e.g., the REP Na-2 had BR-3 fuel), cannot be concluded at this time.

Based on the microstructural differences between MOX and UO_2 fuel, one would expect that appreciable differences exist in the failure behaviour of the two types of fuel. However, the data available on MOX, shown in Fig. 5 and Fig. 6, are too few to ascertain clear differences between MOX and UO_2 failure propensity, at least in terms of failure predictability based on Eq. /1/, and more data are needed in order to draw firm conclusions.

REFERENCE

[1] DAUM, R.S., et al., "Embrittlement of Hydrided and Irradiated Zircaloy-4 Under RIA-type Conditions". 13th ASTM Int. Symp. on Zirconium in the Nuclear Industry", Annecy, France (2001).